

ENGINEERING LIMIT CYCLE SYSTEMS: ADAPTIVE FREQUENCY OSCILLATORS AND APPLICATIONS TO ADAPTIVE LOCOMOTION CONTROL OF COMPLIANT ROBOTS

THÈSE N° 3788 (2007)

PRÉSENTÉE LE 1^{ER} JUIN 2007

À LA FACULTÉ INFORMATIQUE ET COMMUNICATIONS

GROUPE IJSPEERT

PROGRAMME DOCTORAL EN INFORMATIQUE, COMMUNICATIONS ET INFORMATION

ÉCOLE POLYTECHNIQUE FÉDÉRALE DE LAUSANNE

POUR L'OBTENTION DU GRADE DE DOCTEUR ÈS SCIENCES

PAR

Jonas BUCHLI

ingénieur électricien diplômé EPF
de nationalité suisse et originaire de Safien (GR)

acceptée sur proposition du jury:

Prof. W. Gerstner, président du jury

Prof. A. Ijspeert, directeur de thèse

Prof. M. Hasler, rapporteur

Prof. Y. Kuniyoshi, rapporteur

Prof. S. Schaal, rapporteur



ÉCOLE POLYTECHNIQUE
FÉDÉRALE DE LAUSANNE

Suisse
2007

Abstract

IN this thesis, we present a dynamical systems approach to adaptive controllers for locomotion control. The approach is based on a rigorous mathematical framework using nonlinear dynamical systems and is inspired by theories of self-organization.

Nonlinear dynamical systems such as coupled oscillators are an interesting approach for the on-line generation of trajectories for robots with many degrees of freedom (e.g. legged locomotion). However, designing a nonlinear dynamical system to satisfy a given specification and goal is not an easy task, and, hitherto no methodology exists to approach this problem in a unified way.

Nature presents us with satisfactory solutions for the coordination of many degrees of freedom. One central feature observed in biological subjects is the ability of the neural systems to exploit natural dynamics of the body to achieve efficient locomotion. In order to be able to exploit the body properties, adaptive mechanisms must be at work. Recent work has pointed out the importance of the mechanical system for efficient locomotion. Even more interestingly, such well suited mechanical systems do not need complicated control. Yet, in robotics, in most approaches, adaptive mechanisms are either missing or they are not based on a rigorous framework, i.e. they are based on heuristics and ad-hoc approaches.

Over the last three decades there has been enormous progress in describing movement coordination with the help of Synergetic approaches. This has led to the formulation of a theoretical framework: the theory of dynamic patterns. This framework is mathematically rigorous and at the same time fully operational. However, it does not provide any guidelines for synthetic approaches as needed for the engineering of robots with many degrees of freedom, nor does it directly help to explain adaptive systems.

We will show how we can extend the theoretical framework to build adaptive systems. For this purpose, we propose the use of multi-scale dynamical systems. The basic idea behind multi-scale dynamical systems is that a given dynamical system gets extended by additional slow dynamics of its parameters, i.e. some of the parameters become state variables. The advantages of the framework of multi-scale dynamical systems for adaptive controllers are 1) fully dynamic description, 2) no separation of learning algorithm and learning substrate, 3) no separation of learning trials or time windows, 4) mathematically rigorous, 5) low dimensional systems. However, in order to fully exploit the framework important questions

have to be solved. Most importantly, methodologies for designing the feedback loops have to be found and important theoretical questions about stability and convergence properties of the devised systems have to be answered.

In order to tackle this challenge, we first introduce an engineering view on designing nonlinear dynamical systems and especially oscillators. We will highlight the important differences and freedom that this engineering view introduces as opposed to a modeling one. We then apply this approach by first proposing a very simple adaptive toy-system, consisting of a dynamical system coupled to a spring-mass system. Due to its spring-mass dynamics, this system contains clear natural dynamics in the form of resonant frequencies. We propose a prototype adaptive multi-scale system, the adaptive frequency oscillator, which is able to adapt its intrinsic frequency to the resonant frequency of the body dynamics. After a small sidetrack to show that we can use adaptive frequency oscillators also for other applications than for adaptive controllers, namely for frequency analysis, we then come back to further investigation of the adaptive controller. We apply the same controller concept to a simple spring-mass hopper system. The spring mass system consists of a body with two legs attached by rotational joints. The legs contain spring-damper elements. Finally, we present results of the implementation of the controller on a real robot, the experimental robot PUPPY II. This robot is a under-actuated robot with spring dynamics in the knee joints. It will be shown, that due to the appropriate simplification and concentration on relevant features in the toy-system the controller concepts works without a fundamental change on all systems from the toy system up to the real robot.

Keywords — limit cycle, adaptive frequency oscillators, robotics, compliance, under-actuation, nonlinear dynamical system, adaptive system

Zusammenfassung

IN der vorliegenden Arbeit präsentieren wir einen auf dynamischen Systemen basierenden Ansatz für adaptive Regler für die Kontrolle von Fortbewegung. Der Ansatz basiert auf einem rigorosen mathematischen Gerüst welches sich auf nicht-lineare dynamische Systeme abstützt und von Theorien der Selbstorganisation inspiriert ist.

Nichtlineare Dynamische Systeme, wie z.B. gekoppelte Oszillatoren, sind ein interessanter Ansatz für die zeitnahe Generierung von Trajektorien für Roboter mit vielen Freiheitsgraden (z.B. Fortbewegung mit Beinen). Allerdings ist es schwierig ein dem Ziel und den Spezifikationen entsprechendes nichtlineares dynamisches System zu entwerfen. Bis jetzt gibt es keinen Ansatz um dieses Entwurfs-Problem methodisch und einheitlich anzugehen.

Die Natur zeigt uns funktionierende Lösungen für die Koordination von vielen Freiheitsgraden. Ein zentraler Aspekt, der in biologischen Untersuchungen hervortritt ist die Fähigkeit des Nervensystems die natürliche Dynamik des Körpers auszunutzen um effiziente Fortbewegung zu erreichen. Um die Eigenschaften des Körpers ausnützen zu können, müssen adaptive Fähigkeiten vorhanden sein. Neuere Arbeiten haben die Wichtigkeit des mechanischen Systemes für effiziente Fortbewegung aufgezeigt. Interessanterweise benötigen solche gut geeigneten mechanischen Systeme nur einfache Kontrolle. Doch in der Robotik fehlen solche Ansätze entweder oder sie basieren nicht auf einer rigorosen theoretischen Grundlage, d.h. sie basieren auf Heuristiken und ad hoc Ansätzen. Während der letzten drei Jahrzehnte wurde ein grosser Fortschritt in der Beschreibung von Bewegungs-Koordination mithilfe von Synergetischen Ansätzen erzielt. Dieser Fortschritt hat zur Theorie der dynamischen Muster geführt. Diese Theorie ist mathematisch rigoros und gleichzeitig direkt anwendbar. Die Theorie gibt jedoch keine Hilfe und Hinweise für synthetische Ansätze wie sie für die Konstruktion von Robotern mit vielen Freiheitsgraden gebraucht werden. Auch erklärt die Theorie nicht direkt adaptive Systeme. Wir werden zeigen wie wir die Theorie erweitern können um adaptive Systeme konstruieren zu können. Dafür schlagen wir multi-skalen dynamische Systeme vor. Die grundlegende Idee die solchen multi-skalen dynamischen Systemen zugrundeliegt ist, dass ein gegebenes dynamisches System mit zusätzlicher, langsamer Dynamik ihrer Parameter ausgestattet wird, d.h. einige der Parameter werden Zustandsvariablen des Systems. Der Vorteil von multi-skalen dynamischen Systemen für adaptive Regler sind: 1) voll dynamische Beschreibung 2) keine Tren-

nung von Lernalgorithmus und Lernsubstrat 3) keine Auftrennung von Lernversuchen und Zeitfenstern 4) mathematisch rigoros 5) niedrig-dimensionale Systeme. Allerdings müssen wichtige Fragen beantwortet werden um diese Ansätze voll ausnützen zu können. Allen voran müssen methodische Ansätze für den Entwurf der Rückkopplungsschleifen gefunden werden, und wichtige Fragen über Stabilitäts- und Konvergenzeigenschaften solcher Systeme müssen beantwortet werden.

Um diese Herausforderung anzugehen, werden wir zuerst eine konstruktionsorientierte Sicht auf den Entwurf von dynamischen Systemen entwickeln. Wir werden die wichtigen Unterschiede und die Freiheit die eine solche konstruktionsorientierte Sicht, im Gegensatz zu einer modellierungs-orientierten Sicht erlaubt, erkennen. Die Ansätze werden dann auf die Entwicklung eines adaptiven Einfachst-Modell, bestehend aus einem dynamischen System gekoppelt an ein Feder-Masse System angewandt. Wegen der Feder-Masse Dynamik hat dieses System eine klare natürliche Dynamik in der Form von resonanten Frequenzen. Wir schlagen ein prototypisches adaptives multi-skalen System, den frequenz-adaptiven Oszillator vor. Dieser kann seine intrinsische Frequenz den Resonanzfrequenzen der Körperdynamik anpassen. Nach einem kurzen Exkurs, um zu zeigen wie die frequenz-adaptiven Oszillatoren auch für andere Anwendungen, in unserem Beispiel Frequenz-Analyse gebraucht werden können, fahren wir mit der Untersuchung der adaptiven Regler weiter. Wir wenden dasselbe Kontrollkonzept auf ein einfaches Masse-Feder-Sprungsystem an. Das Masse-Feder System besteht aus einem Körper an den zwei Beine mit einem Rotationsgelenk angebracht sind. Die Beine enthalten Feder-Dämpfer Elemente. Zuletzt zeigen wir die Resultate der Implementierung des Reglers auf einem richtigen Roboter, dem PUPPY II. Dies Roboter ist ein nicht vollständig aktuierter Roboter mit Federdynamik in den Kniegelenken. Wir zeigen, dass Aufgrund der korrekten Vereinfachung und dem Fokus auf die relevanten Eigenschaften im Einfachst-Modell das Regler-Konzept ohne grundsätzliche Änderung in allen Systemen vom Einfachst-Modell bis zum richtigen Roboter erfolgreich angewendet werden kann.

Schlagwörter – Grenzyklus, frequenz-adaptiver Oszillator, Robotik, Nachgiebigkeit, unvollständige Aktuierung, nichtlineares dynamisches System, adaptives System

Acknowledgments

AT this place it is my extraordinary pleasure to acknowledge all the great people I had the chance to meet and work with over the last few years. It's the right time and place to thank them for all for their the support in all the various forms: discussions, hints, support, flying activities, French lessons, and Absinth deliveries.

First and foremost I would like to express my gratitude to my advisor Auke Jan Ijspeert, he only made this work possible by accepting me as a PhD student. He managed in an almost perfect manner the balance between giving me freedom to pursue my own ideas on one hand, and good feedback and guidance on the other. Even under the heaviest workloads he remains a calm, friendly and accessible person. His feedback was certainly invaluable for the presented work. His personality is for sure a very important factor for the enjoyable experience that my PhD at the BIRG was.

Then, it is surely in order to thank wholeheartedly Ludovic Righetti, whom I have met as a student to supervise and who has become a good research colleague, but even more important a very good friend since. A lot of the ideas presented in this thesis we developed together in many hours of discussion and many results are an outcome of our collaboration. And, I shall not forget: “Un grand merci pour m’avoir donné l’opportunitié d’apprendre le français soutenu.”

I would like to thank the members of the thesis committee: Martin Hasler, Yasuo Kuniyoshi and Stefan Schaal, as well as the president Wulfram Gerstner for accepting to serve in my thesis committee, their invested time and effort, and giving me good feedback.

Then, I would like to thank Marlyse Taric for always being very friendly, helpful and efficient. Without her, the lab would come to a grinding halt in the shortest of times. Her experience and effectivity was surely an important part of making the organization of the LATSIS conference a much more enjoyable experience. Of course here I shall not forget to thank to Natascha, who supported Marlyse in the beginning of my time at the EPFL.

Further, I would like to thank Christof Teuscher, he not only introduced me to many of the deep secrets of a doctoral student's life at the EPFL and our lab but also later supported me in many important ways.

“Muito obrigado” to Cristina, it was fascinating to get to know a person with such a concurring view on the world of science, others of our preferred past times and much more. I always enjoyed spending my time with you. Many thanks for

your continuing support and encouragement!

A warm thanks goes to Paula who supported me in my decision to start this PhD and for the good times we had.

A big thank certainly also goes to Alessandro. He started at the same time finishing at the same time, but was already a long-term EPFL-dweller, so he was very helpful to the newcomer to find his way through the complicated organism that such a school represents. And of course thanks to him all our IT infrastructure always runs as perfectly as one could only imagine in a dream.

To Fumiya, not only for the support in robotics questions – he made a part of the experiments only possible – but also for sharing a good time around some beers and Long Island Ice Teas.

A further big thanks goes to my fellow pilot and preferred tandem passenger Fabien for all the good moments we spent on all our smaller and bigger flying trips. I wish you always happy landings, not too fast, not too hard!

Many thanks to the people at Cyberbotics: Olivier and Yvan, for always improving their, already great, simulator and listening to our needs.

To Pierre-André for what must be many liters of Pastis, sharing breakfast in the Café des Bouchers, consulting on electronic problems – and, bringing good mood into the lab!

To Joël, first of all for “le bière” [sic], being one of the only one not to despair and still attempt to correct my terrible French, and also for sharing most memorable moments in a Lausanne that comes alive only long after nightfall.

To Sarah for having me introduced to some excellent music and bringing true mathematical insight into the lab.

To Masoud for his placidity, his reliable personality and for sharing a different culture with us.

To Ralf who remains a quiet, friendly and courteous person – until you give him a laser pistol in his hands.

To Andres and Carlos, my columbian office mates for their good mood and atmosphere they created in INN 233.

To Yann for the funky time while sharing our hype corner office.

To our latest arrival at BIRG, Alexander, bringing order and organization into that said corner office - your clean desk will always remain a culture shock to me.

To Aleksandar and Ricardo, visiting our group for some months, bringing new ideas and creating exciting opportunities.

A big thanks also to the LASA tribe: Biljana, Eric, Florent, Micha, Sylvain and all the others, the “meetings” with you were certainly highlights in my life as a young researcher! And a special acknowledgment to Eric, it was a pleasure to discover parts of the Chinese culture with you, I would probably have traveled north forever.

I should certainly not forget to say “merci beaucoup” to Bertrand for many interesting discussions about science, the world and the deeper implications of what I am actually doing!

At this place I would also like to acknowledge all the students that where adventurous enough to embark on a project with me: Anurag, Fritz, Jérôme, Marc-Antoine, Martin, Etienne, Giorgio, Matteo. It was a pleasure working with you guys and I certainly learned and benefitted a lot from our interaction.

I shall certainly not forget to thank the members of the “ancient” Logic Systems Lab under the lead of its director Daniel Mange: André “Chico”, André, Eduardo, Enrico, Gianluca and Jacques. They were always very supportive to the Junior Enterprise under the command of Auke and gave us youngsters a very warm welcome.

Science and research is certainly exciting and a fulfilling pastime, but there are times when a certain life-work balance has to be restored. There was a good group of people around always ready for a change of air. I would like to thank all the people of the RNVL, at Air Turquoise and all the other free flyers around: Alain, Alexandre, Christian, Claude, Enrice, Gilles, Greg Randi, Ricardo, Sebastien, Simon, Stéphane, Tom, and all the countless others! Thanks for making this corner of the alps a a free-flight mecca – it’s a pleasure to share the sky with you!

Last but not least, and most importantly to me, I would like to express a deep gratitude and respect to my parents Annamaria and Robert, as well as to my brother Frank for being very supportive and understanding for my career choices and and the way I organize my life. This was certainly very important for achieving the presented results.

*

My work was mainly funded through a Young Professorship Award to Auke Ijspeert from the Swiss National Science Foundation (SNF). I would like to thank the SNF for the support and the opportunities created through their funding.

Jonas Buchli
Lausanne, April 2007

Contents

Abstract	i
Zusammenfassung	iii
Acknowledgments	v
1 Introduction	1
1.1 Motivation	1
1.2 Outline of the thesis	4
1.3 Contributions	4
2 Background & Related Work	5
2.1 Modeling adaptive systems	11
3 Simpler Systems – Analyzable Solutions	13
3.1 Improving a CPG	14
3.1.1 Introduction	14
3.1.2 Designing Biologically Inspired Distributed Controllers for Walking Robots	15
3.1.3 Outline	16
3.1.4 A Distributed Quadruped Central Pattern Generator	17
3.1.5 Discussion	25
3.2 An engineering view on oscillators	31
3.2.1 Introduction	32
3.2.2 Limit cycle systems	34
3.2.3 The design space	46
3.2.4 Design approaches	55
3.2.5 Design results: From reactive to adaptive oscillators	55
3.2.6 Conclusion & Discussion	59

4	A Toy System	65
4.0.7	Introduction	66
4.0.8	A Simple, Adaptive Locomotion Toy-System	68
4.0.9	Simulation Results	74
4.0.10	Discussion	82
5	Adaptive Frequency Oscillators	89
5.1	Proof of convergence	89
5.1.1	Introduction	90
5.1.2	Learning frequencies with a Hopf oscillator	92
5.1.3	Model description	92
5.1.4	Proof of convergence with the Hopf oscillator	95
5.1.5	Numerical simulations	100
5.1.6	Simple example of learning	100
5.1.7	Error evaluation of the analytic approximation for a simple perturbing force	101
5.1.8	Predicting learning with multi-frequency inputs	103
5.1.9	Learning pseudo-period of chaotic signals	105
5.1.10	Generalization to non-harmonic oscillators	106
5.1.11	An adaptive Van der Pol oscillator	106
5.1.12	Other examples of adaptive oscillators	112
5.1.13	Discussion	114
5.2	Frequency analysis with AFOs	116
5.2.1	Introduction	116
5.2.2	A dynamical system for frequency analysis	117
5.2.3	Simulation Results	122
5.2.4	Probabilistic Treatment: Fokker-Planck Equation	127
5.2.5	Conclusions & Discussion	131
5.2.6	Appendix – Calculation of c_n for small K	137
6	From Abstract to Reality	139
6.1	A simulated hopper robot	139
6.1.1	Introduction	140
6.1.2	Adaptive Frequency Oscillators	141
6.1.3	The adaptive active spring-mass hopper	143
6.1.4	Simulation results	146
6.1.5	Discussion	148
6.2	First real world tests	151
6.2.1	Introduction	152
6.2.2	Adaptive frequency oscillator on a real robot	154
6.2.3	Adaptive Hopf Oscillator with Linear Feedback loop	156
6.2.4	Examples of linear feedback loops	161
6.2.5	Conclusion & Discussion	162
6.3	More real world experiments	165

6.3.1	Introduction	166
6.3.2	Adaptive Controller	168
6.3.3	Hardware	169
6.3.4	Experimental Results	171
6.3.5	Toward a theory for AFOs in feedback loops	181
6.3.6	Conclusions & Discussion	187
7	Epilogue	193
7.1	Original contributions	193
7.2	Discussion & Conclusions	194
7.3	Outlook	195
	Bibliography	217

Chapter 1

Introduction

Goals

In this thesis we pursue three main goals. First, we investigate a dynamical systems approach to adaptive systems. We study aspects of a dynamical systems approach to adaptivity and learning which is based on self-organizing systems. Second, we would like to propose new ideas for robotic locomotion. We do that by studying the application of such adaptive dynamical systems systems to agile legged robotic locomotion. Third, we attempt to present an engineering view on oscillators and dynamical systems in general. More specifically we clarify aspects of the use of oscillators for technological applications.

1.1 Motivation

Nature has always been a major inspiration source for those seeking solutions to technical challenges. A particular area of research which has continued to pose unsolved challenges is agile robotic locomotion, especially for complex terrains. If we look around, we see solutions to those problems every day on many scales, from insects up to mammals. And, as a matter of fact, we ourselves have implemented a solution to this problem. It is thus natural to turn to these natural systems, study them and try to unlock some of the key principles, in the hope this will boost our technological progress.

Despite the recent excitement about bio-inspiration it is nothing new, but has an age old tradition. However, there are a few things which have given new dimensions and momentum to bio-inspired approaches today. First of all, theoretical approaches in biology are more and more commonplace and accepted. Theoretical biology is a well established research area by now. This theoretical fundament helps in singling out fundamental principles and putting hypotheses on firm ground. Second, we can put those ideas to the test on several levels, from theoretical, over simulation to real world implementations. We have powerful dig-

ital computers which allow to do simulation of large complex processes. Building complex machines such as robots gets simpler and more accessible every day. This means we can test out concepts that were not easily testable a few years ago at a reasonable effort in terms of time, cost and material. In this thesis we show work on all this levels, from theoretical to real world implementations.

However, on the downside, bio-inspiration has some issues. First and foremost we have to be clear that bio-inspiration is not always useful and does not automatically lead to good engineering solutions. Nature can be messy and nobody needs to understand how a given “solution” works in order to maintain it. Furthermore, in many bio-inspired contributions there is no clear separation between modeling and application oriented work, goals and aims are not clearly formulated, which often leads to a choice of inappropriate systems and methodology. Sometimes there is careless use and transfer of concepts and terms which dilutes the clarity of the work instead of being beneficial. All this has negative consequences on the quality and usefulness of the contributions. Furthermore, in the engineering field, bio-inspiration can not be an excuse to propose solutions which do not serve the purpose. Consequently, a part of this thesis is devoted in resolving some of these issues in the subject of oscillators applied to robotics.

A key property of natural system is their plasticity and adaptivity. In contrast, technical solutions can get very inflexible, especially when they grow to a certain complexity. It is very difficult to change even small aspects after the deployment of a technical solution. Even worse, such changes can lead to very far-reaching, sometimes catastrophic, changes in the overall systems behavior and performance. Not so in natural systems, where often even very dramatic changes in the environment, the operating conditions and the system itself do not impair the functioning, or at least not completely, i.e. often there is graceful degradation.

And, almost most importantly, there is a fundamental difference on how engineers tackle problems and how nature resolves “problems”. Engineers tend to separate a problem in to smaller problems until they are of manageable and understandable size and structure. From the solutions to those smaller problems, the overall solutions is then assembled. When assembling the partial solutions one needs to take care that the single units still operate as expected. This is an extremely powerful approach, but it bears certain problems and shortcomings. The problems are mainly in terms of scalability and efficiency. Each single property of the system needs to be carefully planned for, implemented and tested. While due to the divide-and-conquer approach it has been tried to make as many sub-systems as independent from each other as possible, there are certain aspects which can not be separated and furthermore, there will always been mutual influences that have not been taken in account. Thus ideally the system would need to be planned, analyzed and tested for all “combinations” of the systems state in order to be sure of its proper function. For large systems evidently this becomes impossible due to a combinatorial explosion. It would thus be desirable to design systems which can sort out certain aspects by themselves without – or with less – need of human specification.

So, Nature works differently, and key to understand this difference is the point of view lies in the theories of self-organization, i.e. how spatio-temporal structure comes about without explicit design and despite a noisy and imperfect world. Nature works more the other way round than the established engineering processes, there are structures which emerge due to self-organizing processes. If they are useful and stable for long enough, i.e. they survive, they are usually exploited in one way or the other, to “solve” a problem. This leads to very robust solutions since the underlying processes are already very robust, they are “attractors” of the system, after a perturbation the system returns back. If the perturbation is too large, the system wanders off and settles into a new stable mode which satisfies the new conditions.

Unfortunately, while we have a large body of knowledge of self-organizing systems, we are largely missing a methodology to deal with self-organized systems in a methodological way and harness them for engineering purposes.

Locomotion is a very good example for all the aspects introduced above. It is a very clearly defined problem with abundant natural examples. It bears clear signs of the importance of self-organization and there is a large body of knowledge which can be scrutinized. Hence, in this thesis we investigate a small aspect of adaptivity in robotic locomotion under the light of self-organization.

It has long been proposed to use oscillators and networks of oscillators to generate movement for robotic locomotion. Oscillators have a long tradition in physical and biological modeling. But there are certain shortcomings when transferring to applications, often models are not used in an appropriate fashion. For example a neural inspired oscillator is used in places where first of all there is no real justification to use a neural oscillator as the level that it concerns is not the neural one and secondly, the model is too complicated for the task to be achieved. I hope to have contributed with my work to clarifying some of these issues. In this work, I am mainly interested in the engineering aspect, as opposed to a modeling aim. This means we have more freedom in proposing radical changes to the systems in order to make them work in a certain way. We exploit this insight by showing that network of oscillators serving as a trajectory generator becomes more useful when it is built with harmonic oscillators instead of “neural” inspired ones. Employing such harmonic oscillators means focusing on the key properties which are important for the application. And, we design an adaptation scheme that comes out of set of “specifications” which is derived from some general observations/principles instead of a direct biological mechanism. But, even if the presented work is somewhat orthogonal to the efforts in the modeling community it is my conviction that some of the results are important for the biological modeling community as will be discussed later.

1.2 Outline of the thesis

The thesis is structured into seven chapters and contains mostly already published papers and two unpublished ones. The papers are organized in a thread leading from basic considerations about the systems to be used over the formulation of an abstract, proof of principle example, to the proof that the proposed system is also working in real world.

After a discussion of the background and related work in the next chapter, in Chapter 3 we will lay out our approach to engineering with the help of nonlinear dynamical systems, especially oscillators, and how important it is to get a clear picture about the goal that should be achieved by using such systems, as this largely influences many choices that need to be made. It will be shown how appropriate choices of systems and design parameters enable successful application.

Then, with Chapter 4 we arrive at a central part of the thesis namely the application of the aforementioned ideas to research in adaptive locomotion. We will introduce a very much simplified and abstract adaptive locomotion system. In this chapter we introduce and motivate the formulation of the adaptive frequency oscillator (AFO).

In Chapter 5, the AFOs will be treated in more detail. Their convergence is proven, in numerical examples the broad applicability of the simple adaptation rule is shown and finally, as a small side-track, another application of the AFOs, namely in a feedback connected pool of many such AFOs for signal processing is presented.

After the small digression into signal processing, in Chapter 6 we come back to the use of AFOs for adaptive locomotion on compliant systems. We show on gradually more complex and realistic systems that the basic idea works without fundamental modification. Concretely we present results on a simulated spring mass hopper and a real robot.

Finally, in Chapter 7 we conclude the thesis with a few general conclusions and an outlook.

1.3 Contributions

In this thesis we present original contributions which can loosely be grouped into the following four topics: (1) The development of a novel type of oscillator, the adaptive frequency oscillator (AFO) which can tune its intrinsic frequency on the frequencies of arbitrary external signals. (2) The application of the AFOs for adaptive controller for compliant robots and systems with resonant frequencies in general. (3) The application of AFOs for signal processing. (4) An engineering view on oscillators, on the application of dynamical systems approaches and on self-organization. These contributions will be detailed further at the end of the thesis.

Chapter 2

Background & Related Work

THE background for the presented work is a confluence of inspiration from many different areas of science and engineering. In the following I will point out the most important and influential contributions and some concepts which are important to give the scientific frame of the work that will be presented in the remainder of the thesis. In particular I will review relevant work in locomotion research and neurobiology, robotics, statistical physics and systems theory.

Central Pattern Generators When investigating on the origin for the locomotion patterns seen in vertebrates, researchers started to realize the importance of the spinal cord for the pattern generation. Early evidence for so called half-centers are documented at the beginning of the 20th century [17, 18]. A very influential experiment is documented in [205]. In the experiment a spinalized cat (i.e. a cat in which the connection between the spinal cord and the rest of the brain has been cut) is put on a treadmill. If the treadmill is set in motion, not only can locomotion pattern be observed that are very close to the normal patterns, but, moreover the cat *changes gaits* when the speed of the treadmill is continually increased. Similar gait transitions can be induced by the electrical stimulation of the brain stem. It seems that the spinal cord is enough to autonomously coordinate large parts of the movement necessary for locomotion. In other experiments, where isolated spinal cords of the lamprey [46] or the salamander [40] are stimulated, fictive swimming is observed. Such observations have led to the formulation of the concept of a Central Pattern Generator (CPG). A CPG is a neural center which generates coordinated high-dimensional output for the different muscle groups, controlled by simple (often tonic, i.e. non-phasic) input signals. A review of CPGs and the development of the concept can be found in [56] and another overview in [82]. Two of the model organisms to study CPGs were the lamprey [46, 83, 84] and the salamander [40]. They have been used because being lower vertebrates and thus a locomotion system of moderate complexity makes them particularly suited for this kind of research.

CPGs can show very different modes, such as the different gaits of mammals or as in the salamander. The Salamander is an amphibian animal, whose body is propelled through the water by traveling wave running over the body. When going to land, the traveling waves are superseded by standing waves, which have the knots between each pair of legs. The salamander CPG is meanwhile very well investigated, there are extensive biological studies [40], there is a lot theoretical work about CPGs [35–37, 47, 77, 78, 195] and experimental studies of model CPGs [104, 108, 109] and implementation of such models on robots [42, 52, 141, 224]. Meanwhile we have many other documented CPGs, not only for locomotion, but also for breathing, digestion, flying etc (cf. [9] for a review). The CPGs can be identified in some animals, e.g. the lobster, neuron by neuron [203]. In vertebrate locomotion things are much more complicated, there are more neurons involved, usually the centers can not be isolated as such and are intertwined with other functions [115]. Nevertheless, there is good evidence that the CPG also plays an important role in those animals and in humans. These concepts are the support for walking rehabilitation treatments for patients with partially lesioned spinal cord [113]. CPGs are an important concept for the research presented in this thesis. It turns out that CPGs are a useful concept for robotics, especially for the reduction of the dimensionality of the control problem, e.g. in the coordination of the degrees of freedom for legged locomotion (see [107]).

Control theory & Linear Systems Theory Modern control theory is a vast field. In its essence it deals with the problem of how to give inputs to a given system to make it go to, or stay in, certain states. In other words, control theory mostly investigates the problem of how to make the system to follow certain trajectories in the state space. But it does not address the question about where the trajectories to follow come from in the first place. The largest part of control theory deals with linear systems (c.f. [68, 206] for some introductory books). Usually nonlinear plants are linearized, for some special cases of nonlinear systems there are direct methods [124, 207].

Thus classical control theory covers a somewhat different domain than what we would like to achieve with CPGs for robots. And typically the application of a CPG in a robot is on top of a rather classical level of low level control that ensures that the trajectories are followed (as in [107]). However, if this is really the best way of applying CPGs is debatable, and we show in our applications that it can often be beneficial to not fully control every aspect of the robot (cf. Chapter 6).

Yet, control theory clearly is powerful and has its place in many industrial applications. As we put it, what we present should be by no means a replacement of classical methods. It should be more looked at as an extension. Consequently we will use tools of control theory in the treatment of the systems.

An important aspect in our work is also the notion of resonant frequencies. Which are readily defined in linear systems theory and a very central aspect of control engineering. Yet, the identification of the resonant frequency of a given

real world system is not exactly straight forward. The usual way is to excite the system in an appropriate way (i.e. by frequency sweeps or step inputs), measure the system response. From the system response the resonant frequency has to be extracted by help of the Fourier transform (or variants of it) and some additional algorithms (i.e. to find peaks in the spectrum). As we will see, by shifting away the focus from linear to nonlinear systems we find a much simpler way of achieving the same goal.

Nonlinear Dynamics, Dynamical Systems In the present work we make extensive use of oscillators. Oscillators have been investigated a lot over the last 30 years and they are often used in biological modeling but also in physics. Some important work can be found in [45, 61, 63, 130, 132, 134, 135, 214, 215, 234]. Oscillators are inherently nonlinear systems, but they still belong to a class of nonlinear systems which show a rather simple attractor behavior, namely a closed curve. They possess a very interesting feature, namely the tendency to synchronize on rhythmic inputs. The inputs do not even need be large, very small inputs suffice. This has to do with the special stability properties of the limit cycle attractor. This issue will be discussed in more depth in Chapter 3. An excellent introduction to oscillators and synchronization phenomena can be found in [166]. The synchronization property makes oscillators a nice building block to build pattern generators, where we need high dimensional coordinated output. Early work of CPGs modeled by oscillators [41, 43, 44, 47, 129, 131, 195, 218–220]. The dynamical systems formalism allows to investigate many interesting aspects of the system, e.g. bifurcation studies [85, 171].

Self-organization & Pattern formation Investigation on self-organization has now a quite long tradition in statistical physics. By studying open systems, far from equilibrium it has been realized that in such systems pattern formation is the rule and not the exception [87, 88, 90]. Later on it has been realized that similar ways of looking at the systems is also successful in the biological context, and especially in movement research [121, 196]. In locomotion and movement coordination research the HKB model [91] is quite well known. For an overview of work related to movement science see [79, 119, 192], some applications [117, 118, 190] and samples of recent research in [114].

CPGs are clearly open system, composed of many nonlinearly interacting elements, they show high-dimensional coordinated output modulated by simple control parameters, thus they possess all elements for a self-organized system which will show pattern formation. Thus it not surprising from the more theoretical point of view the CPG can be treated with theories of self-organization and pattern formation [195]. In such studies CPGs are very often modeled by coupled oscillators as will be discussed below.

Besides the application to movement coordination the ideas of self-organization and their related dynamical systems framework have also been investigated for

robot navigation [12, 60, 193, 194] and robot arm coordination [188, 201].

Unfortunately for the interested engineer, the studies of self-organization do not show how to use the knowledge for synthetic approaches. But, they highlight the importance of non-linear features and the interesting phenomena that such systems can exhibit. Realizing this, an investigation of such systems under the light of engineering application is more than justified and logical. Engineers usually have to take care to rule out “excessive pattern formation” capabilities in their systems. Self-organization for engineering is yet a mostly a unstructured effort, distributed over many disciplines (cf. [33]). Early inspiration to the formulation of our adaptation framework are in [191, 197–200].

Spring-mass models in locomotion Blickhan and Full [13, 14, 70] were among the first to put forward the use of spring mass models for modeling animal locomotion in a systematic fashion. Other early work can be found in [7, 150].

More recently a large body of knowledge about the common features of the mammalian locomotion mechanisms has been accumulated by Fischer and co-workers. Based on studies in which they filmed animals with sizes spanning several orders of magnitude with fast X-ray cameras they could propose unifying principles for mammalian legged locomotion. Based on the insight gained in these studies they introduced the concept of “anti-gravity” muscles or muscle groups. And, they concluded that the pivot around the hip joint is the important movement that contributes to forward locomotion (c.f. [66] and references therein).

On the more abstract side in [204] Seyfarth investigated a very simple spring mass hopper, very similar to the concept we will use in Chapter 6. He could prove the passive stability of the spring mass hopper. Geyer et al could show that simple spring mass systems have different stable modes and that this simple spring mass model can unify modeling of running and walking [74].

There is a large body of work showing that animals and humans, under some circumstances, work near the optimum in terms of cost of transportation [10, 11, 80, 86, 95, 99]. It is however not clear yet how animals know about this optimum. Especially it looks like the adaptation to this optimum works too fast, compared to the known processes that would possibly allow to sense the optimum. Could it be that a purely mechanical fact coupled with a simple mechanism as presented with the adaptive frequency oscillators is the key to this question? Even more, could it be that the efficiency is only a secondary product of the adaptation to resonant frequencies, that then has been favored by evolution? These questions will be addressed in Chapter 6.

Robotics Traditionally robots are built as strongly and fully actuated rigid machines. This has also to do with the fact, that in this way they are fully controllable and its easy to know their state. Unfortunately for tasks requiring high agility such as autonomous robotic locomotion those robots become either slow or very energy consuming, or the actuators become prohibitively large etc.

Compliance is usually not a wanted feature since it makes the control problem harder and it is more difficult to know the state. All this makes perfectly sense for industrial robotics (which is hitherto the main market for robotics) where usually the robots have to repeat certain tasks with very high precision and as fast as possible and flexibility is not a major concern. Furthermore, these robots are deployed in a very controlled environment and task. Thus, it is feasible to develop accurate models of the working space and the robot.

But on the experimental side, In 80s and 90s Raibert experimented with hopping robots [172, 173] with hydraulic actuators, which already possess a certain compliance which is helpful for the legged locomotion that is performed. This research was followed by the work of Pratt [169, 170] who designed a planar bipedal robot exploiting natural dynamics. Research on robots which make use of passive compliant elements to improve the performance for certain tasks is a more novel strain of research. While meanwhile a range of autonomous robotic systems can be bought off the shelf they do not support the features which are needed for the kind of research that we present. In the area of locomotion research there are mainly two fully working robots which are of interest: Tekken by Kimura and Fukuoka [126] and Puppy by Iida [100]. A second version of Puppy is the experimental platform used in some of our own research (cf. Chapter 6). A very impressive robot, of which unfortunately not many details are known is BigDog by Boston Dynamics [167]. The robot employs compliant elements, not much is known about the internals of the control system to us.

In the Leg lab at the University of Jena, there are furthermore robotic legs with compliant elements under investigation [187] as well as a biped with compliant legs [102] and a spring-mass hopper.

Notably in addition to the aforementioned research robots there is a toy which exploits the resonant dynamics of its body to locomote in an efficient manner. This small humanoid robot called Robo-sapien (by Wow Wee) has springs in its torso and rocks its body from one side to the other in order to unload the legs for the forward swing. This rocking movement is excited by the simple controller exactly in the resonant frequency of the body. This toy-robot is an off-spring of Hasslacher and Tildens research into exploiting the self-organizing capabilities of controller-robot systems [92, 93, 174, 210, 222] - as exciting this work is, many questions remain that hinder the easy transfer of this knowledge into research robots.

There are some existing applications of CPGs to robots, e.g. to a quadruped with compliant elements [126], other quadrupedal robots [42, 224], for amphibious snake and salamander robots [51, 52, 106, 107] and to bipedal robots [141]. In the thesis we will present controllers which are loosely inspired by the CPG concept.

Learning systems and search algorithms There is a large number of methods, systems and algorithms for adaptive and learning systems nowadays. Research in machine learning was a very prolific area in the last 20 years. One of

the contributions setting off this research area was certainly Rosenblatt's perceptron [183] and later-on the formulation of the back-propagation algorithm which made a training of the multi-layer perceptron possible [186, 230]. Later many variants of so called artificial neural networks (ANN) have been proposed [94], before it got clear that they are mostly variants of one and the same topic.

Another important strand of algorithms has more been inspired by evolution and is hence called genetic (GA) or evolutionary algorithms (EA), they are stochastic search algorithms. Furthermore, there are some physics inspired search algorithms such as simulated annealing (SA) [128]. Then, another important flavor of algorithms are those which should uncover hidden structure in the data, e.g. clustering algorithms and statistical learning such as training of Hidden-Markov-Models.

Common to those algorithms is that they are basically all search algorithms in different flavors, i.e. gradient descent (ANN), stochastic gradient descent [209] or a type of random search (SA, GA, EA). Consequently there are general methods that encompass many of these methods, e.g. kernel methods [226]

The advantage of such methods and algorithms is their universal use for any type of problem which can be parameterized, one of the central points is the fact that all of the methods have an explicit cost function, i.e. an estimation of quality or similar (sometimes the cost function is somewhat implicit, such as the energy terms in the clustering algorithms). It turns out that the formulation of the cost function is more critical than the search algorithm. A problematic point is the disproportion of the overhead of such algorithms to their performance (training duration, system sizes, e.g. the layers of a NN). Usually there is no rule to dimension the system, what means it has to be dimensioned conservatively what leads to suboptimal solutions in terms of overhead. Furthermore, they have the conceptual property that learning algorithm and learning substrate are separated entities. Depending on the view point this can be considered an advantage or disadvantage. But, even more the two parts of the system are very often formulated in different formalisms (e.g. in a NN, the learning substrate is a general function, the learning is formulated as an algorithm). This is in stark contrast to the facts we are presented with in Nature (e.g. the brain is learning substrate and the implementation of the "learning mechanism" in one system), tells us that we should at least make an attempt to unify the two parts of the system and see to what insight this leads. Furthermore, the pattern-formation theories suggest that the dynamic nature of such processes is important. A fully dynamic description of the algorithms does not come naturally to the discussed methods. It might be useful and interesting to explore alternatives, i.e. methods that do not have an explicit cost function, no separation between learning substrate and algorithm and that are formulated in a dynamic way. The language of dynamical system might be helpful for sorting out fundamental facts of learning and adaptation, much as it helped to sort out fundamental facts for pattern formation. While we have a mathematical language for pattern formation we are only in the beginning for such a language for adaptation. But, this is the key to exploit it for engineering

purposes as the history of control theory for example has shown [140]. In the dynamical systems approach of course there is still an objective function in the wider sense, but it is implicit, it is encoded into the attractor dynamics of the system, this can have some advantages (e.g. [60]) but bears the problem that we have to find a way to develop this dynamics as outlined in the next section.

2.1 A note about modeling adaptive systems in the framework of self-organization

Pattern formation is an inherently nonlinear process, linear systems can not produce stable patterns. Furthermore, systems that show pattern formation are open systems and very often very high-dimensional. Yet, the observed, emergent patterns can very often be described by a small number of variables. The key mechanism for this reduction of the degrees of freedom is captured by the center manifold theorem, also known as slaving principle or adiabatic elimination [87,89]. It is this principle what justifies the usually proposed low dimensional models for CPGs, such as oscillator networks, producing coordinated spatio-temporal patterns.

The variables use to describe the low dimensional structures emerging are called *order parameters*, their behavior is controlled by a set of parameters, the *control parameters*. Thus, the simple models that we usually employ of large scale systems reflects the behavior of the order parameters.

If now we want to build on top of this pattern formation formalism to investigate on adaptive systems, we need to enhance this framework. If such a system now slowly adapts, another – even slower – mode becomes important in the system. Therefore, we propose to enhance a given pattern-forming system with an additional feedback loop, which accounts for the adaptation mechanism. The time constants of this loop will be in general larger then the time constants of the rest of the system.

While the control parameters are usually constant, they become now a function of the systems behavior. This means we have to find the law that determines their evolution over time. In the dynamical systems framework this law should have the form of a differential equation. The AFO based controller that we are going to present is in this way an example of such an adaptive system. It adapts to properties of the pattern which is formed by the interaction of the controller with the body on a faster timescale.

This multi-scale property also amounts into a practical challenge for the simulation, i.e. numerical integration of such systems. Since we have slow effects on one hand and fast effects on the other hands, which can not be separated, i.e. it is exactly their interaction which we are after, we need to integrate the system at high precision for a long time, which means computational demanding runs. To support the integration of such systems, especially also in high-dimensions, with the help of Ludovic Righetti I programmed an integration framework in C++. The framework allows for a very efficient yet flexible numerical integration of dynam-

ical systems. The data analysis is done in Matlab for its ease of use, availability of numerical algorithms and graphical features.

To summarize, the basic properties which such adaptive systems will have are: (1) system modeling the order parameter is usually non-linear (2) the system has a multi-scale property which can not be separated, otherwise the sought phenomena of adaptation are lost, and (3) the feedback loop is in general non-linear.

One can now ask about the relationship of such multi-scale systems with adaptive control and adaptive filters, which are a widely used technique in signal processing and control engineering. While the idea of slowly varying parameters is also at the center of adaptive control and adaptive filters, they are inherently building the linear systems theory. We have pointed out why the systems that we are interested in usually will be inherently nonlinear (otherwise they will not show pattern formation capabilities). Yet, in the theory of adaptive control and filters very powerful results and methods have been developed which should be used as long as appropriate.

Chapter 3

Engineering: Simpler Systems – Analyzable Solutions

IN this chapter we show first in an example and then in a more systematic way how important it is to assess well the model systems which are employed in terms of their suitability for the chosen goal.

In the first example we show that we can improve existing networks of oscillators serving as a model CPG by using a simpler oscillator, namely a harmonic oscillator. We can calculate and design in a straight forward manner key properties of the network. The results of this paper will be reused in Chapter 6 to construct the adaptive controllers for an actual robot.

In the second section we extend the discussion, to a general discussion about the use of oscillators for engineering applications, and how this viewpoint on oscillators allows to sort out the common basic principles behind such systems.

3.1 Improving a CPG

Distributed Central Pattern Generator Model for Robotics Application Based on Phase Sensitivity Analysis

Jonas Buchli and Auke Jan Ijspeert

This paper has been originally published as J. Buchli and A.J. Ijspeert. Distributed central pattern generator model for robotics application based on phase sensitivity analysis. In A.J. Ijspeert, M. Murata, and N. Wakamiya, editors, *Biologically Inspired Approaches to Advanced Information Technology: First International Workshop, BioADIT 2004*, volume 3141 of *Lecture Notes in Computer Science*, pages 333–349. Springer Verlag Berlin Heidelberg, 2004

Abstract A method is presented to predict phase relationships between coupled phase oscillators. As an illustration of how the method can be applied, a distributed Central Pattern Generator (CPG) model based on amplitude controlled phase oscillators is presented. Representative results of numerical integration of the CPG model are presented to illustrate its excellent properties in terms of transition speeds, robustness and independence on initial conditions. A particularly interesting feature of the CPG is the possibility to switch between different stable gaits by varying a single parameter. These characteristics make the CPG model an interesting solution for the decentralized control of multi-legged robots. The approach is discussed in the more general framework of coupled nonlinear systems, and design tools for nonlinear distributed control schemes applicable to Information Technology and Robotics.

3.1.1 Introduction

Information Technology has seen an unprecedented growth in possibilities and capacity in the second half of the 20th century. Powerful theories have emerged along with engineering principles that turn these theories into successful real world applications. Almost all of this progress has been made by adopting a linear and sequential approach to analyze and design systems. Under this view, each of the subsystems must be carefully engineered, in order to make them as reliable as possible. When connecting them, one is striving for a linear interaction as this allows one to guarantee that the prediction made for interacting subsystems remains valid. The order of operation, tasks and information flow is usually sequential as this simplifies the understanding of the mode of operation of the system and the identification of possible problems.

This is in contrast to how natural systems work. In nature, the subsystems are usually unreliable, non-uniform, noisy but in huge numbers. The subsystems and

their interaction are of active, nonlinear nature, leading to emergent phenomena on the system level. Therefore, these systems often work naturally in a parallel fashion. This tends to give interesting properties to natural systems such as robustness, fast computation, high energy efficiency and versatility despite slow, noisy and unreliable components. In order to be able to construct systems with similar properties, it is crucial to have adequate theoretical tools for modeling and designing these complex systems.

In this article, we would like to contribute to this effort in the field of oscillatory systems. We develop a method for predicting phase relationships in systems of coupled oscillators, and use it to design systems that can switch between well-defined phase-locked states. In particular, we apply our approach to a concrete example: the distributed control of locomotion in robots with multiple degrees of freedom.

3.1.2 Designing Biologically Inspired Distributed Controllers for Walking Robots

Controlling walking in robots has proved to be a difficult engineering challenge. It requires coordinating multiple degrees of freedom using signals of the right frequencies, phases, and amplitude. As nature presents very robust and elegant solutions to that problem, some engineers have turned to biology as a source of inspiration. At first sight, the animal locomotory system seems to be of enormous complexity. But, despite the large number of elements taking part in locomotion control, a few simple common features have been observed by biologists among a large variety of different species. One of these is the notion of the Central Pattern Generator (CPG) [81, 82]. A CPG is a network of neurons, capable of producing oscillatory signals without oscillatory inputs. For locomotion, CPGs are located in the spine, and receive relatively simple signals from higher centers of the brain for the control of speed and direction. Sensory feedback is usually not needed to produce the basic patterns, although it plays an important role in adapting the patterns to the given situation the animal is faced with.

Another important concept is to classify different walking patterns by the phase relationships between the individual limbs. This method allows to uncover striking similarities between the gait patterns observed in very different animals. In quadruped locomotion there are three gait patterns that are very often observed: walk, trot and bound.

Models of different complexity and based on different assumptions have been devised that can produce the abstract gait patterns [47, 69, 218, 223, 235]. One important approach is – motivated by the oscillatory limb movements – to use the most simple mathematical model that produces stable oscillatory behavior as gait pattern generator for one limb. This mathematical model is a nonlinear oscillator of some form. These oscillators are then connected together in order to achieve inter-limb coordination (see [47, 69, 223]).

Except [223, 235] most previous models use nonlinear oscillators that are mo-

tivated by neuronal circuits and that have therefore limit cycles with irregular shapes. In this contribution, the point is made to use the simplest oscillators possible as canonical subsystems, in order to have systems that are well understood and are simpler to treat analytically. The canonical subsystem is taken out of the class of nonlinear oscillators. In this article, the canonical subsystem which serves as model for the pattern generator of a single limb will be a simple amplitude controlled phase oscillator (ACPO). By this choice of the canonical subsystem one does avoid the problems involved with the aforementioned neuronal oscillators. The analytical treatment leads to a understanding of the system behavior that allows to apply synthetic approaches to construct a network with these canonical subsystems with desired global behavior. Furthermore, the network is constructed to have one single parameter by which the exhibited gait pattern can be controlled. This is a simplification comparing to previous approaches which usually need several parameters to be changed at the same time.

The desired properties that our CPG model should exhibit are the following. First, the CPG model should be independent of initial conditions and robust against perturbations. Second, the expressed gaits should ideally be controlled by one simple control variable. This simplifies control, and also replicates the biological observation that the modulation of a simple electrical stimulation signal is sufficient to change gait in cats [205]. Finally, when changing the control variable, the CPG should exhibit fast transitions, ideally within one cycle. The transitions are a critical moment since the animal can loose its stability if the transitions are not appropriate. Furthermore, fast transitions are also observed in nature. To the best of our knowledge, hitherto there exists no simple model that fulfills all the criteria just stated.

3.1.3 Outline

A short outline of our approach will be given as follows. First, the canonical subsystem will be presented. The notion of the phase will be introduced, since the phase is crucial to understand synchronization behavior. Then, it will be shown, that by examining the form of the limit cycle the sensitivity of the phase on perturbations can be derived. With this result, it will be shown how the phase relationship between two unidirectionally coupled oscillators can be derived. Out of the insights gained by that treatment, a method is presented to chose an arbitrary phase relationship between the two oscillators.

Next, a quadruped walking controller composed of four coupled oscillators will be constructed. The additional couplings give raise to additional constraints on the phase relationships. It will be shown by numerical experiments that only phase relationships that fulfill these constraints are stable. In a next step, it will be shown how we can exploit these additional constraints to have an continuous valued parameter that allows us to chose the gait pattern expressed. In the discussion we show how the results presented in this article fit in the larger picture and show that our assumptions and simplifications are based on firm theoretical grounds.

3.1.4 A Distributed Quadruped Central Pattern Generator

Predicting the Phase Between Two Oscillators

Our goal in this section is to predict how an oscillator reacts to perturbations by looking at its limit cycle from a geometrical point of view, and to use this prediction for determining the phase relationship between coupled oscillators.

To start with the concepts needed to discuss nonlinear oscillators, the notion of a perturbed nonlinear dynamical system is introduced:

$$\dot{\mathbf{q}} = F(\mathbf{q}) + \mathbf{p} \quad (3.1)$$

where \mathbf{q} is the vector of state variables and \mathbf{p} a perturbation vector. In the case the unperturbed system ($\mathbf{p} = 0$) converges to a periodic solution, it is called an oscillator and the set of \mathbf{q} on which it continues to evolve is called the limit cycle of the system. As described in [166], every oscillator can be transformed into a phase (θ) – radius (\mathbf{r}) coordinate system:

$$\dot{\theta} = \omega_0 + p_\theta \quad (3.2)$$

$$\dot{\mathbf{r}} = F_r(\mathbf{r}, \theta) + \mathbf{p}_r \quad (3.3)$$

where ω_0 is the natural frequency of the (unperturbed) oscillator, F_r is the dynamical system describing the evolution of \mathbf{r} , p_θ is the component of the perturbation acting on the phase and \mathbf{p}_r is the component of the perturbation acting in direction of the radius. Perturbations on a stable limit cycle have different effects on the phase depending on the p_θ and \mathbf{p}_r components. The p_θ component will modify the phase, since the phase is marginally stable [166]. On the other hand, the \mathbf{p}_r component, i.e. in the direction of the radius, will be damped out and will have little effect on the phase.

When two oscillators (F_1, F_2 with corresponding state vectors $\mathbf{q}_1, \mathbf{q}_2$) are coupled together ($p_{\theta,2} = f(\mathbf{q}_1)$), several types of dynamics can result including chaos (i.e. no periodic behavior) and phase-coupling. In this article, we are interested in 1:1 phase-locked regimes, i.e. when the oscillators synchronize such that [166]

$$\theta_d \equiv \theta_2 - \theta_1 \approx \text{const} \quad (3.4)$$

Assuming that the system has phase-coupled¹, we are now interested in how to predict θ_d given two oscillators and their coupling. The general outline of our method is as follows:

1. From the limit cycle of the perturbed oscillator a sensitivity function $S_p(\mathbf{p})$ is derived.

¹Determining which conditions are necessary for phase-coupling is out of the scope of the current article.

2. From the limit cycle of the perturbing system (the other oscillator), the coupling and the sensitivity function, the perturbation term p_θ is calculated. p_θ is usually a function of the phase difference *and* the phase of the perturbed system.
3. From the requirement of phase synchronization (3.4) a differential equation (DE) for the phase difference between the perturbed and the perturbing system (θ_d) can be derived. This DE is usually a function of the phase difference *and* the phase of the perturbed system.
4. By integrating p_θ over the evolution of the perturbed limit cycle the perturbation of the phase that stays in the system is computed. This allows to derive a DE that only depends on θ_d . By help of that DE, the fixed points for θ_d can be found.
5. By applying a stability analysis of the DE, the stable and unstable fixed points can be distinguished.

When looking at the phase space representation of a nonlinear dynamical system we can conclude that changes in the derivative of phase can only stem from components of the perturbation that are in direction of θ , i.e. tangential to the limit cycle. The unit vector tangential to the limit cycle is

$$\mathbf{e}_\theta = \frac{\dot{\mathbf{q}}}{|\dot{\mathbf{q}}|} \quad (3.5)$$

Therefore, the effective perturbation on the phase is

$$p_\theta = \mathbf{p} \cdot \mathbf{e}_\theta \quad (3.6)$$

The derivative of the phase becomes

$$\dot{\theta} = \omega_0 + \mathbf{p} \cdot \mathbf{e}_\theta \quad (3.7)$$

So we found the sensitivity of the phase on perturbations:

$$S_p(\mathbf{p}) \doteq \frac{p_\theta}{|\mathbf{p}|} = \frac{\mathbf{p}}{|\mathbf{p}|} \cdot \mathbf{e}_\theta = \frac{\mathbf{p}}{|\mathbf{p}|} \cdot \frac{\dot{\mathbf{q}}}{|\dot{\mathbf{q}}|} \quad (3.8)$$

With (3.7) we found an explicit form for the time evolution of θ . By using the definition in (3.4) we can derive a differential equation for θ_d . We require synchronization after some transient phase which is not discussed here:

$$\int_{t_1}^{t_2} \dot{\theta}_d dt = 0 \quad (3.9)$$

On the other hand

$$\dot{\theta}_d = \dot{\theta}_2 - \dot{\theta}_1 \quad (3.10)$$

$$\dot{\theta}_d = \omega_{0,2} + p_{\theta_2} - (\omega_{0,1} + p_{\theta_1}) \quad (3.11)$$

This is usually a function of θ_d and θ_2 . As we are mainly interested in the steady state of the system, we integrate it over time. The integration over time is done implicitly by integration over θ_2 (which increases monotonically with time), after the system reached the steady phase locked state. We assume the criterion for phase locking to be fulfilled at $\theta_2 = \Theta_0$, and that the system subsequently is in the steady phase locked state for $\theta_2 > \Theta_0$. From (3.9) we see that the integral should be zero

$$\dot{\theta}_{d,res} = \lim_{\Theta \rightarrow \infty} \int_{\Theta_0}^{\Theta} \dot{\theta}_d d\theta_2 = \sum_{n=1}^{\infty} \int_{2(n-1)\pi + \Theta_0}^{2n\pi + \Theta_0} \dot{\theta}_d d\theta_2 \equiv 0 \quad (3.12)$$

We now have outlined all the steps needed to arrive with a differential equation for θ_d . In the following, we will show the analysis of the phase oscillator that will be used to construct the CPG.

The Amplitude Controlled Phase Oscillator

As outlined before, the CPG model will be constructed of simple canonical subsystems. In this case the subsystems are an amplitude controlled phase oscillator (ACPO). The ACPO is defined by the following dynamical system:

$$[\dot{\theta}, \dot{r}]^T = [\omega, -g(r - r_0)]^T \quad (3.13)$$

The description of this system can be transformed into an equivalent description in the Cartesian coordinate system ($x = r \cos \theta, y = r \sin \theta$):

$$\dot{\mathbf{q}} = \begin{bmatrix} \dot{x} \\ \dot{y} \end{bmatrix} = \left[g \left(\frac{r_0}{\sqrt{x^2 + y^2}} - 1 \right) x - y\omega, g \left(\frac{r_0}{\sqrt{x^2 + y^2}} - 1 \right) y + x\omega \right]^T \quad (3.14)$$

A short hand notation of this system is introduced: $\dot{\mathbf{q}} = F_{\text{ACPO}}(\mathbf{q})$, where $\mathbf{q} = [x, y]^T$ is the state vector of the system. This system shows a limit cycle that has the form of a perfect circle with radius r_0 (Fig. 3.1(a)). The intrinsic frequency of the oscillator is ω .

Two Coupled ACPO

We introduce now a system of two ACPO where one ACPO is coupled unidirectionally to the other one.

$$\dot{\mathbf{q}}_1 = F_{\text{ACPO}}(\mathbf{q}_1) \quad (3.15)$$

$$\dot{\mathbf{q}}_2 = F_{\text{ACPO}}(\mathbf{q}_2) + \mathbf{p}_c(\mathbf{q}_1) \quad (3.16)$$

where $q_1 = [x_1, y_1]$, $q_2 = [x_2, y_2]$. Next will be shown, how we can derive the phase relationship θ_d from the knowledge of the shape of the limit cycle and \mathbf{p}_c . We

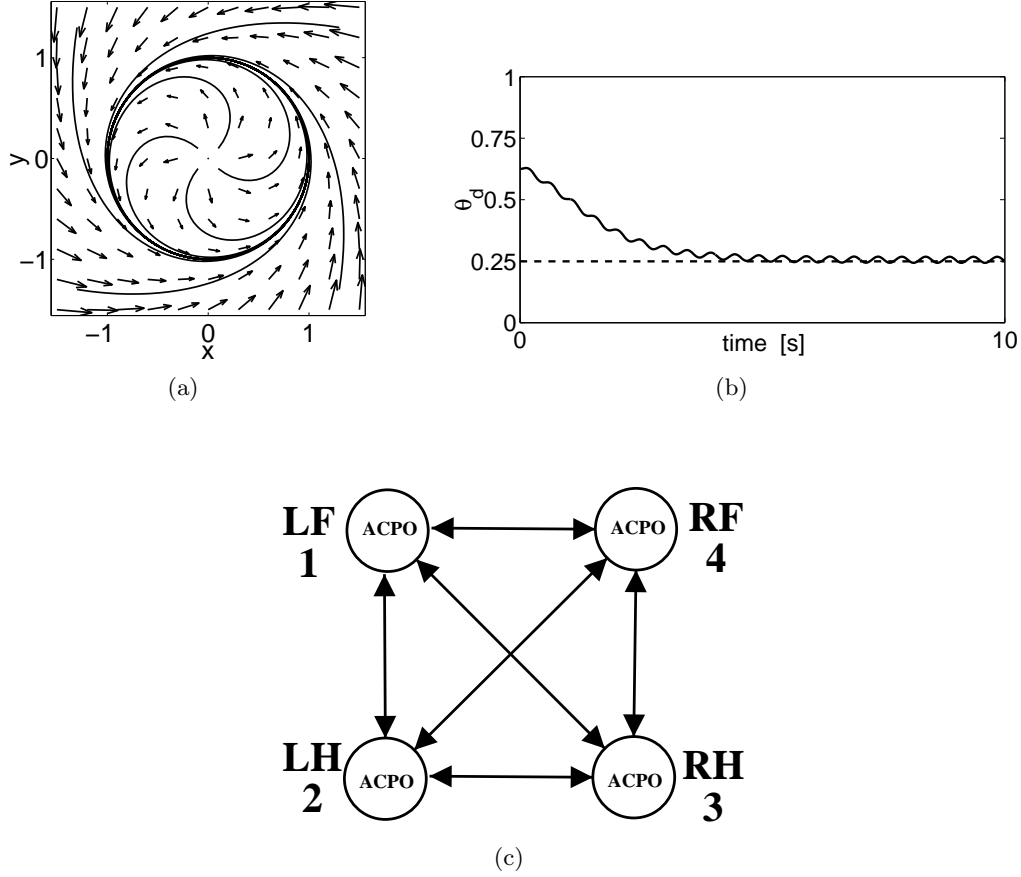


Figure 3.1: **a)** Limit cycle of the amplitude controlled phase oscillator for $r_0 = 1, g = 10, \omega = 2\pi[\text{rads}^{-1}]$. The arrows show the flow $\dot{\mathbf{q}}$ defined by the F_{ACPO} (3.13). **b)** This figure shows the phase difference established for the following values of $\omega_d = -0.0042$, $\lambda = 2$ and $g = 1000$. With help of (3.23) predicted value is $\theta_d = 0.2493$ (dashed line). The value from numerical integration is shown with the solid line (mean over $t = [10, 20]$ is $\theta_d = 0.2554$). **c)** The structure of the ACPO-CPG. Note that the connections illustrated by arrows involve rotation matrices (compare to text).

will do this in an analytical way to illustrate how the method works. However, the method is not limited to cases where we know the form of the limit cycle by analytical derivation, but also works for cases where we get the form of the limit cycle and f_c by numerical integration. To illustrate how the method works, consider the simple connection scheme:

$$\mathbf{p}_c = \lambda[0, x_1]^T \quad (3.17)$$

In words: State variable x from ACPO 1 is coupled on the derivative of state y of ACPO 2 with a coupling constant λ .

1. We derive

$$\mathbf{e}_{\theta_2} = \frac{\dot{\mathbf{q}}_2}{|\dot{\mathbf{q}}_2|} = [-\sin(\theta_2), \cos(\theta_2)]^T \quad (3.18)$$

2.

$$\mathbf{p}_c = \lambda[0, x_1]^T = \lambda[0, r \cos(\theta_1)]^T \quad (3.19)$$

From (3.6) we get

$$p_{\theta_2} = \lambda r [0, \cos(\theta_1)]^T \cdot [-\sin(\theta_2), \cos(\theta_2)]^T = \lambda r \frac{1}{2} [\cos(\theta_d) + \cos(2\theta_2 - \theta_d)] \quad (3.20)$$

3. Using (3.10) and (3.20)

$$\dot{\theta}_d = \omega_{0,2} - \omega_{0,1} + \lambda r \frac{1}{2} [\cos(\theta_d) + \cos(2\theta_2 - \theta_d)] \quad (3.21)$$

4. From (3.12) and (3.21) we get

$$\begin{aligned} \dot{\theta}_{d,res} &= \int_0^{2\pi} \dot{\theta}_d d\theta_2 \\ &= \int_0^{2\pi} \left[\underbrace{\omega_{0,2} - \omega_{0,1}}_{\omega_d} + \lambda r \frac{1}{2} \left[\underbrace{\cos(\theta_d)}_{const} + \underbrace{\cos(2\theta_2 - \theta_d)}_{\text{periodic, zero mean}} \right] \right] d\theta_2 \\ &= 2\pi\omega_d + \lambda r \pi \cos(\theta_d) \equiv 0 \end{aligned} \quad (3.22)$$

From this equation we can calculate the (averaged) fixed points for θ_d

$$\theta_d \Big|_{\dot{\theta}_{d,res} \equiv 0} = \arccos \left(-\frac{2\omega_d}{\lambda r} \right) \quad (3.23)$$

We note that we need $|\frac{2\omega_d}{\lambda r}| < 1$ for this particular system to phase-lock (i.e. for (3.23) to have equilibrium points). Since we assume steady phase locked state, $r \approx r_0$ can be assumed. We are interested in the stable fixed points, since they determine to which phase relationship the system will evolve. For example, for $\omega_d = 0$, we find solutions at $\frac{\pi}{2} + n\pi, n \in \mathbb{Z}_0$.

5. The stability of the fixed points is determined by the one-dimensional Jacobian for θ which can be obtained by differentiating (3.22)

$$\frac{\partial \dot{\theta}_d}{\partial \theta_d} = -\lambda r \pi \sin(\theta_d) \quad (3.24)$$

From this equation we can calculate that $\frac{\partial \dot{\theta}_d}{\partial \theta_d} = -\lambda r < 0$ for $\theta_d = \frac{\pi}{2} + 2n\pi$ and $\frac{\partial \dot{\theta}_d}{\partial \theta_d} = \lambda r > 0$ for $\frac{3\pi}{2} + 2n$ (for $\lambda > 0$, opposite if $\lambda < 0$). Therefore, for $\omega_d = 0$ only phase differences $\theta_d = \frac{\pi}{2} + 2n\pi$ are stable fixed points.

Using (3.23) we can therefore determine the phase difference to which the two oscillators evolve when coupled, under the assumption that they phase-lock. For $\omega_d \neq 0$ the fixed points for θ_d have slightly different values and are dependent on the choice of r_0 , as can be seen from (3.23). In Fig. 3.1(b) the results for numerical integration of the system treated above are presented for $\omega_d \neq 0$ and compared to the value predicted by the analytical treatment.

Method for Choosing Arbitrary θ_d

Based on the insight gained in the previous section a method will be presented to choose arbitrary θ_d . Therefore, a more general coupling scheme is introduced:

$$\mathbf{p}_2 = \lambda \mathbf{P} \mathbf{q}_1 \quad (3.25)$$

where \mathbf{P} is the coupling matrix. In the aforementioned example (3.17) it would be

$$\mathbf{P} = \begin{pmatrix} 0 & 0 \\ 1 & 0 \end{pmatrix} \quad (3.26)$$

We define a rotation matrix

$$\mathbf{R} = \begin{pmatrix} \cos \theta_R & -\sin \theta_R \\ \sin \theta_R & \cos \theta_R \end{pmatrix} \quad (3.27)$$

By taking $\mathbf{q}_{1,r} = \mathbf{R} \mathbf{q}_1$, we get a vector that is equivalent to the vector $\mathbf{q}_1(\theta'_1)$, $\theta'_1 = \theta_1 + \theta_r$. In other words, if we take $\mathbf{q}_{1,r}$ to perturb the second oscillator the effect is the same as if the first oscillator would be in state θ'_1 . Thus,

$$\mathbf{p}_2 = \lambda \mathbf{P} \mathbf{q}_{1,r} = \lambda \mathbf{P} \mathbf{R} \mathbf{q}_1 = \lambda r [0, \cos \theta_1 \cos \theta_R - \sin \theta_1 \sin \theta_R]^T \quad (3.28)$$

Using the same approach as in (3.20)-(3.23) we get

$$\dot{\theta}_{d,res} = 2\pi\omega_d + \lambda r \pi [\cos \theta_d \cos \theta_R - \sin \theta_d \sin \theta_R] \equiv 0 \quad (3.29)$$

By exploiting the trigonometric addition theorems this transforms into

$$\theta_d \Big|_{\dot{\theta}_{d,res}=0} = \arccos \left(-\frac{2\omega_d}{\lambda r} \right) - \theta_R \quad (3.30)$$

where again $r \approx r_0$ is the steady state behavior. As can be seen θ_d is directly proportional to the rotation angle θ_R . Using (3.30) we can design couplings between the oscillators such as to obtain arbitrary phase difference between them. Note that the coupling does not need to be unidirectional. It is straight forward to introduce bidirectional coupling by changing (3.15) to

$$\dot{\mathbf{q}}_1 = F_{\text{ACPO}}(\mathbf{q}_1) + \mathbf{p}_c(\mathbf{q}_2) \quad (3.31)$$

and working out the math as outlined above. Equivalently to (3.28), a second rotation matrix \mathbf{P}_2 is introduced. Therefore, a third additive term in (3.29) arises.

The ACPO CPG

The three most common gaits observed in quadrupeds are walk, trot and bound. To ease the notation, the legs of the quadruped are numbered in the following way: left front 1, left hind 2, right hind 3, right front 4 (cf. Fig. 3.1(c)). If we define $\theta_{d,ij} = \theta_i - \theta_j$ as the difference between the phase of limb i and j then, the gaits can be classified according to Table 3.1(a) (the phases are normalized: $\theta = 1$ corresponds to the full circle).

A quadruped CPG is constructed from four fully connected ACPO, i.e. all oscillators are coupled bidirectionally to every other one (see Fig. 3.1(c)). The coupling matrix is of the form

$$\mathbf{P} = \begin{pmatrix} 1 & 0 \\ 0 & 1 \end{pmatrix} \quad (3.32)$$

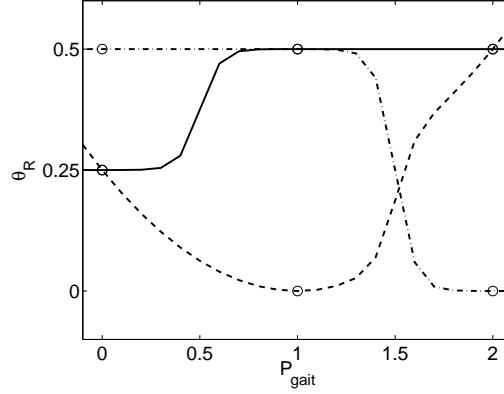
and $\lambda = 2$ for all connections. A ring structure basically is enough to build the CPG, cf. [47, 195]. However, the additional, redundant connections increase the speed of the gait transitions.

Let us outline how we can design specific gait patterns into this network. First of all, for this gait pattern the phase difference between the pairs of oscillators that are connected need to be known. We can derive these phase differences by help of Table 3.1(a). Then, for each connection a corresponding rotation matrix can be derived. If we take as an example the walk pattern we see that we come up with four different rotation matrices ($\theta_d = \pm 0.25 \pm 0.5$) for the 12 connections. In order to be able to change from one gait pattern to another we make the rotation matrices dependent on a parameter P_{gait} and we exploit the fact that $\mathbf{R}(\theta_d) = \mathbf{R}^{-1}(-\theta_d)$. By analysis of the requirements needed to generate walk, trot and bound we come up with three parameter sets of θ_R (cf. Table 3.1(b)). Instead of fixing the θ_d we can define continuous functions that provide these values when a parameter P_{gait} is increased. We chose the functions given in 3.33-3.35. This allows to chose the gait pattern by the single continuous valued parameter P_{gait} . The three corresponding rotation matrices are used in the connection scheme as presented in Table 3.1(c) (using the short notation $\mathbf{R}_i = \mathbf{R}(\theta_{R,i})$).

Table 3.1: (a) The table shows the phase differences corresponding to the three most common gaits observed in quadrupeds. (b) The table shows the 3 different rotation angles that are needed in the construction of the ACPO-CPG. (c) Connection scheme used for the ACPO-CPG.

(a)				(b)			
	$\theta_{d,12}$	$\theta_{d,13}$	$\theta_{d,14}$		$\theta_{R,1}$	$\theta_{R,2}$	$\theta_{R,3}$
walk	0.75	0.25	0.5	walk	0.25	0.25	0.5
trot	0.5	0.0	0.5	trot	0.5	0.0	0.5
bound	0.5	0.5	0.0	bound	0.5	0.5	0.0

		connection origin			
		LF/1	LH/2	RH/3	RF/4
connection target	LF/1	$\mathbf{0}$	\mathbf{R}_1^{-1}	\mathbf{R}_2	\mathbf{R}_3^{-1}
	LH/2	\mathbf{R}_1	$\mathbf{0}$	\mathbf{R}_3^{-1}	\mathbf{R}_2^{-1}
	RH/3	\mathbf{R}_2^{-1}	\mathbf{R}_3	$\mathbf{0}$	\mathbf{R}_1
	RF/4	\mathbf{R}_3	\mathbf{R}_2	\mathbf{R}_1^{-1}	$\mathbf{0}$



$$\theta_{R,1} = \frac{1}{4} \left(\frac{1}{1 + e^{-20(P_{\text{gait}} - \frac{1}{2})}} + 1 \right) \quad (3.33)$$

$$\theta_{R,2} = \frac{1}{4} \left((P_{\text{gait}} - 1)^2 + \frac{1}{1 + e^{-20(P_{\text{gait}} - \frac{3}{2})}} + 1 \right) \quad (3.34)$$

$$\theta_{R,3} = \frac{1}{2} \left(\frac{1}{1 + e^{-20(P_{\text{gait}} + \frac{3}{2})}} \right) \quad (3.35)$$

Figure 3.2: $\theta_{R,1,2,3}$ as a function of the chosen gait parameter. $P_{\text{gait}} = 0$ corresponds to the walk pattern, $P_{\text{gait}} = 1$ to trot, and $P_{\text{gait}} = 2$ to the bound. Solid line: $\theta_{R,1}$, dashed line: $\theta_{R,2}$, dash-dotted line: $\theta_{R,3}$. The dots correspond to values that correspond exactly to the values for the different gait patterns. However, also for settings quite far from these points the gait patterns are stable.

Simulation Results of the ACPO-CPG

In the following, the results of numerical integration of the ACPO-CPG are presented. The system was integrated with a variable step Runge-Kutta solver [146]. The tolerance settings were $T_{\text{rel}} = 10^{-3}$ and $T_{\text{abs}} = 10^{-6}$. The initial conditions were always chosen randomly in $\theta_{1,2,3,4} \in [-1, 1]$. Because the system is robust against random initial conditions, we do not present the transient behavior at the beginning of the integration procedure but rather focus on the more interesting phenomena during gait transitions. In Fig. 3.3, all possible transitions are shown. The time $t = 0$ always corresponds to the time when the gait control parameter P_{gait} is changed abruptly from one setting to another. Noteworthy here is that not all transitions are made with the same ease. Especially the transitions from walk to bound and back take up to about 1.5 s to begin. Also the transient time is higher for these transitions. Furthermore, we have an asymmetry in transitions. The transitions from walk to bound is faster than from bound to walk. Interestingly, Kelso et al. [118] have shown the same effects when human subjects are asked to consciously switch from one coordination task to another. The authors also establish the link to the physical theories of complex systems that will be addressed in the discussion.

Random fluctuations play a very important role in synergetic systems. It turns out that they are fundamental to any pattern formation process. Furthermore, we want our model to be robust against noise. Therefore, we use a noisy model to test the influences of noise. For that the differential equation of the system gets transformed into a stochastic difference equation

$$\Delta \mathbf{q} = (1 + \xi) F(\mathbf{q}) \Delta t \quad (3.36)$$

where ξ is a uniformly distributed random number in $[-0.1, 0.1]$. The stochastic difference equation was then integrated using the Euler method with a time-step of $\Delta t = 10^{-4}$ s. Representatively, for the illustration of the effect of the noise, the transition from bound to walk has been chosen, because from the above presented results it is known to be slowest. In Fig. 3.4(a) the results are presented and as can be seen the begin of the transition occurs about one second earlier, while the steady states are basically not affected by that noise level. Thus, our system is not only robust against noise, but even benefits from it. Such noise induced improvements have been shown in a variety of systems [72] and are now commonly called stochastic resonance.

Finally, in order to illustrate one significant advantage of dynamical systems based CPG models for controlling walking over other methods (e.g. trajectory replay), we present the behavior of the model in case of an external disturbance in Figs. 3.4(b) and 3.4(c).

3.1.5 Discussion

The ACPO CPG. We have presented a model for a quadruped central pattern generator. The model is of distributed nature and shows fast transitions and only one

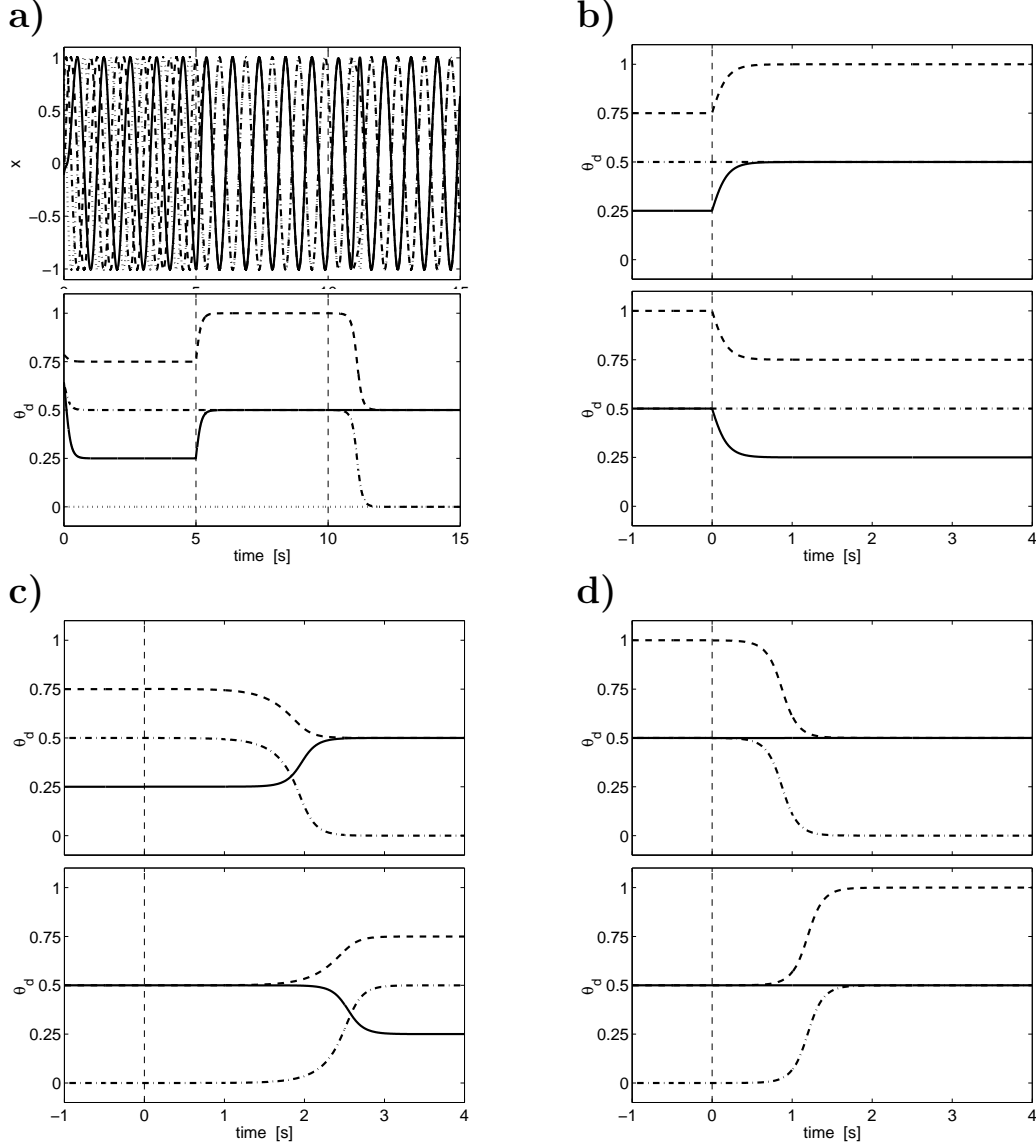


Figure 3.3: Results of the numerical integration of the ACPO CPG. **a)** Trajectories of the ACPO-CPG when switching from walk to trot to bound and the corresponding phase difference plots ($\theta_{d,ij}$). Dashed line: $\theta_{d,12}$, solid line: $\theta_{d,13}$, dash-dotted line: $\theta_{d,14}$. The upper figure presents the oscillatory activity (x_i), while the lower figure shows the corresponding phase difference evolution. **b)** phase difference plots for walk to trot (upper figure) and trot to walk (lower figure). The dashed vertical line indicates the time at which P_{gait} is changed. **c)** walk to bound and bound to walk **d)** trot to bound and bound to trot.

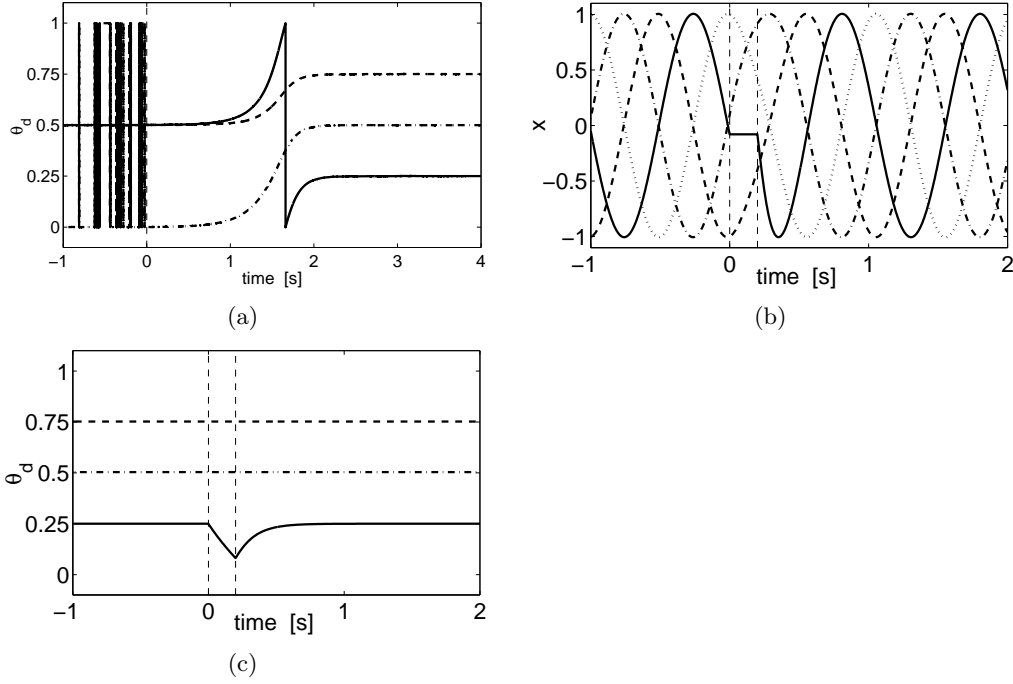


Figure 3.4: **a)** Further experiments on the influence of perturbations on the transition speed. Representatively the bound to walk transitions is chosen which is the slowest. Noise is added during the integration procedure (see text). As can be observed the transition is initiated about 1 s earlier than in the case without noise. **b), c)** To illustrate the robustness against perturbation that is inherently built in the structurally stable dynamical system model of the CPG we present the case when the state variable for the left hind leg gets fixed for 0.2s and then released again during walk. The two vertical lines show the time when the legs is fixed and released again. As can be observed, the leg increases in speed in order to catch up with the other legs to fulfill the requirements of the gait pattern. Within less than 0.5s, the normal gait is re-established.

global attractor. It is robust against noise and perturbations. By one continuous variable we have the control over the chosen gait patterns. From the algorithmic point of view the model is very simple. Considering all these properties, we conclude that the ACPO-CPG is a viable candidate for the implementation in a robot. The presented CPG is however only applicable to interlimb coordination. Additional oscillators are needed for intralimb coordination (i.e. coordinating different DOFs at the hip, knee, and ankle). However, the presented methodology is applicable for these problems as well.

The choice of the subsystem in form of simple oscillators [47, 69, 218], and more specifically phase oscillators [223, 235] has been presented before. However, we motivate our choice with concepts from physics of complex systems rather than base the model on simplified cell models. That this abstraction implied by the choice of simple oscillators makes sense and is based on firm theoretical grounds can be seen when looking on the observations made by biologists from a complex systems perspective.

Modeling in the complex systems framework. We argue that these observations (i.e. low dimensional dynamics and autonomous oscillatory behavior of nerve centers) and the resulting abstract concepts (i.e. CPG) are not a coincidence, but rather a necessity. The reason for that necessity can be understood by physical theories of complex systems developed over the last few decades. These theories deal with systems that are constructed from active subsystems. Understanding the concepts covered by these theories and gaining the insight that modeling controllers for walking robots is an example of a much broader class of problems, we can turn the physical theories into a design methodology that allows us to decide which features need to be preserved in our model and which one can be abstracted away in order to arrive with a controller that satisfies given global properties.

Haken [89] puts the argument forward that a large ensemble of interacting systems normally exhibits low-dimensional dynamics under very broad conditions. While others have formulated parts of the ideas before it was his contribution to formulate an integrated theory of such systems, which he called *synergetic systems*. He enhances the concept of the order-parameter introduced by Landau [136]. The order parameters are identified as slowly evolving variables in a dynamical system (e.g. in the laser, a prime example of self-organizing systems, the order-parameter is the field strength of the laser light). The order-parameters turn out to be the instable modes of that system and their number remains usually a very few comparing to the full state space of the system. The key point is that all the other variables of the system follow the order parameters, and, on the other hand, the activity of the full system influences the evolution of the order parameters. Haken formulated that fact in the *slaving principle*. One can build hierarchies of systems where the order parameters of one subsystem constitute the subsystems for the next hierarchy level. In the case of the locomotory system the order parameters of interest are the phase relationships between the limbs. The scales of the order parameters and the subsystems differ in about three orders of magnitude (neurons: $\sim 10^{-3}$ s – limb activity $\sim 10^0$ s). The different scales are typical

for synergetic systems. Furthermore, it has been shown theoretically [89] and experimentally [165], that the behavior of the order parameters is very independent of the exact nature of the subsystems. Even more, at the order parameter level, completely new phenomena can occur, which are not foreseeable at the subsystem level².

Conclusion of the complex systems perspective. Considering the aforementioned facts, it gets clear that there are two approaches of modeling the behavior of such systems. Both of them have strengths and weaknesses. The first method is to derive models for the subsystems and couple them to come up with the complete model. This is an important approach, especially if one is interested in the exact behavior of the real system being modeled and the influence of all the parameters (for an example see [162]). However, especially when the chosen level of description is very detailed, this method is rather tedious, it leads to complicated models that are normally computationally intensive and possess a large number of parameters. One has to have an enormous knowledge of the details of the subsystems which in reality is often missing. Especially, if one is successful with this modeling approach, one will rediscover the aforementioned system hierarchies. The other approach is to focus on the order-parameter level, if one is mainly interested in mimicking the overall system behavior. It is an phenomenological approach. The advantage here, is that one is freed from a huge amount of parameters, the systems are usually simple and easy to simulate. Yet, the physics guarantees that we still catch the important aspect of the system behavior, namely the behavior of the order-parameters (i.e. models for human inter-limb coordination see [117, 118]). The model derived by this approach typically consists of one low-dimensional dynamical system describing the behavior of the order parameters (e.g. quadruped CPG see [195]). In this article we are following the second approach.

As we are free to chose which level of the system hierarchy we would like to model in order to arrive with an usable model for a robotic application, a good approach is to keep a distributed model consisting of a few subsystems. The subsystems themselves are still models of complex systems. Therefore, they model order-parameter behavior. Naturally, one splits up the whole system into subsystems, where the system being modeled also shows some modularization (i.e. Body segments, Limbs, ...) or where we identify parts that lend themselves to easy measurement of the subsystem behavior. In case of the walking controller, the order parameters are the population activity of the motoneurons for one limb. The population activity serves to drive the muscles. The subsystems are the single neurons of the limb CPG, the muscle cells and all the other numerous parts that form the neuro-mechanical system. Because we are at the order-parameter level of description, it gets clear that there is no need to use models that are motivated by observations made on the single neuron in order to model the behavior on the CPG level. Another motivation for the choice of the canonical subsystem in form of a simple phase oscillator is the fact that from an mathematical viewpoint all limit

²aka. emergence, network effects, self-organization

cycle systems belong to the same universality class [65]. I.e. effects observed in one limit cycle system are also to be expected in another limit cycle system (However, in practical cases, the relationship is often enough only accessible in a qualitative manner. Even, if, from the mathematical viewpoint, a quantitative relationship exists). Furthermore, with this method we arrive with a model that does not show certain drawbacks of earlier models such as dependence on initial conditions, slow and lacking transitions, or periodic driving and prove therefore that our modeling approach is viable. Most probably the most fundamental advantage for our goal of controlling robots is that by choosing the simple oscillator model, we can predict the phase relationships with more ease and to a certain extent by analytical methods.

The level of abstraction of the ACPO-CPG corresponds to the order parameter description of dynamical systems. At this level of description a very simple model can be derived as shown by [195]. The model presented by Schöner et al. however is not of distributed nature anymore. As mentioned before, one interesting property of synergetic systems is their distributed nature. In a robot one would like to have simple distributed control for low level tasks such as locomotion, thus allowing a central processor to use its power to address more involved tasks, such as path planning, communication and the like. Therefore, in this contribution we constructed a model with a more complex structure, that lends itself for a distributed implementation in a robot built of uniform elements.

Outlook and future work. From a more theoretical point of view it will be interesting to do more rigorous analysis of the model, e.g. bifurcation analysis. Furthermore, it will be interesting to take a closer look at the improvement by noise, and compare the observation to other examples and theoretical considerations about stochastic resonance. It is known that there exists a certain optimal level of noise for a given system. This optimum remains to be found.

Since the characteristics of coupled dynamical systems, that we exploited to construct the ACPO-CPG, are universal characteristics that can be observed in many real world systems such as semiconductors [165], analog electronics [157], chemical reactions [202] and many more, one is basically able to implement this models on top of a variety of substrates. The choice in nature are neurons, but for applications we are not restricted to this substrate. The substrate of choice for implementation in the long term will be the one where we have the appropriate control over the characteristic time and length scales on one hand, and suitable operation conditions (temperature, field strengths, power consumption) on the other hand. In addition to that, it should be cheap and simple to manufacture. Therefore, to find such suitable substrates and the way of implementing the systems on top of them, a lot of experiments have to be done.

Conclusions. In recent years a lot of progress has been made in understanding complex systems from a theoretic point of view. Moreover, advances in technology allows us to implement and partially simulate systems of a complexity hitherto impossible. Yet, for applications, these powerful concepts are not yet exploited in a systematic fashion. Researchers in different fields often make implicit use of the

concepts contained in the theory of complex systems when they make investigations and observations, yet, sometimes make assumptions that are not well aligned with this theory. In the authors opinion, it is important and one of the grand challenges for the next decades to transform the knowledge into design principles and collect experiences in order to harness the full power of active distributed systems. The research presented here, belongs to a more general effort that aims at using theories of coupled dynamical systems in the solution of difficult engineering problems and tries to devise new design principles. The possible fields of application are numerous - network engineering, multichannel information transmission, sensor networks and robotics just to name a few.

Acknowledgments This research is funded by a Young Professorship Award to Auke Ijspeert from the Swiss National Science Foundation. We would like to thank Jun Nakanishi for constructive comments on an earlier version of this article.

3.2 An engineering view on oscillators

Engineering Entrainment and Adaptation in Limit Cycle Systems – From Biological Inspiration to Applications in Robotics

Jonas Buchli, Ludovic Righetti and Auke Jan Ijspeert

This paper has been originally published as
J. Buchli, L. Righetti, and A.J. Ijspeert. Engineering entrainment and adaptation in limit cycle systems – from biological inspiration to applications in robotics. *Biological Cybernetics*, 95(6):645–664, 2006

Abstract Periodic behavior is key to life, and is observed in multiple instances and at multiple time scales in our metabolism, our natural environment, and our engineered environment. A natural way of modelling or generating periodic behavior is done by using oscillators, i.e. dynamical systems that exhibit limit cycle behavior. While there is extensive literature on methods to *analyze* such dynamical systems, much less work has been done on methods to *synthesize* an oscillator to exhibit some specific desired characteristics. The goal of this article is two-fold: (1) to provide a framework for characterizing and designing oscillators, and (2) to review how classes of well known oscillators can be understood and related to this framework.

The basis of the framework is to characterize oscillators in terms of their fundamental temporal and spatial behavior, and in terms of properties that these two behaviors can be designed to exhibit. This focus on fundamental properties is important because it allows us to systematically compare a large variety of oscillators which might at first sight appear very different from each other. We identify

several specifications that are useful for design, such as frequency-locking behavior, phase-locking behavior, and specific output signal shape. We also identify two classes of design methods by which these specifications can be met, namely off-line methods and on-line methods. By relating these specifications to our framework and by presenting several examples of how oscillators have been designed in the literature, this article provides a useful methodology and toolbox for designing oscillators for a wide range of purposes. In particular the focus on synthesis of limit cycle dynamical systems should be useful both for engineering and for computational modelling of physical or biological phenomena.

3.2.1 Introduction

Periodic behavior is central to our lives. Our body functions thanks to many types of periodic behaviors ranging from heart beats, breathing, chewing, locomotion, various rhythms in the brain, down to cycles in gene regulatory networks. Similarly our natural environments have multiple periodic phenomena such as rotations of the earth around the sun and around itself, seasons, tides, cycles in ecological systems (e.g. prey-predator populations), in chemical reactions, etc. Finally, many systems that we engineer are meant to exhibit periodic behavior such as clocks (for watches or CPUs), lasers, music, traffic lights, satellites, to name just a few examples. All these phenomena share many common features, and can be modelled (or controlled for engineered systems) by systems of differential equations that exhibit limit cycle behavior, that is by oscillators.

The importance and ubiquity of periodic behavior explains why oscillator models are published in such a large variety of journals in different fields (nonlinear dynamics, physics, biology, chemistry, engineering, etc.). This makes oscillators a very exciting topic of study, but at the same time makes it difficult to extract common principles from all these models. Indeed each field has its own terminology, variable/parameters names, systems of coordinates, methods of analysis, methods of synthesis and this makes it hard to see similarities and differences between models. Furthermore, the choice of a particular oscillator in a given field is often not transparent, and depends sometimes more on historical reasons than on pure design or modelling considerations. The reason for that is usually a lack of abstraction of the concept of oscillators. Finally, another difficulty with oscillators is that while there are many tools for analyzing the behavior of an oscillator (see [75, 134, 166, 234] for some outstanding textbooks), there is a lack of methodologies for *designing* them to exhibit a particular behavior.

The goal of this article is therefore to provide a framework for characterizing different oscillator models in a systematic way, and to focus on methodologies that can be used for designing them. In this process, we review a large range of oscillator models that have been developed as well as some of our own work in adaptive frequency oscillators. We will try to focuss on the fundamental principles of limit cycle systems, and separate those from unnecessary details of a particular implementation. These principles can then be applied to the *design* of systems,

and used to provide guidelines of how to endow a system with a set of predefined properties. Our perspective is therefore mainly an engineering one, i.e. we want to address the problem of how an oscillator or a system of coupled oscillators can be designed to do something useful (e.g. for coordination, sequencing, and/or pattern formation), but the approach should also be interesting for computational modelling.

Oscillators are of interest for engineers for several reasons. They can be exploited for timing and sequencing. They can synchronize to external signals, and show coordinated behavior with perturbations and other oscillators. Connecting them into networks or lattices they can form coordinate yet flexible spatio-temporal patterns. These networks can act as pattern generators which can reduce the dimensionality of a given control problem, in the sense that a small number of simple (scalar) parameters can control multidimensional output patterns. Of course they also exhibit all the common features of structurally stable dynamical systems such as smooth changes under parameter variation. The structural stability makes it possible to fuse in input without destroying the autonomous dynamics of the system, i.e. the resulting dynamics is a combination of internal and external dynamics.

An interesting example of the use of oscillators in engineering is in the field of locomotion control in robots. Locomotion control is still a difficult and unsolved problem for robots with multiple degrees of freedom (e.g. legged robots). Locomotion requires multi-dimensional coordinated periodic patterns that need to satisfy multiple constraints in terms of efficient locomotion, energy and adaptation to complex terrain. One approach to solve this problem relies on accurate models of the robot and environment dynamics to develop control laws for locomotion. These model-based methods have however significant difficulties dealing with environments that are hard to model properly (e.g. with complex terrains). An alternative approach is to use systems of coupled oscillators and to take inspiration from animal motor control. In vertebrate animals, an essential building block of the locomotion controller is the *central pattern generator* (CPG) located in the spinal cord. A CPG is a neural circuit capable of producing coordinated patterns of rhythmic activity in open loop, i.e. without any rhythmic inputs from sensory feedback or from higher control centers [54, 82]. A CPG can be modelled as a system of coupled oscillators [129, 131]. The motivation for using CPG models in robotics is to produce the periodic patterns necessary for locomotion as limit cycles. If this is the case, the oscillatory patterns are robust against transient perturbations (i.e. they asymptotically return to the limit cycle), and this makes them well suited to deal with unexpected perturbations from the environment. Furthermore, the limit cycle can usually be modulated by some parameters, which offers the possibility to smoothly modulate the gait (e.g. increase frequency and/or amplitude) or even to induce gait transitions (i.e. bifurcations between different types of limit cycles, see for instance [47]). Finally, CPGs can readily integrate sensory feedback signals in the differential equations, and show interesting properties such as entrainment by the mechanical body [220]. Because

of these interesting properties, CPGs are increasingly used in robotics (see for instance [30, 59, 125, 181, 232]).

The paper is organized as follows. First, in Section 3.2.2, we introduce oscillators (i.e. limit cycle systems) by definitions, and present a description of the very basic features common to *all* limit cycle systems. We then discuss the typical stability properties of oscillators, and this leads us to the formulation of two distinct coordinate systems, the Phase-Radius coordinate system and the Q coordinate system (the "physical" coordinate system), and their relationship. Examples of the abstract concepts by help of well known oscillators will be given along the way. This discussion helps us to get clear what properties of an oscillator can be designed. Based on this discussion we then address the issue how we can *construct* an oscillatory system to exhibit specific properties. This part addresses the three core questions: What can we do (Section 3.2.3)? How can we do it (Section 3.2.4)? What are the resulting systems (Section 3.2.5)? Finally, we conclude with a general discussion of design choices and give an outlook on future research in this direction.

We assume some familiarity with basic concepts of nonlinear dynamical systems, a good introduction can be found in e.g. in [213], especially the concept of stability will be used extensively. The mathematical facts presented in this article are often not new (many are on textbook level), however the way of presenting oscillators is new due to the focus of generic properties of all oscillators. This leads to a novel discussion of oscillators centered around the transformation between a canonical system in the Phase-Radius coordinate system in which it is particularly simple to discuss the influence of perturbation of oscillators, and the "physical" system, i.e. the traditional way of representing oscillators. To support the discussion the new concept of radius isochrones is introduced. Finally, we would like to give a note about mathematical detail and completeness. For the sake of clarity we do not discuss every subtlety and every case since we think that would dilute the clarity of the concepts. An excellent and very comprehensive introduction to oscillators and synchronization phenomena is [166].

3.2.2 Limit cycle systems

In this section we will introduce the *mathematical* concept of an oscillator. As will get clear there are some subtle differences of what commonly is called an oscillator and the mathematical concept of an oscillator.

The presented concepts are key to all the design issues discussed later, such as the choice of type of oscillator, coupling etc. This means, an engineer wanting to use an oscillator needs a thorough understanding of those concepts. This will allow him/her to chose the right type of oscillator and gives him/her the tools to engineer its properties.

Definitions In order to support our mathematical discussion of oscillators we start with its definition.

$\mathbf{F}(\mathbf{q}, \rho)$	System of equations describing the dynamics of the system, $\mathbf{F}(\mathbf{q}) = [f_1, \dots, f_D]^T$
\mathbf{q}	State vector $\mathbf{q} = [q_1, \dots, q_D]^T$
ρ	Vector of parameters
$\mathbf{p}(t)$	Vector of perturbations
D	Dimension of the system
ϕ	Phase of the oscillator
ω	Intrinsic frequency of the oscillator
\mathbf{r}	Radius of the oscillator $\mathbf{r} = [r_1, \dots, r_{D-1}]^T$
T	Period of the oscillator
Ω_i	Instantaneous frequency
$\mathbf{e}_\phi, \mathbf{e}_\mathbf{r}$	Unit vectors in direction of phase and radius
\mathbb{T}	Transformation from \mathbf{q} to $[\phi, \mathbf{r}]$
\mathbf{q}_∞	The set of points describing the limit cycle
PRCS	Phase-radius coordinate system
QCS	The \mathbf{q} -coordinate system
LC	Limit cycle
PS	Phase sensitivity
PRC	Phase response curve

Table 3.2: Nomenclature, conventions and common abbreviations used to discuss oscillators in this article.

Definition 1 *An oscillator is a autonomous dynamical system, i.e. a system of differential equations with at least one limit cycle attractor. In other words the solution of the system (after a transient time) is a closed cycle, which is asymptotically stable, i.e. if the system gets perturbed out of the limit cycle it returns back to it.*

We see that the limit cycle attractor is the defining property of an oscillator, hence the name limit cycle (LC) system is used as synonym for oscillator.

This means the system has a self-sustained oscillatory behavior to which it returns after a transient perturbation. Oscillators possess thus an *intrinsic* period (and hence frequency) with which the system repeats the pattern of activity. Thus, a linear 2nd (or higher) order system can not be an oscillator in that sense. It can only exhibit sustained oscillations with an oscillatory input in case the system is damped. If it is not damped, the system is just on the border between stability and instability and oscillations are not structurally stable (i.e. after a transient perturbation possibly another pattern is assumed). On the other side of the stability border the oscillations will increase to infinite amplitude.

Let us detail this definition a bit more, for this we need some nomenclature which we list in Table 3.2.

With the help of those variables we can put above definition in more concise terms:

Definition 2 (equivalent to Def. 1) *If the dynamical system*

$$\dot{\mathbf{q}} = \mathbf{F}(\mathbf{q}) \quad (3.37)$$

has a stationary solution which is a closed curve and the solution is structurally stable, (3.37) is an oscillator.

The limit cycle The set on which \mathbf{q} evolves is called the limit cycle, which we denote with \mathbf{q}_∞ . It is an attractor of dimension 1 (i.e. a curve) which is closed in itself, so it needs to be embedded in a space of dimension $D \geq 2$ (cf. Fig. 3.5). The fact that the attractor forms a closed curve implies that the *time shift invariance* holds: if $\mathbf{q}(t)$ is a solution then $\mathbf{q}(t) = \mathbf{q}(t + nT)$, T is the time of repetition, i.e. the period of the system and is inversely proportional to the intrinsic frequency ω of the system $T = \frac{2\pi}{\omega}$ (cf. Fig. 3.5b).

The fact of having a closed curve implies also a special stability property of the attractor. The flow described by the set of equations lets all solutions within the basin of attraction converge to the limit cycle. Perpendicular to the limit cycle the system is thus asymptotically stable. But the phase point moves along the limit cycle. In other words in every point on the limit cycle the flow is stable/contracting in to $D-1$ directions, but drives the state in the one direction perpendicular to the other directions. This is the very essence of a limit cycle system, these stability properties are the only ones that allow for a closed 1-dimensional attractor. And they are the key to understand the properties of oscillators their particular behavior and phenomena such as synchronization.

We can thus distinguish two characteristic stability directions on the limit cycle by introducing a coordinate system of which one basis vector is tangential to the limit cycle, \mathbf{e}_ϕ , and $D - 1$ vectors perpendicular to the limit cycle, which we do denote representatively by \mathbf{e}_r (cf. Fig. 3.5a).

As we will see in the next section the marginally stable direction tangential to the limit cycle is of central importance to discuss oscillators.

The phase In every oscillator we can identify a variable (which does not necessarily correspond to a state variable but is a function of those) which grows *uniformly* in time and is interpreted $\text{mod } 2\pi$ (or any other convention). This variable is called the phase of the oscillator.

The phase of the oscillator is a measure where the oscillator is in the cycle. We remember that the frequency of the oscillator is $\omega = \frac{2\pi}{T}$. We define the phase in the following way

Definition 3 *For the unperturbed system \mathbf{F} , the variable ϕ for which*

$$\dot{\phi} = \omega (= \text{const}) \quad (3.38)$$

is called phase of the oscillator \mathbf{F} .

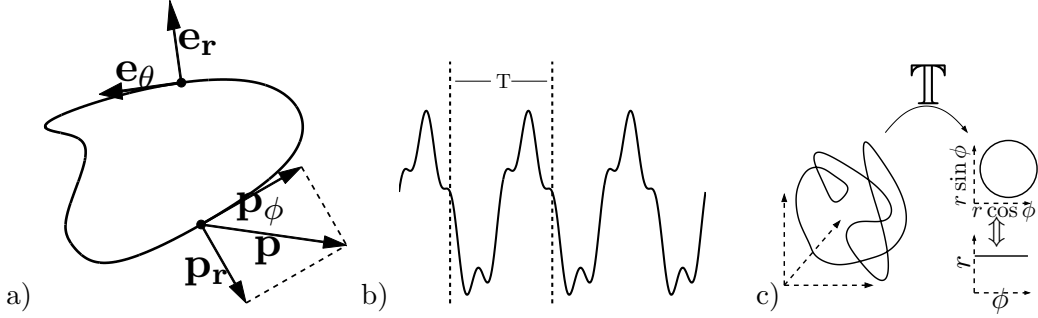


Figure 3.5: a) The schematic illustration of a limit cycle. It is a closed curve in phase space. The stability directions $\mathbf{e}_\phi, \mathbf{e}_r$ are illustrated as well as the projections \mathbf{p}_r and \mathbf{p}_ϕ of a perturbation \mathbf{p} , which has a direction in the phase space, onto those stability directions. b) The time series of an hypothetical oscillator. There is a characteristic period T after which the activity of the oscillator and with this the time series repeat. c) The limit cycle is a 1-dimensional manifold embedded in a D -dimensional space ($D \geq 2$), we can transform the system into a coordinate system in which the manifold shows particularly simple form and of which the stability directions constitute the base vectors.

By help of the phase also the frequency can be cast into a definition

Definition 4 *The rate of change ω of ϕ in the unperturbed oscillator is the intrinsic frequency of the oscillator.*

The reason why we define the frequency by help of the phase will become clear later when we will discuss the oscillator under perturbations. It is important to note that ω is not always an explicit parameter. However, it is always a function of the parameters, $\omega = f(\rho)$.

Now, every oscillator can be transformed into a phase (ϕ) – radius (\mathbf{r}) coordinate system [166]:

$$\dot{\phi} = \omega \quad (3.39)$$

$$\dot{\mathbf{r}} = \mathbf{F}_r(\mathbf{r}) \quad (3.40)$$

where \mathbf{F}_r is the dynamical system describing the evolution of \mathbf{r} (refer to Fig. 3.5c) and has a stable fixed point.

The vectors \mathbf{e}_ϕ and \mathbf{e}_r that we introduced above based on stability considerations form the basis vectors of the phase radius coordinate system. In Eq. 3.39 the fact that the phase is a marginally stable variable ($\frac{d\phi}{d\phi} = 0$) is immediately evident. This coordinate system is the natural one to discuss influences on the oscillator since the stability directions are decoupled.

At this stage it is also worth noting, that in a unperturbed oscillator the phase *completely* describes the state of the system in the stationary regime (cf. phase oscillators in Section 3.2.3). This means we can write $\mathbf{r}_\infty = f(\phi)$.

It is important to realize, that the phase is not necessarily proportional with time. This is only the case when the oscillator is unperturbed, where indeed ϕ is proportional to $t \bmod 2\pi$ - but more importantly and this is the key to the entrainment effects as we will see later, in case of perturbations the phase and time “get decoupled” i.e. the phase can be shifted forward or backwards. The oscillations can be accelerated or de-accelerated. Designing entrainment and other aspects of the oscillator is all about designing these acceleration and de-acceleration effects. We will discuss this in more detail when we look at LCs under perturbations in Section 3.2.2. But first we need to complete our understanding of the phase-radius coordinate system.

The geometry of the limit cycle Normally the oscillator is not readily represented in the ideal phase-radius coordinate system (as in Eqs. 3.39–3.40). We need to discuss the relationship between the oscillators representation in \mathbf{q} and in $[\phi, \mathbf{r}]$. As we will see that is the key to understand the behavior of the oscillator under perturbations.

If we transform the coordinate system and the metrics we could possibly gain a simpler oscillator but the complexity gets transferred into the coupling of the oscillator the input. We will give an example when we discuss phase oscillators in Section 3.2.3.

But then how is the coordinate system usually determined? Let us reflect on the role of the state variables. Usually the state variables are defined by a physical interpretation or they have a concrete conceptual meaning such as a voltage or a chemical concentration, for instance, and that is the way the coordinate system gets defined. This coordinate system is the natural one to formulate the physical laws and interaction between the different physical entities (while, as we have seen, phase radius is the natural one to discuss perturbation because of the separation of variables according to stability properties). And in modeling it is usually the case that the input and outputs of an oscillator are formulated in the physical coordinate system.

But, for engineering, if we want to exploit some of the abstract properties of the oscillator we are not bound to an interpretation of the variables. Thus it can be useful to formulate the inputs and outputs in the phase radius coordinate system or any other suitable coordinate system.

We name thus two coordinate systems, the phase radius coordinate system: PRCS and the coordinate system of \mathbf{q} : QCS. The transformation from QCS to PRCS is given by \mathbb{T} .

$$[\phi, \mathbf{r}]^T = \mathbb{T}(\mathbf{q}) \quad (3.41)$$

Let us look in more detail at this transformation and some of its properties. The transformation can be split up in to components, namely the transformation from \mathbf{q} to ϕ : $\phi = T_\phi(\mathbf{q})$ and the transformation from \mathbf{q} to \mathbf{r} $\mathbf{r} = T_r(\mathbf{q})$, thus

$$\mathbb{T} = \begin{bmatrix} T_\phi \\ T_r \end{bmatrix}$$

Since we are not only interested in the transformation of the state variables but also in the transformation of the dynamics under this transform let us investigate the derivatives of the transformed coordinates, we do this exemplary on ϕ since it works the same way for all state variables.

$$\phi = T_\phi(\mathbf{q}) \quad (3.42)$$

$$\begin{aligned} \Rightarrow \dot{\phi} &= \frac{dT_\phi(\mathbf{q})}{dt} = \frac{\partial T_\phi(\mathbf{q})}{\partial \mathbf{q}} \dot{\mathbf{q}} \\ &= \frac{\partial T_\phi(\mathbf{q})}{\partial \mathbf{q}} \mathbf{F}(\mathbf{q}) \end{aligned} \quad (3.43)$$

We see that T_ϕ is intrinsically defined (by the fact that Eq. 3.43 has to be equivalent to ω , being a constant) but there is some freedom in the choice of T_ϕ . To remove this ambiguity we define the behavior of an oscillator in the canonical PRCS as

$$\dot{\phi} = \omega \quad (3.44)$$

$$\dot{\mathbf{r}} = 1 - \mathbf{r} \quad (3.45)$$

This is somewhat arbitrary but the choice will become clear later in the discussion of the relationship of PRCS and QCS. At this place its choice is already partially motivated by Eq. 3.45 representing the simplest dynamical system with stable, non-zero fixed point behavior where the fixed point is $\mathbf{r} = 1$.

The inverse of \mathbb{T} , \mathbb{T}^{-1} , transforms the system from the PRCS into the QCS. This means by designing \mathbb{T}^{-1} the PRCS can be mapped into any type of oscillator.

Example: Consider the transform of r into r' , given by $r' = (r - 1)^g + r_0$. This transforms the canonical oscillator (Eqs 3.44 – 3.45) into

$$[\dot{\phi}, \dot{r}']^T = [\omega, -g(r' - r_0)]^T \quad (3.46)$$

We can now transform this system further by applying the well known transformation from a Polar coordinate system into the Cartesian coordinate system: $q_1 = r' \cos \phi$, $q_2 = r' \sin \phi$. By this transform we yield the following system

$$\begin{bmatrix} \dot{q}_1 \\ \dot{q}_2 \end{bmatrix} = \begin{bmatrix} g \left(\frac{r_0}{\sqrt{q_1^2 + q_2^2}} - 1 \right) q_1 - q_2 \omega \\ g \left(\frac{r_0}{\sqrt{q_1^2 + q_2^2}} - 1 \right) q_2 + q_1 \omega \end{bmatrix} \quad (3.47)$$

We have thus transformed the canonical oscillator into a phase oscillator in a Cartesian coordinate system. The radius and convergence rate of the oscillator can be controlled by r_0 and g respectively.

While here we can express the transform \mathbb{T}^{-1} and its inverse by rather simple mathematical expressions this is usually not possible. Even more, the transform might often not be expressible in a closed analytical form.

Graphical assessment of \mathbb{T}

We will now discuss a graphical way of assessing relationship of PRCS and QCS, i.e. \mathbb{T} for a given oscillator. For this the notion of time becomes important, i.e. at what velocity the phase point moves through the phase space. What specifies the equivalence of a point in QCS and a point in PRCS? If for time t_0 $\mathbf{q}(t_0) = \mathbb{T}^{-1}([\phi(t_0), \mathbf{r}(t_0)])$, then for all time $\mathbf{q}(t) = \mathbb{T}^{-1}([\phi(t), \mathbf{r}(t)])$. This means if we could find a way of comparing the development of the two points in both coordinate systems at regular intervals and repeat this for different initial conditions we would get an idea of \mathbb{T} .

The activity of the oscillator can be plotted in the QCS (phase portrait) in which the limit cycle will show up as a closed curve. But, the information about the phase velocity is lost. So even that we know that for example the limit cycle in the QCS corresponds to the limit cycle in the PRCS, we do not know which point on the limit cycle in one coordinate system corresponds to which point in the other one. While in PRCS the phase moves along the limit cycle with constant velocity ω , in general, for an arbitrary oscillator \mathbf{F} in the QCS, the phase point will not move along the limit cycle in the phase space with a constant velocity. Thus, the phase does not correspond to the simple “position” on this curve (i.e. an infinitesimal part of the curve does not correspond to the same infinitesimal of ϕ , $d\mathbf{q} \neq d\phi$). In order to investigate on this relationship, we could plot points with always equal $\Delta\phi$.

However, the phase is only uniquely defined on the limit cycle, but we would like to get a global idea of the transformation. We can generalize the notion of a phase outside the limit cycle by the concept of *isochrones*. We follow the definition of [166] and generalize the phase by help of the cycle time T , i.e. the mapping $\mathbf{q}(t) \rightarrow \mathbf{q}(t + T)$.

Definition 5 *Isochrones – The set of points being invariant under the mapping $\mathbf{q}(t) \rightarrow \mathbf{q}(t + T)$ and crossing the limit cycle at \mathbf{q}^* (i.e. \mathbf{q}^* is a fixed point of the mapping) is called an isochrone through \mathbf{q}^* .*

In other words, all points of the phase space which converge to having the same phase on the limit cycle form an isochrone.

If we plot isochrones for every $\Delta\phi = \text{const}$ they show the relationship of the phase with the geometry of the system in the QCS (cf. Fig 3.6). Where they are tightly spaced the phase point moves slowly, thus values of different phase are tighter spaced. If they are equally spaced on the limit cycle, the lengths of an arc of the limit cycle is proportional to a $\Delta\phi$ ($d\phi = \frac{1}{S}2\pi ds$, where s is the arclength and S the total length of the limit cycle). If the isochrones are straight (as in Fig. 3.6b) this means that the DE for ϕ and \mathbf{r} are decoupled, and the transformation \mathbb{T} corresponds to a transformation from Cartesian to Polar coordinates.

Now, the isochrones give us an idea how ϕ is embedded into QCS. But in order to complete our picture of the transformation \mathbb{T} we need to get an idea of how \mathbf{r} is embedded into this coordinate system.

For this we define the Radius-Isochrones, which will give us an idea on how \mathbf{r} evolves over time.

Definition 6 *Radius-Isochrones* – The set of points $\mathbf{q}(t)$ satisfying $\text{dist}(\mathbf{q}(t + \Delta t), \mathbf{q}_\infty) = \epsilon$, are called a Radius-Isochrone with Δt .

Function dist denotes the distance between the point \mathbf{q} and the limit cycle. Intuitively this means all points which converge to the limit cycle in the same time form a radius-isochrone. We see that the definition of the radius-isochrones implies a distance measure from the limit cycle. This distance can be defined in different ways. We use the perpendicular direction to the limit cycle and consider as converged to the limit cycle when it enters the “tube” of radius $\epsilon \ll 1$ around the limit cycle.

We can use the isochrones and the radius-isochrones to get an idea how the abstract phase-radius oscillator is embedded into the coordinate system for \mathbf{q} . The time to get from one isochrone to the next is constant, the time from one radius-isochrone to the next is also constant. The radius-isochrones gives information about the rate of convergence, tightly space radius-isochrones mean a slow convergence to the limit cycle, widely spaced mean fast convergence (see Fig. 3.6 and its description).

If we plot isochrones equally spaced in ϕ and radius-isochrones for equally spaced Δt for the oscillator in the canonical PRCS (Eqs. 3.44–3.45) we get a rectangular grid as seen in Fig. 3.6a with equally spaced vertical lines and exponentially spaced horizontal lines. This means whenever we see those characteristics in an oscillator we know it behaves like the canonical oscillator (i.e. exponential convergence towards the limit cycle and isochrone behavior).

Limit cycles under perturbations

Considering the fact that we can transform *every* oscillator into a PRCS, it gets clear that we can consider all *unperturbed* oscillators are equivalent up to a transformation \mathbb{T} . They only differ in the way how a (physical) input to the system affects its dynamics, i.e. how the input output space is related to PRCS. So far we considered the autonomous, i.e. unperturbed, oscillator. However, the advantage of the use of oscillators (e.g. vs. function based approaches) becomes only effective when using them to be coupled to perturbations. This can mean the oscillator is coupled to some external in- and output or to other oscillators.

If the input and outputs are formulated in a QCS then, in respect to their influence on the limit cycle, they undergo the same transformation \mathbb{T} . We thus have to investigate limit cycle systems under perturbations. Therefore, we have to consider the single oscillator as non-autonomous system,

$$\dot{\mathbf{q}} = \mathbf{F}(\mathbf{q}, \mathbf{p}(t)) \quad (3.48)$$

It is important to stress, that the perturbation can theoretically have any arbitrary functional form, and the perturbation is also not limited on acting on the

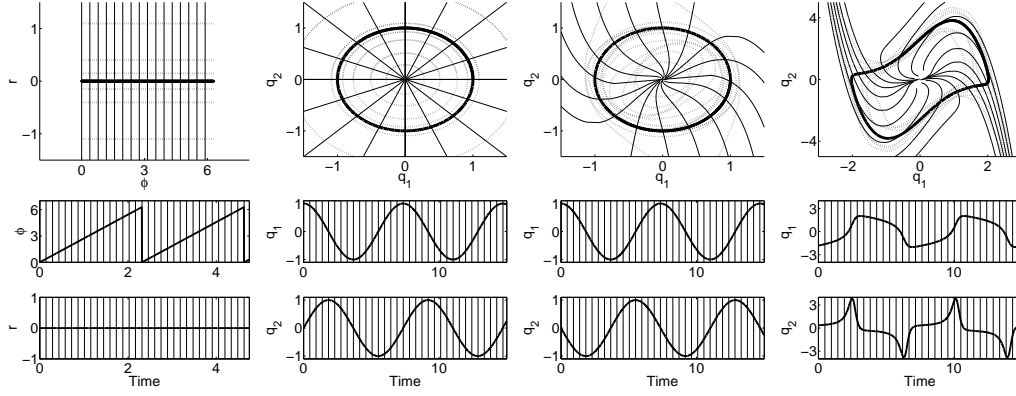


Figure 3.6: Illustrating the transformation \mathbb{T} , by help of the isochrones and the radius-isochrones. For each oscillator 16 equally spaced isochrones are used and a varying number of radius-isochrones with a given Δt are plotted in the phase portrait (upper panels) and below the time series are shown. The fine vertical lines indicate the isochrones (only indicating the temporal position on the time series.) We see while they are always equally-spaced in the time series plot, in the phase plot this is not necessarily the case. a) The phase plot of the canonical oscillator in the phase-radius coordinate system PRCS (Eqs. 3.39–3.40). The isochrones form straight and equidistant vertical lines. The radius-isochrones ($\Delta t = [5, 6, 7]s$) form exponentially spaced straight horizontal lines. b) The Hopf oscillator (Eqs.3.66–3.67). The isochrones form straight rays at equal angles, which reflects the polar interpretation of ϕ in the transformation. The radius-isochrones ($\Delta t = [0.7, 1.4, 2.1]s$ outside of the LC and $\Delta t = [0.7, 1.4, 2.1, 3.5]s$ inside) reflect the 3th order convergence behavior of the radius. In the time-series we see the harmonic nature of the limit cycle reflected. c) The Energy oscillator (Eqs. 3.58–3.59). Due to the appearance of the nonlinear energy term only in the first ODE the system loses its circular symmetry. The isochrones and the radius-isochrones ($\Delta t = [2, 2.4, 2.8, 3.2]s$ outside of the LC and $\Delta t = [2, 2.4, \dots, 5.2]s$ inside) get a characteristic deformation. d) van der Pol Oscillator (Eqs.3.78–3.79). This is a strongly nonlinear oscillator. This fact is reflected in the strong deformation of the isochrones. The strong deformation of the radius-isochrones $\Delta t = [0.3, 0.6, 0.9]s$ away from the limit cycle in the upper left and lower right corner of the figure indicates the rapid convergence of the system in that region. It is immediately visible that the transformation from this QCS to the PRCS is a very complicated one.

first state variable only. However, a discussion of the different types of perturbations is out of the scope of this article. We will focus on an often used form of perturbation, the additive perturbation

$$\dot{\mathbf{q}} = \mathbf{F}(\mathbf{q}) + \mathbf{p}(t) \quad (3.49)$$

We will however realize that the additive form in a QCS transforms into a more complicated functional form in the PRCS. The oscillator in the PRCS becomes

$$\dot{\phi} = \omega + p_\phi \quad (3.50)$$

$$\dot{\mathbf{r}} = \mathbf{F}_r(\mathbf{r}, \phi) + \mathbf{p}_r \quad (3.51)$$

p_ϕ is the component of the perturbation acting on the phase and \mathbf{p}_r is the component of the perturbation acting in direction of the radius.

Expressed by help of the transformation \mathbb{T} we yield for the additive case (i.e. Eq. 3.49)

$$\Rightarrow \dot{\phi} = \frac{\partial T_\phi(\mathbf{q})}{\partial \mathbf{q}} \mathbf{F}(\mathbf{q}) + \frac{\partial T_\phi(\mathbf{q})}{\partial \mathbf{q}} \mathbf{p} \quad (3.52)$$

On the limit cycle $\mathbf{e}_\phi = \mathbb{T}(\mathbf{q})$, thus the relationship between the PRCS and the QCS coordinate system is the determinant for the effect of the perturbations to the oscillator.

Let us give a geometric intuition, which lets us easily derive p_ϕ , without relying on the transformation \mathbb{T} . But, this derivation is only valid on the limit cycle, while above transforms are more general.

To arrive at this, it is important to realize that every perturbation has a direction in the phase space. Consider a pulse like additive input, i.e. a infinitely short input at time t_p . The perturbation will bring the phase point away from the limit cycle. The stability properties will bring it back to the limit cycle, but on another position, relative to the unperturbed system. Thus the phase of the system $\phi_{(t_p+)}$ is not the same as before the perturbation $\phi_{(t_p-)}$, the phase is reset hence the term “phase resetting” (cf. Fig. 3.7).

Thus, for small perturbations the effect that remains in the system is the effect of the perturbation in direction of the phase \mathbf{e}_ϕ , this is the direction tangential to the limit cycle or equivalently the direction $\dot{\mathbf{q}}$:

$$\mathbf{e}_\phi = \frac{\dot{\mathbf{q}}}{|\dot{\mathbf{q}}|} \quad (3.53)$$

Therefore, the effective perturbation on the phase is

$$p_\phi = \mathbf{p} \cdot \mathbf{e}_\phi \quad (3.54)$$

The derivative of the phase becomes

$$\dot{\phi} = \omega_0 + \mathbf{p} \cdot \mathbf{e}_\phi \quad (3.55)$$

So we found the sensitivity of the phase on perturbations:

$$S_p(\mathbf{p}) \doteq \frac{p_\phi}{|\mathbf{p}|} = \frac{\mathbf{p}}{|\mathbf{p}|} \cdot \mathbf{e}_\phi = \frac{\mathbf{p}}{|\mathbf{p}|} \cdot \frac{\dot{\mathbf{q}}}{|\dot{\mathbf{q}}|} \quad (3.56)$$

This means that depending on the state of the oscillator, the same perturbation can have a different influence, at one stage it can speed the oscillator slightly up at the other state slow it down. If the sum of this acceleration or de-acceleration is non-zero this leads to entrainment effects.

The sensitivity of the phase to perturbations is summarized in the phase-reset curve (PRC) and its generalization the phase sensitivity (PS). The PRC is a function which describes the effect of a unitary pulse like perturbation as a function of the phase of the oscillator it arrives at. In other words it tells how much the phase is shifted by that perturbation.

The phase sensitivity generalizes this idea as it does not restrict to a single pulse like perturbation per cycle, but it is an “instantaneous” description of the effect of perturbations. Due to its importance in the discussion about influence of perturbation on oscillators a lot of research has been done mainly on PRC but also on PS, see [166] and references therein. For an example of the derivation phase locking with the presented tools see [23].

It can be difficult or impossible to get analytical form of the PRC or PS. However, with the directional idea introduced in Eq. 3.56 it can be estimated from numerical integration. It can also be measured to a certain extent in real-world systems. We will come back to the role of the PRC/PS when discussing the design of entrainment effects in Section 3.2.5.

Since the frequency of the oscillator corresponds to the rate of change of the phase we see that in a perturbed oscillator the observed frequency is not necessarily the same anymore:

Definition 7 *The instantaneous frequency Ω_i is defined as the momentary rate of change of the phase*

$$\Omega_i = \dot{\phi} \quad (3.57)$$

While for the autonomous oscillator the instantaneous frequency is equal the intrinsic frequency and constant ($\Omega_i = \omega = \text{const}$), in the perturbed oscillator the instantaneous frequency is not equal the intrinsic frequency ($\Omega_i \neq \omega$) and is also a function of time ($\Omega_i = f(t)$). Ω_i is the frequency which will be observed or measured at any given time (e.g. by methods like windowed FFT, spectrograms or wavelets). ω is the *parameter*, while Ω_i is a *variable* which can be decoupled from ω by a perturbation.

Remembering the relation $\Omega_i = \dot{\phi}$, this also means that the observed frequency *is not the same as the intrinsic frequency*: if we have phase locking (i.e. when the difference between the phase of the oscillator and the phase of the perturbation remains bounded) the observed frequency will be the frequency of the perturbation. Consider as an example two mutually connected oscillators with intrinsic frequencies $\omega_{1,2}$ which are different but close enough to have mutual entrainment.

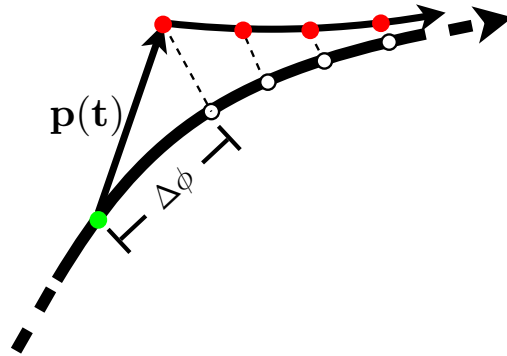


Figure 3.7: Effect of a small pulse like perturbation on the limit cycle. The perturbation $\mathbf{p}(t)$ arrives when the phase point is at the position marked by a the green dot. The phase point is then pushed back to the limit cycle by the stability properties of the system, i.e. it approaches asymptotically the limit cycle. It however retains a phase difference ($\Delta\phi$) in comparison with the unperturbed reference system. The phase difference can be of different amplitude and sign depending on the direction of the perturbation *and* the state the system currently is in when the perturbation arrives. Understanding this fact is key to understanding synchronization phenomena.

The observed frequency Ω_i will be the same for both oscillators, but different from the two intrinsic frequencies, i.e. $\Omega_i \neq \omega_{1,2}$ (it will be in between the two).

Thus, it can be said that the oscillator gets entrained by the perturbation it could be said that it adapts, but this change is only temporary, i.e. reactive. If the input is switched off the system immediately returns to its intrinsic dynamics, there is no memory of the input, no lasting change to the dynamics.

Further, there can be an influence on the radius by the perturbation which can also be exploited. The stability directions here are however less special so this usually reduces to quite standard treatment of ODEs with fixed points under perturbation. Note that however the behavior of the radius under perturbation can still be difficult, especially when there is a strong deformation of the radius-isochrones in the QCS (e.g. as for the van der Pol, cf. Fig. 3.6). Such a deformation means that the convergence behavior is very non-uniform and a perturbation has a completely different effect on \mathbf{r} depending where it arrives.

Thus, summarizing the findings of this section, it must be realized that for the design it is important to know the stability properties and the effect of perturbations in the coordinate systems of the stability directions. Simply said, if we want to change radius only, then we need to act perpendicular the limit cycle, i.e. move the point on the same isochrone, if we want to affect the phase only we need to move the phase point tangential to the limit cycle, to move on the radius isochrones.

3.2.3 The design space

We realize that the oscillator can be completely reduced to the phase radius coordinate system and the inputs can be formulated in that system. We can then possibly use the transformation \mathbb{T}^{-1} into a given interpretation coordinate system to talk about the oscillator in a physically or conceptually more meaningful coordinate system. So all design choices will deal in one way or the other with investigating what the effects of perturbation in the phase radius coordinate system (PRCS) are (and then possibly backwards via \mathbb{T} , what this means for the behavior in the QCS).

We are now at a stage where we can discuss *what can be designed in an oscillator*. There are three basic ways how an oscillator and its in and output can be defined:

1. Chose an ODE system $\mathbf{F}(\mathbf{q}, \rho)$ and functional form of in and output, i.e. $\mathbf{F}(\mathbf{q}, \rho) \rightarrow \mathbf{F}(\mathbf{q}, \rho, \mathbf{p})$.

Then we need to work out the relation of \mathbf{F} to $[\dot{\phi}, \dot{\mathbf{r}}]$, i.e. we have to work out \mathbb{T} (or parts of it), the transformation is *implicitly* specified.

Here we need to be able to convince ourselves either analytically or at least numerically that $\mathbf{F}(\mathbf{q}, \rho)$ represents indeed a structurally stable oscillator. Then we are sure about the existence of the phase radius coordinate system and the stability properties that have been discussed.

Example:

$$\dot{q}_1 = -\alpha \frac{q_1^2 + q_2^2 - E}{E} q_1 - q_2 + p_x(t) \quad (3.58)$$

$$\dot{q}_2 = q_1 \quad (3.59)$$

This oscillator's steady state solution is $\mathbf{q}_\infty = [\sqrt{E} \cos(t + t_0), \sqrt{E} \sin(t + t_0)]$. Structural stability is most easily shown by transforming into polar coordinates and showing that the ODE for the radius has a stable fixed point. We can then show with rather straightforward analysis that in stationary regime:

$$\dot{\phi} = \omega + \sin(\phi)p_x(t) \quad (3.60)$$

2. *Use an ideal phase or phase radius oscillator and given input and output directly in this coordinate system, the transformation is thus implicitly specified by this choice.*

Note that the transformation does not necessarily have to be fully specified, e.g. if only a scalar output is needed it suffices to define a part of the transformation.

Example: Thus, we choose a phase oscillator and add a nonlinearity in the input $\dot{\phi} = \omega + \sin(\phi)p(t)$ will synchronize on $p(t)$ if frequencies are close. The output is chosen to be $o = \sin(\phi)$.

3. *Specify input in QCS and specify \mathbb{T}^{-1} explicitly.*

Example: Choose $\mathbf{q} = [q_1, q_2]$, a Cartesian coordinate system, and \mathbb{T} as the transformation into a polar coordinate system, i.e. $T_\phi = \arctan \frac{q_1}{q_2}$ (\arctan denotes the four-quadrant arcus-tangent), $T_r = \sqrt{q_1^2 + q_2^2}$. The input acts on the first state variable only: $\mathbf{p} = [p_1, 0]$. We can split up the relevant term from Eq. 3.52 in the following way

$$\frac{\partial T_\phi(\mathbf{q})}{\partial \mathbf{q}} = [T_{\partial q_1}, T_{\partial q_2}]^T \quad (3.61)$$

Since $\mathbf{p} = [p_{q_1}, 0]^T$, we can write

$$p_\phi = [T_{\partial q_1}, T_{\partial q_2}]^T \cdot [p_{q_1}, 0]^T = T_{\partial q_1} p_{q_1} \quad (3.62)$$

Using $\phi = \arctan \frac{q_1}{q_2}$

$$\begin{aligned} T_{\partial q_1} &= \frac{d}{dq_1} \arctan \frac{q_1}{q_2} = \frac{1}{1 + (\frac{q_2}{q_1})^2} \frac{-q_2}{q_1^2} \\ &= -\frac{r \sin \phi}{r} = \sin \phi \end{aligned}$$

	Specification	Required Property
1)	Unperturbed avg. frequency: $\overline{\Omega}_i = \omega$	$\int_0^{2\pi} p_\phi = 0$
2)	Frequency locking: $\overline{\Omega}_i = \omega_F$	$\frac{1}{2\pi} \int_0^{2\pi} p_\phi = \omega_F - \omega (= -\omega_d)$ if $\Omega_i = \omega_F$, in differential terms: show that $\phi_d = \phi - \phi_F$ is bounded $\int_0^{2\pi} \dot{\phi}_d = \int_0^{2\pi} p_\phi + \omega_d = 0$
3)	Phase locking: $\phi_d = \Phi_r$	$\phi_d(\Phi_r) = p_\phi(\Phi_r) + \omega_d = 0$ and $\frac{d}{d\phi} \phi_d(\Phi_r) < 0$ (phase locking implies frequency locking).
4)	Spec. instantaneous frequency: $\dot{\phi}(t) = \Omega_r(t)$	$p_\phi = \Omega_r(t) - \omega$
5)	Arbitrary output signal shape: $x(\phi) = x_r(\phi)$ or $x(\mathbf{q}) = x_r(\mathbf{q})$	Appropriate function, i.e. filter
6)	Arbitrary form of LC in QCS: $\mathbf{q}_\infty = \mathbf{q}_{ref}(t)$	stability directions i.e. $\frac{\mathbf{F}(\mathbf{q}_{ref})}{ \mathbf{F}(\mathbf{q}_{ref}) } = \frac{D(\mathbf{q}_{ref})}{ D(\mathbf{q}_{ref}) }$ and $\frac{\partial \mathbf{n}(\mathbf{q}_{ref})}{\partial \mathbf{n}} < 1$

Table 3.3: Common design goals and the required properties of the oscillator.

$$\Rightarrow p_\phi = -\sin \phi p_{q_1}$$

As one can see, the three examples are equivalent in their phase behavior. We also see that it is often not needed to have a full knowledge of the theoretical transformation \mathbb{T} .

In large parts of the literature we see method 1 employed. Often with some complicated \mathbf{F} out of the modeling literature. Immediately we realize that for engineering this is often not the best choice.

By help of the introduction of the stability directions and the geometrical aspects of interpretation of the phase-radius coordinate system (i.e. \mathbb{T}), we can identify two somewhat orthogonal design axes: (1) Timing: Design that influences the phase of the oscillator, here we have (a) influence on (relative) phase, (b) instantaneous frequency, and (c) average frequency. (2) Design that influences the geometry of the oscillator. To name here are (a) influences on r directly and (b) the design of \mathbb{T}^{-1} , i.e. output filter. This is a very interesting and important result, since orthogonal design axis are extremely helpful for engineering tasks. It means we can decouple the influence of parameters on the outcome. In other words, by choosing a more suitable coordinate system, those influences get decoupled while in the original coordinate system they are not.

To detail this more, in the following we address some common design goals and how they translate into properties which the system has to exhibit (summary in Table 3.3).

1. *Specification:* Unperturbed average frequency: $\overline{\Omega}_i = \omega$. Average observed

frequency should be equal to the intrinsic frequency ω .

Required Property: $\int_0^{2\pi} p_\phi = 0$

We need the effect on the phase to have in average zero effect.

2. *Specification:* Frequency locking with an external signal of frequency ω_F i.e. $\Omega_i = \omega_F$

Required Property: $\frac{1}{2\pi} \int_0^{2\pi} p_\phi = \omega_F - \omega (= \omega_d)$ if $\Omega_i = \omega_F$, in differential terms: show that $\phi_d = \phi - \phi_F$ is bounded $\int_0^{2\pi} \dot{\phi}_d = \int_0^{2\pi} p_\phi + \omega_d = 0$ the perturbation in the phase needs in average to make up for the differences between the intrinsic frequency and the frequency of the perturbation.

3. *Specification:* Phase locking with arbitrary phase lag: $\phi_d = \Phi_r$.
Required Property: $\dot{\phi}_d(\Phi_r) = p_\phi(\Phi_r) + \omega_d = 0$ and $\frac{d}{d\phi} \dot{\phi}_d|_{\Phi_r} < 0$. The DE for ϕ_d needs a stable fixed point at Φ_r . This is achieved when the perturbation at every instant cancels for the differences between the intrinsic frequency and the frequency of the perturbation. Note, phase locking implies frequency locking.
4. *Specification:* Arbitrary instantaneous frequency: $\dot{\phi}(t) = \Omega_r(t)$.
Required Property: $p_\phi = \Omega_r(t) - \omega$.
5. *Specification:* Arbitrary T -periodic output signal shape. *Required Property:* An appropriate output function or dynamical system has to be found, i.e. this leads to filter design, or the design of \mathbb{T}^{-1} .
6. *Specification:* Arbitrary form of limit cycle in QCS, i.e. $\mathbf{q} = \mathbf{r}(t)$ – one or several state variables should follow a reference trajectory. This means we want a general form of the limit cycle: We have a closed curve in QCS which should be the limit cycle. *Required Property:* We need thus to design the stability directions to be tangential, i.e. on the curve the flow has to have the direction of the tangent. Normal to the curve the flow has to be stable. If $D(\cdot)$ denotes the tangential and $\mathbf{n}(\cdot)$ the normal direction to a curve, we require (i) flow tangential to reference trajectory $\frac{\mathbf{F}(\mathbf{r}(t))}{|\mathbf{F}(\mathbf{r}(t))|} = \frac{D(\mathbf{r}(t))}{|D(\mathbf{r}(t))|}$ and (ii) contracting perpendicular to the limit-cycle $\frac{\partial \mathbf{n}(\mathbf{r}(t))}{\partial \mathbf{n}} < 1$.

Remember that if we decide to work with a QCS, the the perturbation on the phase is $p_\phi = f(\mathbb{T})$, thus the properties to be satisfied to meet above design goals contain the relationship between a chosen coordinate system (QCS) and the PRCS.

The properties listed above will not necessarily allow a directed design without further assumptions and simplifications as they can lead to very difficult expressions. In the second part of the article we will address how some of the above properties have been designed in previous work.

Classes of Limit Cycles

Here we list a few important classes of oscillators, with properties in terms of the above discussed topics. They are loosely ordered from “simple” to more “complicated” (in the sense of \mathbb{T}). As we have seen above, the classification only makes sense for a given coordinate system. We present them in the coordinate system in which they are usually used and additive input is used.

Phase oscillator – The probably simplest type of oscillator, where the radius is completely neglected, only the phase is retained. The phase oscillator is a linear system defined on the circle \mathbb{S}^1 instead of the Euclidean space \mathbb{R}^1 which implies a closeness of the solution, and with that the system fulfills our definition of an oscillator.

Properties The phase oscillator is essentially a first order linear differential equation, the nonlinearity lies in the interpretation of the phase modulo 2π and input/output relation. It is the most abstract oscillator. An important assumption for applicability of phase oscillator is that the limit cycle is strongly damped, i.e. that the phase point is always on the limit cycle (or very close).

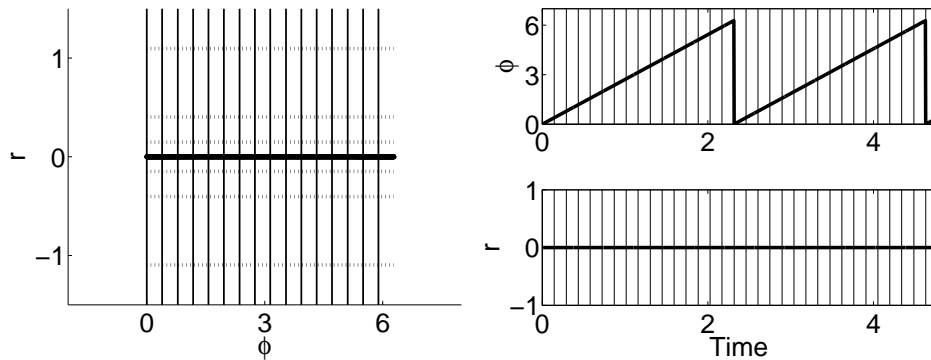
The output signal shape can not change based on input (other than direct functional coupling).

References: The phase oscillator were and are the “work-horse” to work on synchronization effects, e.g. the Kuramoto oscillators [134, 215].

Equations

$$\dot{\phi} = \omega + p(F(t), \phi) \quad (3.63)$$

Illustration



Isochronous oscillator

Properties The isochronous oscillators has straight isochrones, i.e. they are perpendicular to the limit cycle.

Equations

In the simplest case, the isochronous oscillator is a *linear differential equation system*. However not defined on the Euclidean \mathbb{R}^D space but on $\mathbb{S}^1 \times \mathbb{R}^{D-1}$

$$\dot{\phi} = \omega \mod 2\pi \quad (3.64)$$

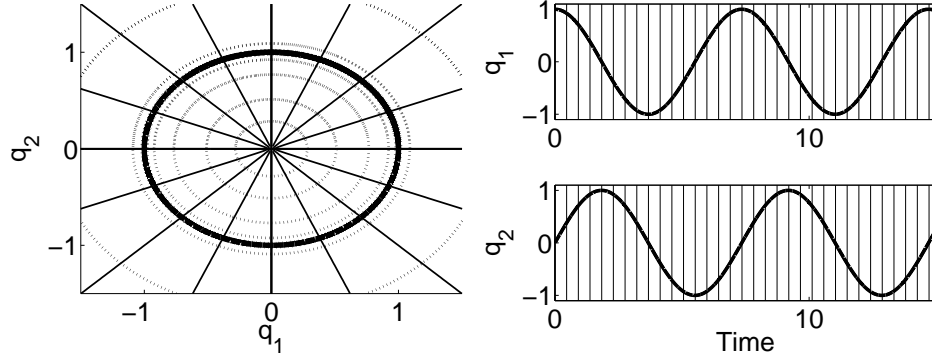
$$\dot{\mathbf{r}} = f(\mathbf{r}_0, \mathbf{r}, \phi) \quad (3.65)$$

Where $f(\mathbf{r}_0, \mathbf{r})$ is DE with stable fixed point \mathbf{r}_0 . The interpretation of ϕ modulo 2π , e.g. in Cartesian coordinates makes it an oscillator, e.g. the Hopf oscillator

$$\dot{x} = (\mu - r^2)x + \omega y \quad (3.66)$$

$$\dot{y} = (\mu - r^2)y - \omega x \quad (3.67)$$

Illustration



References The oscillator in [23] is isochronous.

Amplitude controlled phase oscillators (ACPO)

The ACPO is the extension of the phase oscillator with a radius. The radius is controlled by a differential equation with a fixed point attractor.

Properties The ACPO is simple in the sense that the phase shows up as an explicit state variable. This often allows for analytical treatment [23]. However, in order to achieve higher order locking the input needs to be generating to opportunities for these locking regimes, in the sense that it needs to generate higher order harmonics or sub-harmonics of the input. In contrast to the isochronous oscillator, the differential equation for the radius depends on the phase.

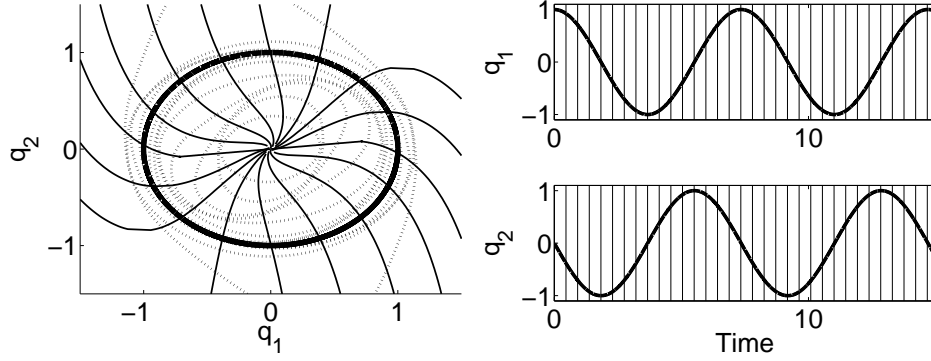
Equations

$$\dot{\phi} = \omega \quad (3.68)$$

$$\dot{\mathbf{r}} = \mathbf{F}(\mathbf{r}, \phi) \quad (3.69)$$

f is a nonlinear function with stable fixed point.

Illustration



Harmonic oscillators – An oscillator with a harmonic limit cycle: i.e. stationary solution $\mathbf{q}_\infty(t) = [r \cos(t), r \sin(t)]$. Note that this term conflicts with the common use to describe a linear second order system. Such a system is however not an oscillator after our definition as discussed above.

Properties Due to its harmonic limit cycle some analytical results on the PS/PRC are possible and thus closed form solutions for phase relationships and locking behavior can be derived.

Typical for harmonic oscillators is a possible description in Cartesian coordinates where the linear second order oscillatory system shows up with an addition of nonlinear terms stabilizing the radius.

Equations

$$\dot{q}_1 = \omega q_2 + f_1(\mathbf{q}) \quad (3.70)$$

$$\dot{q}_2 = -\omega q_1 + f_2(\mathbf{q}) \quad (3.71)$$

See Eqs. 3.58– 3.59 for a concrete example.

Illustration See illustrations for the isochronous oscillator and ACPO which are both harmonic oscillators.

References The Hopf oscillator [98] and the oscillators in [23, 106] are harmonic oscillators.

Piecewise Linear Systems – A system constructed of a set of linear systems of the same order, of which always one is active depending on conditions on the state variables.

Properties Rather straight forward to design and analyze (piece wise solution), can be problematic to simulate. Physical interpretation of switching effect is some fast effect.

Equations Consider the oscillator from [217]

$$\dot{q}_1 = -q_1 - w \max(q_3, 0) - \beta q_2 + 1 \quad (3.72)$$

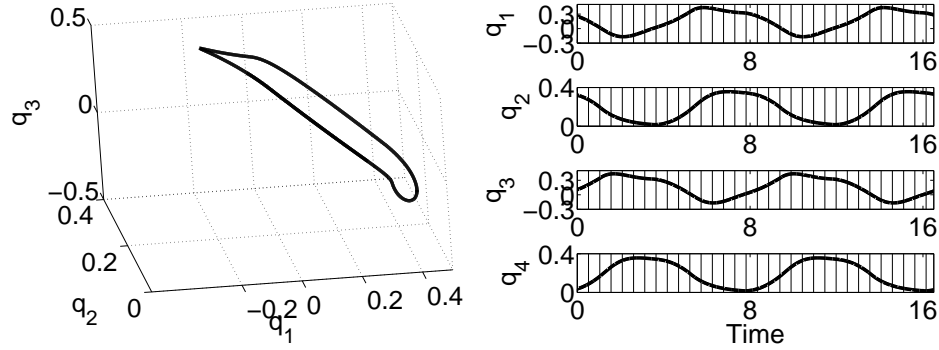
$$\dot{q}_2 = -q_2 + \max(q_1, 0) \quad (3.73)$$

$$\dot{q}_3 = -q_3 - w \max(q_1, 0) - \beta q_4 + 1 \quad (3.74)$$

$$\dot{q}_4 = -q_4 + \max(q_3, 0) \quad (3.75)$$

The system is switched whenever one of the state variables $q_{1,3}$ crosses 0, so the above form is a short form to describe four different systems and oscillates for certain parameter values (e.g. $w = 2.5, \beta = 2$)

Illustration



References The well known Matsuoka oscillators [147], applications of the Matsuoka oscillator in [69, 217]. Such systems are also known as switched linear system or hybrid systems.

Linear systems with reset – A linear, often second order system, which is reset if a variable passes a certain threshold. Those system are an approximation of the relaxation oscillators where we can consider the fast effect to be infinitely fast.

Properties In between resets they behave like a linear system which implies that they are analyzable under this condition, i.e. a partial tractability. Can be problematic for certain solver schemes due to the discontinuity in the ODEs introduced by the reset. Due to the fact that by the reset the whole semi-plane $q_2 > 1$ is reduced to a point ($\mathbf{q} = [0, 1]$), the isochrones and radius-isochrones are identical except for the point on the limit cycle. Therefore, the transformation \mathbb{T} is mathematically problematic.

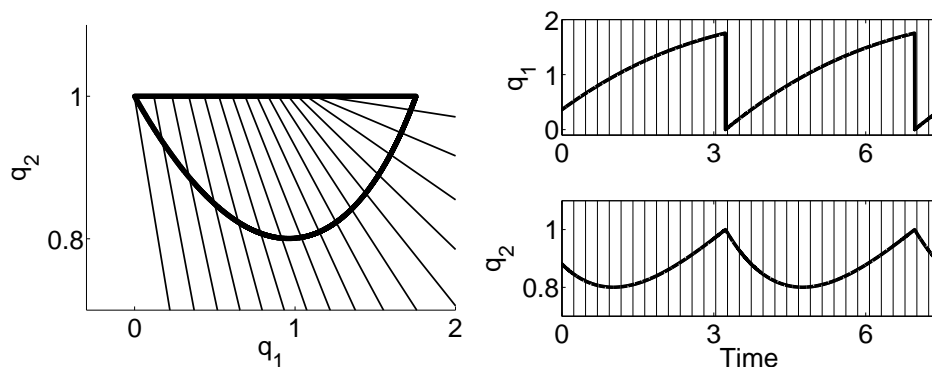
Equations From [112]

$$\dot{q}_1 = bq_1 - \omega q_2 + I \quad (3.76)$$

$$\dot{q}_2 = \omega q_1 + bq_2 \quad \text{If } q_2 > 1, [q_1, q_2] = [0, 1] \quad (3.77)$$

where $b < 0$ and I are constants.

Illustration



References The resonant and fire neurons in [112].

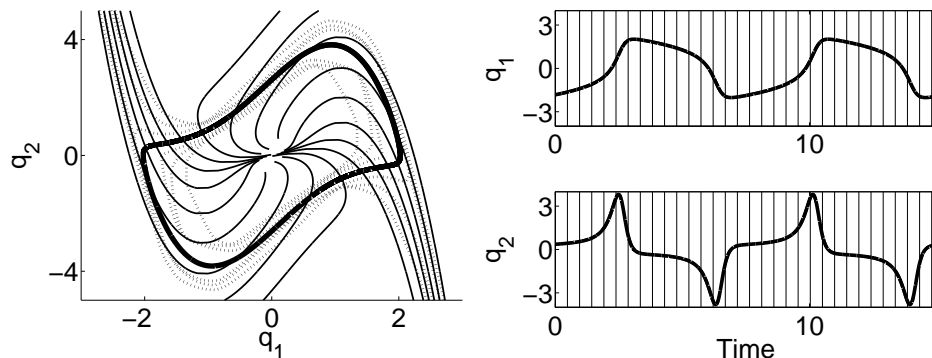
Relaxation oscillators – Properties In general no closed form solution, characteristic phase space with sharp corners, a fast/slow system i.e. two involved time scales which can often be related to physical mechanisms. Relaxation oscillators allow for fast phase locking due to their bent isochrones. Furthermore, they allow naturally higher order locking.

Equations The van der Pol Oscillator

$$\dot{q}_1 = q_2 + p(t) \quad (3.78)$$

$$\dot{q}_2 = \mu(p^2 - q_1^2)q_2 - \nu^2 q_1 \quad (3.79)$$

Illustration



References The well known Hodgkin-Huxley (HH) model of the giant squid axon [96] can exhibit relaxation type oscillatory activity, by a simplification of HH the Fitzhugh-Nagumo (FHN) Oscillator [67] have been derived. The FHN is very closely related to the van der Pol Oscillator.

It is important to realize that a given oscillator can belong the several of the here presented classes (i.e. isochronous, harmonic, ACPO are not mutually exclusive).

3.2.4 Design approaches

Thus so far we have seen *what* can be designed. In this section we address the issue *how* the design goals can be achieved. Thus, as we have seen we need to find structure and parameterization of either \mathbf{F} or \mathbf{T} . Those can be found in different ways, with off-line and online methods.

Off-line – Here the structure and parameters are found by some process before the systems is deployed. Once the system is working they remain fixed. There are different ways to find a suitable structure and parameterization of the ODEs:

- (1) System can be designed by hand, by help of suitable mathematical tools.
- (2) By search/optimization (i.e. an algorithm outside of the dynamical system)
- (3) Dynamically shaped (i.e. the tuning is part of the dynamical system), but once deployed this process is frozen.

On-line adaptation

We could also imagine having some of the parameters changing over time as the system is deployed. This basically means that the parameters are not constant any more. They are turned in a certain sense into state variables as well. Again different approaches can be used: (1) By an algorithm which is outside of the dynamical system. Usually this includes the assessment/measurement of the some predefined quality of the system and an algorithm which tunes the parameters to achieve a better quality. (2) Dynamically – Here the relevant parameters are turned into state variables and a dynamic law in form of ODEs has to be found that will tune the system into the required dynamics. This is very recent research with oscillators (early work [61, 158, 159], more recent [24, 178]). We only call such systems adaptive, since they combine the to be exploited dynamics *and* the adaptation process into a *single* dynamical system. This is also in line with the use of the term adaptive in the framework of adaptive control but is in contrast to the use of the term in many applications of oscillators.

We can thus change the properties as discussed before in Section 3.2.3: (1a,b,c,2a,b) and use the here described design approaches. In table 3.4 we list some of the literature in which oscillators are used either in modeling which had influence on robotic applications, are related to or are directly robotic applications. In the next section we will discuss some aspects of Table 3.4 in more detail.

3.2.5 Design results: From reactive to adaptive oscillators

Thus, we have come a long way in describing the basic characteristic of oscillators, how they lead to design specification and properties. Finally, we would like to discuss some aspects of the resulting system. The resulting systems can have

different properties in terms how they react to the perturbation, how long information about the perturbation is retained. The oscillator can be purely *reactive*, i.e. the perturbation has only a short term, transient effect. Or the system can be *adaptive*. The system has a memory and the effect of the information stays possibly for infinite time. We note this classification in Table 3.4 in the first column by R/A.

Reactive: Temporary entrainment and shape changes

The basic property of structurally stable dynamical systems can be exploited. In other words, the fact that their behavior is a combination of their intrinsic dynamics *and* external input. This means external inputs can partially modify or even “override” the autonomous behavior of the system (annihilate attractors/induce bifurcations). This can possibly be exploited for applications. The changes to the system are reactive in the sense that there is no lasting change in the system. If the input signal is switched off the system will immediately behave according to its original autonomous dynamics. In other words the parameter, i.e. intrinsic dynamics, stays constant. Memory effects can only be realized by the state of phase point and are transient and shortlived. In this category we can count all the exploitation of synchronization, phase resetting etc. (such as in [23, 47, 59, 64, 69, 106, 147, 148, 188, 189, 195, 200, 201, 217–219, 233]). As an example, in case of phase locking the oscillator is matching its frequency to the frequency of the input. This is reactive since the frequency does not stay in the system. The system has no memory of the frequency. The very moment the input is switched off it rotates with the intrinsic frequency. The only remaining perturbation is a possible shifted phase compared to the hypothetically same but unperturbed oscillator. Thus the system is more reactive than adaptive (despite the use of the word in many contributions). One can argue that the above made distinction a reactive and an adaptive system is somewhat arbitrary, but often we can argue by separation of time scales. The “parameters” will usually evolve on time scales slower than the “state variables”. This separation of time-scales is an important concept in physics and engineering to decide which variables are considered static and which dynamic [50, 87].

Entrainment, synchronization & phase locking As we have seen in the previous section, the limit cycle has very characteristic stability properties: It is marginally stable in the direction of rotation. This implies that a perturbation in this direction is not “forgotten” by the system, while the perturbation perpendicular, i.e. asymptotically stable direction, to the limit cycle are damped out.

We can exploit the synchronization properties of a limit cycle system to slightly modify the oscillators timing so that it works “in step” with some outside process. A meanwhile very common application in robotics is to exploit synchronization for legs to work in step with some sensorial input (e.g. touch sensors on the foot,

cf. [69, 155, 217]).

An important aspect in the design of oscillator especially if they are coupled with others into networks is often the question how to design the phase relationship, i.e. with which phase lag the activity of the oscillator is synchronized with the perturbation. An interesting approach to desing specific phase lags is the to use contraction theory [228].

As we have seen important concepts for the designing are the phase response curve (PRC) [166] or the more general concept of Phase sensitivity (PS) [23, 62, 133]. PRC/PS can be derived in an analytic fashion only for some types of oscillators (i.e. harmonic oscillators, phase oscillators; thus they might be the oscillator of choice for this reason). Basically having a closed form of PRC/PS is equivalent in knowing the closed form of the limit cycle. However for other, non-tractable oscillators, we can measure the PRC/PS by numerical integration. The PRC and PS typically have zeros which means that a perturbation arriving when the oscillator is at this phase does not affect the phase. The phase of the oscillator will thus be shifted by a perturbation until it reaches this point and remain there (given it is a stable point). This means to design a certain phase relationship, we have to design either the PRC/PS of the system, i.e. its zeros or need a filter to the input that the desired phase relationship is attained (e.g. rotation of signal as in [23]).

In [23] a discussion about the choice of oscillators can be found an it is shown that the simpler oscillators allow for a good design of some of the properties of network of oscillators used as CPG.

A key requirement for synchronization is that the frequency of the oscillator needs to be close to the frequency of the input. If the differences between the frequencies is large the oscillator does not fully synchronize, it will only show a tendency to synchronization, an effect which is called phase slips [166]. In average the signals of the oscillators will drift relative to each other. A way around this problem is to make the frequency adaptive which will be discussed in the next subsection.

Another way of designing phase relationship in networks of coupled oscillators is by help of the theory of symmetry, where the phase pattern can be achieved without the single oscillator satisfying necessarily the correct properties in the PRC/PS [76, 180, 195]. However, even along with this method the consideration of the properties of the single oscillator helps to design non-frustrated systems, i.e. systems where the individual behavior is in accordance with the global pattern, which settle down faster and are more stable. The synchronization properties can also be exploited to sequence and time actions as outlined in [188, 189, 201].

Inter cycle timing Another desired property could be that the input signal should influence the instantaneous frequency without changing the average observed frequency. The key to such behavior is the property 1) in Table 3.3 and discussed before. While we are not aware of a contribution directly exploiting this

characteristic it would be straight forward to impose an additional constraint on the oscillator used in [180] to satisfy this property.

Reactive shape changes Changes of radius are less frequently exploited than the entrainment effects. But of course due to the stability properties we can very well imagine an input which deflects the limit cycle by changing temporarily the fixed point for the radius. This translates in the outputs to have temporarily a larger or smaller amplitude. An example can be found in [181].

Shaping the dynamical system Another way of designing an oscillator with given output is to use a system which is a universal approximator and approximate the oscillator with this dynamical system. In [71,139,185] the authors use recurrent neural networks to achieve arbitrary limit cycles. The disadvantage of this method is that it usually leads to a very high dimensional system of which the influence of the parameters can not easily be grasped.

An alternative way to changing the intrinsic dynamics of the oscillator is to shape its output into to some given form with filters. One possibility is to design the filter purely functional or to design a dynamical dynamical system which transforms the output (cf. linear filter). In [110] the authors use Gaussian filters shaped by locally weighted learning. In [236] the authors use Neural Networks as filters. The use of filters has the disadvantage that a discontinuous change in the parameters of the filter can lead to a discontinuous change in the output (i.e. one of the advantages of using dynamical systems is negated). In [163] shaping of arbitrary limit cycles is discussed by a direct design of the flow. In [181] the authors shape the limit cycle by help of a network of adaptive frequency oscillators.

Adaptation: Lasting changes to the dynamics

In this section we address *lasting changes to the intrinsic dynamics*, i.e adaptation. Such lasting changes could also be called learning and in some communities this is the preferred term. We do use the terms as equivalent here.

As we have seen the limit cycle system is parameterized by a set of parameters ρ , which are usually kept constant. Adaptation means now that we find a law to change some or all of the parameters so that an adaptation goal is achieved. There are two conceptually different ways of achieving that, either the parameters are changed by an external process or algorithm, or the dynamical system itself gets enhanced with additional state variables and ODEs that represent the parameters and their evolution respectively. This means we have to find suitable differential equations $\dot{\rho} = \mathbf{F}_{\rho}(\mathbf{q}, \rho, t)$. This implies that the set of parameters reflects the state of the adaptation process, especially also after the system is halted. We can thus possibly also read out certain information about the system. This adaptation process constitutes a longer-term memory, in contrast to the reactive changes in the previous section which are forgotten and do not get remembered in the state of the parameters.

The first, algorithmic method, is from the methodological point of view simpler since standard optimization, learn and search techniques can be employed. In [144] Powell's method is used to optimize the parameters of an oscillator network. Many other optimization methods could be used for similar tasks. The second, dynamic method, is more appealing from the conceptual point of view and leads to more efficient and robust solutions (cf. [30]).

Dynamic adaptation of limit cycle systems is a more recent development and young field of research. There are some investigations on adaptation of parameters (frequency, others), e.g. in [24, 137, 159, 178].

An example is introduced in [24] and analyzed in detail in [178] where a Hopf oscillator (Eqs. 3.66–3.67) is enhanced with a evolution law for the frequency ω in the following way

$$\dot{\omega} = -k \frac{y}{\sqrt{x^2 + y^2}} p(t) \quad (3.80)$$

where k is a coupling constant and $p(t)$ an additive perturbation to Eq. 3.66. This law allows the oscillator to adapt to the frequency of the perturbation $p(t)$. Such an additional law for the parameter ω endows the system with many very nice properties and can be exploited for different tasks such as adaptation to body dynamics [24, 28, 30] or programmable CPGs [181].

As can be seen in Table 3.4, the column with the adaption is only sparsely populated. A lot of questions have to be answered and methodologies have to be found.

Adaptation can also be used in the design phase and then the adaptation process is frozen for the deployment phase (i.e. online vs off-line adaptation). This means the dynamics is adapted, then remains fixed for the application (learning/exploitation phase is distinguished) whereas in the first case the adaptation works continuously.

3.2.6 Conclusion & Discussion

Discussion of design choice Oscillators have been used widely in robotics over the last few years with a lot of success, however a lack of abstraction often leads to suboptimal solutions for the given goal. These suboptimal choices arise due to a lack of abstraction of the concepts and/or a fixation on traditionally used oscillators.

For engineering of an application with oscillators we first of all have to get clear what feature of an oscillator is the important one for the task. In other words, we have to decide if its a *generic* feature of oscillators, of a class of oscillators, or if its unique to a certain oscillator/input/output.

We have to think about readouts, what information needs to be available, e.g. an oscillatory output signal with certain properties (e.g. harmonic), or does the phase of the oscillator have to be available as output? We can then think if one of the well known oscillator/coupling schemes which is suitable for the task at hand.

Of course sometimes it can be helpful to take an existing oscillator and modify it to fit (cf. e.g. [116, 180])

Most of the time oscillators are used for their synchronization properties. Thus, we are interested in how the phase ϕ behaves over time. In addition influence on the radius can be exploited, but this is far less common. This means that for many applications the phase oscillator will be a good and completely sufficient choice.

While it is often very convenient to use a phase oscillator we have to be careful with coupling which explicitly use the phase of the input signal (i.e. as it is often done in work on coupled phase oscillators). Because couplings that worked out this way do usually not generalize so easily to a general periodic signal of which the phase is not directly accessible. A way to bridge the gap and to investigate arbitrary periodic signals are Fourier series.

As always in engineering it is not possible to give rules that are valid for all cases, but important questions to guide the choice of oscillator and design strategy are:

- First and foremost: get clear about the design goals, i.e. what property of an oscillator do you want to exploit and why?
- Is direct access to the phase or the frequency required? In other words, should they be presented as explicit variable and parameter?
- Is there a restriction in the number of state variables and complexity of integrating the system (e.g. for embedded computing)?
- Should it be possible to prove or predict analytically properties of the system (convergence, phase relationship)?
- How many elements should the system contain, i.e. is a network of oscillators needed (e.g. half-center, interneurons) or might a single oscillator be enough?
- Is there an advantage to use a strongly nonlinear oscillator or is a harmonic/phase oscillator enough, e.g. is a “neural” oscillator really the right one to achieve my goal? In modeling, does my model really concern the neural level so that the use of a neural oscillator is justified?
- Try to make the design space as orthogonal as possible (e.g. in the Matsuoka oscillator there is a strong influence on the shape if the oscillator gets coupled to others).
- Should the complexity and nonlinearity be placed into the oscillator or into the coupling (e.g. for higher order locking: either, phase oscillator and coupling which generates the higher order frequency components, or complex oscillator and simple couplings.)?

An often made assumption to treat limit cycle systems is the assumption that influence on phase and radius can be completely separated, this assumption directly follows out of the stability directions as discussed. However, a perturbation

perpendicular to the limit cycle can in general very well have an influence on the phase and vice versa (e.g. in the van der Pol) the separation of the directions is a very useful approximation but is limited to a region “close” to the limit cycle. If we want to have a complete separation the oscillator has to be chosen accordingly, i.e. a harmonic isochronous oscillator.

Sometimes it is desired to synchronize the signal in another ratio than 1:1, in general oscillators can phase lock in any ratio n/p $n, p \in \mathbb{N}$. However, harmonic oscillators are not sufficient to achieve this task unless the input contains higher harmonics (ideally pulse like). Relaxation oscillators can phase lock with other ratios to a harmonic signal.

Finally, it is important to stress that there are many design aspects which in this article could not be discussed. As an example consider transient time for locking. It turns out that relaxation oscillators are well suited for rapid phase locking [208], this is due to the bent isochrones, i.e. even a small perturbation can drive oscillator over many isochrones and thus advance it rapidly in towards a stable phase. We see that also for such discussions the basics are the topics discussed in the paper.

We do not address another way of distinguishing two dynamical systems namely by their bifurcation behavior. In dynamical systems it is a typical phenomenon that if some parameters are changed beyond a critical value the qualitative behavior of the system can completely change, e.g. an oscillator can bifurcate to fixed point behavior. If two systems differ in their bifurcation behavior it is usually not possible to transform one into the other by only a change of coordinate systems. Different oscillators can have different bifurcation behavior. It is important to realize, that we do only discuss the oscillators in their oscillatory regime, far away from the bifurcation points and the above made statements are only valid in this parameter range.

Furthermore, we have simplified the discussion by the fact that we do only concentrate on the limit cycle attractor of the system, while it can possibly have other attractors. Thus our discussion is limited to the basin of attraction of the limit cycle attractor (e.g. every limit cycle encloses a unstable fixed point from which the solutions would not converge to the limit cycle).

Outlook and future research It is an immense task to classify the design of oscillators and many details could not be discussed in this article.

We are convinced that taking an engineering perspective on oscillators is needed in order to make full use of them in robotics applications. This paper is only a first step in that direction.

It is possible that an engineered system might lack some of the self-organization properties and flexibility of natural oscillatory networks, but this is a fundamental problem when trying to exploit systems capable of self-organization to engineering. On the other hand we gain methodology, guarantees, but clearly such questions are open for research, see [33] for a deeper discussion.

There are many substrates other than digital computers which allow for structurally stable oscillators, i.e. chemical oscillators, (analog) electronic, biological (see also [33]). Choosing such a substrate however narrows down the degrees of freedom in the design, but still the key to understanding and engineering those systems is presented in this article. It would of course be interesting to exploit such substrates for engineering applications.

Acknowledgments This work is funded by the Swiss National Science Foundation (A.I. & J.B.) and by the European Commission's Cognition Unit, project no. IST-2004-004370: RobotCub (L.R.).

contribution	R/A	offline			online	
		“by hand”	algorhythmic	dynamic	algorhythmic	dynamic
[64]	R	1a				
[233]	R	1a				
[106]	R	1a				
[147, 148]	R	1a				
[195]	R	1a				
[200]	R	1a				
[59]	R	1a				
[155]	R	1a				
[180]	R	1b				
[217–219]	R	1a				
[23]	R	1a				
[69]	R	1a				
[188, 189, 201]	R	1a				
[47]	R	1a				
[104]	R		1a/2			
[236]	R		2b			
[163, 164]	R		2a			
[110]	R		2b			
[185]	R		2			
[71, 139]	R		2			
[181]	R			1a/2b		
[144]	A				1a	
[159]	A					1c/1a
[61]	A					1c
[137, 138]	A	1a				1c
[24, 28, 30, 178]	A					1c

Table 3.4: Table classifying some of the contribution of the field oscillators applied to robotics and related modeling. The contributions are classified according the the design method as discussed in Section 3.2.4. The labels in each case correspond the design goals identified in Section 3.2.3: (1) Timing: Design that influence the phase of the oscillator: (a) influence on (relative) phase, (b) instantaneous frequency, and (c) average frequency. (2) Design that influences the geometry of the oscillator: (a) influences on r , (b) the design of T^{-1} / output filter. The column “R/A” indicates whether the resulting system is reactive or adaptive. This table has sparsely populated columns which point to open research question.

Chapter 4

Adaptive Locomotion Reduced to the Essential: A Toy-System

THIS chapter introduces one of the central concepts of the thesis, *the adaptive frequency oscillator*, along with their use as adaptive controllers.

The motivation for the introduction of the AFO was to find the simplest controller which can adapt to a clearly defined body property. The body property has been chosen to be the resonant frequency as this is a clearly defined concept and we can easily construct simple systems with clearly defined resonant frequencies. (And as we will see later, 2nd order LTI systems possess this property which comes handy for more advanced analysis of the AFOs in feedback loops, cf. Chapter 6).

Moreover, the system is an application of the previously introduced ideas. It shows that based on the ideas in the last chapter, namely a simplification of the dynamical systems and a reduction to the essential features of the locomotion system.

While the original formulation of the AFOs was very much oriented on the application to the toy-systems, only later on –step by step– many more interesting properties of the AFOs and their possible applications have been discovered.

The proposal of a toy-system is very much in the tradition of physics, where it is a successful method to propose systems which allow to study certain aspects of a problem by deliberately neglecting certain, for the problem irrelevant, aspects of the real system. By this the systems get simpler and amenable to scientific investigation. Since it is not always clear from the on-set what the relevant mechanisms are, such systems have to prove their suitability to explain the investigated phenomena later on. As we will see in the next chapter, the concept that we propose does work without fundamental modification from the simplest system, as proposed here, to real robots. We can thus argue that some of the assumptions that are the basis of the formulation of the toy system are at least not completely wrong.

A Simple, Adaptive Locomotion Toy-System

Jonas Buchli and Auke Jan Ijspeert

This paper has been originally published as
 J. Buchli and A.J. Ijspeert. A simple, adaptive locomotion toy-system.
 In S. Schaal, A.J. Ijspeert, A. Billard, S. Vijayakumar, J. Hallam,
 and J.A. Meyer, editors, *From Animals to Animats 8. Proceedings of
 the Eighth International Conference on the Simulation of Adaptive
 Behavior (SAB'04)*, pages 153–162. MIT Press, 2004

Abstract In order to successfully transfer biological principles to engineering problems, it is important to study the fundamental properties of biological systems. The goal is to arrive with useful abstractions that are (1) implementable, (2) testable by experiments and sample implementations, (3) retain the, for an engineering point of view, essential good properties of the biological systems. At BIRG, we are interested in the fundamentals of locomotion control and their possible applications to robotics. In this article, we present a simple, adaptive locomotion toy system that is of oscillatory nature. It is composed of two parts: an adaptive controller based on a nonlinear oscillator, and a mechanical system made of two blocks attached by an active and a passive spring. The controller is designed to be robust against perturbations, and to adapt its locomotion control to changing body kinematics or added external load. The tools to develop such a toy-system are a 2-scale nonlinear dynamical system, namely a Hopf oscillator with adaptive frequency, and a understanding of synchronization behavior of oscillators. A further central ingredient that will be discussed is the concept of asymmetric friction forces. We show that the system possesses several critical parameters. It is illustrated that the bifurcations connected with some of these parameters can be identified as non-smooth phase transitions and power law behavior. Links to biology and possible applications to robotics are discussed.

4.0.7 Introduction

Natural locomotion systems are of great interest for robotics as they present refined and robust solutions to a difficult engineering challenge. Namely, they manage to coordinate multiple degrees of freedom needed for locomotion, using signals of the right frequencies, phases and amplitudes [105]. However, any given natural locomotion system is of great complexity. In the case of a vertebrate locomotion system, it consists of an enormous number of muscle and neural cells and many other types of body parts such as bones, tendons, etc. And even the locomotion apparatus of single cell organisms turns out to be of astonishing complexity [145].

However, as many people have pointed out, simple copying of biological processes can not be what we have to strive for when trying to enhance engineering principles by biological inspiration. It is rather the identification of the principles

at a given level of abstraction that makes adaptation of biological principles for engineering problems successful [23].

Therefore, we have to look for fundamental principles underlying locomotion. In order to identify these principles, a broad range of locomotion systems have to be looked at. This includes single cell movement, worm, snail, snake, insect and mammalian locomotion, different types of flying and swimming but also more abstract concepts like active Brownian particles and ratchet systems.

When we try to find a few abstract principles common to all types of locomotion the following key observations arise:

- Locomotion is the process of transforming energy (unordered movement of many parts, particles) into directed movement (coordinated movement of the particles).
- From the first point we can directly conclude that locomotion always implies an active system and consumes energy¹.
- Any form of locomotion implies asymmetric interaction forces with the environment, e.g. an asymmetric friction mechanism (it turns out that this mechanism is what renders locomotion into a energy consuming process).
- Biological locomotion is robust, i.e. works under a very broad range of external (temperature, external forces, textures, ...) and internal (body properties, fatigue, sicknesses, ...) conditions. There are adaptation processes inherent in the locomotion systems to ensure this robustness.
- The adaptation processes work on many, very different timescales. In other words, the time scales of, for instance, locomotion control, adaptation to fatigue, and adaptation to body development span over several orders of magnitude.

In order to make these fundamental principles accessible to theoretical and experimental investigation without the overhead of complicated experimental setups and difficult to control environments and subjects (all of which can easily hamper clear insight) we are looking for simple systems that, nevertheless, show all the properties listed above. Here we will report on a particular simple instance of a nonlinear dynamical system that possesses the described properties.

Modeling neuro-mechanical systems with oscillators During the last decades there have been growing numbers of attempts to model locomotion control systems with the help of oscillators [23]. On the other hand bio-mechanical systems were modeled by spring mass systems or inverted pendulums - and are therefore of oscillatory nature [13, 70]. The logical consequence to model the complete neuro-mechanical systems by coupled oscillators has been used [218] and

¹The consumed energy can be potential energy (e.g. passive walkers) as well as energy from active mechanisms.

robotics controllers have been developed on the base of oscillators [156]. Oscillators are an important and widely used system to model phenomena in a broad range of fields. Often, simple oscillators with fixed parameters such as frequency and damping are used. Recently however, it was found that for modeling certain phenomena, oscillators with fixed frequencies are not sufficient. Therefore, oscillators with adaptive frequencies are investigated [4, 5].

Exploiting adaptive frequency oscillators for locomotion control In this contribution we show that by using a Hopf oscillator with adaptive frequency we can devise a controller that adapts to the resonant frequencies of the mechanical system and therefore excites it. Together with asymmetric interaction forces with the environment – which turn out to be a fundamental property of any locomotion system – this leads to directed movement. There are 3 core ideas in our approach.

- The (bio)mechanical system is of oscillatory nature. I.e. it possesses resonant frequencies at which it can easily be excited.
- The controller is of oscillatory nature.
- The intrinsic frequency of the oscillator is adaptable and gets influenced by the mechanical system.

by the proper choice of the mechanical system and the controller, a system that is self-exciting and adaptable can be devised. In order to convert the oscillatory movement of the mechanical system into directed movement a fourth fundamental property is necessary: The system needs some type of asymmetric interaction forces in our case asymmetric friction, i.e. the friction coefficients are lower for one direction compared to the other.

We use a simple mechanical spring-mass system to investigate the requirements needed for such a system to make directed movement. Furthermore, we are interested in a (simple) controller that is able to adapt to changing properties of the mechanical system (i.e. growth, mass changes, length changes).

4.0.8 A Simple, Adaptive Locomotion Toy-System

In order to study the aforementioned fundamental principles we devised a simple mechanical system controlled by an oscillator. We will describe the two main constituents of the system and their important properties along with how the two subsystems get connected in order to build the adaptive locomotion system.

Mechanical system The mechanical part of the system consists of two masses connected by two parallel springs S_a, S_p (cf. Fig. 4.1(a)), with different resting lengths l_a and l_p . For convenience, we will express them as $l_a = l_m + l_d$ and $l_p = l_m - l_d$, where l_m is the mean value and $2l_d$ the difference between both lengths. Both springs are linear springs with spring constant k_a, k_p . The system

presented in this article is one-dimensional, in other words, the masses are assumed to move on, and remain in contact with, a horizontal plane and moving on a straight line. In the following, we present the mathematical description of such a system in terms of a system of differential equations. The system can be written as follows:

$$\dot{\mathbf{q}} = \mathbf{A}\mathbf{q} + F_c + F_r(\mathbf{q}) \quad (4.1)$$

where $\mathbf{q} = [x_1, v_1, x_2, v_2]^T$ are the state variables of the system (position and velocities of the two masses), \mathbf{A} is the matrix describing the action of the spring on the masses (without any friction), F_r is the friction present in the system and F_c is constant force arising from the differences and mean value of the resting length of the springs. \mathbf{A} takes the following form

$$\mathbf{A} = \begin{pmatrix} 0 & 1 & 0 & 0 \\ -\frac{k_a+k_p}{m} & 0 & \frac{k_a+k_p}{m} & 0 \\ 0 & 0 & 0 & 1 \\ \frac{k_a+k_p}{m} & 0 & -\frac{k_a+k_p}{m} & 0 \end{pmatrix} \quad (4.2)$$

where m are the masses attached at each end of the springs. And,

$$F_c = \frac{l_d(k_p - k_a) - l_m(k_a + k_p)}{m} [0, 1, 0, -1]^T \quad (4.3)$$

With the choice of l_m and l_d the resting position of the masses can be influenced. The choice of the friction term F_r will be discussed below. Such a second order linear system possesses a resonant frequency, which can be calculated as:

$$\omega_m = \sqrt{\frac{2(k_a + k_p)}{m}} \quad (4.4)$$

In other words, this type of mechanical system can be interpreted as a band pass filter with the pass band around ω_m . For generating displacements of the system, we replace the spring S_a described above with an active spring whose spring constant k_a can be modulated by a controller (see next section). The active spring can be seen as an abstract muscle-like actuator that can both pull and push.

Hopf oscillator As controller/activator of the mechanical system, we use a Hopf oscillator:

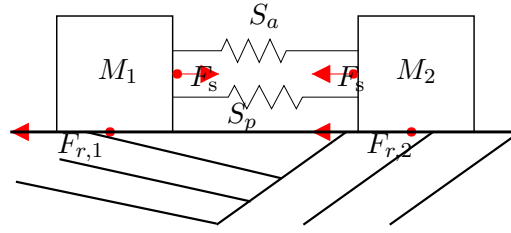
$$\dot{z} = (\mu_h + i\omega_h)z - |z|^2 z + F(t), \quad z \in \mathbb{C} \quad (4.5)$$

which can be written in Cartesian coordinates:

$$\dot{x}_h = (\mu_h - r^2)x_h + \omega_h y_h + F_x(t) \quad (4.6)$$

$$\dot{y}_h = (\mu_h - r^2)y_h - \omega_h x_h + F_y(t) \quad (4.7)$$

a)



b)

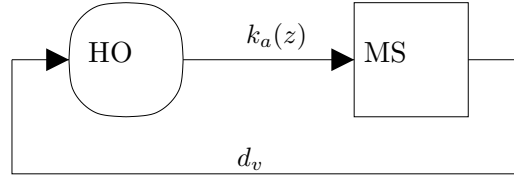


Figure 4.1: a) The mechanical sub-system of the adaptive locomotion toy system. It consist of two identical masses connected by a spring. From the mechanics of the system the forces acting on the body can be determined: F_s is the force that the springs exert on the blocks. It is of the same amplitude and opposite sign for the two masses. $F_{r,i}$ are the friction forces acting on the masses. With the help of this forces and Newton's law we are able to derive the system of differential equations that govern the mechanical system (Eq. 4.1). b) Schematic of the adaptive locomotion toy-system with its two main parts: The Hopf Oscillator (HO) and the spring mass system (MS). The Hopf Oscillator influences the mechanical system via the spring constant $k_a(z)$. The mechanical in turn disturbs the Hopf oscillator by coupling in the velocity difference d_v as an additive disturbance to the Hopf Oscillator equations.

where $x_h = \text{Re}(z)$, $y_h = \text{Im}(z)$ and $r = |z| = \sqrt{x_h^2 + y_h^2}$. ω_h is the intrinsic frequency of the oscillator and $F_x(t) = \text{Re}(F(t))$ and $F_y(t) = \text{Im}(F(t))$ are perturbing forces. The solutions of this system will be discussed below. The Hopf oscillator is coupled to the mechanical system in the following way (cf. Fig. 4.1(b)): First, the spring constant k_a is made a function of z in the following form:

$$k_a = k_0 + a \frac{x_h}{r} \quad (4.8)$$

where k_0 is a constant for the offset of the spring constant and a is a coupling constant, where $a < k_0$ to ensure S_a remains a spring ($k_a > 0$). Since x_h will be an oscillating term, this choice of coupling leads to an undulatory modulation of k_a , where the frequency of the modulation will be ω_h . The division by radius r serves to normalize the maximum of the modulation term to 1.

Second, the Hopf oscillator has feedback from the mechanical system:

$$F(t) = c d_v \doteq -c(v_1 - v_2) \quad (4.9)$$

where c is a coupling constant. Here, the choice has been on the considerations that mainly the coordination between the two bodies is important. Therefore, the choice of a difference term². The choice of the difference of velocities is chosen in order to have a more sensitive coupling in contrast to choosing the difference of positions³.

Properties of the Hopf Oscillator The Hopf oscillator acts as a frequency selective amplifier [58], i.e. frequency components of $F(t)$ that are close to ω_h are amplified. Especially the setting $\mu_h = 0$ is special in the sense that the system undergoes a fundamental change at that point: For $\mu_h < 0$ the system exhibits a stable fixed point at $z = 0$, whereas for $\mu_h > 0$ a stable limit cycle occurs with radius $r = \sqrt{\mu_h}$. This phenomena is known as a Hopf bifurcation [98]. At $\mu_h = 0$, there is no signal oscillating at ω_h weak enough not to get amplified by the Hopf oscillator. Therefore, for that setting the Hopf oscillator can be considered an ideal amplifier⁴. This means that, if the resonant frequency ω_m of the mechanical system and the intrinsic frequency ω_h are close enough, any signal components close to the resonant frequency of the mechanical system get amplified. Thus, an excitation of the system can be expected.

In case of a biological setting, this would correspond to a case where the activation pattern of the muscles is well adapted to the properties of the mechanical system, and, therefore, a very energy efficient mode of locomotion can be expected where only a small amount of energy has to be spent in order to maintain

²Such a difference is also more plausible from the practical and biological point of view, where no absolute values can play a role.

³It is expected, however, that with a proper choice of the coupling constant the qualitative behavior should not depend on this choice.

⁴We can not delve into the mathematical details of the Hopf oscillator in this contribution. For a more detailed treatment see e.g. [123] and references therein.

high locomotion velocity⁵. Animals possess adaptive processes which bring the locomotion system to (near) optimum mode of operation.

Adaptive frequency oscillator In our toy-system, adapting the oscillator to the mechanical systems means a proper choice or a tuning of ω_h . But, we can avoid manual tuning of ω_h by enhancing the dynamical system describing the Hopf oscillator. Instead of fixing ω_h we treat it as a variable with a corresponding differential equation describing the time evolution:

$$\dot{\omega}_h = f(\omega_h, q, t) \quad (4.10)$$

The choice of $f(\omega_h, q, t)$ that serves our purpose is chosen by understanding the synchronization behavior of two coupled oscillators. To get a good grasp on the effects of perturbations on a limit cycle system it is helpful to look at it in the phase plane representation (cf. [213]). In the phase plane all perturbations have a direction, i.e. they can be represented as a vector in that plane. It is known that a small perturbation of a limit cycle system can only affect that phase strongly if it perturbs the oscillator in direction tangential to the limit cycle, the perturbations perpendicular to the limit cycle are damped out⁶. Thus, depending on the state of the oscillator (the position of the phase point on the limit cycle) the perturbation accelerates the phase point or slows it down. If the perturbation is a periodic signal, with a frequency close to the intrinsic frequency of the oscillator, this results in an average acceleration or deceleration depending on the frequency difference and to synchronization. If we take this same effect to tune the frequency of the oscillator (on a slower time scale) the frequency should evolve toward the frequency of the perturbation. Therefore, the effect of $f(\omega_h, q, t)$ is the same as the effect leading to synchronization. Thus, (in average) driving ω_h toward ω_m . On that ground, we chose

$$\dot{\omega}_h = -\tau_h d_v \frac{y_h}{r} \quad (4.11)$$

where $\tau_h \ll 1$. However, the adaptation of ω_h happens on a slower time scale than the evolution of the rest of the system. This adaptation time scale is influenced by the choice of τ_h .

As explained, the output of the Hopf oscillator is coupled via setting $k_a = f(z)$ to the mechanical system. The mechanical system serves as a bandpass filter. Therefore, the Hopf oscillator, via the aforementioned feedback, slowly adapts its frequency to the mechanical system.

⁵Everybody knows this effect from sitting on a swing and trying to get it to move. If one moves the legs at the right frequency, with a minimum effort the swing can be brought to breathtaking heights.

⁶This is, of course, a simplification of the real facts. In fact, perturbations perpendicular to the limit cycle can, in general, perturb the phase of the oscillator. However, for the case of phase oscillators, such as the Hopf oscillator, the above simplification comes very close to the real thing. To discuss the general case is beyond the scope of this article.

In order to measure the excitation of the system we can use the energy content of the mechanical part. There are two contributions to the energy of the mechanical system: The kinetic energy of the masses $E_k = \frac{1}{2}m(v_1^2 + v_2^2)$ and the potential energy of the springs $E_p = \frac{1}{2}(k_a(x_2 - x_1 - l_m + l_d)^2 + k_p(x_2 - x_1 - l_m - l_d)^2)$. We will use this formalism to investigate the optimal excitation frequency of the system in the next section.

Friction Friction dissipates the energy of the system. Therefore, if no energy is pumped into the system the system will always come to standstill from any initial condition. We have tested the system with two different friction schemes: viscous friction and Coulomb friction. Both are introduced as asymmetric friction forces, i.e. the parameters are lower for one direction compared to the other. In viscous friction, the friction force is proportional to the velocity of movement:

$$F_r = [0, -\rho_1 v_1, 0, -\rho_2 v_2]^T \quad (4.12)$$

where

$$\rho_i = \begin{cases} \rho_+ & \text{if } v_i > 0 \\ \rho_- & \text{if } v_i < 0 \end{cases} \quad (4.13)$$

The second model that has been tested is the Coulomb friction model, in which the friction coefficients are constant:

$$F_r = [0, F_{c,1}, 0, F_{c,2}]^T \quad (4.14)$$

$$F_{c,i} = \begin{cases} -|F_s| & \text{if } F_s < \mu_S |F_N| \text{ and } v_i = 0 \\ -\frac{v_i}{|v_i|} \mu_{r,i} |F_N| & \text{otherwise} \end{cases} \quad (4.15)$$

where $F_N = gm$ is the normal force of the body on the ground, and F_s is the spring force acting on the body. Coulomb friction has a static mode (when $v_i = 0$) and a dynamic mode. In our case, the dynamic friction is made asymmetrical as follows

$$\mu_{r,i} = \begin{cases} \mu_+ & \text{if } v_i > 0 \\ \mu_- & \text{if } v_i < 0 \end{cases} \quad (4.16)$$

With the Coulomb friction scheme the system would be unstable since the increase in the input of energy is increasing faster than the dissipation of energy due to friction. In order to avoid this instability problem, the coupling from the Hopf oscillator is slightly changed. The coupling constant a is made dependent on the rate of change of distance of the two masses, i.e. the velocity difference:

$$a_{coulomb} = \begin{cases} a & \text{if } |v_1 - v_2| < v_{thr} \\ 0 & \text{if } |v_1 - v_2| > v_{thr} \end{cases} \quad (4.17)$$

In other words, the coupling is switched off, if, due to heavy excitation the masses separate too fast. Thus, the mechanical system runs passively for a short moment when reaching this maximum velocity until the spring forces and dissipation of energy bring it again below that threshold.

For this article the default friction model is the viscous model unless otherwise noted.

4.0.9 Simulation Results

The basic mode of locomotion is presented in Fig. 4.2(a). We show in vertical order consecutive snapshots of the mechanical system, at every 0.05 s. The locomotion of the system most closely resembles rectilinear-movement observed in some types of worms and snakes. The two masses exhibit an undulatory movement by which they are constantly stretching and compressing the springs between them. Due to the asymmetric friction forces one of the bodies is pushed (dragged respectively) toward one direction.

For the remainder of this section we would like to illustrate a few other important aspects of the presented locomotion toy-system. First, we list the parameters and initial conditions used in the simulations (unless otherwise noted):

Default parameter values				Default initial conditions	
parameter	value	parameter	value	variable	initial value
μ_h	0	l_m [m]	12	z	0
τ_h	0.1	l_2 [m]	0.5	ω_h [rads ⁻¹]	12
c [sm ⁻¹]	0.1	ρ_+ [Nsm ⁻¹]	0.2	x_1 [m]	0
a [Nm ⁻¹]	10	ρ_- [Nsm ⁻¹]	0.1	v_1 [ms ⁻¹]	0
m [kg]	1	μ_s	0.3	x_2 [m]	11.595
k_0 [Nm ⁻¹]	10	μ_+	0.21	v_2 [ms ⁻¹]	0
k_p [Nm ⁻¹]	100	μ_-	0.19		
v_{thr} [ms ⁻¹]	10				

In order to verify that the frequency calculated above is really the resonant frequency of the whole system (Hopf oscillator included) we make the following numerical experiment. We set $\tau_h = 0$, i.e. we go back to the fixed frequency oscillator. Then, we numerically integrate the system for different values of ω_h over a duration of 100 s. In Fig. 4.3, the resulting average energy content of the system is plotted against ω_h . The vertical lines depict the resonant frequency of the mechanical system and its 0.25, 0.5, 2,3 and 4 folds. As expected, the broadest peak is measured around the mechanical resonant frequency. Furthermore, there is a second strong peak (even higher amplitude but less broad) close to the harmonic $2\omega_m$. Apparently, the resonant effects at that point are very strong. Also around $0.25\omega_m$ and $0.5\omega_m$ resonant effects can be observed. They are however, much less strong. Furthermore, there seems to be a systematic shift of the resonant frequencies toward lower values for $\omega_h < \omega_m$ and toward higher values for $\omega_h > \omega_m$. In the lower panel the attained mean velocity of the center of mass is given. We see that that it follows the same pattern as the energy content of the mechanical system.

Henceforth, we introduce frequency adaptation into the Hopf oscillator by setting $\tau_h = 0.1$ and investigate the adaptation capability. We illustrate that the adaptation of ω_h leads to an increase of the forward velocity of the system. To get a first idea of how the system adapts ω_h and how this influences the speed of the mechanical system, we show a representative plot of ω_h and x_1 in Fig. 4.4(a) and

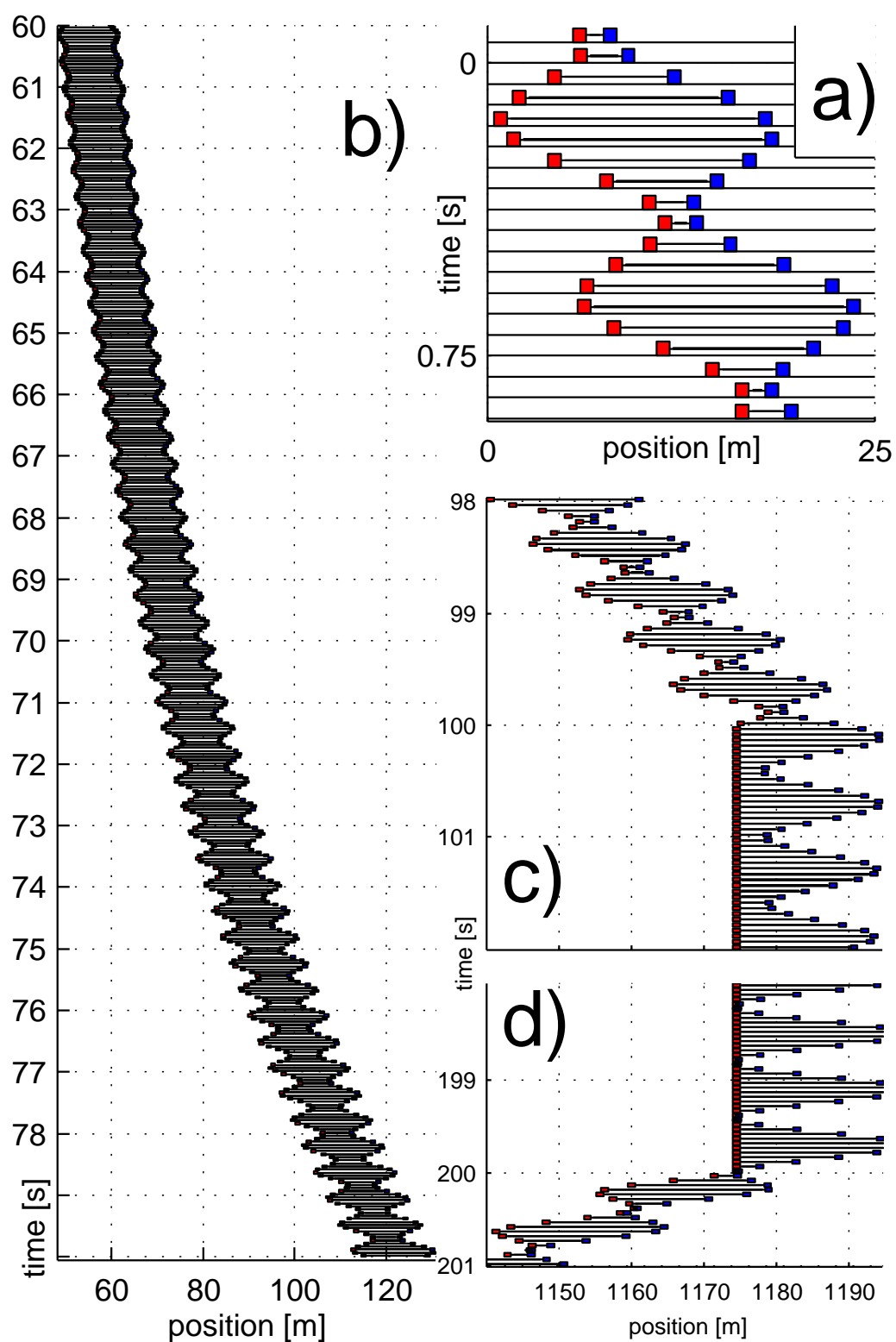


Figure 4.2: Illustration of the basic mode of locomotion. See text for description.

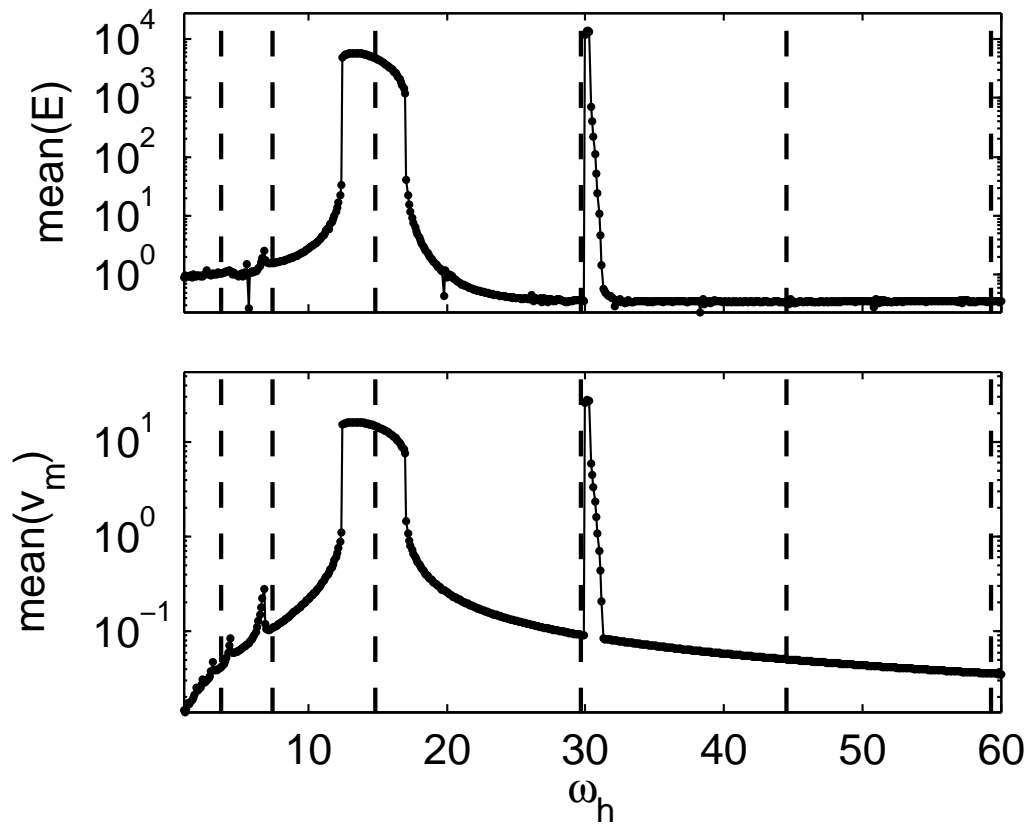


Figure 4.3: Top panel: Mean energy ($E_p + E_k$) content of the mechanical system for different $\omega_0 = [0, 60]$ at steady state. Bottom panel: Mean velocity. As clearly can be seen we have a broad peak around the resonant frequency of the mechanical system $\omega_m = 14.8324$.

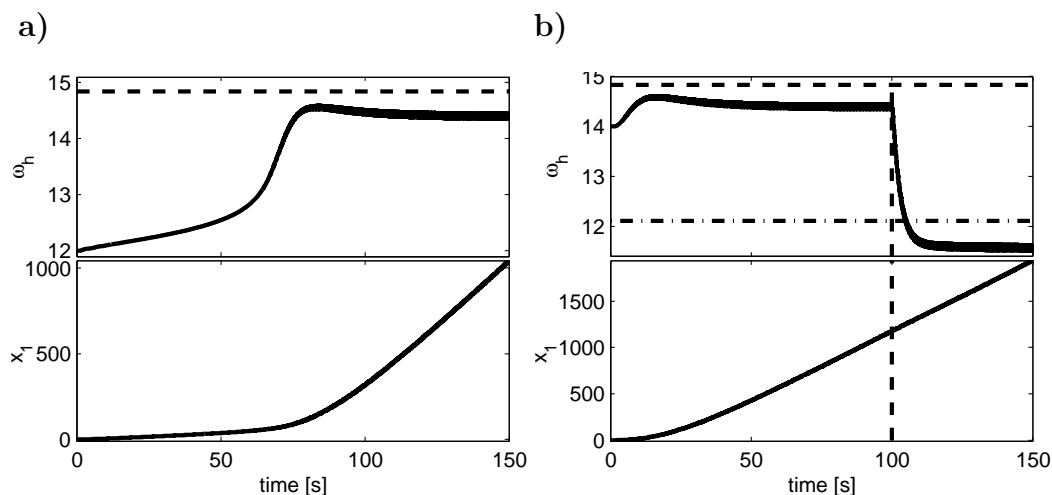


Figure 4.4: (a) This representative plot shows how the adaptation of ω_h increases the velocity of the locomotion system. ω_h starts at 12. The top panel shows the development of ω_h , the second panel shows the position x_1 of M_1 . There is some activity in the system from the beginning, however the excitations gets much stronger the closer ω_h comes to the resonant frequency of the mechanical system ω_m (vertical line). The steady state for ω_h is around 14.4, which is lower than the calculated resonant frequency of the passive mechanical system: $\omega_m = 14.8324$. (b) To illustrate the robustness that is built into the locomotion system by its frequency adaptation we show a representative experiment in which the mass of the bodies is 1kg to 1.5kg at $t=100$ s (vertical line). Immediately, the frequency of the oscillator ω_h starts to adapt to the new resonant frequency of the mechanical system (dash-dotted horizontal line).

the illustration of what happens with the masses from 60 to 80 seconds in Fig. 4.2(b). It can clearly be seen how the frequency adapts, first slowly then faster and finally reaches a steady state around $\omega_h = 14.4$. As can be seen the resonant effects start to excite the mechanical system heavily when ω_h passes at around 13 and the system starts to move forward at high speed.

In the next experiment, the mass is changed during the experiment at time $t = 100$ s from $m = 1$ kg to $m = 1.5$ kg. As we can see in Fig. 4.4(b) the oscillator quickly adapts its frequency to the new resonant frequency of the system and there is little change in the forward velocity. This corresponds for example to the biological case of growth of an animal or an addition of an external load. The adaptation to the massive change in the properties of the body immediately sets in, and after a few seconds the system has reached the new steady state.

As a further important aspect, the role of initial conditions of ω_h at $t = 0$ for the adaptation capability has been explored. As can be seen in Fig. 4.5, ω_h will always converge to the same value, but the initial conditions strongly affect the time ω_h needs to reach steady state. Furthermore, from the results in Fig. 4.3

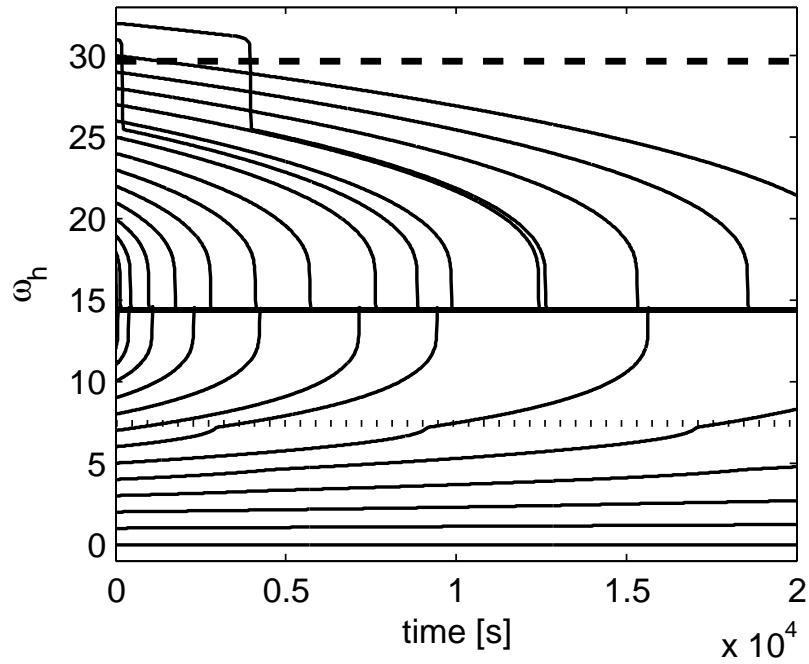


Figure 4.5: Adaptation of ω_h with viscous friction scheme. Different initial values for $\omega_h(0) = 0, 1, \dots, 32$ have been chosen. Clearly, the further away the longer ω_h takes to reach its stable steady state. The horizontal lines depict $0.5\omega_m$ and $2\omega_m$, where from the energy diagram (Fig. 4.3) resonant effects have to be expected and their influence on ω_h clearly can be observed here. Refer to text for further description.

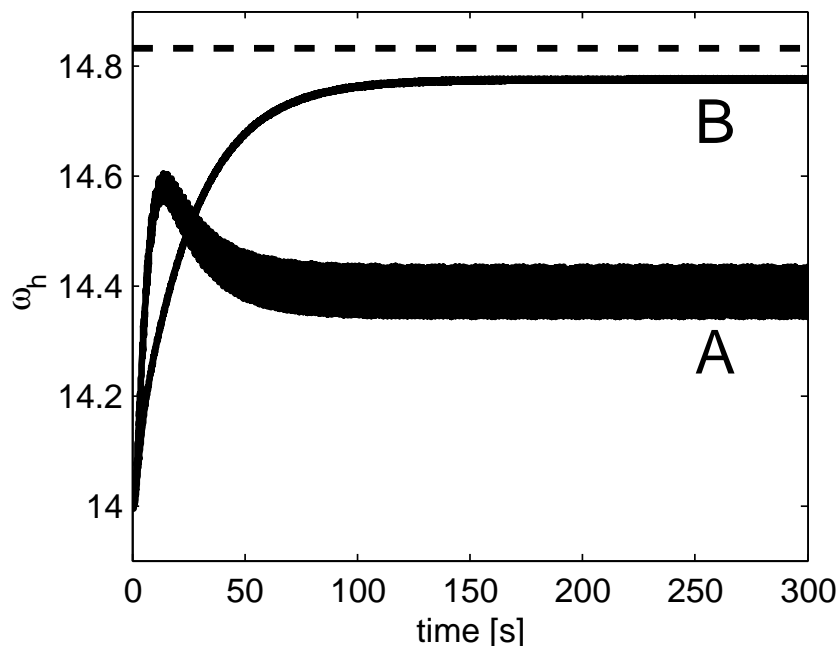


Figure 4.6: Comparison of the development of ω_h for viscous and Coulomb friction scheme. The Horizontal line indicates the resonant frequency of the passive mechanical system. (A) Viscous friction. (B) Coulomb friction. See text for further discussion.

we expect to see some clearly visible effects at $0.5\omega_m$ and $2\omega_m$ (the 1:2 and 2:1 resonant frequencies). At around $0.5\omega_m$ this leads to a slightly attractive area for ω_h (so called ghost points). Even more interesting is the effect at $2\omega_m$. From the energy diagram (Fig. 4.3) we know that the system reacts very strongly at that point. We can see that this violent reaction basically kicks the ω_h out of that region toward ω_m . So we see that even if the possible attained velocity is higher at $\omega_h = 2\omega_m$, this mode is not an attractor of the adaptation process.

Finally, in Fig. 4.6, a comparison between the viscous friction scheme and the Coulomb are presented. We see that the convergence for ω_h is slower in the case of the Coulomb scheme, and the final value is closer to the calculated resonant frequency of the passive mechanical system.

Influences of the Parameters Next, we want to shed light on the influence of the different parameters of the system. Note that the results in this section are of preliminary nature, since a lack of space and time does not allow to treat this topic in all detail in this article. There are a number of parameters which we can expect to influence the system fundamentally: First, the adaptation time scale of the Hopf oscillator τ_h directly influences the adaptation speed, but also

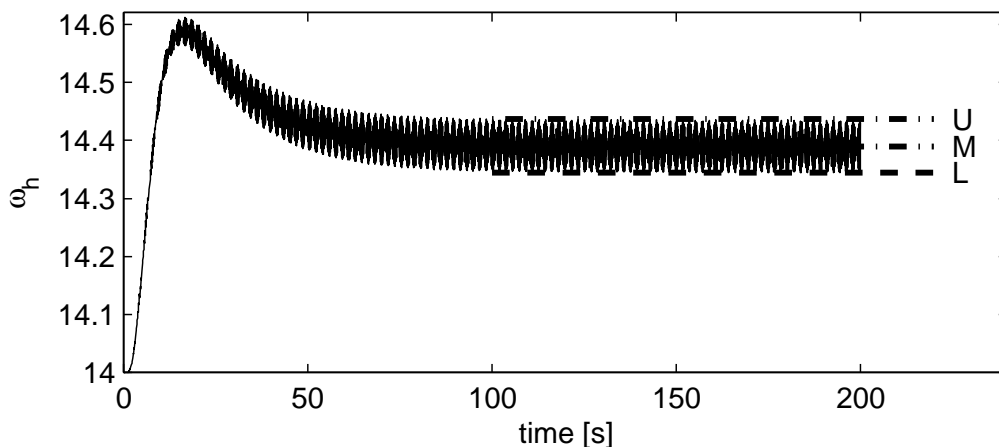


Figure 4.7: In order to quantify the steady state behavior of ω_h the mean m_{ω_h} and variance σ_{ω_h} have been measured after the system reached steady state (horizontal lines). Therefore, m_{ω_h} is a measure for (M) and σ_{ω_h} correlates with the distance (U)-(L). Note this figure is illustrative only – the actual values can change.

the stability of the adaptation process. Second, the coupling constants between the Hopf oscillator and the mechanical system (a, c) can influence transient times as well as stability of the system. Third, the choice of the friction parameters ($\rho_+, \rho_-, \mu_r, \mu_s, \mu_d$) obviously influences the locomotion speed of the system.

The mechanical parameters, such as masses, resting distances and spring constants, which seem to be important at first sight, turn out to be not so fundamental in a second look. They merely determine the time and length scales on which the solutions will be found but do not influence the type of solutions that are possible.

We will now present results of numerical simulations, highlighting the influences of the parameters listed above. First of all, the behavior of the attained steady state values for ω_h depending on the choice of the coupling parameter c will be illustrated. The parameter c influences how strongly the mechanical system perturbs the Hopf oscillator. In order to quantify the dependence of ω_h on this (and other) parameters, we use the mean (m_{ω_h}) and variance (v_{ω_h}) of ω_h after it reached the steady state (cf. Fig. 4.7). These values are measures for location and shape (width/depth) of the attractor for ω_h .

In Fig. 4.8(a), can be seen that there is a bifurcation⁷ for a critical value of $c = C_c$. For $c < C_c$ there is a deviation of m_{ω_h} from the resonance frequency of the mechanical system ω_m . The deviation grows with an exponential increase in the variance when approaching C_c . At $c = C_c$ the mean and variance drop to 0, i.e. the system gets quenched. Such discontinuous behavior in the mean value and power law behavior of the variance are ubiquitous phenomena in phase transitions (bifurcations).

⁷Note that the names *bifurcation* and *phase transition* are basically two names for the same

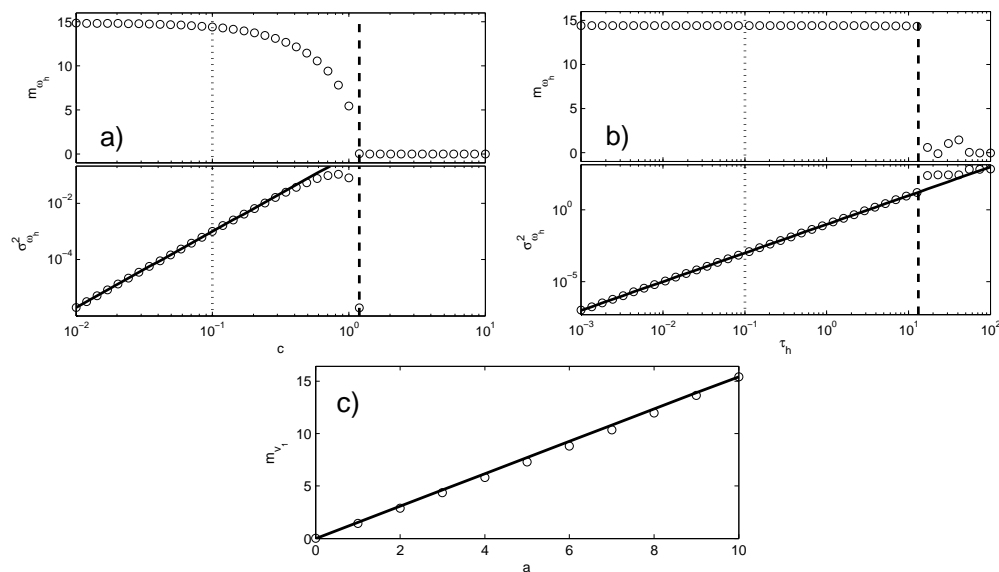


Figure 4.8: (a) Upper panel: the mean value attained for ω_h dependent on c (note the log scale). Lower panel: Variance for ω_h (note log-log scale). Note that for $c > C_c$ the variance drops to 0, therefore it is not drawn on the log scale. The vertical dotted line indicates the default setting of $c = 0.1$ and the dashed lines indicates the approximate value of C_c . The variance can be fitted with a power law $\sigma^2 \sim \tau^\alpha$. The exponent of the fit is $\alpha = 2.6959$. This behavior is typical for phase transitions.

(b) Dependence of mean and variance of ω_h on τ_h for steady state behavior. Again, the dotted line indicates the default setting of $\tau = 0.1$ and the dashed lines indicates the approximate value of $\tau_{h,c}$. The variance can be fitted with a power law $\sigma^2 \sim \tau^\alpha$. The exponent of the fit is $\alpha = 1.9903$. (c) The attained mean values m_{v_1} of v_1 after the system reached steady state depending on coupling parameter a . There is a very clear linear relationship $m_{v_1} = qa$. The fit is for $q = 1.5451$.

Next, we shed light on the influence of τ_h (cf. Fig. 4.8(b)) again we have a clear bifurcation behavior for a critical value of τ_h . For high values of $\tau_h > \tau_{h,c}$ it seems the system sets out onto a route into chaos (data not shown). The reason for that might be that for higher values of τ_h the timescales of the adaptation process and the other time scales of the system start to overlap, and therefore irregular behavior may occur. This conjecture however bases on visual inspection and is not confirmed yet. Again, we have a very clear power law behavior of σ_{ω_h} .

Now we turn our attention to the coupling from the Hopf oscillator to the mechanical system. The corresponding parameter is a . This parameter determines how strongly k_a is modulated by the activity of the Hopf oscillator (cf. Eq. 4.8). We measure the influence by calculating the mean value m_{v_1} of the attained velocity of M_1 at steady state. Here, we find a very clear linear dependence of m_{v_1} on a (cf. Fig 4.8(c)) for the explored range.

Finally, in Fig. 4.9, the influence of the friction asymmetry (ρ_+, ρ_n) is presented. After the transient phase the attained mean velocity of the center of mass is measured. As can be seen there is an exponential dependence of the velocity on the friction parameters.

Loss of feedback and disturbances It is also interesting to see how the system reacts when the feedback is cut from the mechanical system to the Hopf oscillator by setting $c = 0$. In Fig. 4.10(a), one can observe, that because of the setting of $\mu_h = 0$, the system keeps on moving, but at much reduced speed. If μ_h is set to slightly negative values $\mu_h = [-1, -10]$, the oscillations of the Hopf oscillator fade out and the system comes to a stand still (data not shown).

In a next step, we inhibit the frequency adaptation only by setting $\tau_h = 0$. In Fig. 4.10(b), can be seen how the system keeps on moving as normal, however it is not able to adapt to changing conditions anymore (data not shown).

In order to get an idea how the system behaves when it gets disturbed, we blocked one of the masses for 100 s. In Fig. 4.11, can be observed how the system reacts. Immediately the adaptation mechanism for ω_h starts to tune the system to the new resonant frequency $\omega_m = \sqrt{\frac{k_a + k_p}{m}}$. After releasing the blocks the system moves backward for a moment, before converging to the normal steady state again. What happens with the masses around $t = 100$ and $t = 200$ can also be seen in Fig. 4.2(c) and 4.2(d). Especially from Fig. 4.2(d) it can be understood where the backward movement comes about. In the moment of the release of M_1 , M_2 happens to move with high velocity toward M_1 , which leads to acceleration backward in the moment of the release.

4.0.10 Discussion

In this article we have shown that, by using a Hopf oscillator with adaptive frequency, we can devise a controller that adapts to the resonant frequencies of a

phenomena, even though with emphasis on different aspects. See [87] for a discussion.

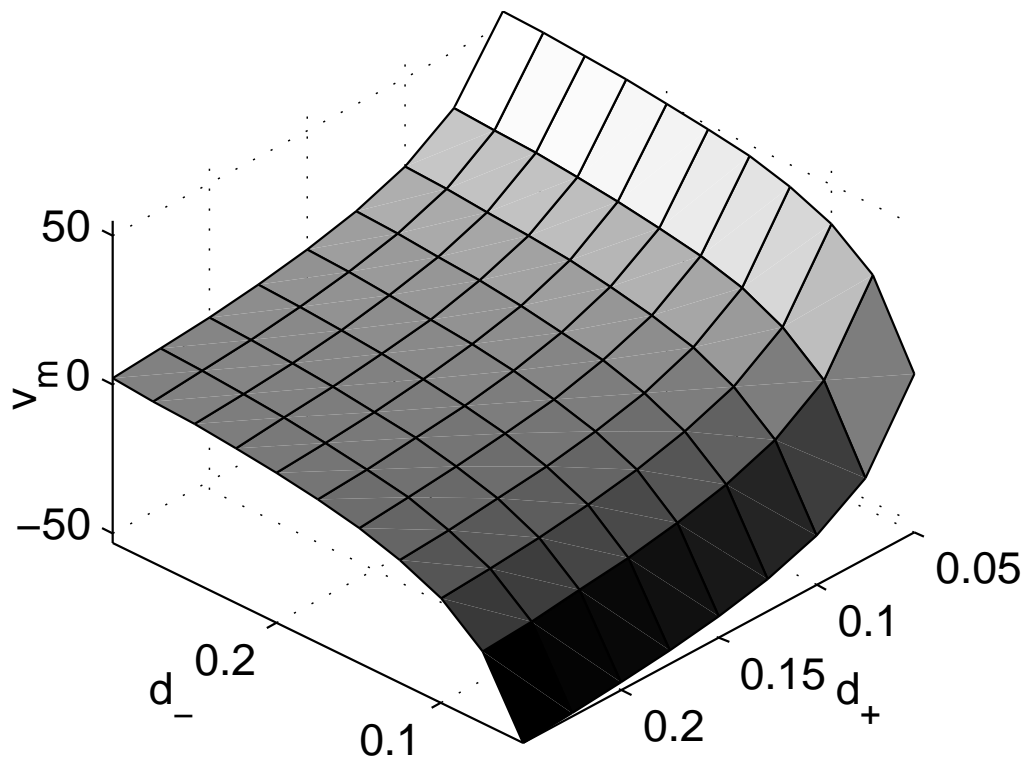
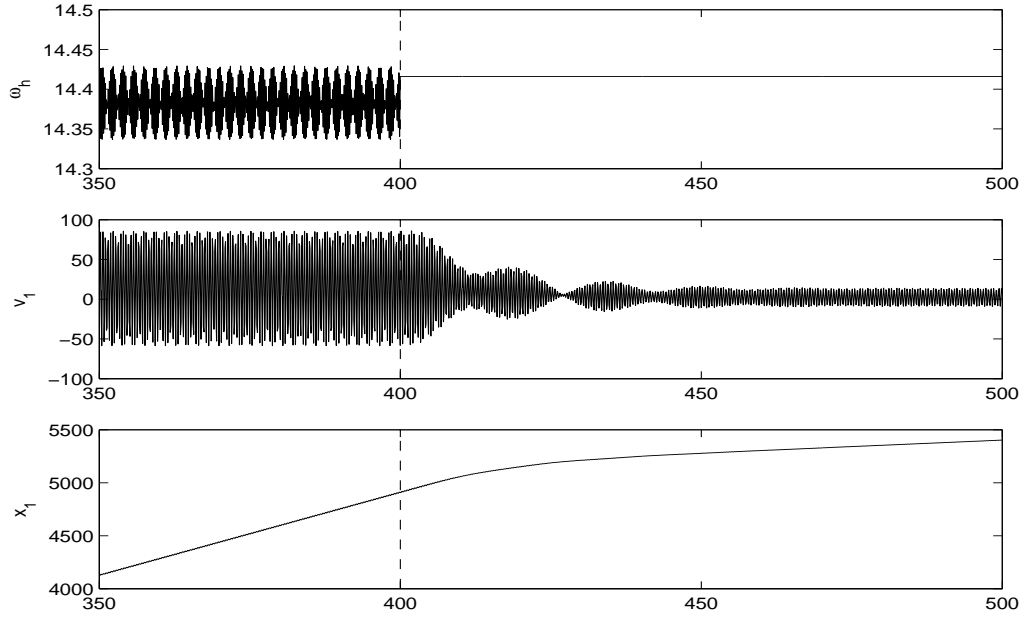


Figure 4.9: Influence of the friction asymmetry in viscous mode. The z axis is the position of m_1 after 200s for a given setting of ρ_- and ρ_+ . White regions correspond therefore to fast forward locomotion, black to fast backward locomotion.

a)



b)

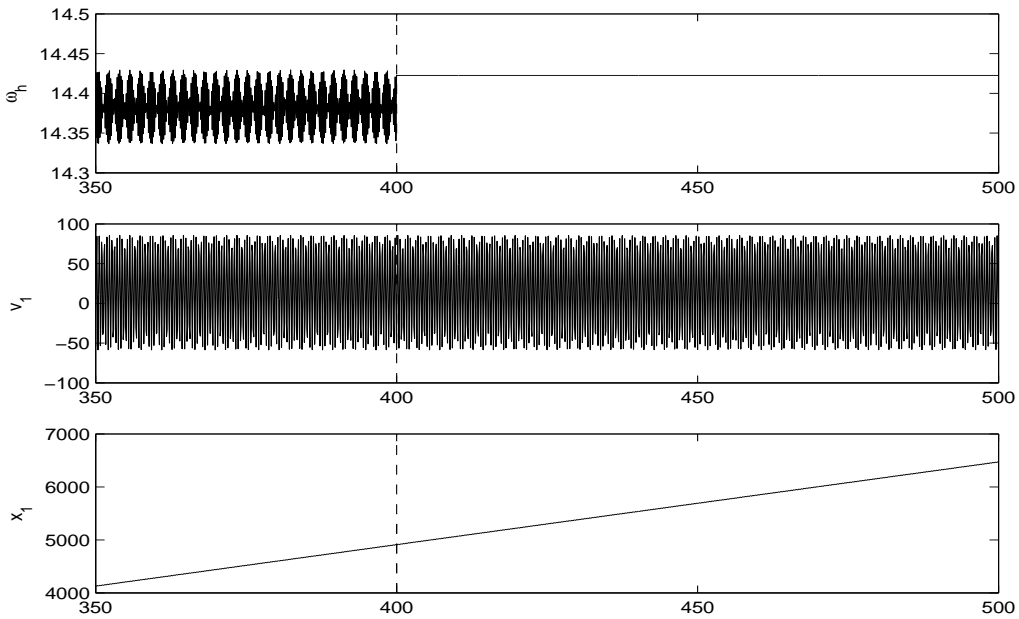


Figure 4.10: a) At $t = 400$ the feedback from the mechanical system to the Hopf Oscillator is cut by setting $c = 0$. This as well inhibits the frequency adaptation. b) At $t=400$ only the frequency adaptation is cut by setting $\tau = 0$. This means there is still feedback from the mechanical system to the Hopf oscillator. Therefore, the system keeps moving with the same speed. However, it can not react to changing mechanical properties anymore (not shown).

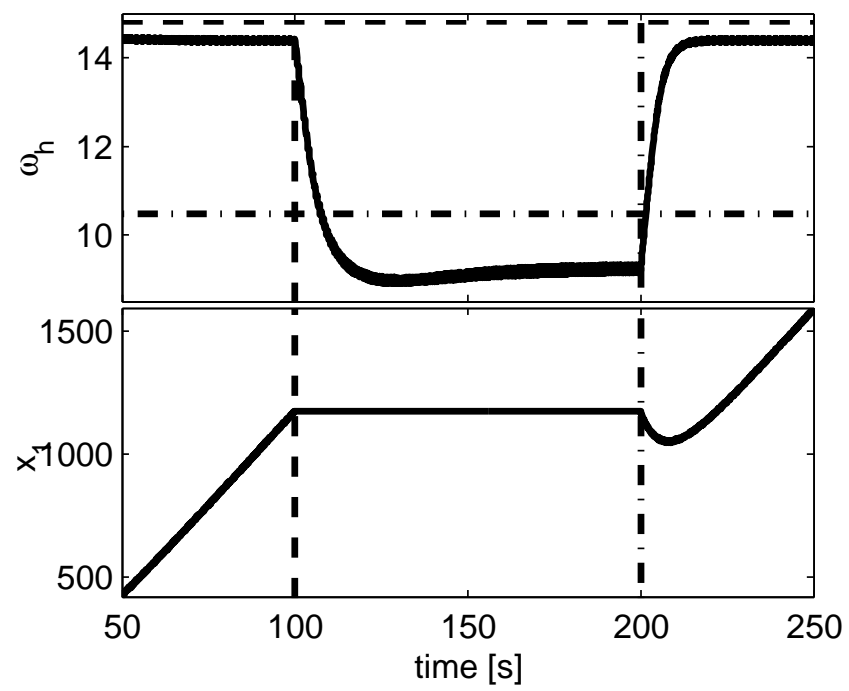


Figure 4.11: M_1 blocked at $t = 100$ (dashed vertical line) and released at $t = 200$ (dash dotted vertical line).

mechanical system and therefore excites it. We exploited the oscillatory nature of the systems and the understanding of synchronization behavior of oscillators. Together with asymmetric friction – which turns out to be a fundamental property of any locomotion system – this leads to directed movement. Asymmetric friction generalizes to asymmetric interaction forces for other types of locomotion, e.g. the elongated body of fishes have a low longitudinal and a large perpendicular drag coefficient, which by proper undulation of the body leads to forward movement. In the case of legged locomotion, the asymmetric interaction forces are implemented by having a stance phase with ground contact forces and a swing phase with zero interaction forces.

Two distinct time scales have been introduced into the dynamical system. Therefore, the system is a simple instantiation of a multi-scale⁸ dynamical system. The fast time scale is what normally is associated with the control of locomotion. The slow time scale can be associated with learning or, more generally, with adaptive behavior. Thus, we see the descriptive power that is naturally built into such multi-scale dynamical systems. Especially, there is no distinction between learning algorithm and learning substrate. Moreover, it is worthwhile noting that for a full understanding of the behavior of such a system, the two time scales can not be treated completely separately.

Hitherto, multi-scale dynamical systems did not receive a lot of attention. One reason might be that there are some problems inherent in their investigation. One first problem that one encounters, is that, since there are many, possibly quite different, time scales in the system, the system has to be integrated in a way to encompass all time scales. In other words, the integration has to be exact enough (i.e. sampled fast enough) in order to calculate correctly the phenomena on the fastest time scale. On the other, hand the simulation has to run long enough in order to see the phenomena on the slowest time scale. The time scales are not fully separable since it is exactly the influence between them that is of interest. Furthermore, the interesting multi-scale systems usually exhibit strong nonlinear behavior and complicated bifurcation structure with many critical parameters, all of which makes it difficult to get a good understanding of the systems behavior. Recently, however, the interest in such systems is rising. One important reason is that cheap, fast workstations allow fast simulation of such systems and thus make their investigation more amenable.

Relation to biology We would like to stress the fact that the presented system is not meant to model detailed biological processes. It is rather a biologically inspired experimental system to investigate fundamental properties of locomotion (i.e. the generation of directed movement).

Nevertheless, and this is our hope, the treatment of such toy systems might

⁸As a matter of fact it contains more than 2 time scales. Already a nonlinear oscillator possesses at least two time scales: One is the time scales of the oscillations and the other is the time scale at which it approaches its limit cycle.

lead to interesting questions for biologists. For instance, we have seen that our model reaches high velocities on higher order locking with the mechanical system. It would be interesting to see if the same phenomenon is observed in CPGs, and potentially, experimentally modify the CPG frequencies (e.g. through the application of excitatory neurotransmitters), and investigate whether it starts to work at these other resonant frequencies. In our case we saw a strong reaction, and it would be interesting to analyze the reaction of the natural system.

Furthermore, it is clear that the resonant frequencies of a locomotion system change very dramatically in an animal life time, and this at different time scales, e.g. due to the addition of external loads (e.g. carrying a prey) and to the growth of the animal. The natural locomotion systems have to cope with all such changes, and it would be interesting to explore the different types of adaptation mechanisms that play a role in keeping locomotion efficient. This is an area where the interplay between biology, engineering and mathematics can prove very fruitful.

Future work and outlook There are several avenues to build up on the presented results. First, there are many theoretical questions that may be asked. Even if the system seems to be a quite simple one, the influence of the parameters is far from trivial. It will be interesting to further investigate the bifurcation behavior of the system. A careful investigation of the influence of the parameters remains to be done. We know that the system contains several critical parameters as outline above. In the presented results, most of them have been chosen in order to be on the safe side, e.g. τ_h has been chosen small enough in order to have two well separated time scales in the system.

Second, there are several extensions that can be made to the systems, such as an extension to non-oscillatory systems, for instance. We see that by exploiting synchronization behavior we can devise a useful system. On the other hand, there exist generalizations of the notion of phase locking and synchronization for aperiodic and non-oscillatory systems [134]. This could indicate that the presented approach is an interesting path to follow also for investigation of other problems, such as cognition, pattern recognition, evolutionary models and the like. Other extensions include introducing other coupling schemes and different types of oscillators.

The control of speed and direction also needs to be addressed. More springs and oscillators can be introduced in order to get a system that can change its direction of locomotion (2/3D system). Furthermore, the system should have some control over speed. Currently there is only stop and full speed (disregarding the transients between the two modes). However, a control of speed could be introduced, e.g. with an intentional detuning of the oscillator and/or with a modulation of the amplitude of oscillatory control signals. There are various other possibilities, of which the respective advantages and disadvantages and their implications on the system have to be carefully studied.

Finally, it would be interesting to construct a real-world robotics implemen-

tation of this toy-system as well as to implement it as a realistic dynamical simulation in a physics-based simulator. The system (most probably in a slightly modified form) should prove interesting for several robotics applications such as snake robots, (ad-hoc) modular robotics, and legged robots.

Acknowledgments This research is funded by a Young Professorship Award to Auke Ijspeert from the Swiss National Science Foundation. We would like to thank Jun Nakanishi for constructive comments on an earlier version of this article.

A Prototype Adaptive Dynamical System: The Adaptive Frequency Oscillator

IN this chapter, we continue the analysis of a central building block of the adaptive controller that are developed in the frame of this thesis, the *adaptive frequency oscillator*. The idea has been introduced in the previous chapter on some intuitive grounds and shown to be working by numerical simulation. It is always very desirable to get an analytical grip on the systems that are employed, first of all to have an indisputable argument that the systems work as they are supposed to, making it safer to use them in critical applications and, second, analytical treatment leads to a better understanding of the system, which also will foster further theoretical advances, consequently we will use the results of this chapter for the analysis of AFOs in feedback loops later in the thesis (cf. Chapter 6).

5.1 Generalization and proof of convergence of the adaptation rule

This section shows the following two results (1) the generalization of the concept of the adaptive frequency oscillators. Supported by numerical simulations we show that the same basic adaptation law works for a large number of different oscillators. (2) The proof of convergence for ω for the adaptive frequency Hopf oscillator.

For the content of this section I am particularly indebted to Ludovic Righetti, who was first a master student under my supervision, then a fellow PhD student. While I worked in the beginning on the conceptual basis of the proof by postulating it was possible to treat it with perturbation methods and the Fourier series decomposition, it was him who has the merits of having arrived with the proof, did the hard to job working it out and putting it into complete and readable shape. I

do however not omit this section since I feel that it is an important logical brick in the interesting story of the adaptive frequency oscillators.

Dynamic Hebbian Learning in Adaptive Frequency Oscillators

Ludovic Righetti, Jonas Buchli and Auke Jan Ijspeert

This paper has been originally published as
L. Righetti, J. Buchli, and A.J. Ijspeert. Dynamic hebbian learning
in adaptive frequency oscillators. *Physica D*, 216(2):269–281, 2006

Abstract Nonlinear oscillators are widely used in Biology, Physics and Engineering for modeling and control. They are interesting because of their synchronization properties when coupled to other dynamical systems. In this paper, we propose a learning rule for oscillators which adapts their frequency to the frequency of any periodic or pseudo periodic input signal. Learning is done in a dynamic way: it is part of the dynamical system and not an offline process. An interesting property of our model is that it is easily generalizable to a large class of oscillators, from phase oscillators to relaxation oscillators and strange attractors with a generic learning rule. One major feature of our learning rule is that the constructed oscillators can adapt their frequency without any signal processing nor the need to specify a time window or similar free parameters. All the processing is embedded in the dynamics of the adaptive oscillator. The convergence of the learning is proved for the Hopf oscillator, then numerical experiments are carried out to explore the learning capabilities of the system. Finally, we generalize the learning rule to non-harmonic oscillators like relaxation oscillators and strange attractors.

5.1.1 Introduction

Nonlinear oscillators have been widely used to model various physical and biological processes and for the last two decades, they are also used in engineering fields, as for example autonomous robotics. Models of Josephson junctions [216], lasers, central pattern generators (CPGs) [48, 78, 131, 221], associative memories [15, 161] or beat perception [57, 137] are a few examples that show the importance of oscillators in modeling and control.

Oscillator models are interesting because of their synchronization capabilities, either with other oscillators or with external driving signals. In most cases, it is a difficult task to choose the right parameters of the oscillators to ensure they will synchronize as desired. Most studies are using phase-locking behavior, but when parameters are outside the phase-locking region synchronization fails. This is mainly the case because oscillators lack plasticity, they have fixed intrinsic frequencies and cannot dynamically adapt their parameters.

Some recent studies, however, concentrate on developing dynamic plasticity for oscillators, so they can learn and synchronize with a wider range of frequencies,

without having to tune the parameters by hand [4, 15, 61, 156, 158, 159]. But these attempts are so far limited to very simple classes of oscillators, equivalent to phase oscillators, mainly because this is the only class of oscillators that can be analytically studied and for which convergence can be proved, when adding adaptivity to the system. Adaptive relaxation oscillators were also developed to model rhythm perception [57]. These oscillators are able to adapt their frequencies to synchronize with external input. But these input signals are simple and reduce to periodic pulse trains.

Recently, we designed an adaptive oscillator for studying adaptive locomotion in biologically inspired robotics [24, 28]. In that work we developed an adaptive frequency Hopf oscillator able to adapt to the resonant frequency of a mechanical system. The oscillator is able to adapt its frequency to the frequency of complex input signals. In this contribution, we prove the convergence of this oscillator and generalize the adaptive rule for more complex oscillators so they can learn the frequencies of, and synchronize with, any rhythmic input signal. An interesting property of our method is that we go beyond phase-locking of oscillations. We add plasticity to the system, in the sense that the system can change its own parameters in order to learn the frequencies of the periodic input signals. So the range of frequencies that can be learned is not limited and after learning the oscillator continues to oscillate at the learned frequency, even if the input signal disappears. We call our adaptive mechanism¹ *dynamic Hebbian learning* because it shares similarities with correlation-based learning observed in neural networks [122].

One major aspect of our approach is that an oscillator learns the frequency of any periodic input, without any signal processing. It means that an oscillator can adapt its frequency to any kind of periodic, or even pseudo-periodic, input. The process is completely dynamic, and does not require the specification of time windows or similar free parameters as it is often the case in signal processing algorithms. The whole learning process and the frequency extraction from the input is totally embedded in the dynamics of the system. Another interesting property of the method is that we can directly apply it to many kinds of oscillators, for example relaxation oscillators or strange attractors. An oscillator, perturbed by a periodic signal F , is described by the general equations

$$\begin{aligned}\dot{x} &= f(x, y, \omega) + \epsilon F \\ \dot{y} &= f(x, y, \omega)\end{aligned}$$

with ω some parameter influencing the frequency of the oscillations. We introduce a learning rule for this parameter

$$\dot{\omega} = \pm \epsilon F \frac{y}{\sqrt{x^2 + y^2}}$$

The sign depends on the direction of rotation of the limit cycle in the (x, y) phase space. This general adaptation rule works for many different oscillators, ω will

¹In this article, we use adaptation and learning as synonyms

converge to a value such that one frequency component of the oscillator and one of the input F match. We discuss this general learning rule in this contribution.

In Section 5.1.2, we first present the adaptive learning rule with a simple Hopf oscillator and prove the convergence and the stability of the whole system. Then, in Section 5.1.5, we present some numerical simulations, to show that the oscillator can adapt its frequency to the frequency of any kind of periodic or pseudo-periodic signals. Finally, in order to demonstrate the generality of our method, we construct, in Section 5.1.10, an adaptive Van der Pol oscillator which we discuss in details. We also present examples of frequency adaptation with an adaptive Rayleigh oscillator, an adaptive Fitzhugh-Nagumo oscillator and an adaptive Rössler system. In Section 5.1.13, we finish this contribution with a discussion.

5.1.2 Learning frequencies with a Hopf oscillator

In this section, we introduce the learning rule for frequency adaptation in oscillators. To keep discussion as simple as possible, we use a Hopf oscillator to discuss our learning method, because its phase evolution is simple to describe. Generalization to more complex oscillators will be presented in further sections. We first present the model, then we prove the convergence of the adaptive dynamical system.

5.1.3 Model description

The Hopf oscillator

The dynamics of the Hopf oscillator is governed by the following differential equations

$$\dot{x} = (\mu - r^2)x - \omega y + \epsilon F \quad (5.1)$$

$$\dot{y} = (\mu - r^2)y + \omega x \quad (5.2)$$

Where $r = \sqrt{x^2 + y^2}$, $\mu > 0$ controls the amplitude of the oscillations and ω is the intrinsic frequency of the oscillator. It means that without perturbations (when $\epsilon = 0$), the system is oscillating at $\omega \text{ rad} \cdot \text{s}^{-1}$. This oscillator is coupled with a periodic force F . When the force is zero, the system has an asymptotically stable harmonic limit cycle, with radius $\sqrt{\mu}$ and frequency ω . As the limit cycle of the Hopf oscillator is structurally stable, small perturbations around its limit cycle ($\epsilon > 0$) do not change the general behavior of the system. It means that the limit cycle will still exist, only its form and time-scale will change. Structural stability assures that this change is close to identity.

As we are mainly interested in the phase dynamics, we rewrite the system in polar coordinates. We set $x = r \cos \phi$ and $y = r \sin \phi$. Equations (5.1) and (5.2)

transform into

$$\dot{r} = (\mu - r^2)r + \epsilon F \cos \phi \quad (5.3)$$

$$\dot{\phi} = \omega - \frac{\epsilon}{r} F \sin \phi \quad (5.4)$$

It is well known that when the oscillator has its intrinsic frequency ω close to one frequency component of the periodic input, it will phase-lock (this phenomena is also called entrainment) [166]. It means that the oscillations synchronize with the frequency of the periodic input. The maximum distance between the intrinsic frequency of the oscillator and the periodic input that still permits phase-locking depends directly on the coupling strength. The stronger the coupling is, the larger the entrainment basin. Outside this basin, the oscillator is still influenced by the coupling but does not synchronize. If the periodic input has several frequency components, then several entrainment basins will appear. Phase-locking will be possible with each frequency component. Outside the basin, the oscillator will have tendency to accelerate or decelerate, according to the term $F \sin \phi$, in average the oscillator will tend to oscillate at a frequency which is between the intrinsic frequency of the oscillator and the frequency of the input. In the case of multi-frequency inputs, these oscillations will be influenced in a similar manner.

Adaptive dynamical system

Now we can build our adaptation rule by using the influence of the external perturbation on the activity of the oscillator. The adaptation rule will be a dynamical system of the form

$$\dot{\omega} = f(\omega, r, \phi, F) \quad (5.5)$$

In the following we motivate the concrete choice of the adaptation rule by reasoning about the effects of a perturbation in a geometric way in the phase space of the dynamical system. This provides insights into our choice of the learning rule. In further sections, we will show more rigorously that this reasoning is appropriate and leads to the desired behavior.

To get a good grasp on the effects of perturbations on a limit cycle system (i.e. an oscillator) it is helpful to look at the limit cycle in the phase space representation. In the phase space all perturbations have a direction, i.e. they can be represented as a vector \vec{P} in that space.

Due to the stability properties of a limit cycle system a perturbation can in the long term only affect the phase of the oscillator. The phase is marginally stable whereas the system is damped perpendicularly to the limit cycle. This means that the phase point always returns to the limit cycle, but it can be phase shifted. In other words the system after a singular perturbation will forget all the perturbation's influence except its influence on the phase.

Especially in a small neighborhood of the limit cycle a small perturbation can only affect the phase strongly if it perturbs the oscillator in the direction tangential to the limit cycle. The perturbations perpendicular to the limit cycle are damped

out. The domain where this assumption is valid depends on the coupling of phase and radius. While for the Hopf oscillator this assumption is valid for a very large neighborhood, the neighborhood can be very small for other oscillators, e.g. oscillators with strongly bent isochrones.

To discuss the influence of the perturbation on the phase in this neighborhood, let us introduce a coordinate system with its origin on the phase point. The first base vector \vec{e}_r is chosen perpendicular to the limit cycle, while the second base vector \vec{e}_ϕ is chosen tangential to the limit cycle (cf. Fig. 5.1). Thus, this coordinate system rotates with the phase point along the limit cycle. In order to know the influence $p_\phi = |\vec{p}_\phi|$ of the perturbation on the phase it is sufficient to project \vec{P} on \vec{e}_ϕ

$$p_\phi = \vec{P} \cdot \vec{e}_\phi \quad (5.6)$$

Thus, depending on the external perturbation *and* the state of the oscillator (i.e. the position of the point on the limit cycle) the perturbation accelerates the phase point or slows it down. If the perturbation is a periodic signal, this results in an average acceleration or deceleration depending on the frequency difference. This effect, if the frequency of the oscillator and the external frequency are close, leads to well known phase-locking behavior. Thus, the influence carries the information needed to adjust to the frequency of the external perturbation. Consequently, if we take this same effect to tune the frequency of the oscillator (on a slower time scale) the frequency should evolve toward the frequency of the perturbation. Therefore, the effect of $f(\omega, r, \phi, F)$ on ω has to be the same as the effect of the perturbation on the phase, thus, (in average) driving ω toward the frequency of the perturbation.

While the discussion here is valid for limit cycles of any form and in any dimension, in the case of the Hopf oscillator and the perturbation as chosen in Eqs.(5.3) and (5.4) it is evident that $p_\phi = \frac{\epsilon}{r} F \sin \phi$. We chose accordingly

$$\dot{\omega} = -\epsilon F \sin \phi \quad (5.7)$$

which corresponds in Cartesian coordinates to

$$\dot{\omega} = -\epsilon F \frac{y}{\sqrt{x^2 + y^2}} \quad (5.8)$$

The adaptation of ω happens on a slower time scale than the evolution of the rest of the system. This adaptation time scale is influenced by the choice of ϵ . Note that the r variable is dropped because we do not want a learning rule which is scaled by the amplitude of the oscillations. With this rule, the oscillator will adapt to the frequency of any input signal. As in applications most signals will be non-harmonic, i.e. they have several frequency components, the oscillator will adapt to one of these components, generally the closest to the intrinsic frequency of the oscillator. We must also note that it is required to keep the oscillator coupled with the input, because it is the evolution of $\phi(t)$, i.e. change of frequency correlated with $\dot{\omega}$, that enables adaptation in Equation (5.7). A proof of convergence of

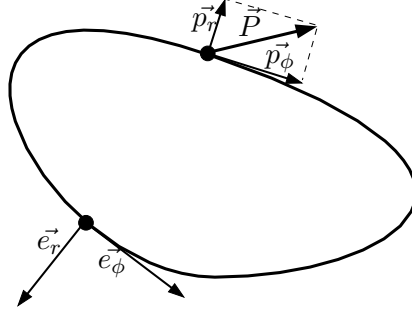


Figure 5.1: We illustrate the coordinate system in which synchronization is most naturally discussed. The figure shows an arbitrary limit cycle. The system is strongly damped in direction perpendicular to the limit cycle \vec{e}_r and marginally stable in direction tangential to the limit cycle \vec{e}_ϕ . This is the reason for the structurally stable limit cycle in the first place and allows for a resetting of the phase on the other hand. Note that the 2-dimensional representation is always valid for discussing a limit cycle since there exists always a 2 dimensional manifold which contains the limit cycle. Refer to text for a discussion of the perturbation \vec{P} .

this adaptive oscillator (Eqs (5.3), (5.4) and (5.7)) in the general case of multi-frequency inputs is given in the next section.

5.1.4 Proof of convergence with the Hopf oscillator

In this section we prove the stability of the adaptive Hopf oscillator, but we will see in next sections that the results we derive in this section can also justify convergence for other types of oscillators. The new dynamical system we study is the one composed of the oscillator and its learning rule for the frequency (Eqs. (5.3), (5.4) and (5.7)). As long as $\omega > 0$, because of structural stability, the behavior of the oscillator (Eqs. (5.3) and (5.4)) is known, so we just have to prove that ω converges to the desired input frequency.

We use perturbation methods (cf. [124]) to discuss the convergence of the system. The solution of the system $\{r(t), \phi(t), \omega(t)\}$ can be written as a perturbation series, with $\epsilon < 1$

$$r(t) = r_0 + \epsilon r_1 + \epsilon^2 r_2 + \epsilon^3 R_r \quad (5.9)$$

$$\phi(t) = \phi_0 + \epsilon \phi_1 + \epsilon^2 \phi_2 + \epsilon^3 R_\phi \quad (5.10)$$

$$\omega(t) = \omega_0 + \epsilon \omega_1 + \epsilon^2 \omega_2 + \epsilon^3 R_\omega \quad (5.11)$$

with initial conditions $r_0(t_0) = r_0$, $\phi_0(t_0) = 0$ and $\omega_0(t_0) = \omega_0$ independent of ϵ . Here, r_i , ϕ_i and ω_i are functions of time and R_r , R_ω and R_ϕ are small residues of the order ϵ^3 . Which means there exists a constant k such that $R_i < k$, generally k is small. The following proof will hold under the hypothesis that $k \ll 1$, numerical

simulations in Section 5.1.5 will confirm this hypothesis. We could also expand the perturbation series to higher order: the finer the approximation is, the wider the time interval valid for the approximation. But we will show that convergence appears on the time-scale associated with the second order approximation. By inserting Eqs. (5.9), (5.10) and (5.11) into Eqs. (5.3), (5.4) and (5.7), and by observing that

$$\begin{aligned}\sin(\phi_0 + \epsilon\phi_1 + \epsilon^2\phi_2 + \epsilon^3R_\phi) &= \sum_{k=0}^{\infty} \frac{(-1)^k (\phi_0 + \epsilon\phi_1 + \epsilon^2\phi_2 + \epsilon^3R_\phi)^{2k+1}}{(2k+1)!} \\ &= \sin\phi_0 + \epsilon\phi_1 \cos\phi_0 + O(\epsilon^2)\end{aligned}\quad (5.12)$$

and similarly that

$$\cos(\phi_0 + \epsilon\phi_1 + \epsilon^2\phi_2 + \epsilon^3R_\phi) = \cos(\phi_0) - \epsilon\phi_1 \sin(\phi_0) + O(\epsilon^2) \quad (5.13)$$

we can identify the terms corresponding to each ϵ^n and derive the following differential equations

$$\dot{r}_0 = (\mu - r_0^2)r_0 \quad (5.14)$$

$$\dot{\phi}_0 = \omega_0 \quad (5.15)$$

$$\dot{\omega}_0 = 0 \quad (5.16)$$

$$\dot{r}_1 = \mu r_1 - 3r_1 r_0^2 + F \cos\phi_0 \quad (5.17)$$

$$\dot{\phi}_1 = \omega_1 - \frac{1}{r_0}(r_1 \dot{\phi}_0 - r_1 \omega_0 + F \sin\phi_0) \quad (5.18)$$

$$\dot{\omega}_1 = -F \sin\phi_0 \quad (5.19)$$

$$\dot{r}_2 = \mu r_2 - 3r_2 r_0^2 - r_2 r_1^2 - F \phi_1 \cos\phi_0 \quad (5.20)$$

$$\dot{\phi}_2 = \omega_2 - \frac{1}{r_0}(r_1 \dot{\phi}_1 - r_1 \omega_1 + r_2 \dot{\phi}_0 - r_2 \omega_0 + F \phi_1 \cos\phi_0) \quad (5.21)$$

$$\dot{\omega}_2 = -F \phi_1 \cos\phi_0 \quad (5.22)$$

with initial conditions $r_0(t_0) = \sqrt{\mu}$, $\phi_0(t_0) = 0$, $\omega_0(t_0) = \omega_0$ and $r_i(t_0) = \phi_i(t_0) = \omega_i(t_0) = 0$, $\forall i = 1, 2$. We consider that the unperturbed system ($i = 0$) has already converged to the limit cycle and that at time t_0 , there are no perturbations. We have to solve Equations (5.16), (5.19) and (5.22) to construct an approximate solution of Equation (5.7) and thus show the convergence properties of the adaptation rule ω . The behavior of the two other state variables is already known since the Hopf oscillator has a structurally stable limit cycle. In order to solve these equations we also have to solve Equations (5.14), (5.15) and (5.18). The error of the approximation will be of order $O(\epsilon^3)$ and will hold for some time interval

$[t_0, t_0 + \sigma]$. The solutions of Equations (5.14)-(5.16) are straightforward

$$r_0(t) = \sqrt{\mu} \quad (5.23)$$

$$\phi_0(t) = \omega_0(t - t_0) \quad (5.24)$$

$$\omega_0(t) = \omega_0 \quad (5.25)$$

To solve the other equations, we first rewrite the periodic input as its complex Fourier series

$$F(t) = \sum_{n=-\infty}^{\infty} A_n e^{in\omega_F t} \quad (5.26)$$

Where ω_F is the frequency of the input. We now consider the case where $\omega_0 \neq n\omega_F$, $\forall n \in \mathbb{N}$, which means that at the beginning the system is not synchronized with any frequency component of the periodic input F . We then get

$$\begin{aligned} \dot{\omega}_1 &= - \left(\sum_{n=-\infty}^{\infty} A_n e^{in\omega_F t} \right) \sin(\omega_0(t - t_0)) \\ &= - \sum_{n=-\infty}^{\infty} A_n \frac{e^{i(n\omega_F + \omega_0)t - i\omega_0 t_0} - e^{i(n\omega_F - \omega_0)t + i\omega_0 t_0}}{2i} \end{aligned} \quad (5.27)$$

Which solves into

$$\omega_1(t) = \frac{1}{2} \sum_{n=-\infty}^{\infty} A_n \left(\frac{-(e^{i(n\omega_F - \omega_0)t + i\omega_0 t_0} - e^{in\omega_F t_0})}{(n\omega_F - \omega_0)} + \frac{(e^{i(n\omega_F + \omega_0)t - i\omega_0 t_0} - e^{in\omega_F t_0})}{(n\omega_F + \omega_0)} \right) \quad (5.28)$$

and

$$\dot{\phi}_1 = \omega_1 + \frac{\dot{\omega}_1}{\sqrt{\mu}} \quad (5.29)$$

which solves into

$$\begin{aligned} \phi_1(t) = & \frac{\omega_1(t)}{\sqrt{\mu}} + \frac{1}{2} \sum_{n=-\infty}^{\infty} A_n \left(\frac{(e^{i(n\omega_F + \omega_0)t - i\omega_0 t_0} - e^{in\omega_F t_0})}{i(n\omega_F + \omega_0)^2} + \right. \\ & \left. \frac{2\omega_0(t - t_0)e^{in\omega_F t_0}}{n^2\omega_F^2 - \omega_0^2} - \frac{(e^{i(n\omega_F - \omega_0)t + i\omega_0 t_0} - e^{in\omega_F t_0})}{i(n\omega_F - \omega_0)^2} \right) \end{aligned} \quad (5.30)$$

By combining Equations (5.25) and (5.28), we have a first order approximation $\omega(t) = \omega_0 + \epsilon\omega_1(t) + \epsilon^2 R_\omega$. This approximation is a periodic solution with mean equal ω_0 . Nevertheless, this first order approximation does not show any adaptation of $\omega(t)$. This seems normal, since we argued before that the learning takes place on a larger time-scale than the perturbation (which is of order ϵ). We now derive the second order approximation to show that learning appears on the associated time-scale. As we are interested in the second order form of ω , we now

solve Equation (5.22)

$$\begin{aligned}\dot{\omega}_2 &= - \left(\sum_{m=-\infty}^{\infty} A_m e^{im\omega_F t} \right) \left(\frac{e^{i\omega_0(t-t_0)} + e^{-i\omega_0(t-t_0)}}{2} \right) \phi_1(t) \\ &= - \frac{1}{2} \left(\sum_{m=-\infty}^{\infty} A_m \left(e^{i(m\omega_F + \omega_0)t - i\omega_0 t_0} + e^{i(m\omega_F - \omega_0)t + i\omega_0 t_0} \right) \right) \phi_1(t)\end{aligned}\tag{5.31}$$

By expanding the equation we find a sum of simpler terms that can be easily integrated

$$\omega_2 = \int_{t_0}^t \left(\frac{1}{4} \sum_{m,n \in \mathbb{Z}} A_m A_n (E_1 + E_2 + E_3 + E_4 + E_5 + E_6) \right) \tag{5.32}$$

where

$$\begin{aligned}E_1 &= e^{i((m+n)\omega_F + 2\omega_0)t - 2i\omega_0 t_0} \left(\frac{-1}{\sqrt{\mu}(n\omega_F + \omega_0)} - \frac{1}{i(n\omega_F + \omega_0)^2} \right) \\ E_2 &= e^{i((m+n)\omega_F - \omega_0)t + 2i\omega_0 t_0} \left(\frac{1}{\sqrt{\mu}(n\omega_F - \omega_0)} + \frac{1}{i(n\omega_F - \omega_0)^2} \right) \\ E_3 &= e^{i(m\omega_F + \omega_0)t + i(n\omega_F - \omega_0)t_0} \left(\frac{-2\omega_0}{\sqrt{\mu}((n\omega_F)^2 - \omega_0^2)} - \frac{4n\omega_F\omega_0}{i((n\omega_F)^2 - \omega_0^2)^2} \right) \\ E_4 &= e^{i(m\omega_F - \omega_0)t + i(n\omega_F + \omega_0)t_0} \left(\frac{-2\omega_0}{\sqrt{\mu}((n\omega_F)^2 - \omega_0^2)} - \frac{4n\omega_F\omega_0}{i((n\omega_F)^2 - \omega_0^2)^2} \right) \\ E_5 &= e^{i(m+n)\omega_F t} \left(\frac{2\omega_0}{\sqrt{\mu}((n\omega_F)^2 - \omega_0^2)} + \frac{4n\omega_F\omega_0}{i((n\omega_F)^2 - \omega_0^2)^2} \right) \\ E_6 &= \left(e^{i\omega_0(t-t_0)} + e^{-i\omega_0(t-t_0)} \right) \left(\frac{-2\omega_0}{(n\omega_F)^2 - \omega_0^2} \right) e^{i(m\omega_F t + n\omega_F t_0)} (t - t_0)\end{aligned}$$

Prior, we postulated that $\omega_0 \neq n\omega_F$, $\forall n \in \mathbb{N}$, consequently, the integration of E_1 , E_2 , E_3 and E_4 gives periodic functions with zero mean. The integration of E_6 gives a function oscillating with some frequency but with its amplitude varying because of the t term, the average contribution of this function is zero. The integration of E_5 is more interesting because when $n = -m$, the exponential disappears and we have a constant instead. Thus when integrating we will find linear terms. For the case $m \neq -n$, after integration, we find a periodic function with zero mean. Therefore, $\omega_2(t)$ is composed of a periodic function $\tilde{\omega}_2(t)$ with zero mean and a deviation $D_\omega(t)$.

$$\omega_2(t) = \tilde{\omega}_2(t) + D_\omega(t) \tag{5.33}$$

where

$$\begin{aligned}
D_\omega(t) &= \int_{t_0}^t \frac{1}{4} \sum_{\substack{n \in \mathbb{Z} \\ m = -n}} A_n A_m \left(\frac{2\omega_0}{\sqrt{\mu}((n\omega_F)^2 - \omega_0^2)} - \frac{4n\omega_F\omega_0}{i((n\omega_F)^2 - \omega_0^2)^2} \right) \\
&= \int_{t_0}^t \left(\frac{-A_0}{2\sqrt{\mu}\omega_0} + \sum_{n \in \mathbb{N}^*} \frac{A_n \bar{A}_n \omega_0}{\sqrt{\mu}((n\omega_F)^2 - \omega_0^2)} \right) \\
&= \left(\frac{-A_0}{2\sqrt{\mu}\omega_0} + \sum_{n \in \mathbb{N}^*} \frac{|A_n|^2 \omega_0}{\sqrt{\mu}((n\omega_F)^2 - \omega_0^2)} \right) (t - t_0)
\end{aligned} \tag{5.34}$$

Then, the solution of $\omega(t)$ in a neighborhood of t_0 is

$$\omega(t) = \omega_0 + \epsilon \omega_1(t) + \epsilon^2 \tilde{\omega}_2(t) + \epsilon^2 D_\omega(t) + O(\epsilon^3) \tag{5.35}$$

The solution is composed of small oscillations of amplitude much smaller than ϵ around ω_0 and a slight deviation $\epsilon^2 D_\omega(t)$. This deviation term determines how the frequency converges to the input frequency. It can also be used to predict the basins of attraction for inputs with several frequency components (cf. Section 5.1.8). For an input signal that has only one frequency in its spectrum, the deviation is obviously done in the direction of this frequency, since $D_\omega(t) > 0$ when $\omega_F > \omega_0$ and $D_\omega(t) < 0$ otherwise. As this approximation is valid for any ω_0 and any t_0 , i.e. the point in time when we make the approximation is not important, the oscillator will always, in average, change its frequency in the direction of the input frequency. For more complex signals with more than one frequency component, because of the $(n\omega_F)^2 - \omega_0^2$ term in D_ω , the system will just change its frequency according to the distance between its intrinsic frequency ω_0 and the frequency components of the input. The amplitudes A_n of the frequency components will also influence this convergence, in the sense that the more intensity a frequency component has, the more it will attract $\omega(t)$. Section 5.1.5 shows examples of such convergence. We must also note that the zero frequency (the mean of the periodic signal) can also influence the convergence because of the A_0 term. Thus, if the input signal has a non-zero mean, ω could eventually converge to 0 if A_0 has a stronger influence than the other frequency components. In this case, the limit cycle of the Hopf oscillator would bifurcate into a fixed point.

We still have to discuss the case $\omega_0 = n\omega_F$ for a given $n \in \mathbb{N}$. In this case, the oscillator is synchronized with one frequency component of the perturbation. Thus, $\omega(t)$ oscillates and deviates from $n\omega_F$. Then there are two cases, either the deviation becomes an attraction as soon as $\omega_0 \neq n\omega_F$ and the intrinsic frequency of the oscillator is always staying in a small neighborhood of $n\omega_F$. Or $\omega(t)$ diverges from this frequency and gets attracted by another frequency component of the input signal, with stronger amplitude.

We notice that ϵ controls both the amplitude of oscillations around $n\omega_F$ and the learning rate of the system (proportional to ϵ^2). So the faster the learning is,

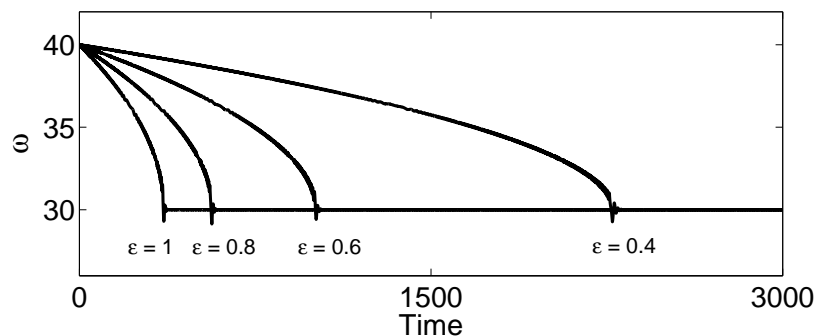


Figure 5.2: Plot of the evolution of ω for four different values of ϵ . Here we set $\mu = 1$, $x(0) = 1$ and $y(0) = 0$, the perturbing force is $F = \cos(30t)$. For every value of ϵ , we see that ω converges to 30, which is the frequency of the input signal. Therefore, the system is able to learn the frequency of the input signal. We also notice that ϵ controls the convergence rate, the higher it is, the faster the system learns.

the higher the error of adaptation will be. But as $\epsilon < 1$, the error of adaptation is bounded and small (of the order of ϵ).

So we have proved that the learning rule makes the frequency converge to a frequency component of the input signal, for any initial conditions (t_0, ω_0) . The attracting frequency component depends on its distance to the intrinsic frequency of the oscillator and its intensity. The proof is global because we did not make any assumption on the initial condition for ω and on the neighborhood of the attracting frequencies.

5.1.5 Numerical simulations

The goal of this section is to study the behavior of the learning dynamical system with numerical simulations. First we give a simple example of adaptation of the oscillator receiving a simple periodic signal as input. Then we confirm the proof of Section 5.1.4 by calculating the second order approximation error for a simple example. We also use the analytic results to predict the behavior of the system when varying several parameters. Finally, we show that the system can adapt to pseudo-periodic signals.

5.1.6 Simple example of learning

First of all, we want to show a simple example of how the system works and discuss the influence of the learning rate ϵ . The adaptive Hopf oscillator is composed of the perturbed Hopf oscillator

$$\dot{x} = (\mu - r^2)x - \omega y + \epsilon F \quad (5.36)$$

$$\dot{y} = (\mu - r^2)y + \omega x \quad (5.37)$$

and of the adaptive frequency learning rule

$$\dot{\omega} = -\epsilon F \frac{y}{\sqrt{x^2 + y^2}} \quad (5.38)$$

Here we use a simple cosine signal $F = \cos(30t)$ as input, with $\mu = 1$ and initial conditions $r(0) = 1$, $\phi(0) = 0$ and $\omega(0) = 40$. We integrate the system numerically for several values of ϵ , the results of the simulations are shown in Figure 5.2. In this figure, we can see that the oscillator adapts its intrinsic frequency to the frequency of the input signal. We also see that ϵ controls the adaptation rate of the system, the higher ϵ is, the faster the learning.

5.1.7 Error evaluation of the analytic approximation for a simple perturbing force

In Section 5.1.4, we derived an approximate solution of the learning dynamical system, in order to prove its convergence. The error of this approximation is bounded by some constant k . We now evaluate numerically the error of the approximation, for a simple sinusoidal input, in order to show that this constant is really small and that the hypothesis made for proving convergence holds. We set $F = \sin(\omega_F t)$, $t_0 = 0$, $\mu = 1$. Then we can derive an approximate solution of $\omega(t)$ using Equations (5.25), (5.28) and (5.32).

$$\omega_0(t) = \omega_0 \quad (5.39)$$

$$\omega_1(t) = -\frac{1}{2(\omega_F - \omega_0)} \sin((\omega_F - \omega_0)t) + \frac{1}{2(\omega_F + \omega_0)} \sin((\omega_F + \omega_0)t) \quad (5.40)$$

$$\begin{aligned} \omega_2(t) = & \frac{\sin(2\omega_0 t)}{16\omega_0(\omega_F - \omega_0)} - \frac{\sin(2\omega_F t)}{16\omega_F(\omega_F - \omega_0)} - \frac{\sin(2(\omega_F - \omega_0)t)}{16(\omega_F - \omega_0)^2} + \frac{t}{8(\omega_F - \omega_0)} \\ & - \frac{t}{8(\omega_F + \omega_0)} + \frac{\sin(2(\omega_F + \omega_0)t)}{16(\omega_F + \omega_0)^2} - \frac{\sin(2\omega_0 t)}{16\omega_0(\omega_F + \omega_0)} + \frac{\sin(2\omega_F t)}{16\omega_F(\omega_F + \omega_0)} \\ & + \frac{\cos(2\omega_F t) - 1}{16\omega_F(\omega_F - \omega_0)^2} + \frac{\cos(2\omega_0 t) - 1}{16\omega_0(\omega_F - \omega_0)^2} + \frac{\cos(2(\omega_F - \omega_0)t) - 1}{16(\omega_F - \omega_0)^3} \\ & - \frac{\cos((\omega_F + \omega_0)t) - 1}{4(\omega_F - \omega_0)^2(\omega_F + \omega_0)} - \frac{\cos((\omega_F - \omega_0)t) - 1}{4(\omega_F - \omega_0)^3} \\ & - \frac{\cos(2(\omega_F + \omega_0)t) - 1}{16(\omega_F + \omega_0)^3} - \frac{\cos(2\omega_F t) - 1}{16\omega_F(\omega_F + \omega_0)^2} + \frac{\cos(2\omega_0 t) - 1}{16\omega_0(\omega_F + \omega_0)^2} \\ & + \frac{\cos((\omega_F + \omega_0)t) - 1}{4(\omega_F + \omega_0)^3} - \frac{\cos((\omega_F - \omega_0)t) - 1}{4(\omega_F + \omega_0)^2(\omega_F - \omega_0)} \end{aligned} \quad (5.41)$$

We can now numerically evaluate the errors of the approximations of order 1, $\omega_\epsilon(t) = \omega_0 + \epsilon\omega_1(t)$, and of order 2, $\omega_{\epsilon^2}(t) = \omega_0 + \epsilon\omega_1(t) + \epsilon^2\omega_2(t)$. The upper plot of Figure 5.3 shows the result of this simulation. First of all, we clearly see that the dynamical system correctly learns the frequency of the input signal. In this figure we also plotted the function $\omega_\epsilon(t)$ and $\omega_{\epsilon^2}(t)$, we clearly see that the second order approximation is really better than the first and explains the behavior of the system on a larger time scale. Actually, it explains very well the convergence process of the learning dynamical system. We see that the learning appears on a

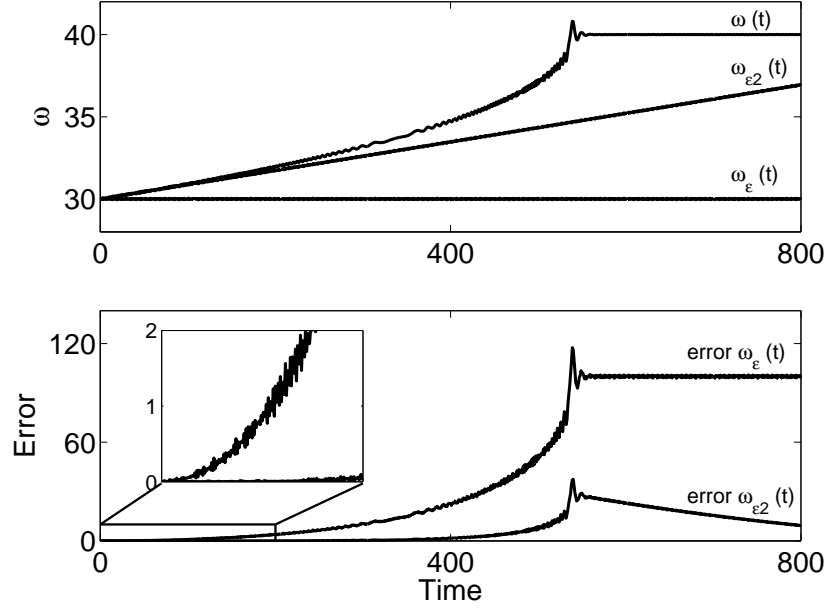


Figure 5.3: Results of the simulation of the first and second order approximations. For a simple input, here $F = \sin(40t)$, $\epsilon = 0.9$, initial conditions are $t_0 = 0$, $w_0 = 30$. The upper figure shows the evolution of the ω variable for the initial dynamical system (Eq. (5.38)), the first order approximation $\omega_\epsilon(t)$ and the 2nd order approximation $\omega_{\epsilon^2}(t)$. The lower figure shows quadratic errors between the initial system and the 2 approximations, for the evolution of ω .

Table 5.1: This table summarizes the maximum errors of the simulation for the first and second order approximations discussed from Figure 5.3

Time	Maximum Error ω_ϵ	Maximum Error ω_{ϵ^2}
0s	0	0
0.001s	$5.18e^{-13}$	$1.70e^{-19}$
0.01s	$4.91e^{-7}$	$1.15e^{-12}$
0.1s	0.0053	$6.30e^{-11}$
1s	0.0114	$1.85e^{-7}$
10s	0.0340	$4.25e^{-4}$

coarser time scale than the oscillations of the system. In the lower plot, we see the square error between the original system and the approximations. We clearly see that the 2nd order approximation follows the real system for quite a long time. Table 5.1 summarizes the maximum square error of the approximations. It must be noted that numerical integration of the dynamical system is done with an embedded Runge-Kutta-Fehlberg(4,5) algorithm, with absolute and relative errors of 10^{-6} . As a matter of fact, errors below this value cannot be taken as significant errors. Obviously, the first order approximation diverges rapidly, at 0.1s of simulation, the error is becoming really significant. On the other hand, the second order approximation is really good still after 10s. These results validate the hypothesis of the approximation methods and so, the analytic proof. It also emphasizes the fact that learning takes place on a larger time-scale than the perturbations on the oscillator and its oscillations. Consequently, the adaptive Hopf oscillator has two distinct time scales. The finer one describes the perturbation on the oscillator and its oscillations. Learning takes place on the coarser one.

5.1.8 Predicting learning with multi-frequency inputs

When learning frequency of multi-frequency input signals, we might expect the system to converge to one of the frequency components of the input. But how can we calculate the range of initial frequencies for which the adaptive oscillator will converge to a specific frequency component of the input? While proving the convergence of the system, we derived a deviation equation, Equation (5.34), that describes the deviation from the initial intrinsic frequency, ω_0 , of the oscillator

$$D_\omega(t) = \left(\frac{-A_0}{2\sqrt{\mu}\omega_0} + \sum_{n \in \mathbb{N}} \frac{|A_n|^2 \omega_0}{\sqrt{\mu}((n\omega_F)^2 - \omega_0^2)} \right) (t - t_0) \quad (5.42)$$

We saw that this equation is depending on the initial frequency of the system ω_0 , the frequency components of the periodic input $n\omega_F$ and their amplitude A_n . Thus, for a given input signal, we can calculate the values of ω_0 for which the function is equal to zero $\forall t$. These zeros give the intervals of convergence, the dynamical system converging towards the frequency components located in the same interval as ω_0 .

For example consider the following input

$$F = 0.2 \sin(20t) + 0.5 \sin(30t) + 0.3 \sin(40t) \quad (5.43)$$

The main frequency of this signal is $\omega_F = 10$. The amplitude of the frequency component are $A_2 = \frac{0.2}{2i}$, $A_3 = \frac{0.5}{2i}$, $A_4 = \frac{0.3}{2i}$ and $A_i = 0, \forall i \in \mathbb{N} \setminus \{2, 3, 4\}$. Thus we only have to find the roots of the following equation

$$\frac{0.2^2 \omega_0}{4(20^2 - \omega_0^2)} + \frac{0.5^2 \omega_0}{4(30^2 - \omega_0^2)} + \frac{0.3^2 \omega_0}{4(40^2 - \omega_0^2)} = 0 \quad (5.44)$$

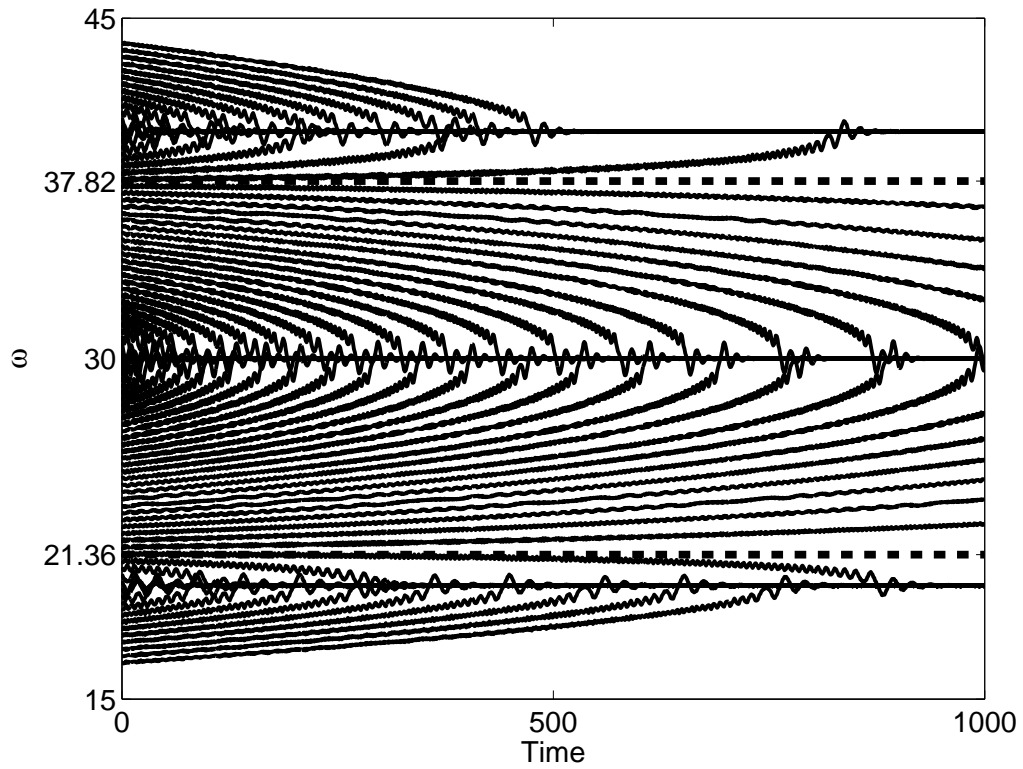


Figure 5.4: In this figure, we plotted $\omega(t)$ for several initial conditions, ω_0 . The periodic input is Equation (5.43), $\epsilon = 0.9$. The dotted lines indicates the boundary between the different basins of attraction, corresponding to the different frequency components of the input, that were predicted analytically.

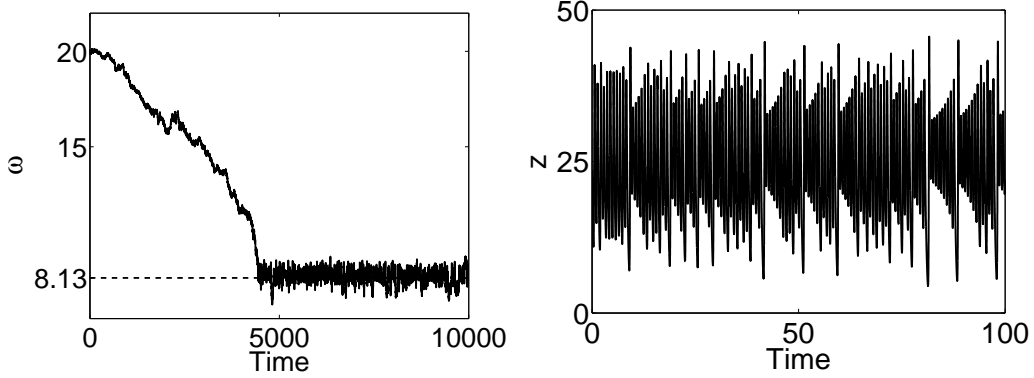


Figure 5.5: The left plot of this figure represents the evolution of $\omega(t)$ when the adaptive Hopf oscillator is coupled to the z variable of the Lorenz attractor. The right plot represents the z variable of the Lorenz attractor. We clearly see that the adaptive Hopf oscillators can correctly learn the pseudo-frequency of the Lorenz attractor. See the text for more details.

The solutions of this equation are 0 and $\pm \sqrt{\frac{717 \pm \sqrt{134089}}{0.76}}$. As we are working with frequencies > 0 we have the following bounds $\omega_{down} \simeq 21.3598$ and $\omega_{up} \simeq 37.8233$. Thus we must expect to have convergence to 20, 30 or 40 when $\omega_0 \in [0, \omega_{down}]$, $[\omega_{down}, \omega_{up}]$, $[\omega_{up}, \infty]$ respectively. With some uncertainty at the limit of the intervals, because of the oscillations of order ϵ that can make the system switch from one interval to the other. Figure 5.4 shows this behavior, the horizontal dotted lines mark the bounds. Convergence corresponds to what we predicted.

5.1.9 Learning pseudo-period of chaotic signals

We proved convergence for periodic signals, but we argue that even pseudo-periodic signals can be used as input for the learning dynamical system. In order to show this fact, we present the result of learning, when coupled to a chaotic pseudo-periodic signal. We couple the oscillator with the z -variable of the Lorenz system [213], whose equation is

$$\dot{x} = -\sigma x + \sigma y \quad (5.45)$$

$$\dot{y} = -xz + rx - y \quad (5.46)$$

$$\dot{z} = xy - bz \quad (5.47)$$

Where $\sigma = 10$, $r = 28$ and $b = \frac{8}{3}$ (parameters for which the system produces a strange attractor). The Fourier spectrum of the z -variable indicates two major frequency components (data not shown). The first one at frequency 0 (A_0 in the Fourier series), because the average of z , $\langle z \rangle \neq 0$, and the second one at $\sim 1.3\text{Hz}$. As the zero frequency component has a really strong amplitude compared to the other and we do not want adaptation to this frequency, we center the z -variable

before coupling to the oscillator. Otherwise, ω converges to 0 and the oscillations disappear. Indeed the basin of attraction corresponding to frequency $\sim 1.3\text{Hz}$ is not very wide and ω gets kicked out of it because of the chaotic nature of the input. Thus the input for coupling we use is $F = z - \langle z \rangle$.

Figure 5.5 shows the result of the learning process. After convergence, $\langle \omega \rangle \simeq 8.13 \text{ rad} \cdot \text{s}^{-1}$ which corresponds to an intrinsic frequency of the oscillator of $\sim 1.29 \text{ Hz}$. Thus our adaptive dynamical system has learned the pseudo-frequency of the strange attractor. As this is not a strictly periodic signal, $\omega(t)$ oscillates, following the constantly changing pseudo-frequency of the attractor.

This experiment enforces the idea that our adaptive dynamical system is able to learn the frequency of any periodic, or pseudo-periodic signal. It learns a frequency component of the input, even if the signal is really noisy or if the frequency is not strictly defined.

5.1.10 Generalization to non-harmonic oscillators

In previous sections, we presented an adaptive Hopf oscillator able to learn the frequency component of a periodic signal. The goal of this section is to show how we can easily apply our adaptive rule to non-harmonic oscillators like relaxation oscillators. The problem with such oscillators is that they have two time scales (slow buildup and fast relaxation) so it is difficult to treat them analytically to prove convergence of the adaptive rule. In this section, we discuss in details the case of the Van der Pol oscillator, then we show results of the adaptive rule with the Rayleigh oscillator, the Fitzhugh-Nagumo oscillator and the Rössler system.

5.1.11 An adaptive Van der Pol oscillator

The Van der Pol oscillator

The Van der Pol is a classical example of relaxation oscillator and is often used in biological modeling, for example to model CPGs for quadrupedal locomotion [47]. Its equation is

$$\ddot{x} + \alpha(x^2 - p^2)\dot{x} + \omega^2 x = 0 \quad (5.48)$$

Here α controls the degree of nonlinearity of the system (the relaxation part), p the amplitude of the oscillations and ω mainly influences the frequency of the oscillations. In this study we set the amplitude of oscillations to $p = 1$. We rewrite the system in a 2-dimensional form and perturb it in the direction of x as we did in Section 5.1.2

$$\dot{x} = y + \epsilon F \quad (5.49)$$

$$\dot{y} = -\alpha(x^2 - 1)y - \omega^2 x \quad (5.50)$$

Because of the relaxation property of the oscillator, the frequency spectrum contains, in addition to the frequency of the oscillations, an infinite number of frequency components. They are all multiples of the frequency of the oscillations

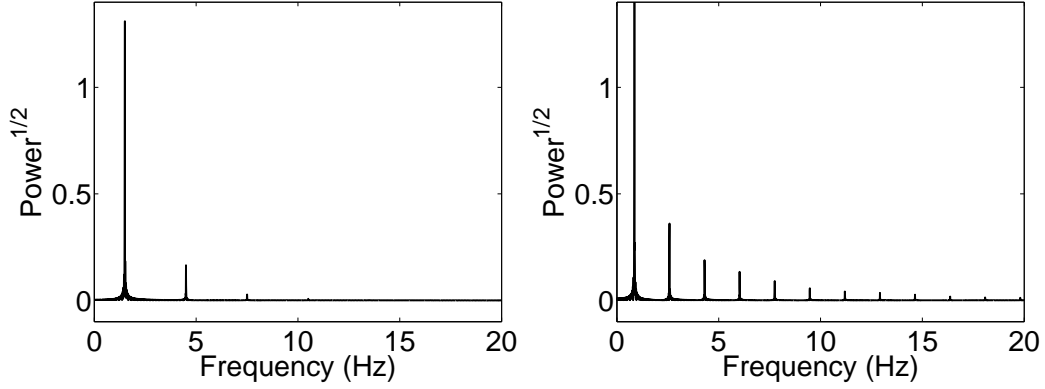


Figure 5.6: Frequency spectrum of the Van der Pol oscillator, both plot with $\omega = 10$. The left figure is an oscillator with $\alpha = 10$ and on the right the nonlinearity is higher $\alpha = 50$. On the y-axis we plotted the square root of the power intensity, in order to be able to see smaller frequency components.

and have smaller intensities. The nonlinear part of the system, whose importance is driven by the α variable, influences the intensity of these components. It means the higher α is, the more intensity high frequency components have. The frequency of the oscillations are mainly defined by ω , but α also influences this frequency. In fact an increase of the nonlinear term α tends to slow the oscillator down.

Figure 5.6 shows the frequency spectrum of the x variable for two different values of α . We clearly see that the intensities of the fast frequency components increase as α increases. We also observe that the oscillator gets slower when α increases (the peaks shift to the left). But still ω is a good control parameter of the frequency of the system.

The complexity of the frequency spectrum of such oscillators complicates learning. Indeed, according to the initial conditions (i.e. according to the distance between the frequency of the periodic force and the main frequency of the oscillator), the oscillator may learn different frequencies and synchronize one of its higher frequency components to the input, instead of adapting its main frequency.

The adaptive dynamical system

The adaptive rule we introduced in this article dynamically changes the parameter that mainly controls the frequency of the oscillations. Thus, in this case we will make the ω parameter a dynamical system. Before discussing adaptation, we want to discuss the locations of the entrainment basins in function of ω , in order to understand how the adaptive rule will work. The entrainment basins are the regions of frequencies where the oscillator phase-lock with an input signal [166].

Figure 5.7 shows the entrainment basins of a Van der Pol oscillator with high

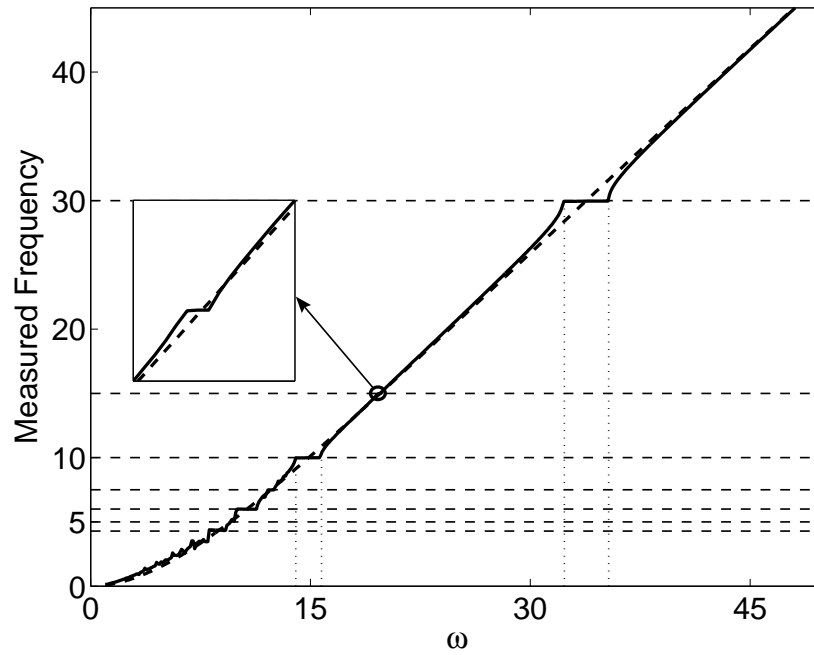


Figure 5.7: Plot of the frequency of the oscillations of the Van der Pol oscillator according to ω . Here $\alpha = 50$. There are 2 plots, in dotted line the oscillator is not coupled and in plain line the oscillator is coupled to $F = \sin 30t$. The strength of coupling is $\epsilon = 2$. We clearly see basins of phase-locking, the main one for frequency of oscillations 30. The other major basins appears each $\frac{30}{n}$ (dotted horizontal lines). We also notice small entrainment basins for some frequencies of the form $\frac{30p}{q}$. For a more detailed discussion of these results refer to the text.

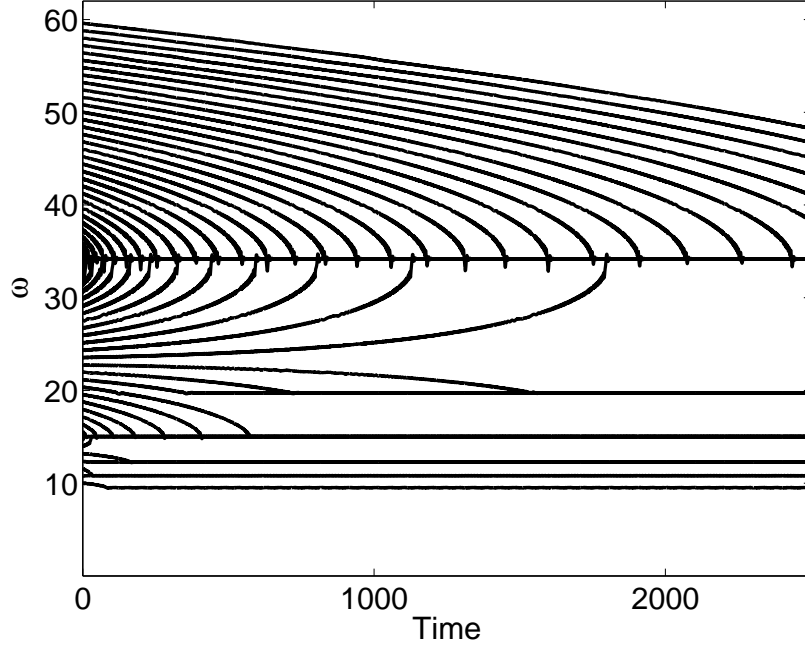


Figure 5.8: This figure shows the convergence of ω for several initial frequencies. The Van der Pol oscillator is perturbed by $F = \sin(30t)$, with coupling $\epsilon = 0.7$, $\alpha = 50$. We clearly see that the convergence directly depends on the initial conditions and as expected the different kinds of convergence correspond to the several entrainment basins of Figure 5.7.

nonlinear component $\alpha = 50$, which is forced by a periodic signal $\sin(30t)$. As expected, we see phase locking at frequency of oscillations 30, with an entrainment basin of $\omega \in [32, 35]$. We also explained that the oscillator may phase lock its higher frequency components, as these frequency components are equally spaced, one should expect phase lock for fractions of the frequency of the perturbing force. In this case, for example, we see phase locking at frequencies of oscillations $\frac{30}{2}$, $\frac{30}{3}$ and $\frac{30}{4}$.

This figure may become even more complex if the input signal has several frequency components. We would see entrainment basins every time a frequency component of the oscillator is close enough to any frequency component of the external signal. Then, when using our adaptive rule, one should expect convergence to any entrainment basins, depending on the initial conditions. Therefore, the oscillator might adapt its higher frequency components to the frequency of the input.

We now discuss the learning rule we introduced in Section 5.1.2, applied to the Van der Pol oscillator. We just change the sign of Equation (5.7). This is justified because when looking to the limit cycle of the Van der Pol oscillator, we see that it is rotating in the opposite direction of the Hopf oscillator limit cycle. So the

learning rule is

$$\dot{\omega} = \epsilon F \frac{y}{\sqrt{x^2 + y^2}} \quad (5.51)$$

We do not give an analytical proof of convergence for the Van der Pol oscillator because to use perturbation methods, as we did for the Hopf oscillator, we need to know the solution of the unperturbed Van der Pol oscillator, but to the best of our knowledge, only implicit solutions are known [55] and thus such a proof is beyond the scope of this article. But the general behavior of the system should be qualitatively the same, because of the linear coupling on the oscillator. Lets rewrite Equations (5.49) and (5.50) into polar coordinates

$$\dot{r} = \epsilon F \cos \phi + (1 - \omega^2)r \cos \phi \sin \phi + \alpha r^3 \sin^4 \phi \quad (5.52)$$

$$\dot{\phi} = -\omega^2 \cos^2 \phi - \sin^2 \phi + \alpha r^2 \sin^3 \phi \cos \phi - \frac{\epsilon F}{r} \sin \phi \quad (5.53)$$

Even if the phase evolution is more complex than for the Hopf oscillator, the interaction between the phase of the oscillator ϕ and the perturbation F is of the same kind. Indeed, we clearly identify the same $-\frac{\epsilon F}{r} \sin \phi$ terms for the phase of both oscillators (Eqs. (5.52), (5.53) and Eqs. (5.3), (5.4)). So we can expect the same deviation of ω and therefore, the same convergence properties.

Now that we discussed the different expected behaviors, we present a series of experiments in order to confirm our predictions and the functionality of the adaptive dynamical system.

Numerical confirmation

We predicted that the adaptive Van der Pol oscillator will either adapt its frequency of oscillations or one of its higher frequency component to the frequency of the input. In order to show this, we study convergence of ω for different initial conditions, when the oscillator is coupled with a simple sinus input ($F = \sin(30t)$). Figure 5.8 shows the result of the simulation.

When the initial condition $\omega_0 > 23$, we clearly see that ω converges to 34 which corresponds to a frequency of oscillations of $30 \text{ rad} \cdot \text{s}^{-1}$. In this case the oscillator is correctly adapting its frequency to the frequency of the input. For lower values of ω_0 , we see convergence to other frequencies, corresponding to the entrainment basins of Figure 5.7. We can conclude that the adaptive rule is changing ω in order to get one frequency component of the oscillator to the same frequency than the input signal. In fact, ω is falling into the nearest entrainment basin. Therefore, we see how useful entrainment basins studies are to understand the dynamics of the adaptive oscillator.

Moreover, even if there is not a direct relation between ω and the frequency of the oscillations, the adaptive learning rule can appropriately tune ω so that the frequency of oscillations (or one of the other frequencies of the oscillator) are the same than the frequency of the input signal. Figure 5.9 shows the result of the adaptation of the oscillator for various input signals. From these experiments, we

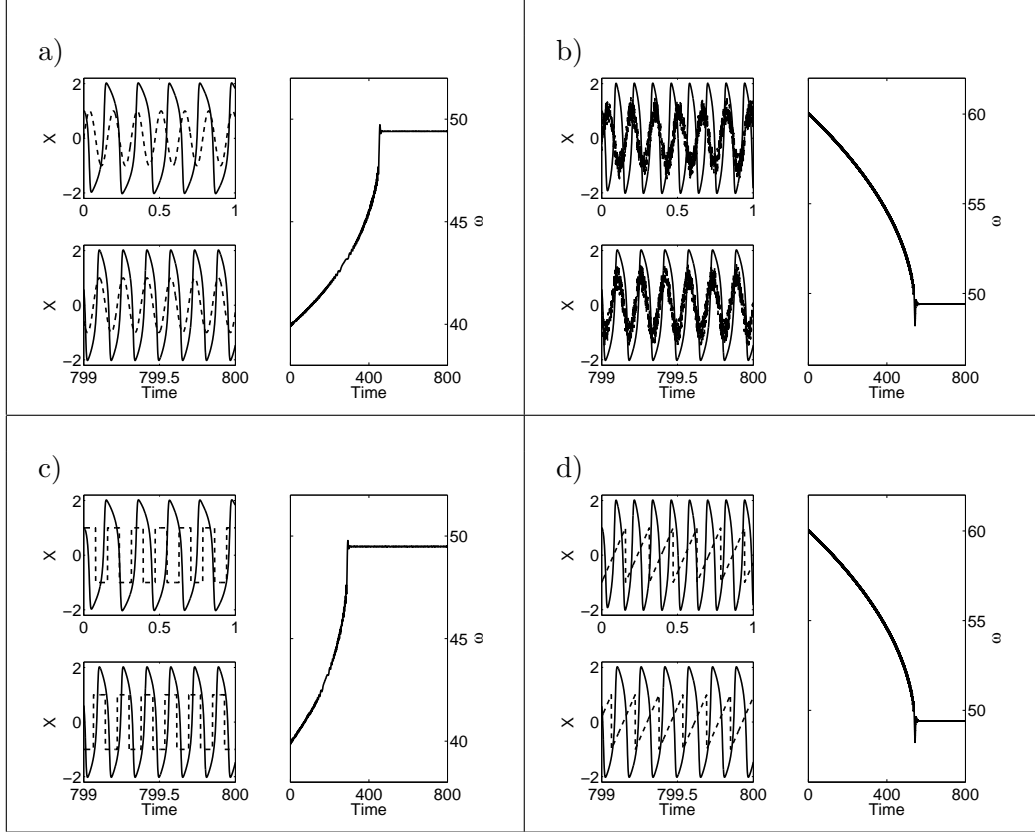


Figure 5.9: We show the adaptation of the Van der Pol oscillator to the frequency of various input signals: (a) a simple sinusoidal input ($F = \sin(40t)$), (b) a sinusoidal input with uniformly distributed noise ($F = \sin(40t) + \text{uniform noise in } [-0.5, 0.5]$), (c) a square input ($F = \text{square}(40t)$) and (d) a sawtooth input ($F = \text{sawtooth}(40t)$). For each experiment, we set $\epsilon = 0.7$ and $\alpha = 100$ and we show three plots. The right one shows the evolution of $\omega(t)$. The upper left graph is a plot of the oscillations, x , of the system, at the beginning of the learning. The lower graph shows the oscillations at the end of learning. In both graphs, we also plotted the input signal (dashed). In each experiment, ω converges to $\omega \simeq 49.4$, which corresponds to oscillations with a frequency of $40 \text{ rad} \cdot \text{s}^{-1}$ like the input and thus the oscillator correctly adapts its frequency to the frequency of the input.

see that ω converges to a value that corresponds to a correct adaptation of the frequency of the oscillations to the frequency of the input. In each experiment, we see that after learning, the Van der Pol oscillator and the input signal are oscillating at the same frequency.

The adaptive Van der Pol oscillator demonstrates how to generalize our adaptive rule to complex oscillators. But, an increase in the complexity of the frequency spectrum of an oscillator also generates side effects, like adaptation toward synchronization of the higher frequency components of the oscillator and the frequency of an input signal. Thus, when using highly nonlinear oscillators, one should always know the kind of frequency spectrum it has, in order to be able to predict the behavior of the oscillator. Even if we cannot analytically prove the convergence of our model, by numerically calculating the positions of the entrainment basins of the oscillator when perturbed, we are able to predict the behavior of the system in a quite powerful way.

In this section, we also discussed a very important property of the adaptive learning rule. Although, the parameter we tune has not a linear relation with the frequency of the oscillator, as it is often the case in highly nonlinear oscillators, the adaptive oscillator is able to correctly adapt this parameter and find the appropriate frequency of oscillations. It seems that a monotone relation between the frequency of the oscillations and the parameter we tune is sufficient for frequency adaptation.

5.1.12 Other examples of adaptive oscillators

In this section, in order to show the generality of the adaptive rule, we present experimental results with three other oscillators. We build an adaptive Rayleigh oscillator, an adaptive Fitzhugh-Nagumo oscillator and an adaptive Rössler system.

The construction of the adaptive dynamical system is straightforward. The main task is to identify in each oscillator the parameter that mostly influences the frequency of the oscillations. Then, we only have to make this parameter a dynamical system in the same way we did for the Hopf or the Van der Pol oscillator. The right column of Figure 5.10 gives the resulting equations for each oscillator.

In order to demonstrate the frequency adaptivity of these modified oscillators, we made experiments for each oscillator. The results of the experiments are summarized in Figure 5.10. In these experiments, the oscillators were perturbed by a simple sinusoidal input and each oscillator was able to adapt its ω parameter in order to learn the frequency of the input. Moreover, although the parameters controlling the frequency in each oscillator are not linearly related to the frequency of the oscillations, the adaptive rule is able to correctly find the correct value for the ω parameter to learn the desired frequency.

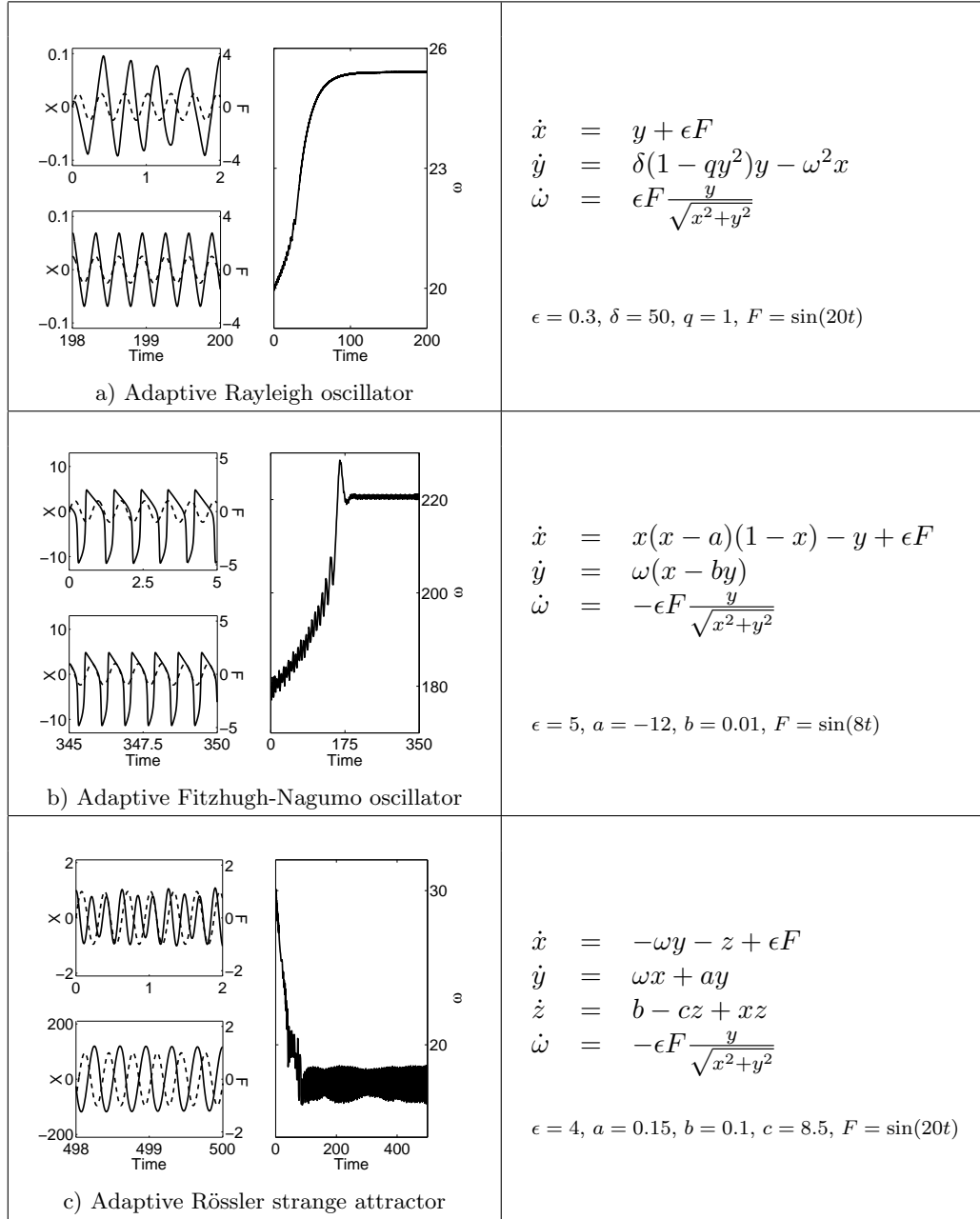


Figure 5.10: We show results for several adaptive oscillators. For each oscillator, we give its equation in the right column, ω corresponding to the adaptive parameter. We also specify the values of the different parameters used in the experiments. In the left column we plotted results of the experiment. Each figure is composed of 3 plots. The right one is a plot of the evolution of ω . The left ones are plots of the oscillations (the x variable) and of the input signal F (dashed line), before (upper figure) and after (lower figure) adaptation.

5.1.13 Discussion

Fields such as control of autonomous robots or signal processing may need models of plastic dynamical systems to adapt to a constantly changing environment. Moreover, plasticity in nonlinear oscillators might become an important aspect in modeling adaptive processes, as for example in biology where adaptivity and memory are major properties of living systems. The learning rule presented in this article is a step towards a general framework of plastic dynamical systems, which are systems for which learning is embedded in their dynamics and not an offline optimization process.

The evolution of the parameter controlling the frequency of the adaptive oscillators that we discussed can be viewed as the correlation between the phase of the oscillator and the input signal. So we defined a type of correlation-based learning for periodic functions. In neurobiology, correlation based-learning rules are known as Hebbian learning [122], hence we call our rule *dynamic Hebbian learning* to highlight its correlation properties. Possible relevance to biology has to be investigated in further research.

The construction of adaptive oscillators that we presented is simple, and general enough to be applied to non-harmonic oscillators and not only to phase oscillators. The adaptive rule is general for an oscillator, perturbed by a signal $F(t)$, with general equation

$$\begin{aligned}\dot{x} &= f(x, y, \omega) + \epsilon F(t) \\ \dot{y} &= f(x, y, \omega)\end{aligned}\tag{5.54}$$

with ω influencing the frequency of the oscillations. We have the general learning rule

$$\dot{\omega} = -\epsilon F \frac{y}{\sqrt{x^2 + y^2}}\tag{5.55}$$

Only the sign in front of F may change according to the orientation of the flow of the oscillator in the phase space. In this sense we generalize the concept of learning presented by Nishii in [158, 159], in which learning rules were only derived for phase oscillators. Nevertheless, in addition to frequency adaptation, Nishii also derived learning rules for coupling strength in populations of oscillators, which is an issue we do not address in this contribution.

The learning rule we presented is not rigid and can be modified. For instance, for the Hopf oscillator, a change in the learning rule in Eq. (5.7), from $\sin\phi$ to $\cos\phi$ or any combination of periodic functions will not change the convergence properties. This would only correlate the force to more complex periodic functions instead of $\sin\phi$. Intuitively, the proof of convergence should give the same results, since the learning part of the approximation (Equation (5.34)) depends on the conjugate symmetry of the complex Fourier series of the input signal, which is true for every real input signal.

The mathematical proof given in this paper leads to a better comprehension of the learning process, which takes place on a coarser time scale than the oscillations of the system. This proof also allows us to predict what the oscillator would learn

in the case of multi-frequency inputs. Nevertheless, we only give a proof for the adaptive Hopf oscillator and even if we numerically show that more complex adaptive oscillators can be designed, a general rigorous proof for a larger class of oscillators is still missing. Constructing such a proof is a very difficult task.

A major feature of our learning rule is that the oscillator can extract the frequency of any input signal without any explicit signal processing (Fourier transform) or any explicit time window or similar parameters. All the processing is embedded in the dynamics of the oscillator. We also showed that the system can learn frequencies from really noisy signals or from pseudo-periodic signals, like a signal from the Lorenz strange attractor. The adaptive rule is also valid to tune parameters that do not control linearly the frequency of the oscillations. A monotonic, possibly nonlinear, relation between the frequency of oscillations and the adapted parameter is sufficient for correct adaptation of the parameter as we showed for the case of relaxation oscillators. In this case, the system is able to correctly find a value that produces oscillations at the same frequency as the input signal.

Dynamic Hebbian learning for adaptive oscillators has an important implication in the design of CPG models. Actually, coupled nonlinear oscillators are often used for modeling CPGs [48, 78, 131, 221], but the coupling has to be defined by hand and this is a non-trivial task. By using adaptive oscillators, one could build CPGs that can dynamically adapt their frequencies and consequently, create a desired pattern of oscillations. For instance, we are currently exploring how a population of adaptive oscillators can implement some kind of dynamic Fourier transform [175]. Furthermore, one can imagine using this adaptation mechanism to model various processes where self-synchronization is observed.

Acknowledgments We would like to gratefully acknowledge Jun Nakanishi and Biljana Petreska for their useful comments on a previous version of this article and the anonymous reviewers for their constructive comments. This work was made possible thanks to the support of the European Commission (Integrated Project RobotCub) and of the Swiss National Science Foundation (Young Professorship Award to Auke Ijspeert).

5.2 Frequency analysis with AFOs

In this section we show that it is natural to use the same building block for other applications than robotics. We do this by showing how we can do dynamic frequency analysis with a pool of adaptive frequency oscillators.

Frequency Analysis with Coupled Nonlinear Oscillators

Jonas Buchli, Ludovic Righetti, Auke Jan Ijspeert

This paper is under review.

Abstract We present a method to obtain the frequency spectrum of a signal with a nonlinear dynamical system. The dynamical system is composed of a pool of adaptive frequency oscillators with negative mean-field coupling. For the frequency analysis, the synchronization and adaptation properties of the component oscillators are exploited. The frequency spectrum of the signal is reflected in the statistics of the intrinsic frequencies of the oscillators. The frequency analysis is completely embedded in the dynamics of the system. Thus, no preprocessing or additional parameters, such as time windows, are needed. Representative results of the numerical integration of the system are presented. It is shown, that the oscillators tune to the correct frequencies for both discrete and continuous spectra. Due to its dynamic nature the system is also capable to track non-stationary spectra. Further, we show that the system can be modeled in a probabilistic manner by means of a nonlinear Fokker-Planck equation. The probabilistic treatment is in good agreement with the numerical results, and provides a useful tool to understand the underlying mechanisms leading to convergence.

5.2.1 Introduction

Frequency analysis is an important method in science and engineering. It has been realized that the frequency spectrum of a signal carries important information that is not easily accessible and exploitable in the time domain. Consequently, frequency domain methods are of major importance in many disciplines both for signal processing and for signal generation.

Several well-known techniques have been developed to carry out frequency analysis, most prominently techniques based on Fourier transforms, filter banks, and wavelets. The goal of this article is to explore alternative methods and to answer the following question: is it possible to carry out frequency analysis using a dynamical system and nothing else? As we will see, the answer is yes, by using a system of coupled (adaptive frequency) oscillators.

This work was mainly driven by intellectual curiosity, and the resulting system is therefore not meant to outperform current techniques nor to model a particular biological or physical phenomenon. Nonetheless, as discussed at the end of

the article, the system presents several interesting properties which might lead to interesting applications in engineering, and/or in science, e.g. for exploring questions of adaptation in rhythmic systems.

Oscillators and systems of coupled oscillators are known as powerful modeling tools [166] and are widely used in physics and biology to model phenomena as diverse as neuronal signaling, circadian rhythms [214], heart beating, flashing of fireflies [154], inter-limb coordination [91], Josephson junctions [231], lasers to name a few. Quite often the oscillator's parameters (such as the intrinsic frequency) are kept fixed. Recently, we proposed an adaptive frequency mechanism for oscillators which enables the oscillator to adapt its intrinsic frequency to one of the frequency components of an input signal [24, 178].

Here, we present a system consisting of a population of mean field coupled adaptive frequency oscillators which is able to extract the frequency components of any arbitrary teaching signal $T(t)$ presented to the system and to reproduce it by a signal $O(t) \approx T(t)$. The main results presented here are twofold: First, we show, verified by numerical integration, that the system indeed reproduces the frequency spectrum of a given signal. The spectrum is reflected in the distribution of individual intrinsic frequencies of the population of oscillators. The system works for signals that have discrete and continuous spectra, where these spectra can be stationary or time-varying. Second, we show that the frequencies of the oscillators can be treated as particles under external forces and this allows one to use the Fokker-Planck formalism to pose a macroscopic model which serves to study its convergence properties in an additional way.

Central to the system are: a) the adaptive frequency property of the basic oscillators, b) a negative feedback mechanism exerting influence via the mean field, and c) a large number of oscillators. The oscillators serve as discrete building blocks to construct the desired signal. After convergence, the distribution of the frequencies of the oscillators corresponds, with respect to the fundamental limits, to the frequency spectrum of the input signal, which could otherwise be obtained e.g. via the FFT. To the best of our knowledge the presented system is the first of its kind, exploiting the properties of oscillators to do frequency analysis.

5.2.2 A dynamical system for frequency analysis

In this section, we will first describe the basic unit out of which the whole the complete system is constructed, namely the adaptive frequency oscillator that we developed. We then present the complete system build as a pool of adaptive frequency oscillators coupled with a negative mean-field feedback mechanism.

Basic unit: The adaptive frequency oscillator

The basic unit of the system is an adaptive frequency Hopf oscillator [24, 178]. The oscillator receives an input $I(t)$ which is an additive perturbation to \dot{x} and

which also influences the evolution of the frequency ω

$$\dot{x} = (\mu - (x^2 + y^2))x + \omega y + KI(t) \quad (5.56)$$

$$\dot{y} = (\mu - (x^2 + y^2))y - \omega x \quad (5.57)$$

$$\dot{\omega} = KI(t) \frac{y}{\sqrt{x^2 + y^2}} \quad (5.58)$$

where x, y are the states of the oscillator and ω its intrinsic frequency, $0 < K$ is a coupling constant, μ determines the steady state amplitude of oscillations ($x_\infty^2 + y_\infty^2 = \mu$). We choose for simplicity $\mu = 1$.

The convergence properties of adaptive frequency oscillators as presented in Eqs. (5.56)–(5.58) are discussed in detail in [178]. Important for the frame of this article is the fact that an adaptive frequency oscillator adapts its intrinsic frequency ω to one of the frequency components present in the input signal. By perturbation series analysis it can be proved that the adaptive frequency Hopf oscillator converges. From this analysis it gets furthermore clear that the convergence behaves according to [178]

$$\dot{\omega} = K^2 \sum_{n \in \mathbb{N}} \frac{|A_n|^2 \omega}{(n\omega_F)^2 - \omega^2} + \tilde{F}(t) \quad (5.59)$$

where ω_F is the fundamental frequency of the perturbation and A_n are the Fourier components of the signal $I(t)$ perturbing the oscillator. $\tilde{F}(t)$ summarizes other driving terms which have average zero or are of very small order and do thus not contribute to the long-term evolution of ω . Equation 5.59 furthermore shows that there exist several basins of attraction (i.e. one for each $A_n \neq 0$).

At this point, it is important to point out that the convergence of the frequency adaptation (i.e. the behavior of ω) should not be confused with the locking behavior (i.e. the classic phase locking behavior, or synchronization, as well documented in literature, cf. [166]). The frequency adaptation process is an *extension* of the common oscillator with fixed intrinsic frequency. (1) The adaptation process changes the intrinsic frequency and not only the resulting frequency, (2) the adaptation generally has an infinite basin of attraction (i.e. for every initial condition $\omega(0)$ it will converge to a frequency $n\omega_F$ as opposed to the limited range in which synchronization can take place, also known as Arnol'd tongues structure [8, 166]), (3) the frequency stays encoded in the system when the input is removed (e.g. set to zero).

In Figure 5.11 the typical convergence of the intrinsic frequency ω for different input signals is shown. Here, we only show a *single* adaptive frequency oscillator in these examples, *without* the mean-field feedback, to give the reader a feeling of the properties of the building block of the full system. It is important to realize that the adaptive frequency oscillator will find not only the frequency of harmonic signals (Fig. 5.11a), but also of nonharmonic signals (Fig. 5.11b–f).

Adaptive frequency oscillators will also track non-stationary signals with varying frequencies (Fig. 5.11d). If the input has several frequency components the

final value of ω is dependent on its initial condition $\omega(0)$ and the structure of the frequency spectrum of the input signal, i.e. there exist several basins of attraction (see Fig. 5.11e). The size and boundaries of a basin of attraction depend on the energy content of the frequency component constituting the attractor in this basin and can be inferred from Eq. (5.59) (see [178] for details). Finally the oscillator also adapts to the pseudo-frequency of non-periodic signals like the output of the Rössler system [184] in its chaotic regime (Fig. 5.11f).

In Fig. 5.12 we show how the adaptation rate can be modulated by choosing different coupling constants K . It is evident that while a larger K means shorter adaptation time, the amplitude of the oscillations at steady state behavior increases as well. The problem of increased steady state oscillations however does to a large extent not affect the final system with the mean-field feedback, as will be discussed later.

All the aforementioned properties of the adaptive frequency oscillator, i.e. extraction of frequencies and tracking are important and exploited for the construction of our system capable of dynamical frequency analysis.

Complete system: Pool of adaptive frequency oscillators

A pool of N such oscillators is used to create the final system. The input $I(t)$ is chosen as the difference between the mean field $m(t)$ produced by the oscillators and the teaching signal $T(t)$

$$I(t) = T(t) - m(t) = T(t) - \frac{1}{N} \sum_i^N x_i \quad (5.60)$$

The output is chosen equal to the mean field $O(t) = m(t)$. Thus, Eq. 5.60 establishes negative feedback via the mean activity of the oscillators. Fig. 5.13 illustrates the construction of the system.

By the negative feedback (Eq. 5.60), the action of the oscillators is subtracted from the teaching signal, thus the remaining oscillators only “feel” the frequency components not fully covered yet by the already adapted oscillators. When the system starts with uniformly or randomly distributed initial frequencies, the different oscillators will gradually populate the frequency spectrum of the teaching signal. Since the Hopf oscillator has a harmonic limit cycle and due to the additive property of the system, the population of oscillators naturally reconstructs the frequency spectrum of the signal by matching the distribution of the intrinsic frequencies to the frequency spectrum of the input signal. In other words, we have a means of frequency analysis in a fully dynamic way. If the power of the signal is different from 1 a normalization of the signal is helpful. But even if the signal power is not normalized, the system is either able to partially recover the spectrum (power larger than 1) or it will be able to recover the whole spectrum with the surplus oscillators adding to the noise floor (power smaller than 1). We will not concentrate on these secondary results as we want to present the basic properties of the system and present results with normalized signals.

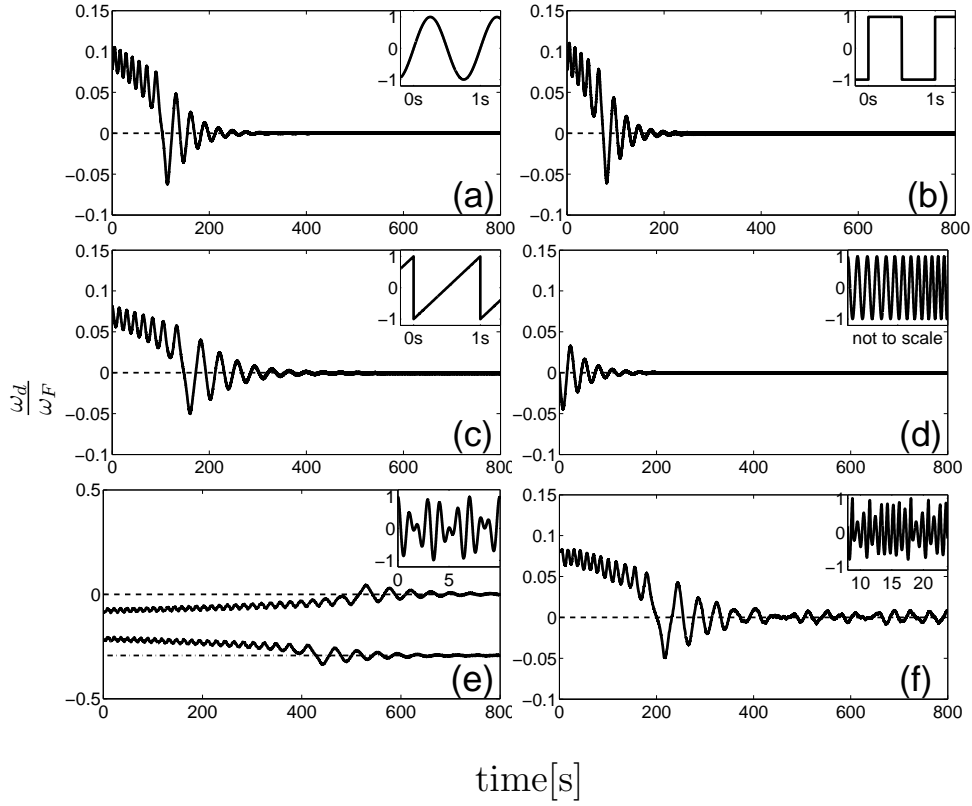


Figure 5.11: (a) Typical convergence of an adaptive frequency oscillator (Eqs 5.56–5.58) driven by a harmonic signal ($I(t) = \sin(2\pi t)$). The frequency converges in an oscillatory fashion towards the frequency of the input (indicated by the dashed line). After convergence it oscillates with a small amplitude around the frequency of the input. The coupling constant determines the convergence speed and the amplitude of oscillations around the frequency of the driving signal in steady state. In all figures, the top right panel shows the driving signals (note the different scales). (b–f) Non-harmonic driving signals. We depict representative results on the evolution of $\frac{\omega - \omega_F}{\omega_F}$ vs. time. The dashed line indicates the zero error between the intrinsic frequency ω and the base frequency ω_F of the driving signals. (b) Square pulse $I(t) = \text{rect}(\omega_F t)$, (c) Sawtooth $I(t) = st(\omega_F t)$ (d) Chirp $I(t) = \cos(\omega_c t)$ $\omega_c = \omega_F(1 + \frac{1}{2}(\frac{t}{1000})^2)$ (Note that the graph of the input signal is illustrative only since the change in frequency takes much longer than illustrated.) (e) Signal with two non-commensurate frequencies $I(t) = \frac{1}{2} \left[\cos(\omega_F t) + \cos(\frac{\sqrt{2}}{2}\omega_F t) \right]$, i.e. a representative example how the system can evolve to different frequency components of the driving signal depending of the initial condition $\omega_d(0)$. (f) $I(t)$ is the non-periodic output of the Rössler system. The Rössler signal has a $1/f$ broad band spectrum, yet it has a clear maximum in the frequency spectrum. In order to assess the convergence we use $\omega_F = 2\pi f_{max}$, where f_{max} is found numerically by FFT. The oscillator converges to this frequency.

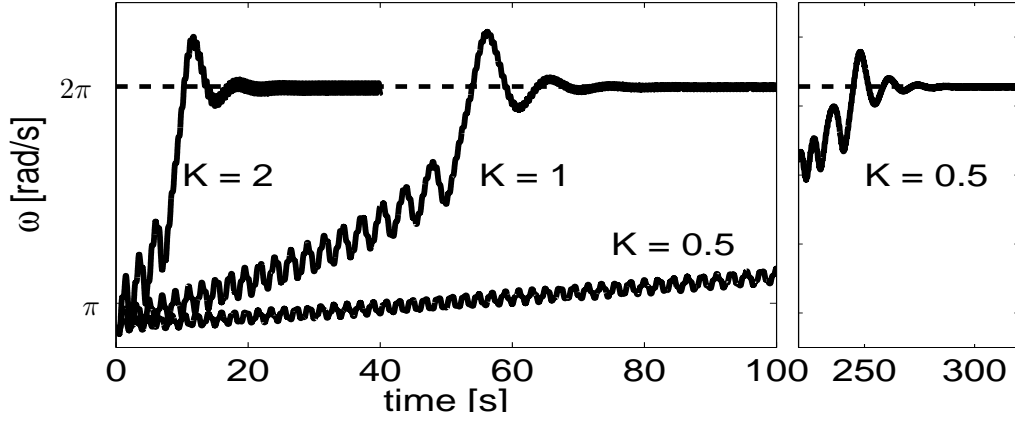


Figure 5.12: Typical convergence of an adaptive frequency oscillator (Eqs 5.56–5.58) driven by a harmonic signal ($I(t) = \sin(2\pi t)$) and different coupling constants K . The coupling constant determines the convergence speed and the amplitude of oscillations around the frequency of the driving signal in steady state – the higher K the faster the convergence and the larger the oscillations.

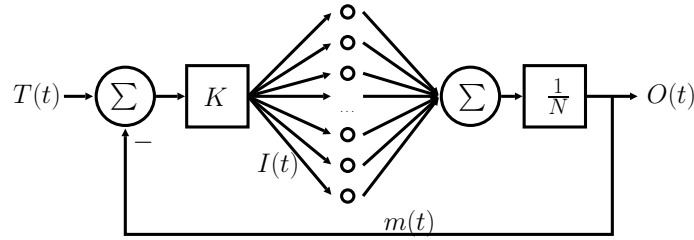


Figure 5.13: The structure of the dynamical system that is capable to reproduce a given teaching signal $T(t)$. The system is made up of a pool of adaptive frequency oscillators. The mean-field produced by the oscillators is fed back negatively on the oscillators. Due to the feedback structure and the adaptive frequency property of the oscillators it reconstructs the frequency spectrum of $T(t)$ by the distribution of the intrinsic frequencies.

5.2.3 Simulation Results

The following results present the numerical integration² of the pool of oscillators. The initial condition for the frequencies is drawn from an uniform random distribution. The presented results are representative for the behavior of the pool of oscillators. Unless otherwise stated, the system is integrated with the following default parameters: $\mu = 1$, $K = 200$, $N = 1000$.

Discrete spectrum In Fig. 5.14 we present the evolution of the system for an input signal $T(t) = \frac{1}{6}[3\sin(2\pi t) + 2\sin(3\sqrt{2}\pi t) + \sin(2\pi^2 t)]$ (cf. Fig. 5.14a) and initial frequency distribution $\omega(0) \sim U(1.5, 21.5)$. Fig. 5.14a shows how the system locks almost immediately to the input signal and reproduces it. In Fig. 5.14b, the system is shown after $t = 1000$ s and we can see that the system matches the input signal very well. The time evolution of the square-root error is shown in Fig. 5.14c and we see that it quickly drops already in the first seconds of the evolution. In Fig. 5.14d the time evolution of the distribution of intrinsic frequencies is depicted. The initial uniform distribution gets structured and converges towards the frequency components, i.e. the system develops from an initial unordered state into an ordered state which corresponds to the input signal. Visible is also how the strongest frequency component in the input signal (at 2π) exerts the strongest attraction which translates into the fastest convergence of the corresponding oscillators. This is in agreement with Eq. 5.59. In Fig. 5.14e,f, two measures of the convergence of the frequency distribution are shown, in (e) the number of oscillators which have converged to the correct frequencies and (f) the average Manhattan distance which is calculated as follows: The distribution of oscillator is sorted and the vector corresponding to the (sorted) distribution of the target spectrum is subtracted, then the sum of the absolute value of this difference is taken and divided by N (i.e. $d = \frac{1}{N} \sum |\omega_i - \omega_{r,i}|$, where $\omega = [\omega_0, \dots, \omega_N]$ is the state of the oscillator frequencies, sorted from highest to lowest, and $\omega_r = [\omega_{r,0}, \dots, \omega_{r,N}]$ is the target distribution, again sorted) between the current state of the oscillators and the target spectrum. Both convergence measures clearly show a rapid convergence to the final correct frequency distribution. While the Manhattan distance shows very fast convergence in the first few seconds, the count of converged oscillators takes a bit more than 20 seconds to raise to around 80%. In Fig. 5.14g the histogram of the intrinsic frequencies of the pool of oscillators at $t = 1000$ s is presented. The bars correspond to the number of oscillators in a given range of frequencies, thus they indicate the frequencies and strength of the components. It is clearly visible that the histogram matches very closely the theoretical frequency components. There are some oscillators which have not yet converged, however their number is small ($\sim 3\%$).

In Fig. 5.15 we show that the final state of the distribution is not dependent on the initial conditions. We also see that the initial condition influences the

²Embedded Runge-Kutta-Fehlberg (4,5) method, $t_{abs} = 10^{-6}$, $t_{rel} = 10^{-3}$

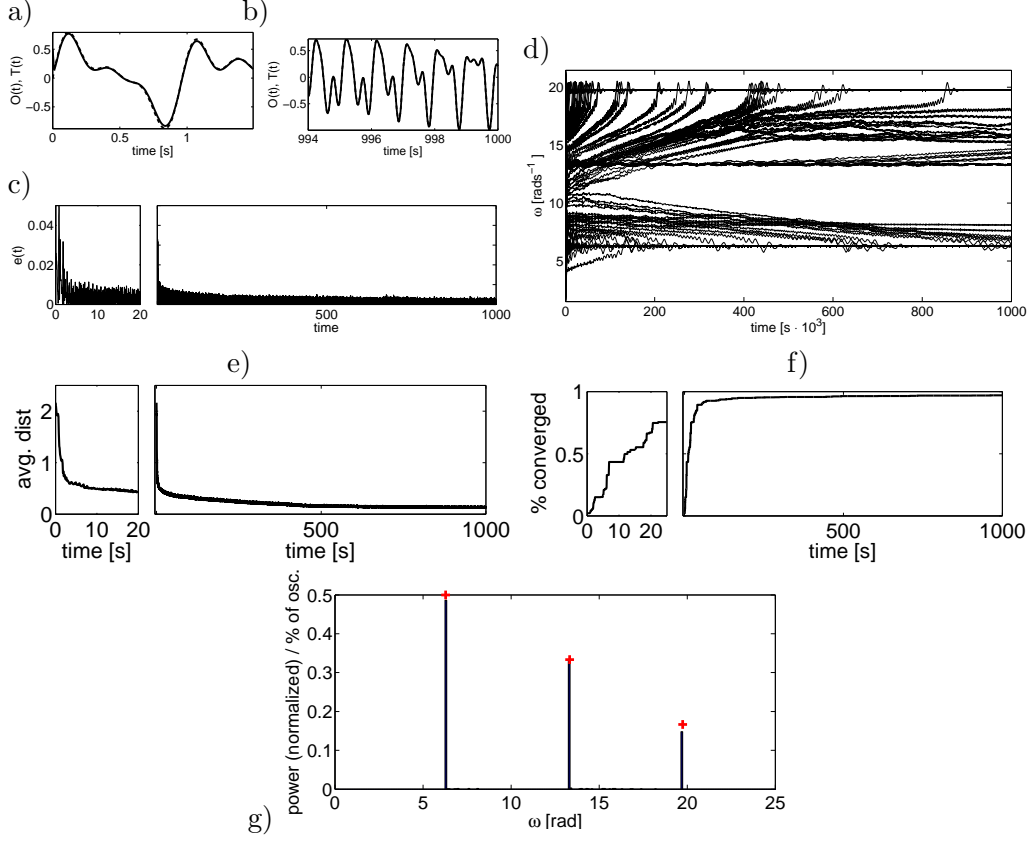


Figure 5.14: ($N = 1000$, $K = 200$) – a) The teaching signal $T(t)$ (dashed) vs. the output signal $O(t)$ (bold) in the beginning ($t = [0, 1.5]$ s) The output almost immediately tracks the teaching signal since we have a very strong coupling constant. b) $T(t)$ vs $O(t)$ after 1000s, now the output signal is basically identical to the teaching signal. c) The square root error $e(t) = \sqrt{(O(t) - T(t))^2}$ d) Evolution of the distribution of ω . The traces of the evolution of the ω_i are shown. Thus, we can clearly see the development of the distribution of the intrinsic frequencies from the initial uniform distribution to the distribution which corresponds to the Fourier spectrum of the signal. e) The average Manhattan distance between the distribution of the frequencies of oscillators and the Fourier spectrum (cf. text). f) The fraction of oscillators which have converged. It can be seen that there is fast convergence of the oscillators in the first few seconds. The measure stabilizes at around 0.96. g) The distribution of the intrinsic frequencies ω distribution after $t=1000$ s (bars) the crosses indicate the theoretical value of the Fourier spectrum of the signal.

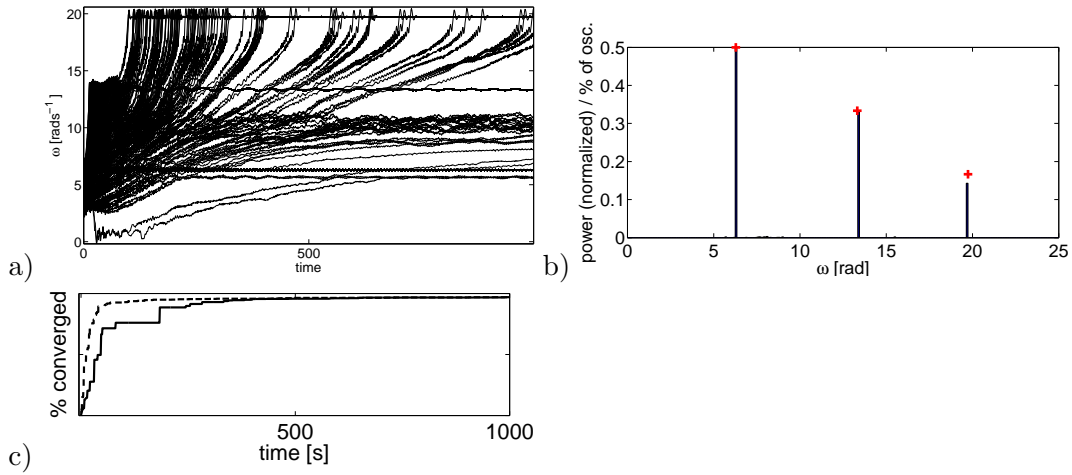


Figure 5.15: ($N = 1000$, $K = 200$) – Simulation with an initial condition which is further off the end target spectrum. As can be seen due to the negative feedback the oscillators cross over the frequencies which are already covered. This means they take longer to converge but the final distribution is very close to the case presented in Fig. 5.14. c) The count of converged oscillators (bold line) in comparison with the example from before (dashed).

transient time. We chose an initial condition $\omega(0) \sim U(3, 6)$, i.e. *all* oscillators start lower than the lowest frequency component of the teaching signal. As can be seen the oscillators do not get stuck at the lowest frequency components and are able to cross over the middle components of the signal. This is because the middle components are already covered by enough oscillators and thus subtracted via the negative feedback; the remaining oscillators thus only “feel” the remaining frequency component. The final state is the same, apart from the position of the oscillators which have not yet converged. Their number is the same ($\sim 3\%$).

As mentioned in the introduction of the basic oscillator, we can influence the convergence speed by increasing the coupling constant K . Thus, we show the effect of varying K in Fig. 5.16 for the mean-field coupled system. The input signal is a simple sinus $T(t) = \sin(10t)$, the initial condition is $\omega(0) \sim U(2, 18)$. The system is using $N = 100$ oscillators. While in the first seconds of the evolution it is clearly the case that the higher the coupling constant K the faster the evolution, for the long term evolution, as can be seen from Fig. 5.16b, there seems to be a value of K for which convergence is the best, i.e. converges to the lowest error, at around $K = 200$. The oscillators with the negative-mean field coupling do not suffer from the negative effects for strong K as encountered for the single oscillator. The reason for this is that the oscillator locks to the input signal and is thus removed from the input via the feedback. Thus there is no large input driving the oscillator even for very strong coupling.

In Fig. 5.17 we show the simulation results for $N = 6$ oscillators, which is the

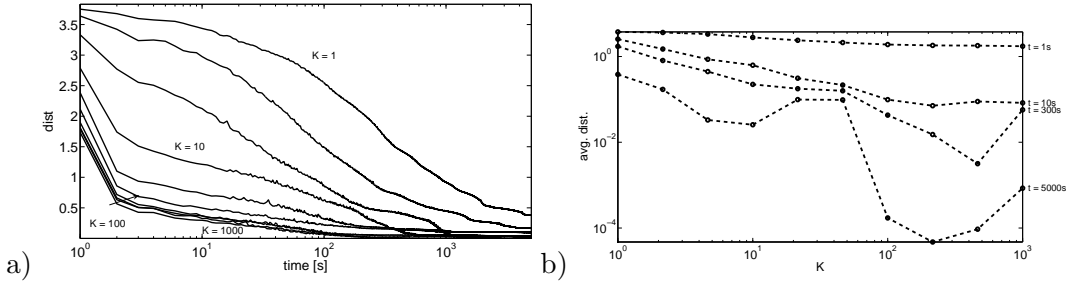


Figure 5.16: ($N = 100$) – a) Convergence over time for different values of K ($T(t) = \sin(10t)$ $\omega(0) \sim U(2, 18)$) as measured by the average Manhattan distance (note the logarithmic scale for the time). We can see that in general larger K mean faster convergence. b) Distance after 1s, 100s, 300s, and 5000s for different values of K .

minimal number of oscillators needed to exactly represent the teaching signal. The results show that the convergence in this example works perfectly. In the presented example an initial condition of $\omega(0) \sim U(1, 50)$ has been chosen. It turns out, that with a lower number of oscillators the initial condition gets more critical. The more spread out the initial condition is the more likely the convergence works perfectly (data not shown). Yet, even if the convergence does not work perfectly, the most important components of the signal are generally correctly identified (data not shown), i.e. a convergence of 3 oscillators to $\omega = 2\pi$ and 3 oscillators to $\omega = 3\sqrt{2}\pi$, instead of 3 to $\omega = 2\pi$, 2 to $\omega = 3\sqrt{2}\pi$ and 1 to $\omega = 2\pi^2$.

Non-stationary spectrum A further important aspect is that the system is able to recover the spectrum of non-stationary input signals. In Fig. 5.18 we show a case where the input signal has strongly varying frequencies (quadratic chirps: $T(t) = \frac{1}{2} [\sin(\omega_1 t) + \sin(\omega_2 t)]$, $\omega_1 = 2\pi(1 + (\frac{t}{3000})^2)$, $\omega_2 = 2\pi(3 - (\frac{t}{3000})^2)$). In the figure the instantaneous frequencies $\dot{\phi}_{1,2}$ ($\phi_{1,2} = \omega_{1,2}t$) are drawn along with the statistics of the frequencies of the oscillators. It is clearly visible that the system tracks the time dependent frequencies. The figure corresponds to spectrograms which can be obtained via wavelet transforms or other multi-scale filter methods.

Continuous spectrum In physics, many signals of interest have a continuous, often broad, spectrum. In the following we show how the system performs on a broad-band chaotic signal from the Rössler oscillator. In Figure 5.19a we show the statistics of the intrinsic frequencies of the oscillators along with the FFT of the teaching signal. We used the y variable of the Rössler oscillator in its chaotic

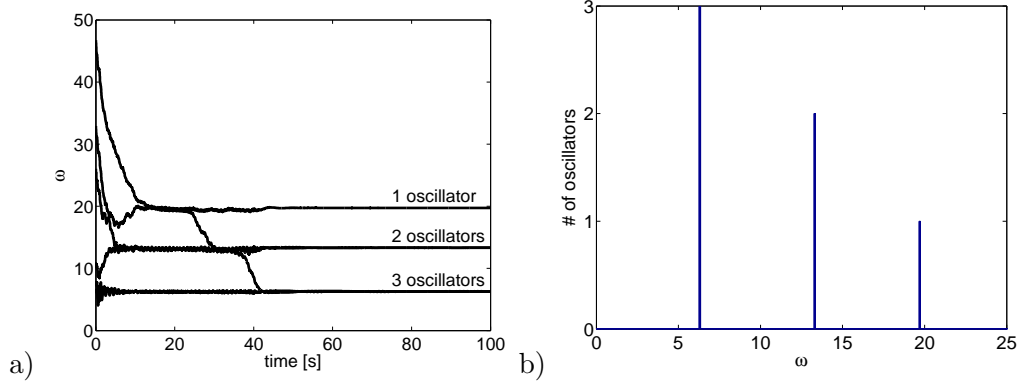


Figure 5.17: ($N = 6$, $K = 200$) – The same input signal as in Figs. 5.14 and 5.15. This time we use the minimal number of oscillators ($N = 6$) needed for perfect convergence to the given input signal. It can be seen that in this example the convergence works perfectly. b) shows the histogram after 100 s - see text for further discussion.

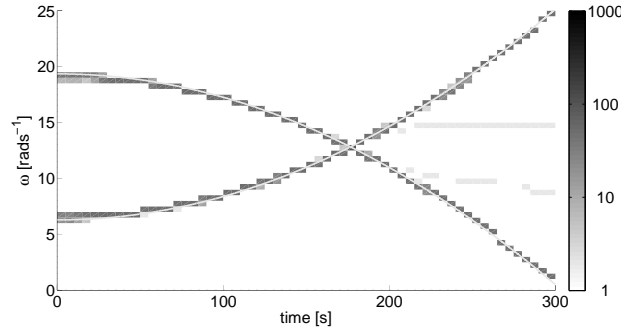


Figure 5.18: ($N = 1000$, $K = 200$) – $T(t)$ is a non-stationary input signal (cf. text), in contrast to Figs 5.14 and 5.15 the histogram of the distribution of the frequency ω_i is shown for every 50s, the grey level corresponds to the number of oscillators in the bins (note the logarithmic scale). The thin white line indicates the theoretical instantaneous frequency. Thus, it can be seen that the distribution tracks very well the non-stationary spectrum, however about 4% of the oscillators diverge after the cross-over of the frequencies.

parameter range as a teaching signal³ [184]. For the pool of oscillators to be able to cover the whole signal, the Rössler signal has been normalized by its mean energy. We used the settings $K = 0.1$, $N = 10^4$, initial conditions $P(\omega, 0) \sim U(1.5, 2.5)$, and show the state of the pool of oscillators after 10^5 s.

As can be seen in Fig. 5.19a the important features of the spectrum are replicated, especially the broad spectrum. However, the distribution is not as broad as the frequency of the driving signal. There is some cut-off effect. The cut-off frequency is dependent on the coupling constant K and the number of oscillators N : the lower K and the higher N , the higher the cutoff frequency (data not shown). Another interesting fact is that the oscillators chose a symmetric spectrum (i.e. about half of them having negative frequencies), this is of course a fully valid solution. Even if the oscillators do not exactly match the spectrum we can see that the *essential* features such as the broad distribution and important peaks of the teaching signal are replicated.

In Fig. 5.19b, where the time-series of the output signal is compared with the teaching signals, we see how the output of the system nicely follows the teaching signal, in terms of zero crossings and general signal shape. However, we also see here the manifestation of the fact that the signal is missing some high frequency components, i.e. it does not accurately follow the teaching signal to its peak values. This is in line with the observation of the spectrum.

5.2.4 Probabilistic Treatment: Fokker-Planck Equation

In order to investigate the convergence properties of our system, the oscillators can be treated in a probabilistic manner, i.e. instead of looking at the single activities of the oscillators we characterize the state of the frequencies by a probability density function $P(\omega, t)$. Instead of looking at the convergence of the large scale system, we can then look at the behavior of this simplified system. Another motivation for the probabilistic formalism is the fact that it is also a very good way of testing the understanding of the important and relevant mechanisms at work. In other words, when the simplified probabilistic model matches to a large extend the results of the full scale system, it strongly suggests that the understanding, assumptions and simplifications that went into the formulation of components of the Fokker-Planck equation are correct, and the retained mechanisms relevant.

For the probabilistic treatment, the frequencies of the oscillators can be treated as massless particles under external forces, which allows us to use the well known

³Rössler system ($a = 0.2$, $b = 0.2$, $c = 5.7$, $T(t) = y$):

$$\begin{aligned}\dot{x} &= -y - z \\ \dot{y} &= x + ay \\ \dot{z} &= b - cz + xz\end{aligned}$$

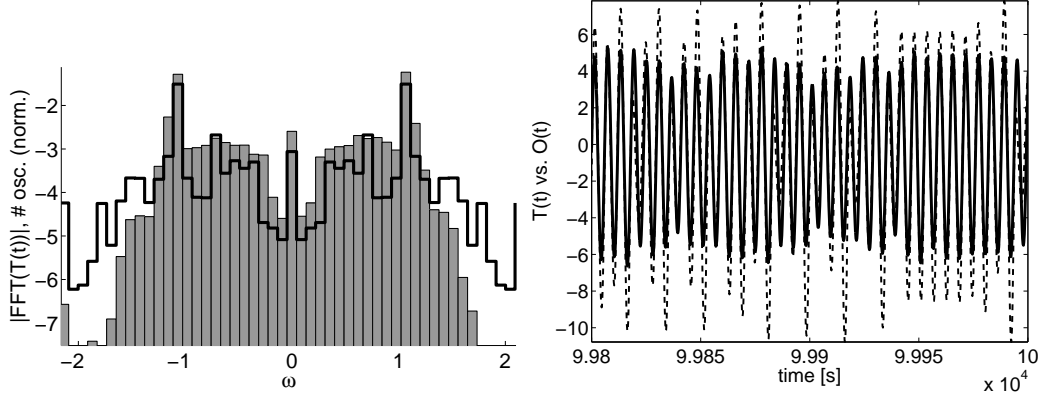


Figure 5.19: ($N = 10000$, $K = 0.1$) – a) The FFT (black line) of the Rössler signal (for $t = [99800, 100000]$) in comparison with the distribution of the frequencies of the oscillators (grey bars, normalized to the number of oscillators) at time 10^5 s. The spectrum of the FFT has been discretized into the same bins as the statistics of the oscillators in order to allow for a good comparison with the results from the full scale simulation. b) Time-series of the output signal $O(t)$ (bold line) vs the teaching signal $T(t)$ (dashed line).

Fokker-Planck equation of the form

$$\frac{\partial P(\omega, t)}{\partial t} = -\frac{\partial}{\partial \omega} \left[A(\omega, P)P(\omega, t) - \frac{1}{2} \frac{\partial}{\partial \omega} B(\omega)P(\omega, t) \right] \quad (5.61)$$

where the probability current is composed of a drift term (first summand) and a diffusion term (second summand).

Drift term The drift term, is a function of the "force" $A(\omega, P)$ acting on the intrinsic frequencies ω of the oscillator. As discussed in Section 5.2.2, without the negative feedback, the force driving the intrinsic frequency can be written as [178]:

$$A(\omega, P) = K^2 \sum_{n \in \mathbb{N}} \frac{|A_n|^2 \omega}{(n\omega_F)^2 - \omega^2} + \tilde{F}(t) \quad (5.62)$$

where ω_F is the fundamental frequency and A_n are the Fourier components of the signal perturbing the oscillator. $\tilde{F}(t)$ summarizes forces which have average zero or are of very small order and are thus neglected for the mean-field treatment. However, in case of the feedback coupled system, the effective force is dependent on the current state of the distribution $P(\omega, t)$ in the following way: Due to the negative feedback, the oscillators that have already converged diminish the forces that make the oscillators converge. In order to account for this fact, a correction factor is multiplied with the actual amplitudes of every frequency component of the signal, i.e. every summand in Eq. 5.62, is multiplied with a factor

$a_n = \left(1 - c_n \left(\frac{|A_n|}{A_\Sigma}\right)^{-1}\right)$. The quantity c_n is the fraction of oscillators which have converged and locked to $n\omega_F$ ($c_n = \frac{C_n}{N}$, C_n : number of converged oscillators), A_Σ is the sum of the absolute values of all Fourier components $A_\Sigma = \sum_{n \in \mathbb{N}} |A_n|$, thus $\frac{|A_n|}{A_\Sigma}$ designates the value of c_n at which there are enough oscillators to replicate the part of the signal with given frequency (we exploit the conjugate symmetry of the Fourier spectrum of real signals to consider only the positive part of the spectrum). Hence, a_n designates the amount of signal energy for a given frequency $n\omega_F$ that can still be felt by the oscillators that have not yet converged, thus, potentially driving them to this frequency. a_n converges to zero for $c_n \rightarrow \frac{|A_n|}{A_\Sigma}$. Hence, the force term reads⁴

$$A(\omega, P) = K^2 \sum_{n \in \mathbb{N}} \frac{\left| \left(1 - c_n \left(\frac{|A_n|}{A_\Sigma}\right)^{-1}\right) A_n \right|^2 \omega}{(n\omega_F)^2 - \omega^2} \quad (5.63)$$

Until here the formulation of the Fokker-Planck equation is general and not does depend on assumptions on the coupling constant K . We need however a way to calculate c_n . The key to assessing c_n is counting the “converged” oscillators in the full scale system, which translates into an integration of P over a certain region of ω for the Fokker-Planck formulation: $c_n = \int_L P(\omega) d\omega$. In Appendix 5.2.6, the approximation of c_n as used in the numerical integration is outlined.

Diffusion term The second part of the Fokker-Planck Equation, the diffusion rate $B(\omega)$ is a function of the noise in the system. For a physical system it has to be non-zero and positive. Obviously we defined the system in Eqs. (5.56) – (5.58) to be purely deterministic. However, it is straightforward to enhance Eqs. 5.56 – 5.58 with additive noise terms and therefore transform them into Langevin equations. Then the diffusion term $B(\omega)$ is a constant, proportional to the variance of the noise σ^2 ($B = 0.5\sigma^2$, Eqs. 5.56–5.58 describing the system are enhanced by an additive white Gaussian noise term with the same variance) [182].

Especially, in the noiseless limit case ($B(\omega) = 0$), as we will see next, the results from the Fokker-Planck equation correspond very well to the results obtained by integration of the full-scale system for large N .

Example: Harmonic signal

Let us take a concrete example with a harmonic teaching signal $T(t) = \sin(\omega_F t)$. In this case we can write down the Fokker-Planck equation straightforwardly and

⁴The term for the absolute value can further be simplified: $|\dots| = |A_n - c_n A_\Sigma|$. However, the origin of the terms is then obscured, thus we prefer the other formulation for its explanatory power.

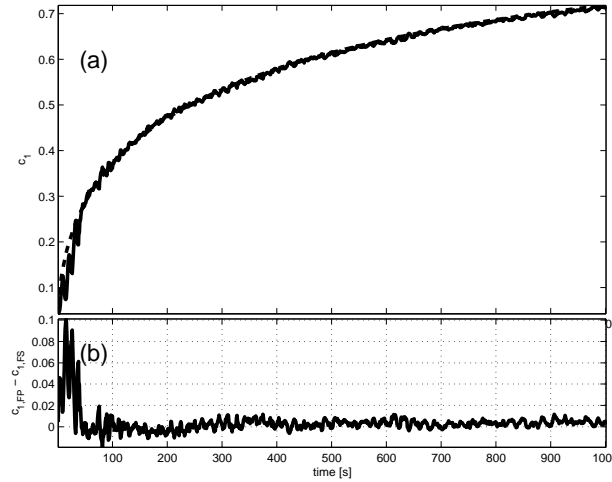


Figure 5.20: $T(t)$ is a harmonic signal a) $c_1(t)$ for Fokker-Planck (dashed) and full-scale simulation ($N = 1000$, $K = 1$) in the noise-less limit ($B(\omega) = 0$) b) The difference between $c_1(t)$ for Fokker-Planck and full-scale simulation.

Eq. 5.63 simplifies to

$$A(\omega, P) = K^2 \left| \left((1 - c_1) \frac{1}{2} \right) \right|^2 \frac{\omega}{\omega_F^2 - \omega^2} \quad (5.64)$$

To compare the dynamical system and its Fokker-Planck interpretation, the quantity c_1 , i.e. the fraction of oscillators which have converged to ω_F , is used, as a measure for the convergence of the system. In Figure 5.20 the results of c_1 in full-scale simulation vs. the integration of the Fokker-Planck equation (Eq. 5.61) are presented. The following parameters have been used for the simulations: number of oscillators in full scale simulation $N = 1000$, initial condition $P(\omega, 0) \sim U(\omega_F - 2, \omega_F + 2)$, $\omega_F = 15$, $x(0), y(0) \sim U(0, 1)$. The nearly perfect coincidence of the results of the Fokker-Planck equations with the full scale simulation is clearly visible. This confirms the validity of the probabilistic treatment. In the beginning c_1 in the full scale simulation is lower than predicted by the Fokker Planck equation, however after about 30 s the match is very close.

In Figure 5.21 we show the results of the full-scale simulation and the Fokker-Planck equation for $B \neq 0$.⁵ Especially for low levels of noise, the correspondence of the frequency distribution in the large scale simulation and the results from the Fokker-Planck equation are very good. Even for high levels of noise the characteristics of the distribution are well preserved. In Fig. 5.21g we compare the measure c_1 in the full-scale simulation with the c_1 from the Fokker-Planck equation. In both, full-scale and Fokker-Planck, we see clearly how the noise does not

⁵Euler Integration $\Delta t = 10^{-3}$ s

affect the system strongly for moderate levels of noise, the mean values are close to one and not affected by the noise. Only for stronger noise ($\sigma > 10^{-4}$) does the influence become evident, the mean values degrade and the fluctuations in the full scale system are enhanced (visible in the increased variance). Interestingly the main peak in the full scale simulation starts to oscillate around the correct value (cf. Fig 5.21, the peak of the histogram shifts left and right of the peak given by the Fokker-Planck solution). This means the oscillators do not de-phase and start having different frequencies, but they fall into a coherent large scale oscillation. This comes from the interaction between the oscillators with close frequencies, an effect not captured by the presented Fokker-Planck equation. This behavior under influence of noise is different than simple diffusion in Brownian motion, where the variance would observed would be exactly the variance of the added noise (i.e. σ^2). Interestingly, the behavior of mean and variance in the full scale simulation as seen in Fig. 5.21g shows the typical fingerprint of a phase transition, and indeed we can also observe in the solution of the Fokker-Planck equation, how this solution qualitatively changes from a clear peak (Fig. 5.21a,b) with two characteristic side lobes to a more tent-shaped distribution (Fig. 5.21e,f).

Example: Discrete spectrum

To present how the Fokker-Planck Equation behaves with more complex spectra, we integrate it for the same signal and initial conditions as used in Fig. 5.14, namely $T(t) = \frac{1}{6}[3\sin(2\pi t) + 2\sin(3\sqrt{2}\pi t) + \sin(2\pi^2 t)]$ and $\omega(0) \sim U(1.5, 21.5)$. The comparison is shown in Fig. 5.22. We see that especially in the beginning the match is very good. For longer evolution the Fokker-Planck equation predicts a slightly better convergence than seen in the full scale simulation. While at $t=15000$ the statistics predicts that all oscillators should have converged, in the full scale system there are still some oscillators which have not converged yet. We will discuss some possible reasons for that below.

5.2.5 Conclusions & Discussion

General properties Summarizing, we have presented a dynamical system which is able to reproduce the frequency spectrum of any incoming signal. Especially interesting are the facts that no preprocessing of the signal is needed, that there is no need to set time windows or similar parameters (see below), and that the input does not need to be stationary. The mechanism that enables the “learning” of the frequency spectrum is the adaptive frequency mechanism of the oscillators, a mechanism which is related to Hebbian learning known in theoretical neurobiology [122, 178]. As a matter of fact, learning and adaptation can be considered as dynamics of the parameters of the system, on a slower time scale. This gives a general and unified point of view of learning and adaptive systems. To the best of our knowledge, our system presents a novel approach to do signal processing using dynamical systems. In order to obtain the frequency spectrum

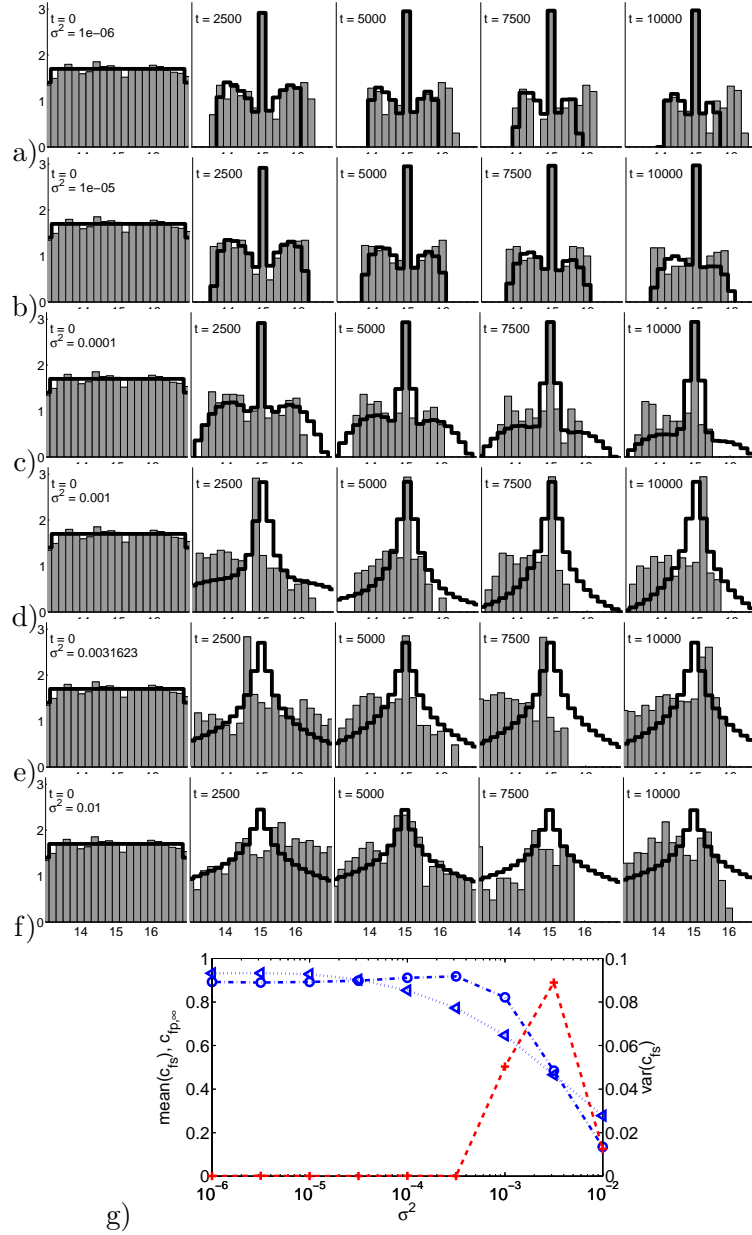


Figure 5.21: Results from integration of Fokker-Planck and full-scale simulation ($N = 1000$, $K = 1$) for different levels of noise: $\sigma^2 = [10^{-6}, 10^{-2}]$ a)–f) Comparison between the distribution of the large scale simulation (bars) and the Fokker-Planck integration (line), note the logarithmic scale. The continuous distribution $P(\omega, t)$ has been discretized in order to allow for a good comparison with the results from the full scale simulation g) Measures of the convergence in steady state. (Triangles) Fokker-Planck c_1 , (Circles) Full-scale simulation c_1 , (Crosses) Variance of c_1 in the full scale simulation. Clearly visible is that the full-scale simulation and the Fokker-Planck equation show the same qualitative behavior under different levels of noise. Interestingly there is a peak of variance for a level of noise between $\sigma^2 = 10^{-3}$ and 10^{-2} in the full-scale simulation (discussion see text).

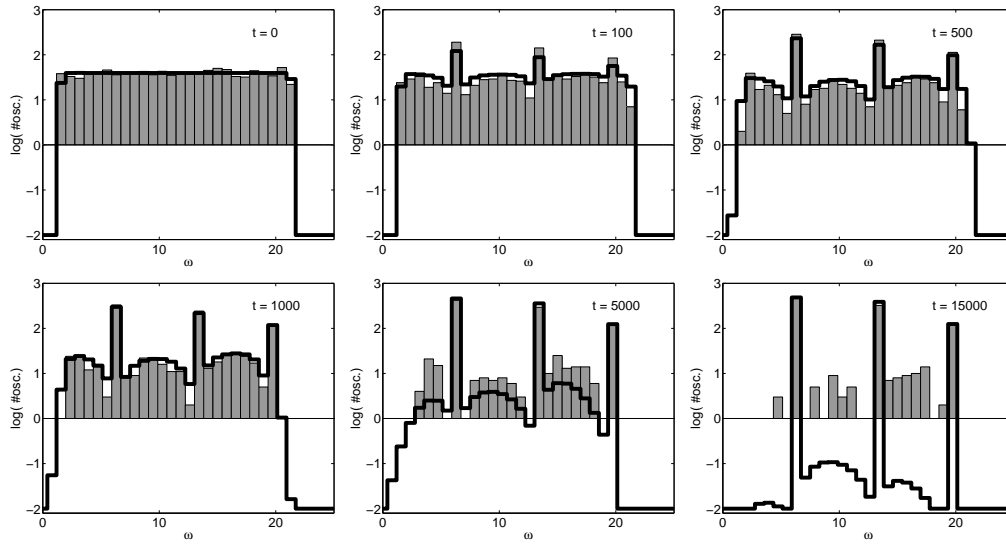


Figure 5.22: Comparison between the results of the Fokker-Planck integration and the full scale simulation ($N = 1000$, $K = 1$) for a more complicated signal, namely the signal used in Fig. 5.14. The grey histogram shows the statistics of the full scale simulation and the black line shows the prediction of the Fokker-Planck integration. Note that the statistics of the oscillator does not show more detail since the single oscillator is the lower limit for resolution (zero line in the plot), this resolution could arbitrarily be pushed up by choosing more oscillators. We see that especially in the beginning the match is very good. For longer evolution the Fokker-Planck equation predicts a slightly better convergence than seen in the full scale simulation (cf. text).

of the input signal $T(t)$ it suffices to feed in the signal as input to the system. The frequency spectrum can be read out from the distribution of ω . The system tracks dynamically any changes in the spectrum and is thus not limited to stationary signals, this is a property which directly follows from the use of dynamical systems.

Fokker-Planck analysis We showed that the full scale dynamical system can be simplified and treated by a non-linear Fokker-Planck equation. Despite not being solvable analytically, the Fokker-Planck equation allows for an integration of the system that is orders of magnitude faster and thus allows for the investigation of convergence properties, with the disadvantage that for its integration the Fourier spectrum of the signal has already to be known. Thus, the Fokker-Planck equation is only a way to analyze the system but does not replace the original setup for possible applications. Furthermore, there are clearly differences between the Fokker-Planck equation and the behavior of the full-scale system in the high noise range. There are interactions in the system which are not caught by the presented Fokker-Planck equation, which, in its current form, only describes the mean-field feedback. Effects that are neglected include nonlinear cooperative effects such as clustering and mutual influence of oscillators with close frequencies. These effects remains to be studied in detail. However, the Fokker-Planck equation and its related probability distribution P is a good description for the system in the thermodynamic limit ($N \rightarrow \infty$) and gives already good results for finite sized systems. While it was rather straight forward to write down the Fokker-Planck equation, deriving its analytical solution is much more difficult or even impossible. The theoretical approximations and the numerical solutions presented in this article should provide a first step towards a full analytical treatment. While for the sake of performance in the first part of the article we used from small to very large K , the theoretical understanding is only firm for lower K . As pointed out in the appendix A, important parts of the theoretical fundament for large K remain to be worked out. Since it is generally known that strongly coupled oscillators are very difficult to analyze, for large K we have much less of theoretical knowledge that we can build upon.

Open parameters: K , N , and initial distribution When applying our system to a new, unknown, signal, three items need to be instantiated: the coupling strength K , the number of oscillators N , and the initial distribution of intrinsic frequencies $\omega(0)$.

As we have seen, the coupling strength K determines the speed of convergence towards the frequency components of the input signal, with large K leading to faster convergence. In the single oscillator case, a large K leads to undesirable overshoots and oscillations of the frequency ω around the input frequency. This problem is however much less significant in the complete system with populations of oscillators because the driving signal gets effectively removed from the input by

the negative feedback after convergence. This means that in practice K can be chosen in a range of several orders of magnitude, from 1 to 1000 (see Fig. 5.16) and still provide good convergence to a stationary input signal. Clearly, the choice of K becomes more critical with non-stationary signals. From the theoretical point of view we know that there must be a limit how fast the system can track a non-stationary signal, this limit is influenced by the choice of K , i.e. the higher K , the faster the system can track non-stationary effects.

Obviously, there is also limit in the approximation capacity of the system due to the discretization by the component oscillators. The level of accuracy can be chosen and scales with $\sim \frac{1}{N}$. We showed that the system is already capable of converging with the minimum number of oscillators, however the smaller the number of N the more critical becomes the initial condition. In practice one should choose an intermediate number of oscillator (e.g. $N = 100, \dots, 1000$) to balance between the dependence on initial conditions and the computational cost. In the way the system is constructed it works best for normalized signals, otherwise the result will have a noise floor or the oscillators are not able to fully cover the spectrum. Furthermore, as we have seen, the system is better suited for discrete spectra, but also performs reasonably well on continuous spectra. However here the choice of a large N becomes more critical.

In summary, it is important state that the exact choice of the parameters is usually not critical.

Last but not least, no special initial conditions need to be given. However, of course the initial conditions (mainly $\omega(0)$) determine the transient times.

Comparison with related signal processing techniques It will further be interesting to investigate how the system relates to the fundamental limits of signal processing, such as the uncertainty relationship. It is evident that the presented system can not circumvent these limits. The choice of K and N do implicitly specify the time-frequency resolution such as in wavelet transforms [143] or windowed FFT. Yet, to work out the analytical dependence of this resolution window on those two parameters remains to be done. But only by knowing this dependence the system will be comparable to the other well established techniques in a quantitative way.

Out of this reasoning it follows that, comparing the statistics of the oscillators against the FFT of the continuous signal in Fig. 5.19 might not be the best method to assess the system, since the FFT is a statistics over a longer time window, while the oscillator statistics shows the system in a given moment with the statistics dependent on the implicit time window that we do not know how to calculate yet.

Filter-banks are a way of analyzing the frequency spectrum of a signal based on (linear) dynamical systems. But the output of the filter-bank needs to be post-processed by algorithmic treatment to get the spectrum. Filter-banks are thus not a way to do the frequency analysis with only dynamical systems as we asked for

in the introduction. Furthermore, in contrast to filter-bank methods, our method works without explicitly specifying different bands for filtering, it adjusts itself to the needed frequency components.

Future work We are currently investigating variants of the presented, basic system, including (i) replacing the simple sum by a weighted sum for the generation of the output signal such that a single oscillator rather than a group of oscillators can produce a given frequency component, (ii) adding direct coupling between the oscillators (i.e. other than through the mean-field) to achieve structurally stable solutions after the teaching signal is switched off (cf. [175] for an example), and (iii) using non-harmonic oscillators (e.g. van der Pol or FitzHugh-Nagumo oscillators). For non-harmonic oscillators, the direct correspondence between distribution of intrinsic frequency and Fourier spectrum would be lost, but these oscillators possess wider stable regions for higher order locking, thus such systems could be more suitable to replicate non-harmonic limit cycles in a structural stable way.

Possible applications As mentioned in the introduction, this work was mainly meant as an exploration of the use of dynamical systems to perform frequency analysis, and its real applicability remains to be explored. It could be used as an alternative to methods such as FFT, wavelets, and filter banks, but its pros and cons compared to those methods remain to be studied in detail. Possible applications include any application that uses frequency analysis, e.g. signal processing, signal filtering, and signal compression. In addition to the interesting properties listed at the beginning of this section, we would like to point out a possible advantage of our system: the system lends itself directly to a fully parallel implementation. This means it would be well suited for a very fast hardware implementation. Furthermore, as discussed above, the system can be extended with direct coupling between oscillators to do robust signal *generation*. For instance, the system could learn a rhythmic gait pattern for a legged robot, and then replay it robustly (i.e. as the limit cycle attractor of the system of coupled oscillators). Compared to fixed pre-recorded gait patterns, such a dynamical systems approach is interesting because it allows online modulation of the gaits and offers robustness against temporary perturbations (i.e. the system will return to the limit cycle after a short transient period). See [181] for an example applied to the walking of a humanoid robot.

The relevance to modeling should also be explored. Several physical and biological systems show similar frequency adaptation mechanism. For instance, many animals have body properties (e.g. dimensions and mass) that change over several orders of magnitude from larval stages to adulthood. The frequencies of locomotion cycles typically also change over a large range. It would be interesting to explore what are the developmental mechanisms that underly this frequency adaptation. Clearly our model is very abstract, and is as such not suitable for mechanistic explanations of such phenomena. But it might be that some of the

adaptation mechanisms present in biological systems could be compared to the adaptation rule that underlies our system.

5.2.6 Appendix – Calculation of c_n for small K

We show in the following how c_n can be approximated for low K , later we discuss what needs to be done to extend the formulation for large K which turns out to be much more difficult. While weakly coupled oscillators are fairly well understood and treated extensively in the literature, the picture changes for strongly coupled oscillators which are much more difficult to handle. In any case c_n is a function of $P(\omega)$, i.e. the state of the oscillators. Hence, the Fokker-Planck equation becomes nonlinear.

For the given assumption that K is small we can calculate the integration region L in a straight forward manner by exploiting the locking condition for weakly coupled harmonic oscillators. The locking condition is a condition on the difference of the intrinsic frequency of the oscillator and the perturbation. As soon as the frequencies are close enough, i.e. the difference of frequencies is below the critical value ($|n\omega_F - \omega| < \omega_c$), the oscillator will phase lock on the perturbation. This means it will oscillate at the frequency of the perturbation (ω_F) instead of the intrinsic frequency ω . As shown in [23], by analyzing the geometry of the limit cycle of system Eqs. (5.56)–(5.57) and the influence of perturbations, the critical difference in frequency can be calculated as

$$\omega_c = \frac{K\mu}{2} \quad (5.65)$$

Because for small K the locking region is about the same size as the region where the frequency convergence mechanism makes the frequency “snap” into the final frequency, we can safely consider the oscillator as converged when it enters the locking condition. This assumption is based on empirical evidence, but the results of the numerical integration in Sections 5.2.4 and 5.2.4 shows that it is justified.

Using condition from Eq. 5.65, which gives the bounds on the frequencies for which component oscillators phase lock, c_n can then be calculated as $c_n \approx \int_{n\omega_F - \omega_c}^{n\omega_F + \omega_c} P(\omega) d\omega$.

While we have seen that this assumption and derivation of c_n gives good results for small K (i.e. up to $K \approx 1$), for large K the correction factor needs further modification. Unmodified the present formulation of c_n would over-estimate the number of converged oscillators because it removes all oscillators from the driving forces when they enter the locking region, which gets large for large K .

But since even if the locking region is very large, the oscillators continue to converge once they enter the locking region, cf. example in Fig. 5.14, where all oscillators start in the locking region of the signal components, nevertheless there is a convergence of the frequencies. Calculating c_n based on critical frequency ω_c would thus lead to an overestimation of the number of converged oscillators. Thus, we have to figure out how to modify the calculation of c_n for large K . In

the following we shortly describe the largest effects that we have observed which will be the basis for the modification.

For large values of K , even if the oscillator has locked on the signal (which happens very early due to the larger locking region) it will not completely remove the associated part of it since it will run phase shifted with the signal. The small remaining signal is amplified by the strong coupling constant to drive other oscillators towards the frequency.

Furthermore, for such strong coupling, the radius of the limit cycle is changed to an extent that the effects need to be taken into account. What happens is that due to the strong coupling the radius of the limit cycle is larger than $\sqrt{\mu}$. This effect accounts for the steady state error (i.e. the oscillators which do not converge), since due to the larger radius, fewer oscillators are needed to actually cover the full signal.

Thus, while we have an idea for the mechanism which have to go into the formulation the modification term for strong K we yet have to work out the theoretical fundament and analytical form of these mechanisms.

Acknowledgments This work is funded by the Swiss National Science Foundation (A.I. & J.B.) and by the European Commission's Cognition Unit, project no. IST-2004-004370: RobotCub (L.R.).

From Abstract to Reality

IN this chapter we develop the ideas from Chapter 4 further. The abstract controller concept is step by step applied to more complex robots, first in simulation and then in the real world. It will be shown that the original concept is not only working without a fundamental modification on all the systems on which it has been tried, but that the results get ever more interesting and promising the more complex the underlying “body” becomes.

In a first simulation study, the adaptive frequency oscillators are applied to a simple 4-DOF spring mass hopper. Finally, the controllers are implemented and put to the test on a real robot, the experimental compliant and under-actuated robot PUPPY II.

6.1 A simulated hopper robot

A Dynamical Systems Approach to Learning: A Frequency-adaptive Hopper Robot

Jonas Buchli, Ludovic Righetti and Auke Jan Ijspeert

This paper has been originally published as J. Buchli, L. Righetti, and A.J. Ijspeert. A dynamical systems approach to learning: a frequency-adaptive hopper robot. In *Proceedings of the VIIIth European Conference on Artificial Life ECAL 2005*, Lecture Notes in Artificial Intelligence, pages 210–220. Springer Verlag, 2005

Abstract We present an example of the dynamical systems approach to learning and adaptation. Our goal is to explore how both control and learning can be embedded into a single dynamical system, rather than having a separation between controller and learning algorithm. First, we present our adaptive frequency Hopf oscillator, and illustrate how it can learn the frequencies of complex rhythmic

input signals. Then, we present a controller based on these adaptive oscillators applied to the control of a simulated 4-degrees-of-freedom spring-mass hopper. By the appropriate design of the couplings between the adaptive oscillators and the mechanical system, the controller adapts to the mechanical properties of the hopper, in particular its resonant frequency. As a result, hopping is initiated and locomotion similar to the bound emerges. Interestingly, efficient locomotion is achieved without explicit inter-limb coupling, i.e. the only effective inter-limb coupling is established via the mechanical system and the environment. Furthermore, the self-organization process leads to forward locomotion which is optimal with respect to the velocity/power ratio.

6.1.1 Introduction

Nonlinear dynamical systems are a promising approach both for studying adaptive mechanisms in Nature and for devising controllers for robots with multiple degrees of freedom. Indeed, nonlinear dynamical systems can present interesting properties such as attractor behavior which can be very useful for control, e.g. the generation of rhythmic signals for the control of locomotion. However, controllers for engineering applications usually need to be tailor-made and tuned for each application. This is in contrast to Nature where multiple adaptive mechanisms take place to adjust the controller (the central nervous system) to the body shape, and vice-versa. For the control of locomotion for instance, there are mechanisms to adapt the locomotor networks to changing body properties (e.g. due to growth, aging, and/or lesions) during the life time of an individual, and this greatly increases its survival probability.

In order to endow robots with similar capabilities, we are investigating the possibility to construct adaptive controllers with nonlinear dynamical systems. This is achieved by letting the parameters of the system change in function of the systems behavior, and, therefore, also in function of external influences. Thus, we aim at designing systems in which learning is an integral part of the dynamical system, not a separate process, in contrast to many approaches in artificial neural networks and other fields.

In an earlier study [24] we presented an *adaptive frequency oscillator* as a controller for a simple locomotion system. The motivation to use an adaptive frequency oscillator was to deploy a controller that is able to adapt to “body”-properties, i.e. properties of the mechanical system. In this case the body property to be adapted to is the resonant frequency of the mechanical system. The presented approach is especially useful when the mechanical properties of the body are not known or changing. In such cases, properties such as the resonant frequencies and similar are not directly accessible, but have to be inferred by some sort of measurement.

In this paper we pursue further the idea of the adaptive frequency oscillator used as an adaptive locomotion controller (cf. [24]). First, we will present how the adaptive frequency oscillator can learn the frequencies of arbitrary rhythmic input

signals. The main interesting features of the adaptive oscillator are (1) that it can learn the frequencies of complex and noisy signals, (2) that it does not require any pre-processing of the signal, and (3) that the learning mechanism is an integral part of the dynamical system.

Then, we will present a more complex and realistic example of a robot that is capable of hopping, namely a 4-DOF spring-mass hopper with an adaptive controller based on the adaptive frequency oscillators. Spring-mass systems have been widely used to study fundamental aspects of locomotion [14, 70] and several robots based on this concept have been presented [34, 53, 172]. In [73] the mechanical stability of spring-mass systems is discussed. Recently, robots with legs including elastic elements have been presented [69, 103, 127]. Coupled oscillators have been extensively studied for locomotion control [47, 69, 220, 223]. However, usually the structure and parameterization of these controllers are fixed by heuristics or are adapted with algorithms which are not formulated in the language of dynamical systems. One exception is [158] where learning is included in the dynamical system. The results are, however, for many coupled phase oscillators and no direct application example is given. Another exception is [39] where an adaptation of the stride period is investigated, with a discrete dynamical system.

In our contribution, thanks to the adaptive mechanisms, the controller tunes itself to the mechanical properties of the body, and generates efficient locomotion. As we will see, the system, albeit its simplicity, shows a rich and complicated emergent behavior. In particular, efficient gait patterns are evolved in a self-organized fashion, and are quickly adjusted when body properties are changed. Interestingly, the emergent gaits are optimal with respect to the velocity/power ratio.

6.1.2 Adaptive Frequency Oscillators

In this section we introduce our adaptive frequency Hopf oscillator, and will show its behavior under non-harmonic driving conditions. The adaptive frequency Hopf oscillator is described by the following set of differential equations. We introduce it in the Cartesian coordinate system (Eqs. 6.1–6.3) as this allows an intuitive understanding of the additive coupling. In order to understand convergence and locking behavior it is also convenient to look at the oscillator in its phase, radius coordinate system which in the case of the Hopf oscillator, having a harmonic limit cycle, coincides with the representation in polar coordinates (Eqs. 6.4–6.6).

$$\dot{x}_h = (\mu_h - r^2)x_h - \omega_h y_h + cF_x(t) \quad (6.1) \quad \dot{r}_h = (\mu_h - r^2)r + \cos(\phi_h)cF_x(t) \quad (6.4)$$

$$\dot{y}_h = (\mu_h - r^2)y_h + \omega_h x_h \quad (6.2) \quad \dot{\phi}_h = \omega_h - \frac{1}{r} \sin(\phi_h)cF_x(t) \quad (6.5)$$

$$\dot{\omega}_h = -\frac{1}{\tau_h} \frac{y}{r} cF_x(t) \quad (6.3) \quad \dot{\omega}_h = -\frac{1}{\tau_h} \sin \phi_h cF_x(t) \quad (6.6)$$

where x_h, y_h are the states of the oscillator, ω_h is its intrinsic frequency, $r = \sqrt{x_h^2 + y_h^2}$ and $F_x(t)$ is a perturbing force (the subscript h distinguishes the

variables of the Hopf oscillator from variables in the mechanical system). If $F_x(t) = 0$, this system shows a structurally stable, harmonic limit cycle with radius $r = \sqrt{\mu}$ for $\mu > 0$. It can be shown [176] that such an oscillator adapts to frequencies present in a rhythmic input signal. In the case of a harmonic signal $F_x(t) = \sin(\omega_F t)$ this means ω_h is evolving toward ω_F . If the input signal has many frequency components (e.g. square signal) the final value of ω_h is dependent on the initial condition $\omega_h(0)$. The size and boundaries of the basins of attraction are proportional to the energy content of the frequency component constituting the basin of attraction, see [176] for further discussion of the convergence properties. Our adaptive frequency oscillators have many nice features which makes them useful for applications and a good example for the dynamical systems approach to learning: 1) no separation of learning substrate and learning algorithm, 2) learning is embedded into the dynamics, 3) no preprocessing needed (e.g. no extraction of phase, FFT, nor setting of time windows), 4) work well with noisy signals, 5) robust against perturbation, 6) they possess a resonant frequency and amplification properties.

Now we shall present a few representative results from numerical integration, to show the correct convergence of the adaptive frequency oscillator. First, we show the convergence for a harmonic perturbation $F_x(t) = \sin(\omega_F t)$. As we are interested to show that $\omega_h \rightarrow \omega_F$, we use $\omega_d = \omega_h - \omega_F$ and $\phi_d = \phi_h - \phi_F$ to plot the results. For all simulations $\tau = 1$, $c = 0.1$, $\omega_d(0) = 1$, $\phi_d(0) = 0$ and $r_h(0) = 1$. We present results of the integration of the system Eqs. 6.4-6.6. In Fig. 6.1 the behavior of variables ϕ_d and ω_d is depicted. In Fig. 6.1(b), we present the phase plot of the system for the harmonic perturbation. Clearly visible is that the system is evolving towards a limit set. The limit set corresponds to the phase locked case $\phi_d \leq \text{const}$ and the frequency has adapted so that $\omega_d \approx 0$. Since we want to be sure that the convergence works for a wide range of input signals (as in the case when the oscillator is coupled with the mechanical system) we show then results with general nonharmonic perturbation by general T_F -periodic functions $f(t, \omega_F)$, $T_F = \frac{2\pi}{\omega_F}$ (Fig. 6.2). The system was subjected to the following driving signals: (a) Square Pulse Signal $f(t, \omega_F) = \text{rect}(\omega_F t)$, (b) Sawtooth $f(t, \omega_F) = st(\omega_F t)$, (c) Quadratic Chirp $f(t, \omega_F) = \cos(\omega_c t)$, $\omega_c = \omega_F(1 + \frac{1}{2}(\frac{t}{1000})^2)$, (d) Signal consisting of two non-commensurate frequency components, $f(t, \omega_F) = \frac{1}{2} \left[\cos(\omega_F t) + \cos(\frac{\sqrt{2}}{2}\omega_F t) \right]$, (e) Chaotic signal from the Rössler system. There are differences in the convergence speed and in the limit set. Yet, in all cases the oscillators converge to the appropriate frequencies. Very interesting cases are signals with 2 or more pronounced frequency components (such as signals (a), (b) and (d)). In this case the initial condition $\omega_d(0)$ determines to which frequency the oscillator adapts (cf Fig. 6.2(d)). The size of the basin of attraction is proportional to the ratio of energy of the corresponding frequency component to the total energy of the signal (due to the lack of space the data is not shown, but can be found in [176]). These simulations show that the adaptation mechanism works despite complex input signals (convergence under broad driving conditions). In the next

section we will explore how these interesting properties can be applied to control a mechanical system.

6.1.3 The adaptive active spring-mass hopper

In this section we will present the spring-mass hopper. We will first present the mechanical structure and then focus on the adaptive controller. As a general idea we will exploit the bandpass, and amplification/attenuation properties of both the mechanical system and the adaptive frequency Hopf oscillator.

Since our main interest is the adaptation in the controllers, we do not discuss the problem of mechanical stability of the locomotion. We avoid stability problems by an appropriate mechanical structure (wide feet, low center of mass), thus the feet of the robot are wide enough to ensure stability in lateral direction, i.e. the robot is essentially working in a vertical (the “sagittal”) plane. The spring-mass hopper consists of 5 rigid bodies joined by rotational and linear joints (cf. Fig. 6.3). A prolonged cubic body is supported by two legs. The two legs are identical in their setup. A leg is made of an upper part M_u and a lower part M_l which are joined by a spring-mass system and a linear joint. The function of the linear joint is just to ensure the alignment of the body axes and is otherwise passive. The spring between the two parts of the leg is an activated spring of the form $F_f = -kd_l$, where $k = f_k(t)$ and d_l is the distance between M_u and M_l . The damper is an ideal viscous damping element of the form $F_d = -c_d v_d$, where c_d is the damping constant and $v_d = v_u - v_l$, is the relative velocity of M_u and M_l . The rotational joints between the upper part of the leg M_u and the body M_b are activated by a servo mechanism which ensures that the desired velocity v_{ref} is always maintained (cf. [3]). The choice of the spring activation function $f_k(t)$ and the choice of the desired velocity $v_{ref} = f_v(t)$ will be discussed below, when the coupling between controller and mechanical system is introduced. Due to the spring-mass property of the legs the contraction mechanism possesses a resonant frequency ω_F ¹. In other words, this type of mechanical system can be interpreted as a band-pass filter with the pass band around ω_F . This fact is important for the controller to be able to activate the body [24]. This will be further discussed towards the end of this section.

The *controller* of the leg consists of an adaptive frequency Hopf oscillator (Eqs. 6.1–6.3), which is perturbed by the activity of the mechanical system (see below for the exact form). The Hopf oscillator acts as a frequency selective amplifier [58], i.e. frequency components of $F_x(t)$ that are close to ω_h are amplified. Especially the setting $\mu_h = 0$ is special in the sense that the system undergoes a fundamental change at that point: For $\mu_h < 0$ the system exhibits a stable fixed point at $z = 0$, whereas for $\mu_h > 0$ a stable limit cycle occurs with radius $r = \sqrt{\mu_h}$. This phenomenon is known as a Hopf bifurcation. At $\mu_h = 0$, there is no signal oscillating at ω_h weak enough not to get amplified by the Hopf oscillator. Therefore, for

¹Note, that the leg can also be considered as a pendulum and thus possesses a second resonant frequency. We will not focus on this intrinsic dynamics in this article.

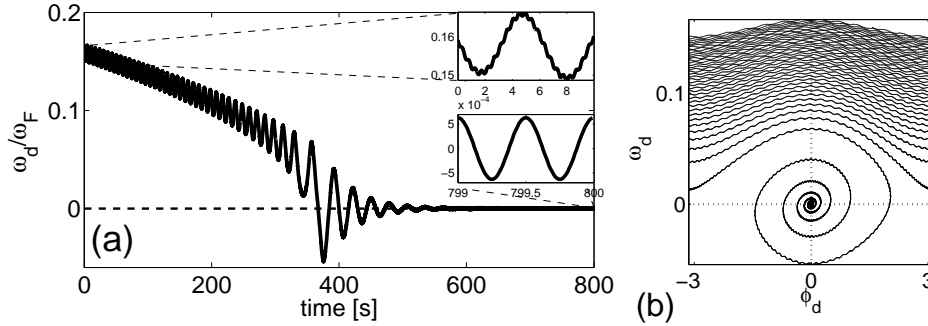


Figure 6.1: (a) Integration of the System Eqs. 6.1-6.3 (b) corresponding phase plot, in which the frequency adaptation and the phase locking can be seen.

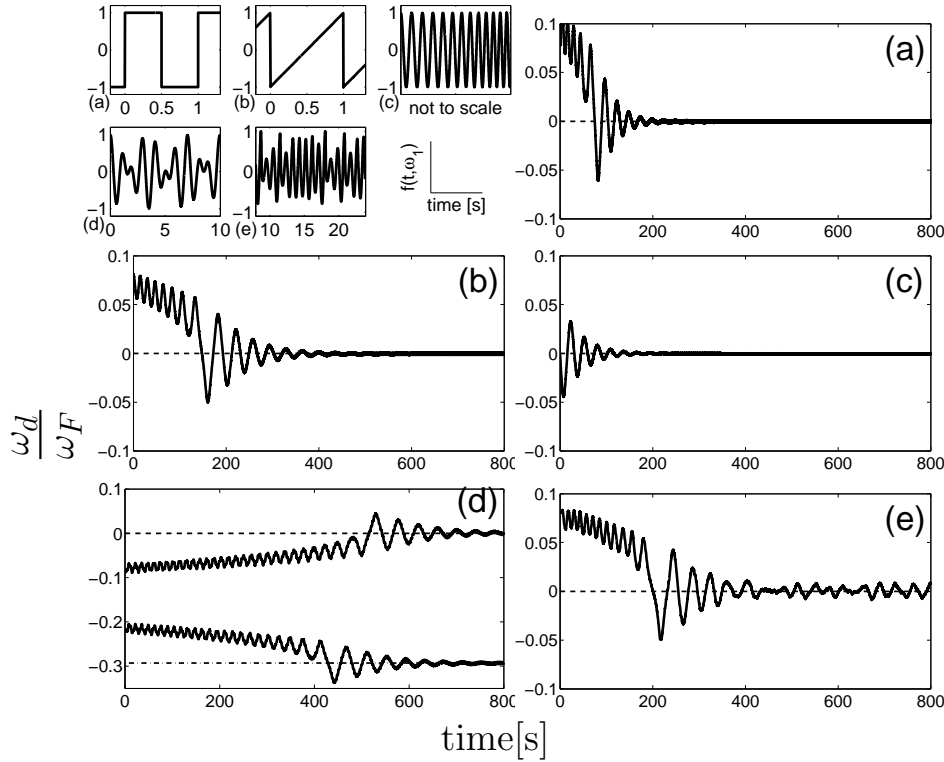


Figure 6.2: On the top left panel the nonharmonic driving signals are presented. (a) Square pulse (b) Sawtooth (c) Chirp (Note that this is illustrative only since the change in frequency takes much longer as illustrated.) (d) Signal with two non-commensurate frequencies (e) Output of the Rössler system. – We depict representative results on the evolution of $\frac{\omega_d}{\omega_F}$ vs. time. The dashed line indicates the base frequency ω_F of the driving signals. In (d) we show in a representative example how the system can evolve to different frequency components of the driving signal depending on the initial condition $\omega_d(0)$.

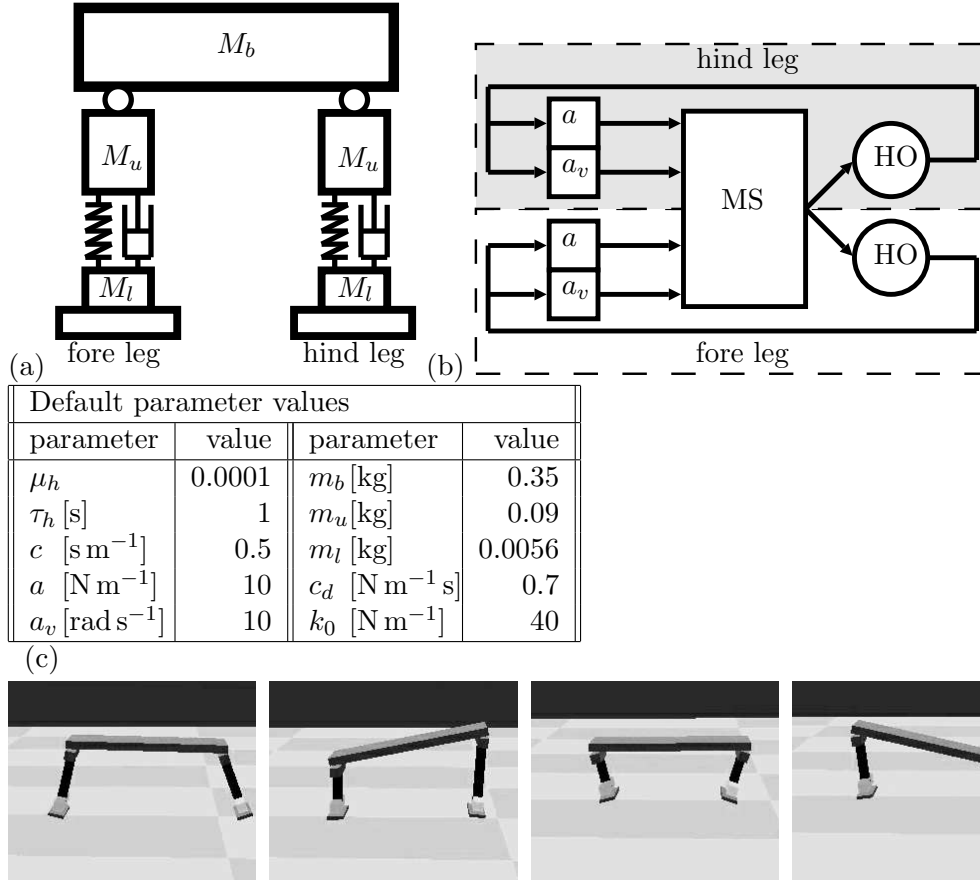


Figure 6.3: (a) The mechanical structure of the spring-mass hopper. The trunk is made up of a rigid body M_b on which two legs are attached by rotational joints. The lower part of the leg is attached by a spring-mass system SD . The lower part consist of a small rigid body. The length of the body is 0.5m (b) The coupling structure of the controller and the mechanical system used for the spring-mass hopper. The upper Hopf oscillator is used for the activation of the fore leg and the lower feedback loop for the hind leg. (c) This table presents the parameters that have been used for the simulations, unless otherwise noted. Note that this parameters can be chosen from a wide range and the results do (qualitatively) to a large extent not depend on the exact values of the parameters. Bottom row: Snapshots of the movement sequence of the spring-mass hopper when the frequency is adapted, i.e. steady state behavior (cf also movie [1]).

that setting the Hopf oscillator can be considered an ideal amplifier. We use a setting $\mu_h \approx 0$. The *coupling* from the oscillator to the mechanics is established via the spring constants $k = f_k(t)$ and desired angular joint velocity $v_{ref} = f_v(t)$. The oscillator therefore drives both a linear actuator (the spring in the leg) and a rotational actuator (the servo in the hip). The function for the spring constant is chosen as $k = k_0 + a \frac{x_h}{r}$, where k_0 is a constant and a a coupling constant. The function for the desired velocity is chosen as $v_{ref} = a_v y_h$ where a_v is a coupling constant. The choice of this function, which introduces a $\frac{\pi}{2}$ phase lag between the spring activity and the joint angular velocity is based on the observation of a phase lag between hip and knee joints in locomoting humans and animals. The coupling from the mechanical system to the Hopf oscillator is established via the relative velocity between upper and lower part of a limb as follows $F_x(t) = cv_d$ Fig. 6.3 illustrates the coupling scheme. Thus, by the coupling scheme a feedback loop is established between the oscillator and the mechanical system. If the resonant frequencies of mechanical system and the Hopf frequency match, i.e. $\omega_F \approx \omega_h$, an increase of the activity in the system is expected due to the amplifying properties of the Hopf oscillators (cf. [24]). Instead of tuning the controller manually to the appropriate frequency, we let the controller adapt its frequency. In order to achieve this adaptation, we introduce an influence of the mechanical perturbation to the evolution of ω_h via an appropriate choice of F_ω .

Adaptive Frequency The coupling of the perturbation of the mechanical system to the evolution of ω_h , allows the controller to adapt to the mechanical system and is equivalent to the perturbation arriving at the oscillator projected on the tangential direction of the limit cycle multiplied with an adaptation rate constant: $\dot{\omega}_h = -\frac{1}{\tau_h} cv_d \frac{y_h}{r} = -\frac{1}{\tau_h} F_x(t) \frac{y_h}{r}$. This is the same coupling as used for the adaptive frequency Hopf oscillator before.

6.1.4 Simulation results

The spring-mass hopper simulation was implemented in Webots, a robot simulator with articulated-body dynamics [153]. In Table 6.3 we present the parameters for the spring-mass hopper that were used for the simulations unless otherwise noted. Note that this parameters can be chosen from a wide range and the qualitative results do to a large extent not depend on the exact values of the parameters.

We first show how the adaptation of the Hopf frequency ω_h leads to an excitation of the system and hopping is initiated. To avoid influence of the hip movements on the generated movement the joints are, in this case, fixed at an angle of zero degrees and $a_v = 0$, i.e. the hopper is just able to hop in place. Thus, the experiment verifies that the frequency adaptation works. As can be seen in Fig. 6.4, indeed, due to the adaptation the feet start to lift from the ground. In a next experiment the coupling from the oscillators to the rotational hip joints is set to its default value ($a_v = 10$). Due to the activation of the hip joints complex movements emerge. The diversity and self-organization of the movement depends on many factors, therefore in this article we will show preliminary results on the

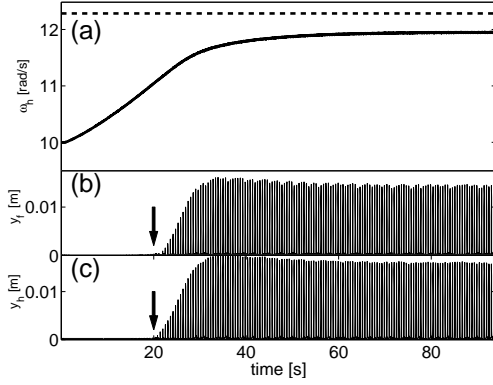


Figure 6.4: Simulation results of the spring-mass hopper when the rotational joints are not activated. a) Evolution of the intrinsic frequencies of the Hopf oscillators ω_h . Note that the frequencies of both oscillators nearly coincide and therefore only one seems visible. b) Fore limb foot elevation. c) Hind limb foot elevation. The adaptation of the frequency is clearly visible and as can be seen in the feet elevation measurements the activity of the system is increased as hopping starts at around 20 s (arrow). The dashed line depicts the theoretical resonant frequency of the spring-mass system when it would not leave the ground. Due to the lift-off of the feet the real resonant frequency is smaller than the calculated value.

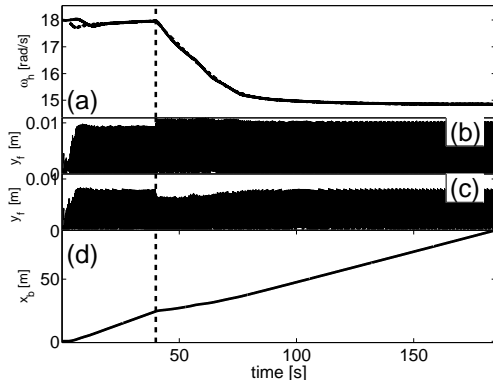


Figure 6.6: Test of the adaptation capability of the controller when the mass is changed. At $t = 40$ s (dashed line) the mass of the body M_b is changed from $m_b = 0.2$ kg to 0.4 kg. See text for discussion.

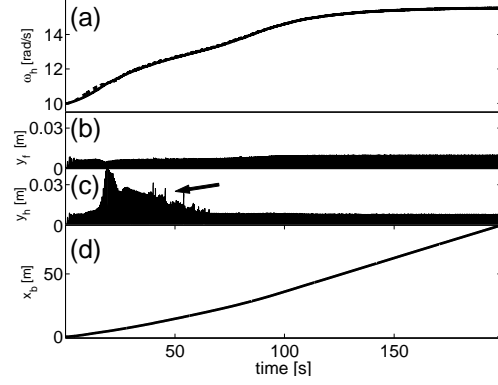


Figure 6.5: Simulation results of the spring-mass hopper when the rotational joints are activated a) The frequencies of the Hopf oscillators ω_h b,c) Foot elevation $y_{f,h}$ d) Displacement of the center of mass of the body x_b . The adaptation of the frequency is clearly visible. As can be seen in the feet elevation measurements and the displacement of the body this adaptation enhances the activity of the leg and initiates a displacement of the body. Interestingly there is a burst of activation (arrow) which increases the adaptation speed before the system settles to steady state behavior.

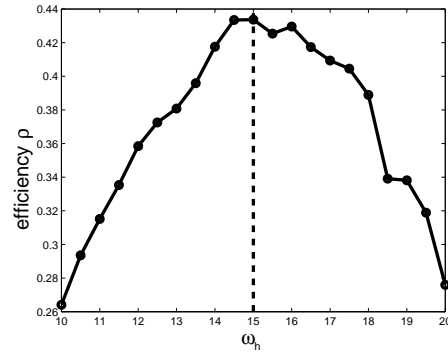


Figure 6.7: Efficiency ρ vs ω_h . See text for the definition of ρ , details of measurement and experimental protocol. The dashed line indicates the frequency to which the oscillators adapt. It is clearly visible that this corresponds to the maximum of the efficiency.

most typical locomotion pattern that was observed. This pattern resembles the bound. The movement sequence of the hopping movement is shown in a series of representative snapshots in Fig. 6.3. In Fig. 6.5, the adaptation, feet elevation and displacement of the body is presented. The average achieved velocity in steady state for $m_b = 0.35$ kg is about 0.53 ms^{-1} (approx. one body length per second). The next experiment shows that the controller correctly tracks changes in the mechanical system. To demonstrate this adaptation capability the mass of the body M_b is changed from $m_b = 0.2$ kg to $m_b = 0.4$ kg at time $t = 40$ s. The results are presented in Fig. 6.6. As the mass is changed, the controller immediately starts to adapt and settles after about 50 s to the new resonant frequency. When looking at the displacement of the body x_b it is evident that the change in the mass slows down the system for a moment but due to the adaptation the velocity is increased again (cf also movies of the experiments [1]). The average velocity before change of mass is about 0.68 ms^{-1} . After the change, when reached steady state behavior again, the velocity is in average 0.49 ms^{-1} .

In a last experiment we investigate the efficiency of the hopper for forward locomotion. We define the efficiency as the ratio $\rho = \frac{\bar{v}_{x,b}}{\bar{P}_\Sigma}$ i.e. the ratio between average forward velocity $\bar{v}_{x,b}$ of the body and the average power \bar{P}_Σ consumed by all activated joints. In order to assure steady state measurements, the learning is disabled ($\tau_h = 0$) and the experiment is repeated for different Hopf frequencies $\omega_h = [10, 10.5 \dots, 20]$. The transient behavior is removed before the efficiency is measured. In Fig. 6.7, the results of the efficiency measurements are presented. The line indicates the frequency to which the system evolves if $\tau \neq 0$, thus it is clear that the adaptive frequency process finds the optimal efficiency. It is worth noting, that this optimum in efficiency does not correspond to the maximum of power consumption nor the maximum of velocity (data not shown). This is in line with the observations on animals.

6.1.5 Discussion

When introducing adaptation into a system it is important to investigate the convergence properties of the adaptation mechanism. From the mathematical point of view adaptivity on one hand and convergence and stability on the other hand are somewhat opposing requirements. We have shown, that the adaptive frequency oscillator can be driven with general, nonharmonic signals and still adapts to the frequency of the signal.

We have presented a 4-DOF spring-mass hopper with a controller based on adaptive frequency Hopf oscillators which adapts to mechanical properties of the hopper. This adaptation has the effect that the spring-mass system starts to resonate and initiates hopping locomotion, similar to the bound. The adaptation is embedded into the dynamics of the system and no pre-processing of sensory data is needed. The system shows fast adaptation to body properties.

The results presented in this paper show that with a simple control scheme, it is possible to initiate complex movements and to adapt to the body properties

which are important for this movement. In order for this simple scheme to be successful it is important that the controller exploits the natural dynamics of the body. This is in line with observations in nature, where the controllers are found to be complementary to the bodies they control. In fact the adaptation can be considered a type of Hebbian learning as it maximizes the correlation between the signal perturbing the oscillator and the activity of the oscillator. Interestingly, there is no direct coupling between the controllers for the hind and the fore limb. The only coupling between the two controllers is via the mechanical structure and the environment. Nevertheless, an efficient inter-limb coordination emerges and a fast, efficiency-optimal locomotion is established. This is interesting as there is no explicit notion of velocity in the system, so it is surprising that the system optimized on velocity/power efficiency.

Immediate possible applications of such adaptive nonlinear dynamical systems are e.g. modular robotics, micro robots, robots which are difficult to model, and adaptive Central Pattern Generators (CPG) for legged locomotion. Furthermore, it will be interesting to explore the use of such adaptive systems in other fields such as in Physics, Biology and Cognitive Sciences, where oscillators are widely used model systems.

Acknowledgments This work is funded by a Young Professorship Award to Auke Ijspeert from the Swiss National Science Foundation (A.I. & J.B.) and by the European Commission's Cognition Unit, project no. IST-2004-004370: RobotCub (L.R.). We would like to thank Bertrand Mesot for constructive comments on earlier versions of this article.

Additional results From the simulation used in the just presented study, more interesting results have been obtained, which were omitted in the publication for lack of space. We do present it in the following as it completes the understanding of the system.

In Fig. 6.8, we show first the two quotients making up the efficiency measure, namely the energy consumed by the robot and the velocity. It is clearly visible that they do not show an extremal value for the found frequency, but only their quotient as presented in the article. Furthermore, we show, that the system finds distinct gait patterns (expressed by the phase difference between hind and fore leg) for each frequency. This data is the motivation for some of the experiments shown later on the real robot with local controllers.

As an additional very interesting result, we show where the energy for locomotion is actually spent. The main contribution is from the motor of the hind limbs ($\sim 45\%$), followed by the motor of the front limbs ($\sim 35\%$), and only then comes the contributions of the springs ($\sim 15\%$ and $\sim 5\%$).

Interestingly this distribution of the power corresponds qualitatively to biological data, where (1) the hind limbs contribute most for locomotion and (2) in the limbs, it is mainly the pivotal action around the hip joint that contributes to the

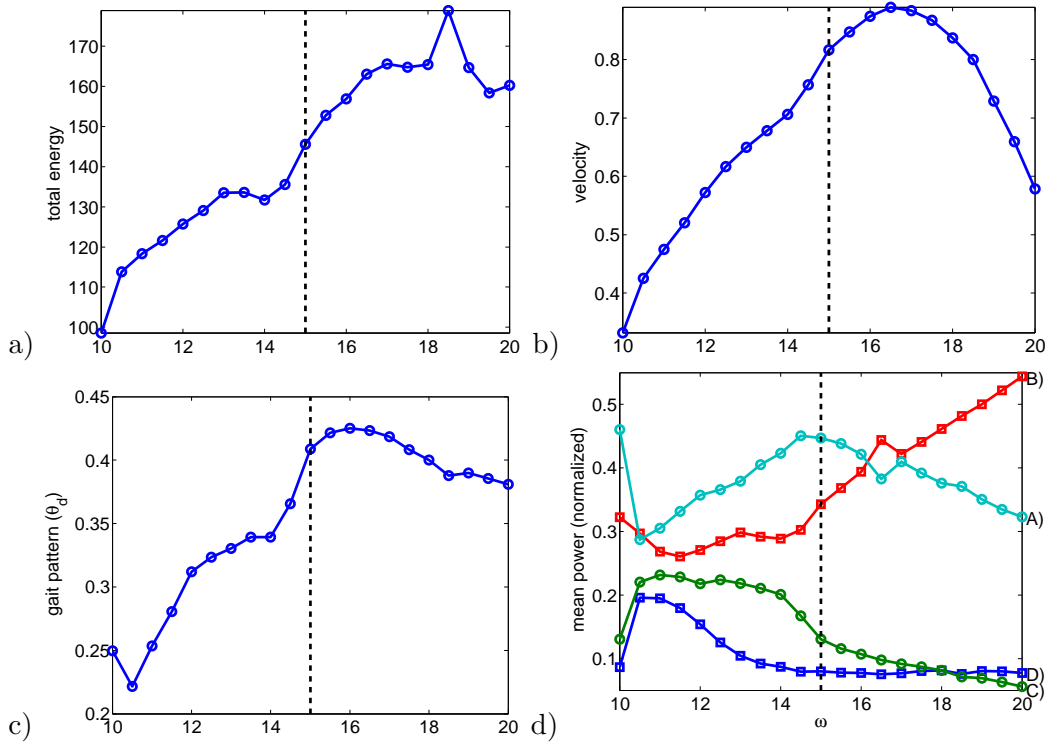


Figure 6.8: Further results from the simulation study a) total energy consumed by the robot over the simulation run b) The mean velocity achieved by the robot. It can be seen that the neither the energy nor the velocity show an extremum at the resonant frequency. c) Gait pattern (phase difference), depending on the detuning of the controller different gait patterns emerge. d) Energy distribution over the different actuators of the robot. After adaptation, the hind legs contribute more to the locomotion. Hip joints more than the springs: Mean energy A) hind hip joint B) fore hip joint C) hind spring D) fore spring.

forward motion. The other muscles are anti-gravity muscles and do not contribute to locomotion. Those muscles correspond to the springs in our systems. In the robot, as we will see below, we will have non-activated knee joints and it is the energy distribution from this simulation which suggested that the approach will work well with non-activated springs - the results we will present will show that this assumption is correct.

We can thus put forward the hypothesis that the observed energy distribution and consequently muscle and limb dimensions in mammals follow from very basic mechanical facts to which evolution has been tuning its solutions.

6.2 First real world tests

This paper shows preliminary results on PUPPY II and a treatment of AFOs in feedback loops. The work is extended in the next section.

Finding Resonance: Adaptive Frequency Oscillators for Dynamic Legged Locomotion

Jonas Buchli, Fumiya Iida and Auke Jan Ijspeert

This paper has been originally published as J. Buchli, F. Iida, and A.J. Ijspeert. Finding resonance: Adaptive frequency oscillators for dynamic legged locomotion. In *Proceedings of the IEEE/RSJ International Conference on Intelligent Robots and Systems (IROS)*, pages 3903–3909. IEEE, 2006

Abstract There is much to gain from providing walking machines with passive dynamics, e.g. by including compliant elements in the structure. These elements can offer interesting properties such as self-stabilization, energy efficiency and simplified control. However, there is still no general design strategy for such robots and their controllers. In particular, the calibration of control parameters is often complicated because of the highly nonlinear behavior of the interactions between passive components and the environment.

In this article, we propose an approach in which the calibration of a key parameter of a walking controller, namely its intrinsic frequency, is done automatically. The approach uses adaptive frequency oscillators to automatically tune the intrinsic frequency of the oscillators to the resonant frequency of a compliant quadruped robot. The tuning goes beyond simple synchronization and the learned frequency stays in the controller when the robot is put to halt. The controller is model free, robust and simple. Results are presented illustrating how the controller can robustly tune itself to the robot, as well as readapt when the mass of the robot is changed. We also provide an analysis of the convergence of the frequency adaptation for a linearized plant, and show how that analysis is useful for determining which type of sensory feedback must be used for stable convergence. This approach is expected to explain some aspects of developmental processes in

biological and artificial adaptive systems that “develop” through the embodied system-environment interactions.

6.2.1 Introduction

Although rigid bodies and high-gain motor control for tracking precise trajectories are the basis for the design of traditional robotic systems, there has been an increasing interest of endowing robots with passive dynamics for locomotion behaviors inspired from biological research. In biological locomotion research it has long been realized that the control systems have to work together with the bodies they are controlling. As observed by Marc Raibert, the central nervous system does not control the body, it can only make suggestions [172]. An increasing number of legged robots are, similarly to their biological counterparts [6, 70], endowed with passive dynamics in the form of springs and/or pendulums, and have demonstrated interesting properties such as energy efficiency, self-stabilization, and simple control [38, 49, 101, 126, 149, 173].

However, an important problem with robots that have passive dynamics is that we do often not know how to properly control them. Because passive dynamics is intrinsically dependent on the physical constraints of the environment, the control architectures have to be highly dynamic and adaptive. For the operation in complex environments, in particular, it is useful for the robot to autonomously find the intrinsic locomotion dynamics. Because the locomotion dynamics is highly dependent on the physical constraints of the body and the environments (e.g. body weight and ground friction), the robot has to constantly and dynamically track and readapt the control parameters to maintain the locomotion dynamics. This is possible since body and sensors yield redundant information and invariants, which a suitable controller can find and exploit. After all, biological systems for locomotion control are extremely adaptive and seem to fulfill these adaptivity requirements.

Therefore, a successful control methodology needs to address the following questions: (1) how can we stabilize the controller-robot systems, (2) control them, and (3) modulate their behavior. These requirements are not different from the ones addressed with traditional linear controller design. For robots with passive dynamics, however additional properties of the controller are needed. Namely, (4) how to find in an autonomous fashion the intrinsic locomotion modalities and, because they can change due to the environment or changes in the body, (5) constantly track and readapt to them.

We propose an approach that addresses the problem of how to automatically and dynamically tune a controller to the, possibly time-varying, properties of a compliant robot body and exploit those properties for locomotion. In particular, we are interested in designing systems made of coupled nonlinear oscillators that are bi-directionally coupled to the robot for the control of locomotion. In this context, it is important for the controllers to be able to track the resonant frequencies of the compliant robot in order to minimize the amount of energy that needs to be

applied for obtaining locomotion. We do not address the problem of mechanical stability in this work, we are mainly interested in the adaptation problem.

In this article, we implement such an approach by using the adaptive frequency Hopf oscillator [24, 178] for controlling the hopping of a compliant quadruped robot. We designed this oscillator to have several interesting properties such as a structurally stable limit cycle and the ability to tune its intrinsic frequency to the frequency components of arbitrary rhythmic input signals. Particularly interesting are the facts that the system is simple, that it does not require complicated preprocessing and signal analysis techniques, and that it does not require external learning/optimization algorithms (learning is part of the dynamical system).

Oscillators for locomotion control have been presented before (e.g. [47, 104, 126, 217]), however the automatic, online tuning of their parameters is usually not addressed. In some studies the intrinsic synchronization properties of the oscillators are exploited to modify the gait patterns slightly based on sensory input. These studies use the well-known synchronization properties of nonlinear oscillators, namely that an oscillator receiving a forcing rhythmic input (e.g. from sensors) will oscillate at the frequency of the input as long as the coupling is strong enough and that the intrinsic frequency of the oscillator is not too different from that of the input. This means (1) that synchronization only works when the intrinsic frequency is designed to be close to that of the input, and (2) that frequency of the input is forgotten once the input is removed. In contrast, our approach based on frequency adaptation has three interesting properties: (1) it tunes the *intrinsic* frequency of the oscillator, not the resulting frequency, (2) the intrinsic frequency converges to the input frequency from any initial condition (ie. even if it is initially very different from it), and (3) after convergence, the intrinsic frequency keeps the value of the input frequency even when the input signal is removed.

In previous work, we have demonstrated in simulation that the adaptive frequency oscillators can be used to adapt to the resonant frequency of the body and initiate locomotion in crawling and hopping robots [24, 28]. In particular, we illustrated how it could adapt to changes in body weight. Here, we extend that work by applying the control architecture to a real robot, the quadruped robot PUPPY II, and by demonstrating that the system can deal with all the noise and time delays of a real system. In addition, we provide a mathematical analysis of the convergence of the frequency adaptation for a linearized plant, and show how that analysis is useful for determining which type of sensory feedback must be used for stable convergence. Interestingly, this analysis explains the experimental facts that the convergence of the adaptation process can be achieved with the sensory information from some sensors but not others (unless the sensor signals are modified). As it becomes clear later in this paper, this finding allows further insights into sensory motor-coupling of adaptive behavior in robots with passive dynamics.

In the next sections, we first describe the adaptive frequency Hopf oscillator and its application to the control of hopping with the quadruped robot (Sec-

tion 6.2.2). Experiments show the nice online adaptive property of the controller but also that convergence of the frequency adaptation is obtained with some sensors but not with others (namely with the inertial sensor but not the knee joint angle sensor). We then present a general analysis of a complete system composed of the adaptive oscillator bi-directionally coupled with a linear plant (Section 6.2.3). We use that analysis to explain the robotic experiments, i.e. how convergence depends on the modality of the sensory information (Section 6.2.4). Finally, results are discussed in Section 6.2.5.

6.2.2 Adaptive frequency oscillator on a real robot

This section explains the control architecture and the initial experimental results with the robotic platform where we use the adaptive frequency Hopf oscillator as a controller. The aim is to motivate the subsequent analysis, more detailed results on the robot experiments will be reported elsewhere. We will see that we need to develop an understanding of adaptive frequency oscillators in feedback loops to explain the experimental results. And hitherto no analysis of adaptive frequency oscillators with feedback loop exists. This article is a first step toward this analysis.

PUPPY II is a small experimental quadruped robot for the investigation of locomotion in robots with passive dynamics. The robot has 4 servo motors in the “hip” joints and passive rotational knee joints with a spring (see Figure 6.9). It is thus under-actuated and has a very pronounced intrinsic body dynamics in terms of the resonant frequency. The used version of this robot has several sensor capabilities: 3-axis inertia sensors, touch sensors, knee angle sensors, force sensors under the feet, and an IR distance sensor. From previous research (see [101]) it is known that such a robot has interesting intrinsic locomotion modalities which are closely linked with its passive dynamics. So far however these modes were found by parameter tuning, trial and error, systematic parameter sweeps or other search techniques. Our research aims at finding controllers which are autonomously capable of finding and exploiting such intrinsic locomotion capabilities. We have shown in simulation how very simple dynamical systems can find intrinsic locomotion modalities and elicit them [28]. This robot allows to test the presented approach on a real robot.

The controller consists of an adaptive Frequency Hopf oscillator which has the form [24, 178]:

$$\dot{r} = (\mu - r^2)r + \cos \phi y \quad (6.7)$$

$$\dot{\phi} = \omega - \frac{1}{r} \sin \phi y \quad (6.8)$$

$$\dot{\omega} = -\frac{1}{\tau} \sin \phi y \quad (6.9)$$

where r, ϕ and ω are the state variables for amplitude, phase and frequency respectively. $u = r \cos \phi$ is the oscillatory output signal and y is an input signal that

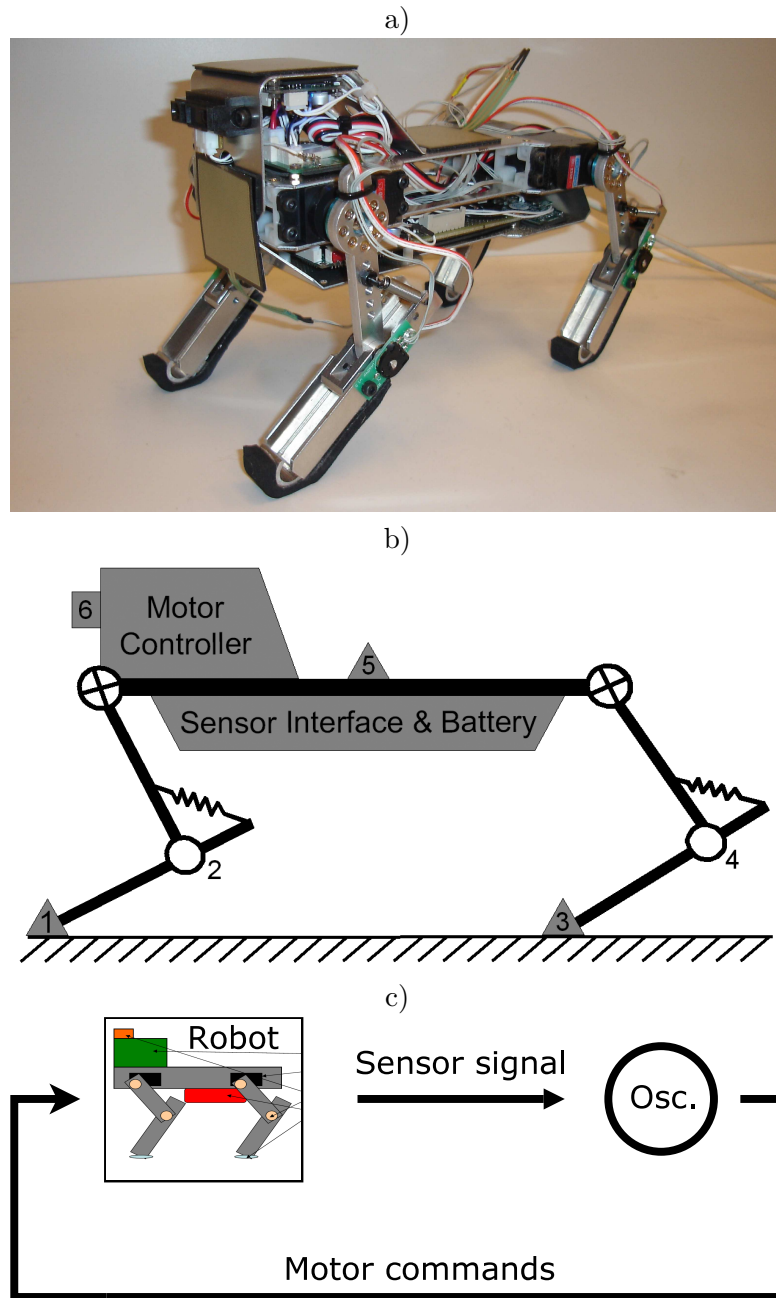


Figure 6.9: a) PUPPY II, a robot “dog” with passive dynamics (cf. springs in the knee joints) and several sensor modalities b) Mechanical structure of PUPPY II and sensor placement: 1,3: FSR (Force Sensitive Resistors) 2,4: Potentiometers of the passive joints 5: 3-axis acceleration sensors 6: PSD (Position Sensitive Detector). Circles with a cross denote actuated joints, blank circles denote passive joints. c) Control structure used in the experiments: One of the sensor channels is used to perturb an adaptive frequency Hopf oscillator, the output of the oscillator (a state variable) is used to send motor commands (position control). Thus, this system constitutes a nonlinear feedback loop.

is used to feed sensory input into the oscillator. u (with an appropriate scaling and offset) is used as position setpoint for the servos. If the input $y = 0$, this oscillator exhibits a harmonic limit cycle with radius $\sqrt{\mu}$ and frequency ω . If the input is a rhythmic signal the oscillator will tune its frequency to the frequency of the input (see [176] for details). Note that this mechanism is more than mere synchronization, it is real frequency adaptation with a theoretically unlimited basin of attraction. τ represents the adaptation time constant. Its choice is to a large extent uncritical (here we use $\tau = 0.3$). The higher this constant the faster the adaptation, but also the larger the fluctuations around the steady state value after convergence. In the presented experiments, one oscillator is used to drive all four legs, i.e. all four legs get the same position set point (i.e. hopping). The aim is to replicate some of the results from [28] on a real robot and then go further and explore more possibilities. As input to the oscillator one of the sensors of the robot is used. The closest match to the setup as in [28] intuitively is using one of the knee sensors (sensor 2 or 4) as input. In Fig. 6.10, the result of the experiment with the knee sensor is shown. It is clear that with the knee sensor there is no convergence. This somehow contradicts the intuition from the previous simulation experiments. Thus, a more formal understanding of such a system is needed to understand the convergence properties. Furthermore, if however the inertia sensor (sensor 5, z-axis) is used as an input to the oscillator, a nice convergence is observed, the frequencies to which the oscillator develops indeed correspond to a hopping forward locomotion of the robot (see movies under [2]). Fig. 6.11 shows an example of the resulting hopping behavior. And, in analogy to the simulation experiments, in Fig. 6.10b we present the capability of the controller to readapt to change of body properties. This dynamic re-adaptation follows directly from the formulation of the controller as a dynamical system.

The question arises how we can understand the convergence properties and ultimately can we use the insight to improve the convergence properties or design the controller to converge to another body property of our choice.

6.2.3 Adaptive Hopf Oscillator with Linear Feedback loop

In order to begin with the analysis of the system, the plant (i.e. the robot) will be modeled by a linear time-invariant system. This is a simplification but as we will see in the remainder of this article this simplification yields already significant understanding of the mechanism that leads to convergence/divergence.

Thus, in the following we treat the “body” as a linear system. Therefore, let's assume the following systems: First, a linear n -th order SISO (the “robot”) of the form

$$\dot{\mathbf{x}} = \mathbf{A}\mathbf{x} + \mathbf{B}u \quad (6.10)$$

$$y = \mathbf{C}\mathbf{x} + \mathbf{D}u \quad (6.11)$$

\mathbf{A} is a $n \times n$, \mathbf{B} a $n \times 1$, \mathbf{C} a $1 \times n$ matrix, and \mathbf{D} a scalar. u is the (scalar) input to the linear system and y the (scalar) output.

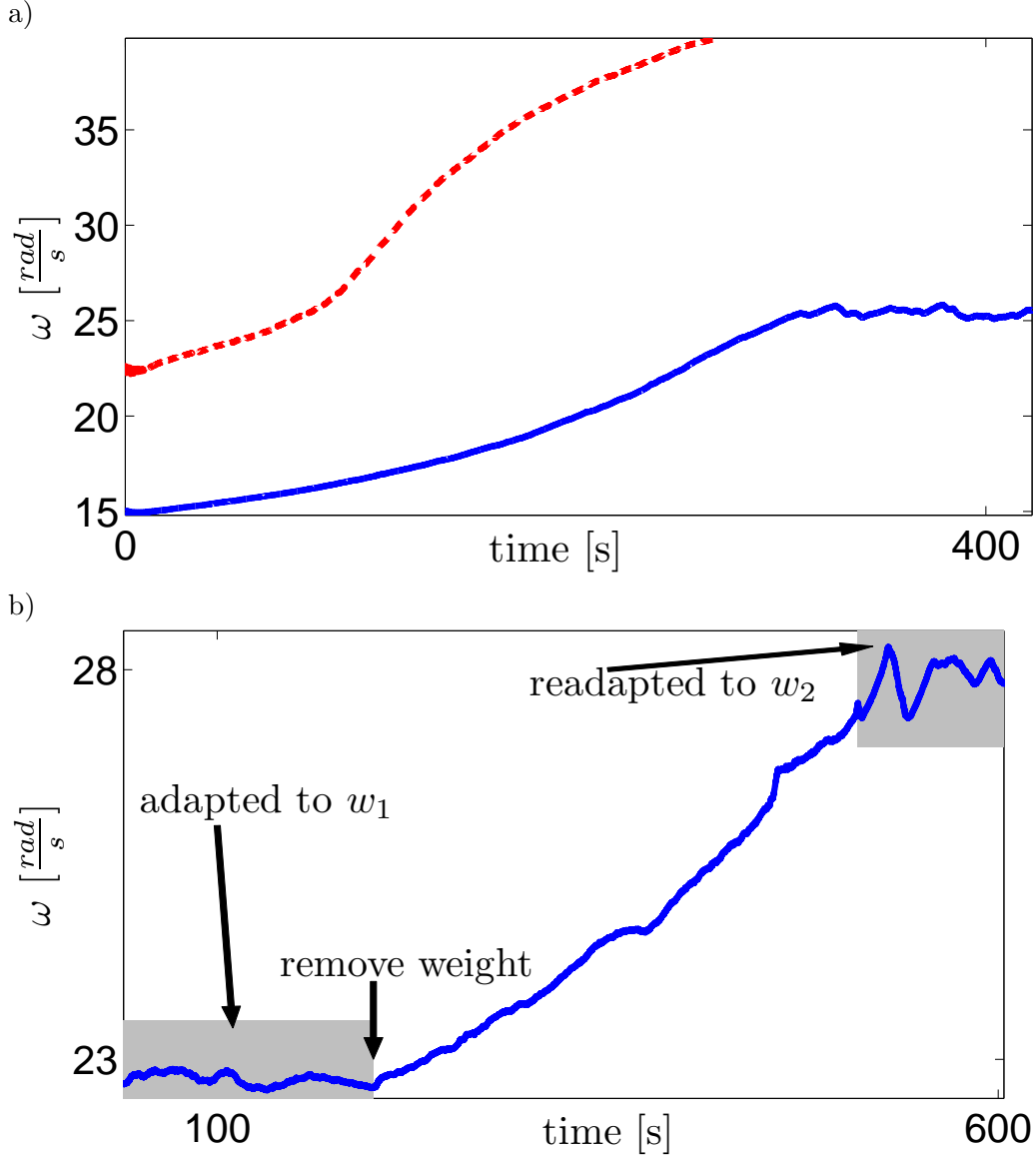


Figure 6.10: Results of adaptation experiments with the real-world robot a) The frequency ω of the oscillator is shown as it changes over time (bold line) adaptation using the z-axis of the inertia sensor: convergence of the frequency adaptation; (dashed line) adaptation using the knee sensor: divergence of the frequency adaptation with increased rate around the resonant frequency b) An experiment showing the advantage of using online adaptive controllers. The body weight is changed from $w_1 = 0.905$ kg to $w_2 = 0.695$ kg. The controller immediately adapts to the changed body property.



Figure 6.11: These snapshots show the hopping movement of the robot after the frequency adaptation has converged. There are moments when the robot has all four legs lifted.

Second, the adaptive frequency Hopf oscillator as described by Eqs. 6.7– 6.9. We set $u = r \cos \phi$. Hence, the Hopf oscillator and the linear systems are connected in a feedback structure through their inputs y (from the linear system to the Hopf Oscillator) and u (from Hopf to the linear system).

As can be shown by linear systems theory, the linear system can not generate other frequencies than already present in the input u , it can however modify phase and amplitude of the signal. Therefore, we can write:

$$y = Ar \cos(\phi + \alpha) \quad (6.12)$$

where $A = |H(s)|$ and $\alpha = \arg(H(s))$. ($H(s)$ is the transfer function of the linear system).

We begin the analysis of the oscillator by writing the phase of the Hopf oscillator perturbed by an input y

$$\dot{\phi} = \omega - \frac{1}{r} \sin \phi y$$

As outlined above we write $y(t)$ to be the Hopf state amplified by A and rotated by α

$$y(t) = Ar \cos(\phi + \alpha)$$

thus

$$\dot{\phi} = \omega - \sin \phi A \cos(\phi + \alpha)$$

Using trigonometric transformations we can write this expression as

$$\Rightarrow \dot{\phi} = \omega + \frac{1}{2} A [\sin \alpha - \sin(2\phi + \alpha)]$$

The results in [178] show that we have a separation of timescale, i.e. the frequency adaptation process works on a timescale much slower then the convergence to the limit cycle with given frequency and radius. Thus, we assume $\omega = \text{const}$ and investigate what the observed frequency will be. If this frequency is different then the intrinsic frequency, it should drive the slower adaptation process. $\omega = \text{const}$ also implies that A and α are constants ($s = j\omega$). We evaluate the average effective frequency with the given assumptions:

$$\bar{\omega} = \frac{1}{2\pi} \int_0^{2\pi} \omega + \frac{1}{2} [A \sin \alpha - \sin(2\phi + \alpha)] d\phi \quad (6.13)$$

Since by assumption ω is a constant and therefore α, A are constant, it follows that the first two summands are constants. The last summand is a 2π -periodic mean-free function, thus we get

$$\bar{\omega} = \omega + \frac{1}{2}Ar \sin \alpha \quad (6.14)$$

Let us define $\Delta\omega$ as $\Delta\omega = \bar{\omega} - \omega$, which is a useful notation to discuss convergence:

$$\Delta\omega = \bar{\omega} - \omega = \frac{1}{2}Ar \sin \alpha \quad (6.15)$$

From [178]

$$\Rightarrow \dot{\omega} \approx \frac{1}{2}A^2 \frac{\omega}{\omega_F^2 - \omega^2} \quad (6.16)$$

where

$$\omega_F = \omega + \Delta\omega$$

Assuming $\omega, \omega_F > 0$ this means if $\Delta\omega > 0$, ω increases, otherwise it decreases. If $\Delta\omega$ has a zero crossing with a negative slope ($\frac{\partial \Delta}{\partial \omega} < 0$), there is an attractive region around $\Delta\omega \approx 0$. Therefore, we expect the adaptation of the frequency to have a stable fixed point in this region. Hence, $\Delta\omega$ gives us information on the convergence of the system.

The magnitude of the linear system $A = |H(s)|$ can not be the determinant for convergence since it is positive, thus we have to focus on the phase of the linear system $\alpha = \arg H(s)$. We see that the term $\sin \alpha$ determines the zeros and the sign of $\Delta\omega$, conclusively the phase of the linear system $\alpha = \arg H(s)$ is the determinant for convergence of the adaption process. We will come back to the use of the phase for determining stability in the presentation of the examples. But first we verify numerically the derived approximation.

Numerical test of the approximation

Indeed the result shows that the observed frequency is *not* the intrinsic frequency. This can be confirmed by computing an FFT on one of the oscillatory state variables (x, y) of the oscillator (data not shown). Here we present another numerical verification of the results.

To test if our assumptions and simplifications are correct we can numerically integrate the differential equation (6.16) and compare the results with the integration of the full system (Eqs. 6.7–6.11). As can be seen in Fig. 6.12, the approximation yields very close results to the full system for $\omega \neq \omega_F$ (using parameters from example A below). Looking at the reasoning in [178] it is clear that the approximation is only correct if $\omega \neq \omega_F$. Thus the observed erratic behavior after convergence at $t > 860$ s is clearly not a surprise and does not invalidate above results. Furthermore, this erratic behavior is partially due to numeric artifacts by integrating the equation in a straight forward manner with a Runge-Kutta solver.

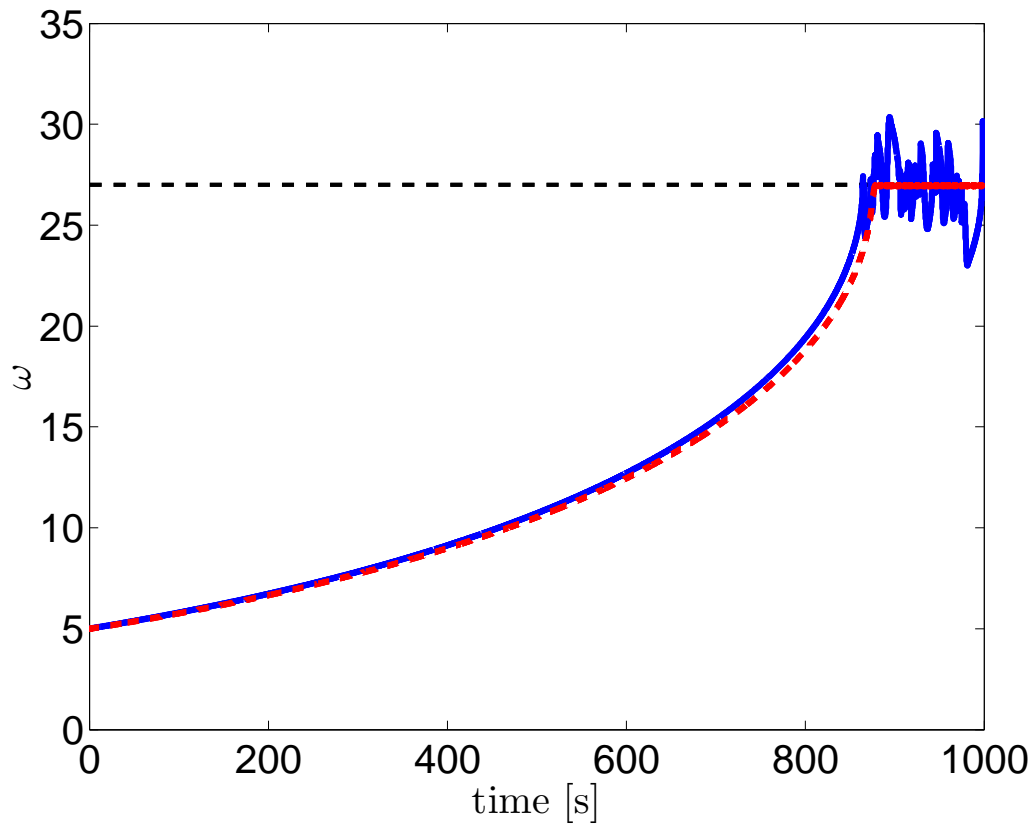


Figure 6.12: In this figure we compare the results of the integration of the full system (Eqs.6.7–6.11) with the results of the approximation (Eq. 6.16): (blue) ω from the integration of the full system, (red dashed) ω predicted by the approximation. The dashed horizontal line marks the resonant frequency of the linear system.

6.2.4 Examples of linear feedback loops

Now that we are confident that our reasoning is correct, let us present two examples for a feedback loop with a linear system. The linear system is inspired by a spring mass system. It does however not represent a detailed modeling of the robot.

The two examples will replicate the basic observations in the two presented experiments in Fig. 6.10. Thus, the goal of these two examples is to show how generic linear systems model for the plant helps to explain the convergence properties of the complete feedback system. We also show that it is very easy to reason for stability once the Bode plots of the linear system are known.

The phase of a linear system is commonly drawn as part of the Bode plot. Bode plots are a very fundamental tool in control engineering for determining stability of feedback loop systems, robust control performance, etc. We can thus exploit all the knowledge experience and tools of working with Bode plots for the analysis of our problem. This means we have a very well developed, rather simple but still very powerful tool to analyze the convergence property of adaptive frequency Hopf oscillators in feedback loops. Furthermore, it can ultimately allow us to design for certain convergence properties, by engineering the phase of the system. This is commonplace in conventional control engineering, thus very well developed techniques exist.

Stable at resonance

Lets assume the following linear system:

$$\begin{aligned}\mathbf{A} &= \begin{bmatrix} 0 & 1 \\ -\frac{k}{m} & -d \end{bmatrix} \\ \mathbf{B} &= \begin{bmatrix} 2 \\ 0 \end{bmatrix} \\ \mathbf{C} &= [1, 0] \\ \mathbf{D} &= 0\end{aligned}$$

This is 2nd order (e.g. spring mass) system, which possesses a clear resonant frequency at $\omega_r = \sqrt{\frac{k}{m}}$. The values of the constants are largely irrelevant for the general result. For the presented data we have chosen $k = 27^2$, $m = 1$ and $d = 0.1$. (Note that we use unit-less constants as their physical interpretation can vary).

In Figure 6.13, we present the Bode diagrams for the linear systems, and the result of the adaptation of oscillator. As discussed above, the bode plot already gives us a hint for stability of the adaptation process. More precisely we need to look at function $\Delta\omega$, but since this is a second order system, we know that the phase shift is maximum 2π , thus the phase can only have a single zero crossing. Since sin is a odd function we also know that the sign does not change, thus we can read the stability of the adaptation directly out of the bode plot. In this

example we see a negative zero crossing at the resonant frequency, thus we expect the adaptation process converge to the resonant frequency.

In cases where we have a higher order linear system, and also for getting an idea about the quantitative behavior of the convergence, i.e. convergence rates, it is indeed helpful to look at the function $\Delta\omega$ which we obtain in a straight forward manner from the data in the bode plot and inserting into Equation 6.14.

Thus, in this example we see that the convergence rate should increase and come to a sudden stop. This is indeed the case as can be seen in Fig. 6.13d, where we show the integration of the full system (Eqs. 6.7–6.11).

Unstable at resonance

Now, let's assume the same system as above but we change the coupling from the linear system to the Hopf oscillator (i.e. “change the sensor modality”), by setting

$$\mathbf{C} = [0, 0.1]$$

i.e. the second state variable of the linear system is now used as input to the Hopf oscillator. Changing only the coupling means, the system has the *same* resonant frequency as before. Nevertheless, as we will see the adaptation does not converge to this frequency. Again, in Figure 6.14, we present the Bode diagram. As before by looking at the phase of the linear system we already gain insight into the expected convergence properties of the frequency adaptation. This time there is no zero crossing, and the rate is positive. Thus, we expect the adaptation process to diverge. Looking at the function $\Delta\omega$, we can see that the convergence rate should be very low, but increases to a peak around the resonant frequency. And indeed, looking at Fig. 6.14c this prediction is confirmed. Thus, with the two presented examples we reproduce the observations in the experiments on the real robot that we have convergence with some sensors but not with others (compare Fig. 6.10 with Figs. 6.13/6.14d).

6.2.5 Conclusion & Discussion

We have presented results on an adaptive controller adapting and exploiting passive dynamics in a robot. This paper showed that the proposed control architecture is able to find the resonance frequency given by the passive dynamics of the real-world robot. The convergence properties are further analyzed by using linear plant models.

The experimental results demonstrated a number of potential advantages of the proposed adaptive frequency oscillator in real-world autonomous adaptive robots. In particular, it is important to note that this architecture requires no pre-programmed models of body dynamics, but it autonomously finds adequate control parameters. The experimental results, however, need to be discussed further toward our comprehensive understanding of adaptive control architectures.

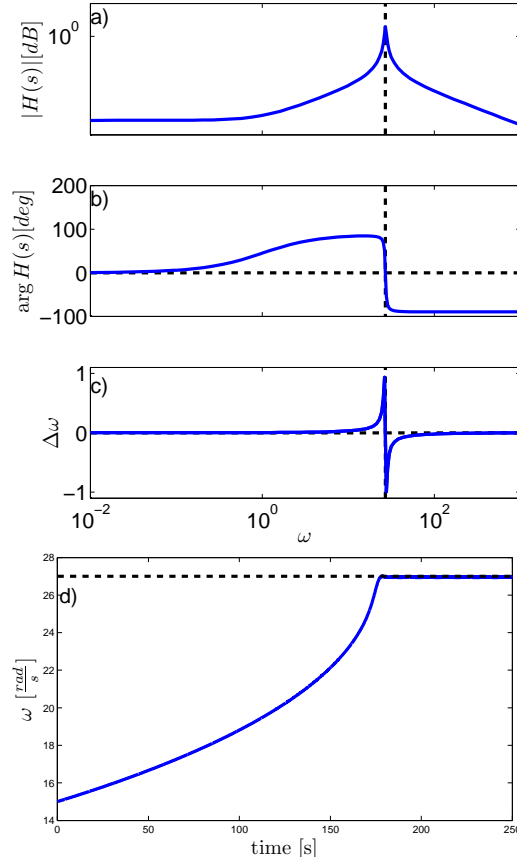


Figure 6.13: A linear system for which the convergence is stable at resonance. a,b) Bode plot for $H(s)$, the dashed line indicates the resonant frequency. Note that the phase has a negative 0 crossing at the resonant frequency, this means the adaptation process has a attractor at the resonant frequency. c) The function $\Delta\omega = \sin(H(s))$. Strictly speaking we need to look at this function to determine stability. d) Time series of the integration of the full system showing the adaptation of the oscillator frequency ω . It is clearly visible how the oscillator frequency adapts to the resonant frequency of the linear system (dashed line), what corresponds to the prediction from the Bode plot and $\Delta\omega$.

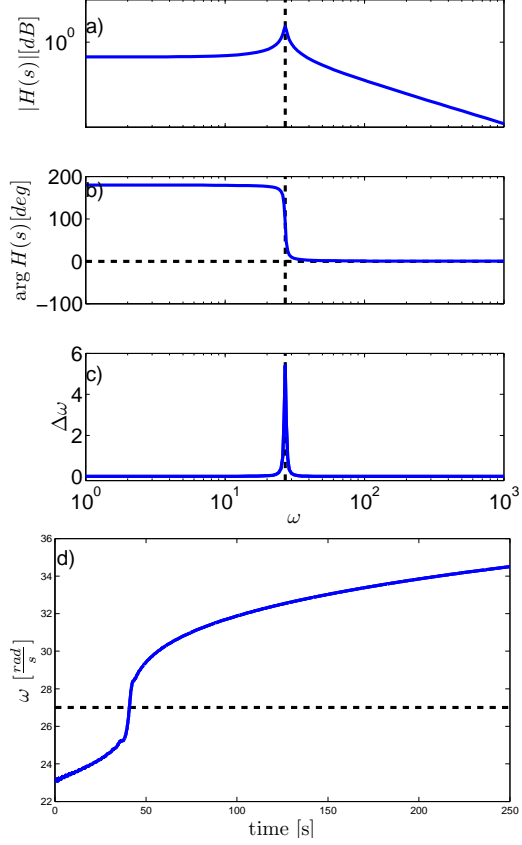


Figure 6.14: A linear system for which there is no convergence at resonance. a,b) Bode plot for $H(s)$, note that the phase has no negative 0 crossing at the resonant frequency, this means the adaptation process has no attractor at the resonant frequency, and especially $\Delta\omega$ (c), is always positive with a distinct peak at the resonant frequency. This means divergence of the oscillator frequency ω with an increased rate to be expected around the resonant frequency. d) Time series of ω . The prediction is confirmed by the data obtained by the integration of the full system.

The presented analysis has brought us a big step forward in understanding adaptive frequency oscillators in feedback loops. If we compare the convergence behavior of the system with the linear feedback loops (Figs. 6.13/6.14d) with the results from the robot experiment (Fig. 6.10) we see that the linear systems already reproduce the basic features observed in the experiment. We conclude that the linear systems analysis is sufficient to understand basic convergence properties of adaptive frequency Hopf oscillators with feedback loops. We have shown that the phase shift of the linear system is the main determinant of the stability of the adaptation process. Treating the body as linear system presents the simplest case for analysis but yields very important results. The presented work is an important step towards the understanding and designing adaptive controllers for robots with passive dynamics.

Furthermore, this paper also shows how with a description of our adaptive systems in the language of dynamical systems, we can readily explore it with powerful mathematical tools. We have seen that Bode plots are a helpful tool for the analysis but they can also help in the design of the controllers.

Such an adaptive controller is able to autonomously find invariants of the sensor-motor system. The state of the controller reflects these invariants (here the resonant frequency). This states can serve as segmented behavior patterns which can serve as a fundament on which more comprehensive and sophisticated sensory-motor control can build on. Those behavior patterns need to be stable over a certain time otherwise they can not be exploited. In a certain sense such an adaptive controller extracts the slowly varying properties out of the sensor-motor dynamics, and thus represents such meta-stable properties. We can also look at the oscillator as a (very rough) model of the robot of which the parameters are tuned to match the real robot. Loosely speaking finding the correct frequency for the oscillator corresponds to adapting the body schema (the oscillator) to the real body. It is likely that the understanding of such adaptive systems leads to an understanding of the development of cognitive capabilities.

Future work We have employed linear models for the plant, but the situation on the real robot is a bit more complicated, it needs to be seen to what extent linear models are valid. In order to arrive there, linear models of the sensor-motor modalities of the robot need to be derived. This can be done either theoretically, model-based or by systems identification methods. The prediction of the linear model need then to be checked against the results obtained from the robot.

Furthermore, in future we can explore the design of convergence properties by designing $H(s)$ or adding additional systems in the feedback loop. As an example, phase shift elements (as used to ensure stability of linear feedback loops) could be used to stabilize/destabilize the adaptation process according to some needs. Design techniques for such linear systems are well developed in control theory.

Furthermore, the implications and potential of feedback loops of adaptive frequency oscillators with linear systems is not fully explored and exploited. It is

well possible that we can obtain further results from the analysis of this system. A further development is to generalize above system by using MIMO systems in the feedback loop. MIMO systems would correspond to the case where several sensors channels and several actuators are used at the same time.

Acknowledgments The authors would like to thank Ludovic Righetti for helpful discussions.

This research is supported by the Swiss National Science Foundation through a Young Professorship Award to Auke Ijspeert (J.B. & A.I.) and grant 200021-109210/1 (F.I.).

6.3 More real world experiments

The next paper presents more results of the application of AFO based controllers on PUPPY II. At this point we would like to point to another study, which started in a supervised master project. In this study the concept has been proven to work on a real robot, namely a Sony AIBO and is summarized in [16]. The AFO controller has been implemented on the AIBO, however, the clarity of the application gets diluted by the fact that the AIBO robot has no intrinsic compliance, so spring dynamics has to be emulated by low level controllers. The study was a test of the concept before we had PUPPY II available for our research. The conceptual results contained in this study are all present in the studies contained in the thesis.

Self-organized Adaptive Legged Locomotion in a Compliant Robot

Jonas Buchli and Auke Jan Ijspeert

This paper has not been submitted for review yet.

Abstract In this contribution we present experiments of an adaptive locomotion controller on a compliant robot. The adaptive controller consists of adaptive frequency oscillators in different configurations. In the experiments we show that (1) the adaptive controller is constantly tracking body properties and readjusting to them (2) that important gait parameters are dependent on the geometry and movement of the robot and the controller can account for that and (3) that local control is sufficient and the adaptive controller can adapt to the different mechanical modes. Furthermore, we show the analytical treatment of adaptive frequency oscillators in closed feedback loops, and compare the results to the real data.

6.3.1 Introduction

The current state of the art in robotic legged locomotion does not compare in any means to legged locomotion observed in the animal kingdom. The fact that there already has been a large research effort devoted to robotic locomotion, points to the fact that it is not just a matter of better implementing the, possibly correctly identified, basic principles. No, it points to a more fundamental problem, namely that the way robots are built *and* controlled simply do not support fast, efficient, robust and elegant locomotion.

While it has been realized for a while now that (1) compliance might be a key factor and (2) body environment system is self-organizing and locomotion can not be understood by separating the single systems, (3) the systems need to be highly adaptive, systems implementing all those key factors are rare.

In this article we investigate on the following three main questions and topics: (1) It is well known that a body, of an animal or robot, has specific resonant frequencies (e.g. from elasticity or pendulum dynamics). Less studied however is how these frequencies depend on the posture and type of gait. We will show that they do depend from posture and type of gait and we will present an adaptive controller which can account for this dependence. (2) One central feature which makes attractor dynamics an interesting tool to design controllers or, in the wider sense, behaviors for a robot is that attractor dynamics is very robust under noisy conditions and perturbations. We show here that concepts earlier only presented in simulations [24, 28] are very robust with noisy signals and therefore the simple systems developed in theory and simulations can readily be implemented in real world systems. (3) We show that we have a theory to understand adaptive frequency oscillators in feedback loops. This gives us a tool to work with resonant dynamics of any type of system, adaptive frequency oscillators can be used to either find them or avoid them.

An important concept from neurobiology which has stimulated a lot of research in robotics is the concept of the Central Pattern Generator (CPG). It has been realized that in vertebrates the neural centers generating the high-dimensional coordinated gait patterns are located in a distributed fashion in the spine rather than in higher brain centers [82]. The CPG is under modulatory control by the brain. Subsequently, a lot of researchers have taken up the ideas and many studies ranging from theoretical [47, 195] to implementation studies (e.g. [52, 104, 107]) about the use and properties of CPGs have been done. Yet, most applications of CPGs are on stiff, fully actuated robots where the trajectories given by the CPG are accurately followed by help of high-gain control. But this is probably not how the CPG work in nature. As observed by Marc Raibert, the central nervous system does not control the body, it can only make suggestions [172]. In this contribution, we show exactly the application of Raibert's insight. There have been difficulties in putting those ideas to realization. We argue that parts of this is due to an inappropriate methodology which is unable to deal with such compliant and self-organizing system in a methodological fashion.

The controllers that we use in this article are loosely inspired by the CPG concept in that they are dynamical systems which can show their own coordinated spatio-temporal pattern. We illustrate their novel property of being truly adaptive, in that the controllers tune key parameters to match the body properties of the robot.

In this paper we will show results of an adaptive controller on a compliant robot. We employ an underactuated compliant robot with strong body dynamics. As [101] shows such a robot as used in our study can show many different modes of locomotion, dependent of many critical parameters. Such modes include bounding (alternating) gaits, hopping gaits, gaits with higher periodicity etc. In the previous studies these parameters were found/tuned by hand. They emphasized the need to adapt to the different environment and body conditions, but do not show a process which can do that. In this contribution we show a first attempt at such an adaptive controller, and we take the concept further and even allow some of the parameters to be determined by the robot environment system itself, namely phase (i.e. gait pattern) and the frequency. This means we exploit the self-organization capabilities of the body-environment system to simplify the control problem and improve the controller performance.

The controller consists of adaptive frequency oscillators. This paper has two parts in which, firstly we show experimental results of adaptive controllers on a compliant robot, highlighting different important aspects and findings, and secondly, show theoretical results about the convergence behavior of such adaptive controllers.

Related work Early work on spring dynamics in animal models can be found in [70] and important contributions from the robotics community showing self-stabilization and simple control in robot with appropriate body dynamics can be found in [39, 49, 101, 126, 149, 173].

Recent studies on mammals have shown that many muscle groups in the mammalian legs effectively are anti-gravity muscles and do not directly contribute to locomotion [66]. These studies have sparked quite some theoretical treatment of locomotion with springy legs [73].

While the idea to “adapt” to resonant body dynamics is not new, usually the systems employed work more in a reactive fashion than truly adaptive, i.e. their parameters remain constant, and especially do not reflect the body parameters after the adaptation process. See [31] for a more in-depth discussion of this issue. In the frame of oscillators this typically means that synchronization (i.e. phase locking) is exploited. However, as we will explain later, the adaptive frequency property that we exploit in our study is a fundamental extension of synchronization or phase locking. An interesting example is [227]. While still not truly adaptive, the remarkable result of this study is that the locking region is extremely large.

The use of adaptive frequency oscillator for adapting to resonant body dynamics has been first presented in [24]. Further result on a more complex robot

simulation has been presented in [28]. In [30] we presented first preliminary results of the adaptation on a real robot. Here we present more detailed data for different experiments. The theoretical understanding of adaptive frequency oscillators has been advanced in [178] by proving its convergence and first results on the treatment of AFOs in feedback loops are shown in [30].

6.3.2 Adaptive Controller

In this section we introduce the dynamical systems and methods that we use to construct the controllers of the robot. The controller consists of one or several oscillators mutually coupled and influenced by sensory information.

The building blocks of our controllers are oscillators. More specifically, we use the Hopf oscillator [98]:

$$\dot{\mathbf{q}} = \mathbf{F}_H(\mathbf{q}_i) = \begin{bmatrix} (\mu - (q_1^2 + q_2^2)) q_1 + \omega q_2 \\ (\mu - (q_1^2 + q_2^2)) q_2 - \omega q_1 \end{bmatrix} + \mathbf{p} \quad (6.17)$$

where, $\mathbf{q} = [q_1, q_2]$ are the state variables, $\sqrt{\mu}$ is the steady state amplitude, and ω the intrinsic frequency of the oscillator. $\mathbf{p} = [p_1, p_2]$ is an additive input to the oscillator. The nice feature of this oscillator is its harmonic limit cycle, i.e. we can write the steady state solution of the system (6.17) by $q_1(t) = \sqrt{\mu} \cos(\omega t + \phi_0)$, $q_2(t) = \sqrt{\mu} \sin(\omega t + \phi_0)$, where ϕ_0 is the angle of the initial condition $\mathbf{q}(0)$. The harmonic limit cycle allows to analytically determine the phase sensitivity and this allows to determine the phase relationship to other oscillators for example [23].

The oscillators receive input from the sensors of the robot. The form of the input is different for different experiments. In general the sensor values are converted into a mean free signal by a high-pass filter and multiplied by a coupling constant to achieve a suitable input range (typically values between -1 and 1). In other words $p_1 = K_s s(t) + \dots$ where s is the (filtered) sensor value.

Adaptive Frequency Oscillators In some experiments the oscillators will be extended to adaptive frequency oscillators. Adaptive frequency oscillators have been introduced in [24] and generalized and treated in more detail in [178].

The idea behind adaptive frequency oscillators is that we endow the oscillators with the capability to tune their intrinsic frequency to the frequency of a perturbation. This can be achieved by posing the following general rule as DE for the intrinsic frequency (or a parameter which tunes the intrinsic frequency):

$$\dot{\omega} = -\tau p_1 \frac{q_2}{\sqrt{q_1^2 + q_2^2}} \quad (6.18)$$

where τ is an adaptation constant. It is important to realize, that the adaptive frequency property that we exploit in our study is a fundamental extension of synchronization or phase locking. (1) The adaptation process changes the intrinsic frequency and not only the resulting frequency, (2) the adaptation generally has an infinite basin of attraction (i.e. for every initial condition $\omega(0)$ it will converge

to a frequency $n\omega_F$ as opposed to the limited range in which synchronization can take place, also known as Arnol'd tongues structure [8, 166]), (3) the frequency stays encoded in the system when the input is removed (e.g. set to zero).

Network of oscillators In some experiments, we use small networks of oscillators. Networks of oscillators can be built by introducing a functional coupling between oscillators, i.e. extending \mathbf{p} by an additional summand comprised of the signals of the other oscillators.

$$\mathbf{p} = \dots + \sum_j \lambda_{ji} \mathbf{P}_{ji} \mathbf{R}_{ji} \mathbf{q}_j$$

where λ is a coupling constant, \mathbf{P} is the, binary, coupling matrix and \mathbf{R} is the rotation matrix (examples of the coupling will be given later).

$$\mathbf{R} = \begin{pmatrix} \cos \theta_{ji} & -\sin \theta_{ji} \\ \sin \theta_{ji} & \cos \theta_{ji} \end{pmatrix} \quad (6.19)$$

The use of harmonic oscillator makes it possible to design arbitrary phase relationships into networks of such oscillators. We use the method outlined in [23] which is based on the idea that we can rotate the signal of an oscillator to introduce phase shifts. As shown in [23] choosing θ is equivalent in specifying the phase shift between the oscillators.

So the complete expression reads

$$\dot{\mathbf{q}}_i = \mathbf{F}_H(\mathbf{q}_i) + \underbrace{\sum_j \lambda_{ji} \mathbf{P}_{ji} \mathbf{R}_{ji} \mathbf{q}_j}_{\text{coupling}} + \underbrace{[K_{k,i} s_k(t), 0]^T}_{\text{sensor input}} \quad (6.20)$$

6.3.3 Hardware

PUPPY II is a 8 DOF experimental quadruped robot designed by F. Iida [100]. For the purpose of this article, its main interesting characteristics are that it is under-actuated and has spring dynamics in the legs. See Fig. 6.15 for an illustration of the robot. We describe in turn the important characteristics of the robot.

Mechanical system Each leg has a rotational “hip” joint and a knee joint. Only the hip joint is actuated, directly by attaching the leg to a strong RC servo motor. The knee joint features a spring (cf. Fig. 6.15 for the geometry of the leg). Thus, the robot is underactuated, only 4 of the 8 DOF are actuated and in addition, due to the springs, it has a very pronounced intrinsic dynamics in form of resonant frequencies. The weight of the robot is roughly 0.7 kg. The robot is energetically not autonomous, the power is fed to the robot by a cable.

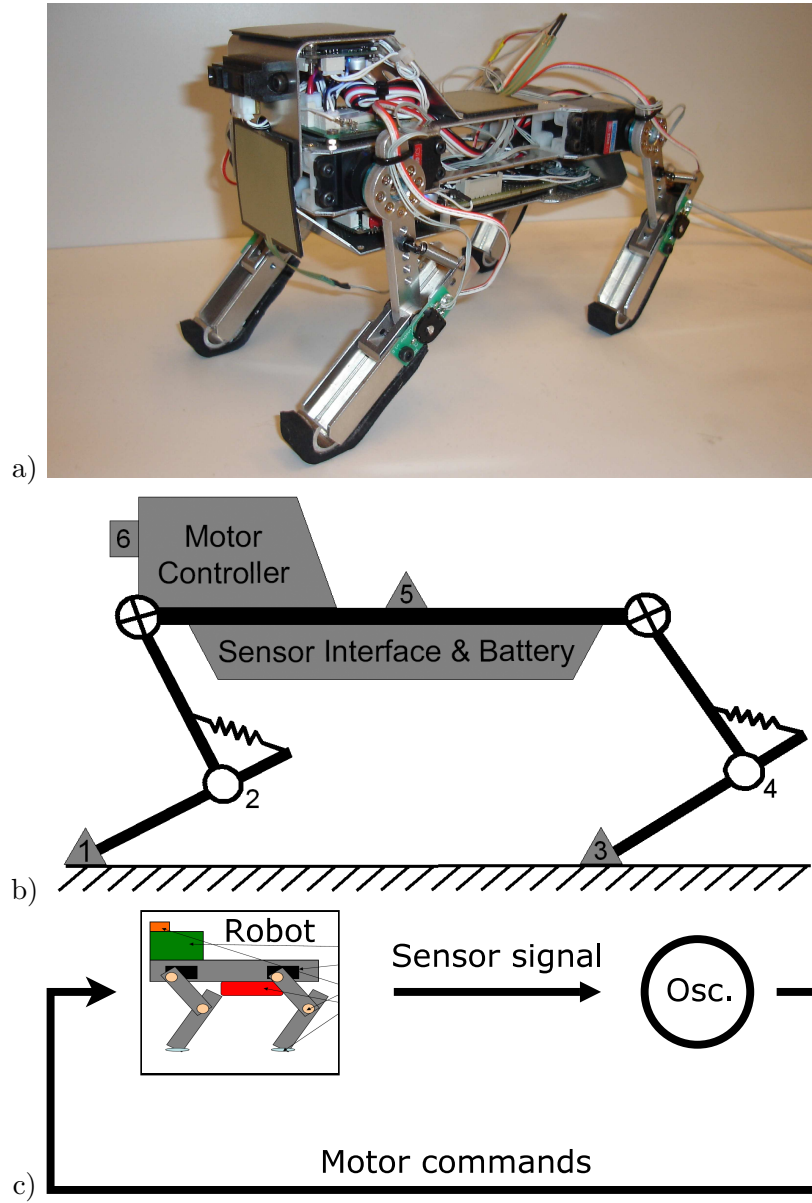


Figure 6.15: a) PUPPY II, a robot “dog” with passive dynamics (cf. springs in the knee joints) and several sensor modalities b) Mechanical structure of PUPPY II and sensor placement: 1,3: FSR (Force Sensitive Resistors) 2,4: Potentiometers of the passive joints 5: 3-axis acceleration sensors 6: PSD (Position Sensitive Detector). Circles with a cross denote actuated joints, blank circles denote passive joints. c) Control structure used in the experiments: One of the sensor channels is used to perturb a controller consisting of one or several adaptive frequency Hopf oscillators, the output of the oscillator (a state variable) is used to send motor commands (position control). Thus, this system constitutes a nonlinear feedback loop.

Sensors & Motors The robot is outfitted with 4 different sensor modalities: Force sensitive resistors on the body of the robot and under the feet of the robot, 3-axis acceleration sensor, IR-position sensitive detector sensor, and potentiometers to measure the knee angles. In the presented work we use the knee angle sensors and the inertia sensor. Those sensors convey a lot of information about the movement of the robot. The motors of the robot are strong off-the-shelf RC servo motors which are controlled in position.

Control loop The oscillators are integrated with Euler integration on a off-board computer with a time-step of $t_s = 10^{-3}$ s. The sensor values are read and calculated setpoints are sent to the robot via the USB bus, with a sampling frequency of 50 Hz, i.e. every 200th integration step the values are read out and the sensor values are updated. The faster integration step for the dynamical system is to ensure the numerical accuracy of the integration scheme.

The signal of the oscillator is converted into an desired angle for the leg in the by a linear transform

$$\alpha_t = \alpha_1 x(t) + \alpha_0 \quad (6.21)$$

where α_t is the desired angle for the leg, α_0 is the center angle, α_1 is the amplitude for a signal of amplitude 1. Later when presenting the results, we will list α_1 and α_0 for each experiment.

There is a low level controller (PD controller in the servos) which controls the position of the motor. The control performance of the low-level position control at the frequencies used for our experiments is sufficiently high that we can assume that the actual angle of the leg corresponds to the desired angle α_t . The delay in the feedback loop is also sufficiently small that it does not pose a problem for the presented application.

Posture For each experiment we will characterize the setup of the robot in the following way (1) controller structure, i.e. number of oscillators, connection to sensors, motors and mutually (2) posture (cf. Fig. 6.16) of the robot and amplitude of movements for a signal of amplitude $x(t) = 1$ and the center angle, i.e. the angle the leg assumes for a signal of amplitude $x(t) = 0$. It is important to note these angles determine implicitly the posture of the robot, i.e. if the body is horizontal or more tilted forward or backwards.

6.3.4 Experimental Results

In the following we describe several experiments which demonstrate some of the interesting features of the adaptive controller working together with the compliant robot.

We show two main results: (1) The adaptive controller is able to track the resonant frequency of the robot which is a function of different body parameters

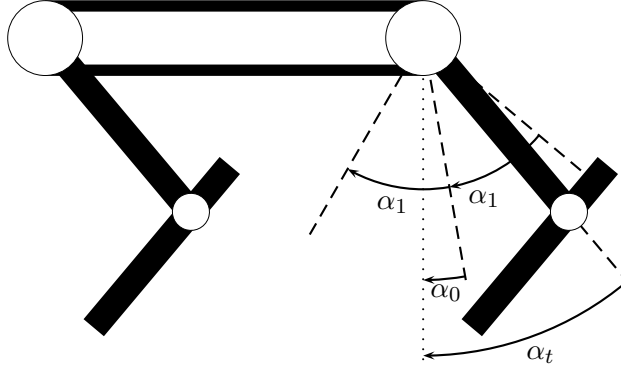


Figure 6.16: Parameters describing the posture of the robot: center angle, i.e. angle for zero signal $x(t) = 0$, angle corresponding to a signal of amplitude $x(t) = 1$. α_t is the actual position of the leg, α_0 is the offset (compared to a vertical position) of the center position of the leg. Note that the vertical position denotes $\alpha_0 = 0$, legs titled backwards from this position have negative angles, and vice versa. This means the larger this angle, to more tilted forward is the leg. α_1 is the amplitude of the leg for a signal of amplitude 1 (measured against α_0).

(2) controllers based on dynamical systems as we present are able to “recognize” mechanically intrinsic modes of locomotion, adapt to them and enforce them.

Further, we show that key properties of the gaits are not only depending on properties of the body but also the actual mode of movement that the body is operating in. And we show that even if we specify the gait pattern on the level of the CPG (by full coupling) the chosen gait pattern (measured by the foot-fall pattern) does not necessarily correspond to the CPGs pattern.

Experiment 1 – Change of body properties In this experiment we demonstrate the capability of the dynamical system to constantly track the resonant properties, i.e. as soon as the body properties, here the weight, is changed the oscillators readjust the frequency to the new conditions.

The posture is: front legs $\alpha_0 = 14.38$, hind legs: $\alpha_0 = 3.23$, the amplitudes for both pairs is $\alpha_1 = 10.8$. The controller setup is illustrated in Fig. 6.17. It consists of a single oscillator which is connected to the output of the z-axis (vertical axis) of the inertia sensor.

To demonstrate the continuous adaptation capability, after the adaptation has converged, the weight of the robot is changed, what changes its resonant frequency. In Fig. 6.17 the data of the adaptation experiment is shown. It can be seen how immediately after the change of the body property the controller starts to tune to the new frequency. Later in the article we also present results with changed leg stiffness (cf. Experiment 5 and Fig. 6.24).

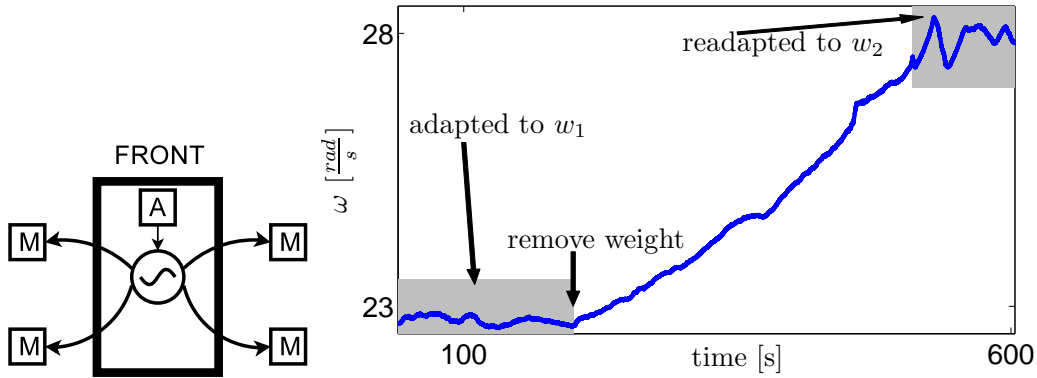


Figure 6.17: Experiment 1 to show the online adaptation of the controller. On the left an illustration of the sensor-controller structure. The z-value of the acceleration sensor (A) is used as an input to the oscillator. The signal of the oscillator is used to set the motor position according to Eq. 6.21. On the right the intrinsic frequency ω of the oscillator is shown as it evolves during the experiment. The body weight is changed from $m_1 = 0.905$ kg to $m_2 = 0.695$ kg. The controller immediately starts to adapt to the changed body property.

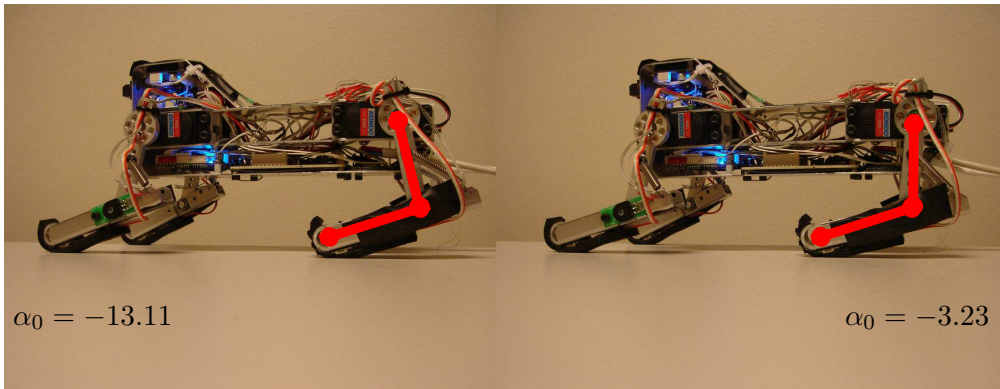
Experiment 2 – Posture dependent frequency In this experiment we show that the frequency is not only dependent of obvious parameters like the weight of the robot but other, e.g. geometrical parameters, can influence the frequency as well. Here we show that it is dependent from the posture of the legs and the adaptive frequency oscillator is able to account for these different frequencies.

For this experiment again the robot is driven by a single oscillator and the inertia sensor is used as input to the oscillators (cf. Fig. 6.17a). While the front leg parameters are kept at $\alpha_0 = 14.38$ and $\alpha_1 = 10.80$, in this experiments the angle of the hind leg is varied from $\alpha_0 = -13.11$ to $\alpha_0 = 3.23$ while all the other parameters remain the same.

In Fig. 6.18 we show the average frequency which is assumed by the oscillator vs the angle of the leg. As can be seen, the steeper the angle of the leg the higher the frequency found by the adaptation process.

By varying the posture angle α_0 of the leg we vary the (average) incident angle of the foot which induces a change in the resonant frequency of the robot. As illustrated in Fig. 6.19 this makes sense considering the geometry of the leg: The steeper the leg the less of the force acting on the foot loads the springs and the larger becomes the force vector pushing along the axis of the foot and thus loading the motor. The force vector acting perpendicular (i.e. in direction of the free movement) to the lower leg gets smaller, thus there is less force loading the spring. The leg feels stiffer. Thus, the further the leg is tilted back, the stiffer the systems becomes, therefore the frequency increases with decreasing α_0 and vice versa.

a)



b)

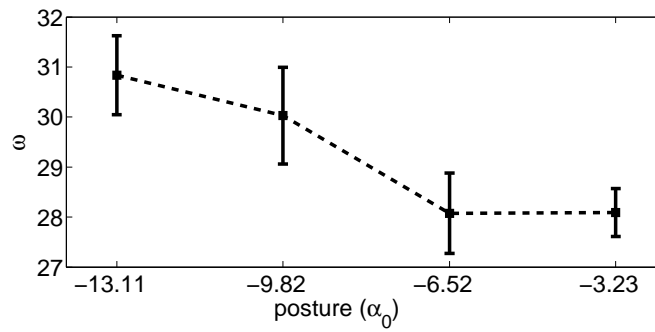


Figure 6.18: a) The range of posture angles used in the experiment illustrated on the robot. b) The average frequency (squares) found by the adaptive frequency oscillator vs posture, i.e. the angle of the leg. The bars show the standard deviation.

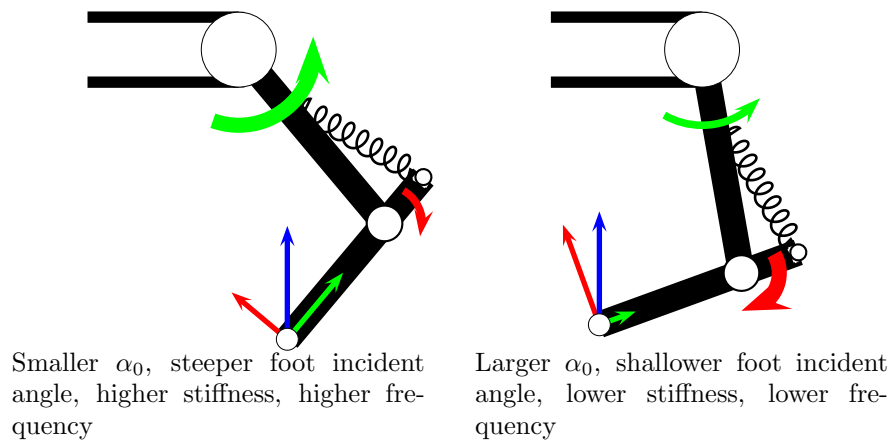


Figure 6.19: Illustration of the effect of the posture angle α_0 on the load distribution on the spring and motor respectively. Of the force acting on the leg (blue), only the part of the force active perpendicular to the foot loads the spring (red), the force acting parallel to the foot will act on the motor (green). Note that this is illustrative only for the principles at work, and that the real case is more complicated (e.g. amongst other things the force vector on the foot is not necessarily vertical).

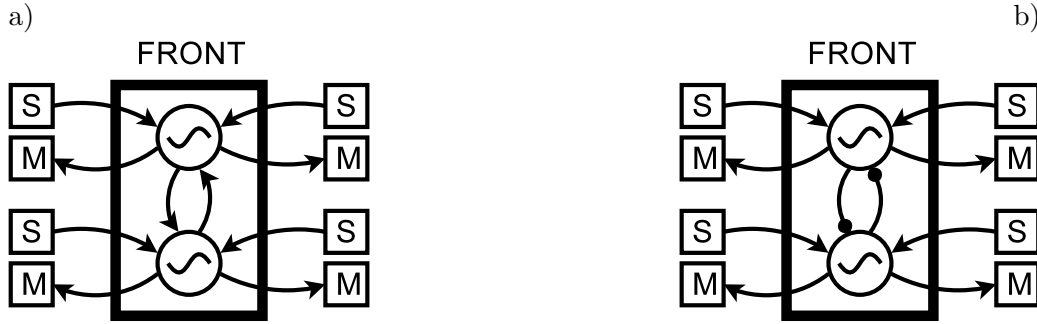


Figure 6.20: Controller setup with two oscillators. a) Setup with $\theta_d = 0$, i.e. the two oscillators will synchronize in phase, this can also be interpreted as excitatory coupling as denoted by the arrow. b) Setup with $\theta_d = \pi$, i.e. the two oscillators will synchronize in anti-phase. This can also be interpreted as inhibitory coupling as denoted by the circle.

Experiment 3 – Gait dependent frequency In this experiment the robot is set up to assume two different gait patterns, by appropriate posture and the different controller setups.

In this experiment the legs are driven by two oscillators (illustrated in Fig. 6.20). Two distinct runs are made, one where the setpoints are given to the robot so that all the legs are in phase (Controller a, $\theta_d = 0$) and the second one so that the hind-legs are in anti-phase with the front legs (Controller b, $\theta_d = \pi$).

Otherwise all the parameters of the robot are the same, especially the angles of the legs (i.e. the posture) to avoid effects on the tuning of the frequency of such parameters (as seen in the previous experiment).

In order to classify the gait pattern that the robot actually assumes we need to know when the feet touch the ground. In PUPPY II, we can infer the different phases (stance/swing) from the knee angle sensor. Since the springs are very stiff and the lower legs very light we can neglect dynamic effects of the rotation of the legs on the knee angle signal and assume that if the knee angle is not zero the leg is loaded, thus the leg is touching the ground.

As a control that the robot really assumes the gait pattern we want, in Fig. 6.21a we show the gait pattern for the two runs. We present the data as it is often presented in the biological/physiological literature, i.e. stance and swing phase. It gets clear that for the in-phase pattern the legs are active at the same time, while for the case when we invert the signal for the back legs we see a more alternating gait. In 6.21b the results of the two adaptation runs are presented, as can be seen the frequency found is very distinct.

In order to investigate the reason for that it's worth while looking at the gait pattern that the robot assumes in the two cases. The reason for the different frequencies stems from the fact that for the in phase gait, the springs of all four legs are loaded in more or less the same time, while for the bounding gait the

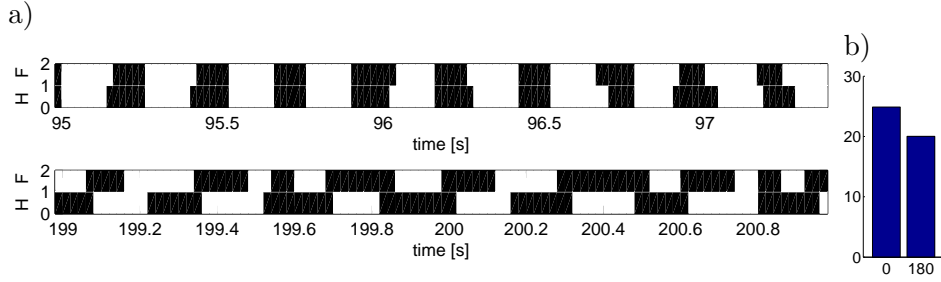


Figure 6.21: Experiment to investigate the influence of the gait pattern on the resonant frequency. a) gait pattern, stance/swing phases, black is stance phase and white is swing phase, H depicts the hind legs and F depicts to fore legs, for simplicity only one leg per pair is shown, the data in each pair looks very similar. Top row for $\theta_d = 0$, it is well visible that the front and hind limbs are active at the same time, while for $\theta_d = \pi$, we clearly see a alternating gait. b) resulting frequency of the adaptation process, the mean is at $\omega = 24.89$ for $\theta_d = \pi$ (alternating gait) and at $\omega_d = 20.02$

springs of the front and hind legs loaded more in an alternating fashion. This can be explained by a very simple spring mass model of the overall robot where we lump the springs of the legs into one single spring with a spring constant k_{eff} . If the springs of the legs are contracting at same time we have to add up the respective spring constants. Thus, for gaits where the leg are active at the same time the system behaves stiffer in average.

Experiment 4 – Self-organization of gait: CPG pattern does *not* correspond to gait pattern The aim of this experiment is to show, that the gait pattern that the robot actually is assuming does not necessarily correspond to the gait pattern commanded by a CPG.

Again we use the same controller setup as before as in the last experiment with a single oscillator, and the two different phase settings. In this experiment we do not focus on the adaptation capability of the controller, but hold the frequency fixed at $\omega = 20 \text{ rads}^{-1}$. The Posture of the robot is tilted forward by choosing a steeper angle for the back leg than for the front leg: hind $\alpha_0 = -10.44$ $\alpha_0 = 10.06$. The amplitude is $\alpha_1 = 10.8$.

In Fig. 6.22 we present the gait patterns as estimated from the knee angles (in the same way as in the last experiment). First, (in Fig. 6.22a) we present again the gait pattern by showing the stance and swing phases. Then, we present the time series of the phase difference of the two signals estimated with the Hilbert transform. We can see that if we specify a phase difference of π for the CPG we indeed get the expected result, a bounding gait where the front and the hind legs touch the ground with a phase difference of around π . However, if the phase difference for the CPG is specified as zero degrees, the robot does not assume a jumping gait in which both legs touch down in the same time, as one would assume.

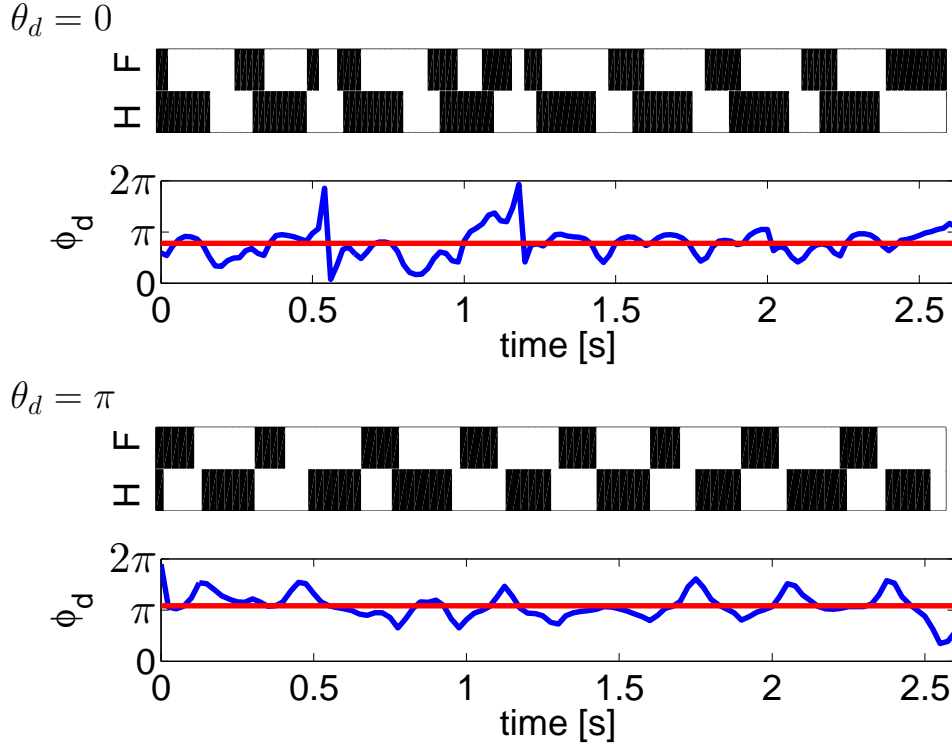


Figure 6.22: Gait pattern estimated by the knee angle data, black is stance and white is swing phase. a) Coupling $\theta_d = 0$, the first panel shows the gait pattern estimated by the knee angle data, the second panel shows the phase differences estimated by difference of the phase of the Hilbert transform of the knee angle data (in red the average difference). b) The information but this time the angle of the CPG is specified as $\theta_d = \pi$.

But, the phase difference estimated by the Hilbert transform varies mainly between 0.4π and π , and in the stance-swing-diagram we can clearly see how the front legs touch down shortly after followed by a longer stance phase of the hind legs which initiates a flight phase. In other words, we command two very *different* patterns, but the body exhibits both times very *similar* gaits. Furthermore, we see that the gait pattern for $\theta_d = 0$ is more irregular and more pseudo-periodic than the pattern for $\theta_d = \pi$, which means that this gait is less robust.

Also one has to note that the robot can be biased by tilting forward, i.e. for this experiment the robot posture is biased towards an anti phase gait, while in the experiment before there was a more symmetrical posture which allow in-phase gaits to be mechanically stable.

Experiment 5 – Self-organization of gait pattern: Local adaptive controllers The aim of this experiment is to show, that we can exploit the tendency of the body of the robot to prefer certain gait patterns to use simpler,

namely purely local control structures. Motivated by the results of the previous experiment and earlier simulation studies [28], namely the fact that the robot has modes which are mechanically more suitable, in this experiment we constrain the controllers of the robot less - there is no direct coupling between the oscillators for the hind and front legs. The only coupling that is established works over the mechanical system. As shown in Fig. 6.23 we use two oscillators, one for each pair of front and hind legs. The sensor feedback is the knee angle data from each leg. The oscillators are not directly coupled. The posture of the robot is as follows: hind leg $\alpha_0 = -10.44$, front leg $\alpha_0 = 10.06$ and $\alpha_1 = 11.88$ for both pairs. Note that we have changed the stiffness of all legs, by attaching the spring differently, so that it has less lever. This makes the leg less stiff, and the frequency decreases. The reasons for this are twofold. First, to show yet another resonant frequency by changing the spring stiffness (as opposed to body mass as in Experiment 1). And secondly, the slower movements facilitate the experiment.

In Fig. 6.24a we show the frequency of the oscillators adapting to the body, and readapting after a perturbation. As can be seen in Fig. 6.24b, where we show the difference between the frequencies of the oscillators, despite the fact that they are not directly coupled, they remain very close. Furthermore, we show the phase difference in Fig. 6.24c, where it can be seen that the oscillators remain phase locked over the whole experiment. So the mechanical influence is enough to keep the oscillators phase locked and adapting *in a coordinated fashion*. Furthermore, it can be seen that the oscillators lock into an anti-phase pattern, what corresponds to the tendency for anti-phase gaits as found in the experiment before. We see that despite the freedom of the system and the loss of the specification of the phase difference, the system settles into a well coordinated movement, which corresponds to the mechanical “mode” of the robot. It can thus be said that this controller adapts to the mechanical properties of the body and current posture. We also see that the phase relationship is not exactly π , thus we see that a phase relationship which does not exactly correspond to π seems more suited for the mechanical system in this setup since it is chosen by letting the body organize the phase difference itself.

Thus from this experiment we can conclude, that for coordinated motion, purely local controllers can be enough, i.e. mechanical coupling is enough to coordinate the different pairs of legs. We can then ask, what is the need of direct coupling then. It turns out that we can make the gait more robust by employing a direct coupling. As an example, in such an experiment if the posture is too “tilted” the two oscillators will converge to two different frequencies, on the other hand the tilted position is good for efficient forward locomotion. We can thus imagine, that the robot learns about the appropriate gait pattern in a more upright fashion, after that the pattern is “fixed” by introducing a coupling which corresponds to the found mechanical gait pattern (i.e. by setting θ_d to the found value). Then, the robot can be tilted forward to make it locomote with a good gait pattern.

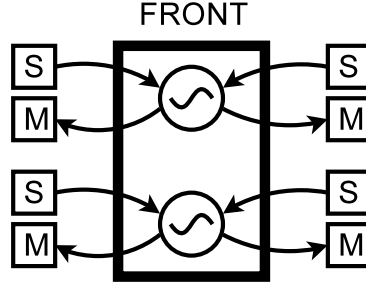


Figure 6.23: Controller schema for Experiment 5. No connection between the oscillators for the hind and front leg.

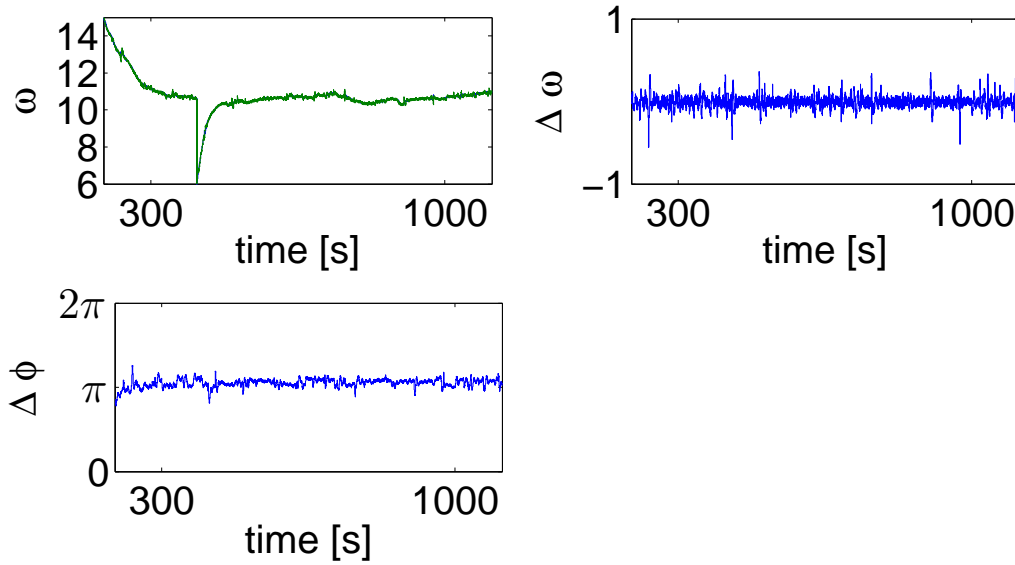


Figure 6.24: Data from the adaptation experiment with local controllers (Ex. 5).
 a) Adaptation of the frequencies, at around 400s the frequencies are reset to 6 rads^{-1} . It is clearly visible that there exists an attractor for the convergence process are around 11 rads^{-1} b) The difference between the frequencies for the front and hind leg. It is clearly visible how closely together the two frequencies evolve. c) The phase difference of the two oscillators, as can be seen they phase lock at a value slightly higher than 0.5. And the phase locking is never lost during the whole experiments, i.e. the legs are always well coordinated.

6.3.5 Toward a theory for AFOs in feedback loops

So far we have presented empirical results, but it would be nice to be able to analyze what frequency the controller converges to. For this we have to develop an understanding of AFOs in feedback loops. While in [178] the convergence behavior of the open loop case is analyzed we need to extend those results for the treatment of the closed loop case. As shown in [22] for certain sensor modalities there is no convergence, but the frequency diverges. We need to develop an understanding for those cases. Thus, here we will show that we can understand the convergence behavior with the help of linear systems theory. In the following we will show the convergence analysis given a few assumptions hold.

For the following treatment it is convenient to write the Hopf oscillator, i.e. system Eq. (6.17), in the polar form, which is done by a straight forward transformation by substituting $\phi = \omega t$ and $r = \sqrt{q_1 + q_2}$. We furthermore assume (without loss of generality) that the perturbation is $p = [p_1, 0]$. The system in the polar form reads

$$\dot{r} = (\mu - r^2)r + \cos \phi p_1 \quad (6.22)$$

$$\dot{\phi} = \omega - \frac{1}{r} \sin \phi p_1 \quad (6.23)$$

$$\dot{\omega} = -\frac{1}{\tau} \sin \phi p_1 \quad (6.24)$$

Adaptive Hopf Oscillator with Linear Feedback loop

In order to begin with the analysis of the system, the plant (i.e. the robot) will be modeled by a linear time-invariant system. This is a simplification (i.e. neglecting nonlinearities from the springs, kinematics of the body etc), but, as we will see in the remainder of this article, this simplification yields already significant understanding of the mechanism of the adaptation process.

Thus, in the following we treat the “body” as a linear system. Therefore, let us assume the following systems: First, a linear n -th order SISO (the “robot”, i.e. the motor commands are all lumped into one variable and only one sensor channel is modeled) of the form

$$\dot{\mathbf{x}} = \mathbf{A}\mathbf{x} + \mathbf{B}u \quad (6.25)$$

$$y = \mathbf{C}\mathbf{x} + \mathbf{D}u \quad (6.26)$$

\mathbf{A} is a $n \times n$, \mathbf{B} a $n \times 1$, \mathbf{C} a $1 \times n$ matrix, and \mathbf{D} a scalar. u is the (scalar) input to the linear system and y the (scalar) output. Here, we can interpret y as the sensory feedback and u as the motor command.

Second, the adaptive frequency Hopf oscillator as described by Eqs. 6.22–6.24. We set $u = r \cos \phi$ and $p_1 = y$. Hence, the Hopf oscillator and the linear systems are connected in a feedback structure through their inputs y (from the linear system to the Hopf Oscillator) and u (from Hopf to the linear system). See Fig. 6.25 for an illustration of the feedback structure.

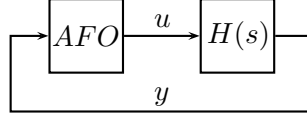


Figure 6.25: Illustration of the feedback loop of the adaptive frequency oscillator with the linear system and the conventions used. The adaptive frequency oscillator (AFO) is connected to the plant, which is modeled as a linear system $H(s)$ through u (the motor commands) and the sensory feedback from the robot to the AFO is modeled by y .

As can be shown by linear systems theory, the linear system can not generate other frequencies than already present in the input u , it can however modify phase and amplitude of the signal. Therefore, we can write:

$$y = Mr \cos(\phi + \alpha) \quad (6.27)$$

where $M = |H(s)|$ and $\alpha = \arg(H(s))$ ($H(s)$ is the transfer function of the linear system).

We begin the analysis of the oscillator by writing the phase of the Hopf oscillator perturbed by a signal y

$$\dot{\phi} = \omega - \frac{1}{r} \sin \phi y \quad (6.28)$$

As outlined above we write $y(t)$ to be the state of the Hopf oscillator amplified by M and rotated by α

$$y(t) = Mr \cos(\phi + \alpha) \quad (6.29)$$

thus

$$\dot{\phi} = \omega - \sin \phi M \cos(\phi + \alpha) \quad (6.30)$$

Using trigonometric transformations we can write this expression as

$$\Rightarrow \dot{\phi} = \omega + \frac{1}{2}M[\sin \alpha - \sin(2\phi + \alpha)] \quad (6.31)$$

The results in [178] show that the systems shows a separation of timescale, i.e. the frequency adaptation process works on a timescale much slower then the convergence to the limit cycle with given frequency and radius. Thus, we assume $\omega = \text{const}$ and investigate what the observed frequency of the closed loops system will be. If this frequency is different from the intrinsic frequency, it should drive the slower adaptation process. $\omega = \text{const}$ also implies that M and α are constants ($s = j\omega$). We evaluate the average *effective* frequency $\bar{\Omega}$ with the given assumptions:

$$\bar{\Omega} = \frac{1}{2\pi} \int_0^{2\pi} \omega + \frac{1}{2}[M \sin \alpha - \sin(2\phi + \alpha)] d\phi \quad (6.32)$$

Since by assumption ω is a constant and therefore α , M are constant, it follows that the first two summands are constants. The last summand is a 2π -periodic mean-free function, thus we get

$$\bar{\Omega} = \omega + \frac{1}{2}Mr \sin \alpha \quad (6.33)$$

Let us define $\Delta\omega = \bar{\Omega} - \omega$, which is a useful notation to discuss convergence:

$$\Delta\omega = \bar{\Omega} - \omega = \frac{1}{2}Mr \sin \alpha \quad (6.34)$$

From [178], we know that the slow variation of ω is as follows

$$\Rightarrow \dot{\omega} \approx \frac{1}{2}M^2 \frac{\omega}{\omega_F^2 - \omega^2} \quad (6.35)$$

where ω_F is the frequency of the rhythmic signal applied to the AFO. Here, with the feedback loop $\omega_F = \bar{\Omega}$ and as we shown above this can be written as

$$\omega_F = \omega + \Delta\omega$$

Assuming $\omega, \omega_F > 0$ this means if $\Delta\omega > 0$, ω increases, otherwise it decreases. If $\Delta\omega$ has a zero crossing with a negative slope ($\frac{\partial \Delta}{\partial \omega} < 0$), there is an attractive region around $\Delta\omega \approx 0$. Therefore, we expect the adaptation of the frequency to have a stable fixed point in this region. Hence, $\Delta\omega$ gives us information on the convergence of the system.

The magnitude of the linear system $M = |H(s)|$ can not be the determinant for convergence since it is positive, thus we have to focus on the phase of the linear system $\alpha = \arg H(s)$. We see that the term $\sin \alpha$ determines the zeros and the sign of $\Delta\omega$, conclusively the phase of the linear system $\alpha = \arg H(s)$ is the determinant for convergence of the adaption process. In the following we illustrate the result with a simple linear system for two different “sensory channels”.

Stable at resonance

Let us assume the following linear system:

$$\mathbf{A} = \begin{bmatrix} 0 & 1 \\ -\frac{k}{m} & -d \end{bmatrix}$$

$$\mathbf{B} = \begin{bmatrix} 2 \\ 0 \end{bmatrix}$$

$$\mathbf{C} = [1, 0]$$

$$\mathbf{D} = 0$$

This is 2nd order (e.g. spring mass) system, which possesses a clear resonant frequency at $\omega_r = \sqrt{\frac{k}{m}}$. The values of the constants are largely irrelevant for the

general result. For the presented data we have chosen $k = 27^2$, $m = 1$ and $d = 0.1$. (Note that we use unit-less constants as their physical interpretation can vary).

In Figure 6.26, we present the Bode diagrams for the linear systems, and the result of the adaptation of oscillator. As discussed above, the bode plot already gives us a hint for stability of the adaptation process. More precisely we need to look at function $\Delta\omega$, but since this is a second order system, we know that the phase shift is maximum 2π , thus the phase can only have a single zero crossing. Since \sin is a odd function we also know that the sign does not change, thus we can read the stability of the adaptation directly out of the bode plot. In this example we see a negative zero crossing at the resonant frequency, thus we expect the adaptation process converge to the resonant frequency.

In cases where we have a higher order linear system, and also for getting an idea about the quantitative behavior of the convergence, i.e. convergence rates, it is indeed helpful to look at the function $\Delta\omega$ which we obtain in a straight forward manner from the data in the bode plot and inserting into Equation 6.33.

Thus, in this example, according to the peak in the convergence rate in Fig. 6.26c the convergence rate should increase and come to a sudden stop. This is indeed the case as can be seen in Fig. 6.26d, where we show the integration of the full system (Eqs. 6.22–6.26).

Unstable at resonance

Now, let us assume the same system as above but we change the coupling from the linear system to the Hopf oscillator (i.e. “change the sensor modality”), by setting

$$\mathbf{C} = [0, 0.1]$$

i.e. the second state variable of the linear system is now used as input to the Hopf oscillator. Changing only the coupling means, the system has the *same* resonant frequency as before. Nevertheless, as we will see the adaptation does not converge to this frequency. Again, in Figure 6.27, we present the Bode diagram. As before by looking at the phase of the linear system we already gain insight into the expected convergence properties of the frequency adaptation. This time there is no zero crossing, and the rate is positive. Thus, we expect the adaptation process to diverge. Looking at the function $\Delta\omega$, we can see that the convergence rate should be very low, but increases to a peak around the resonant frequency. And indeed, looking at Fig. 6.27c this prediction is confirmed. Instead of convergence, this means that ω crosses the resonant frequency with increased rate (Fig. 6.27d).

Comparison with real world data

In Fig. 6.28, we present data from the real robot for the two cases (convergence/divergence) and compare it with a fitted model of the basic system used before. The convergent behavior is observed by using the acceleration sensor, the

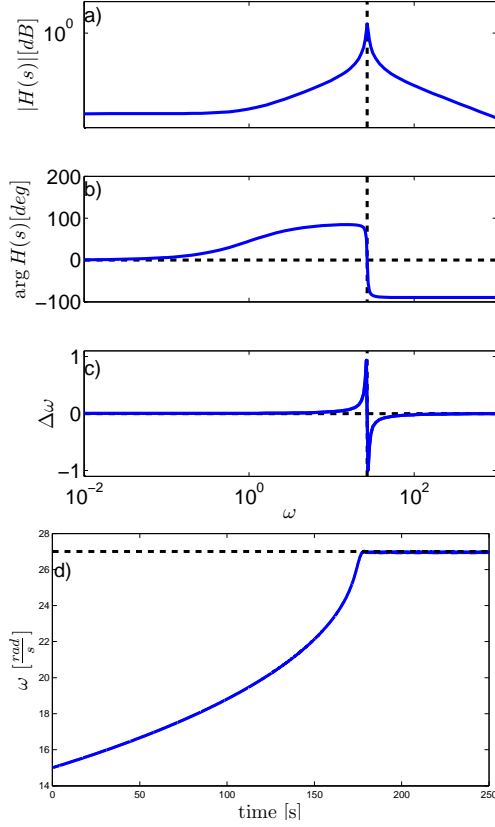


Figure 6.26: A linear system for which the convergence is stable at resonance. a,b) Bode plot for $H(s)$, the dashed line indicates the resonant frequency. Note that the phase has a negative 0 crossing at the resonant frequency, this means the adaptation process has a attractor at the resonant frequency. c) The function $\Delta\omega = \sin(H(s))$. Strictly speaking we need to look at this function to determine stability. d) Time series of the integration of the full system showing the adaptation of the oscillator frequency ω . It is clearly visible how the oscillator frequency adapts to the resonant frequency of the linear system (dashed line), what corresponds to the prediction from the Bode plot and $\Delta\omega$.

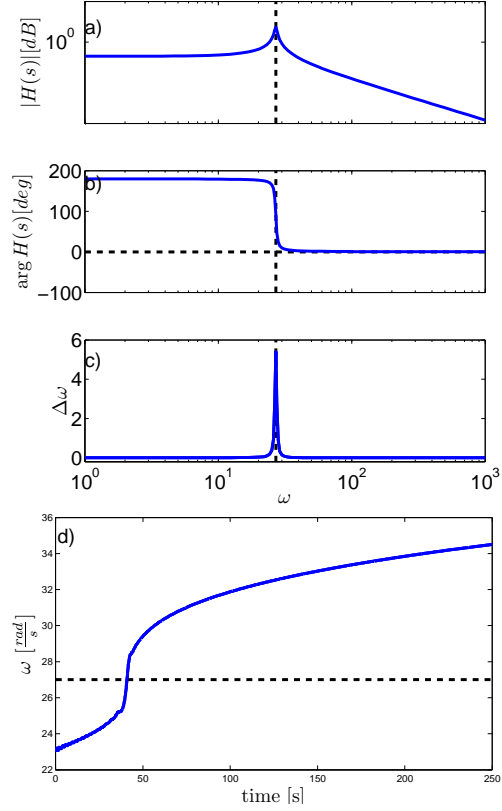


Figure 6.27: A linear system for which there is no convergence at resonance. a,b) Bode plot for $H(s)$, note that the phase has no negative 0 crossing at the resonant frequency, this means the adaptation process has no attractor at the resonant frequency, and especially $\Delta\omega$ (c), is always positive with a distinct peak at the resonant frequency. This means divergence of the oscillator frequency ω with an increased rate to be expected around the resonant frequency. d) Time series of ω . The prediction is confirmed by the data obtained by the integration of the full system.

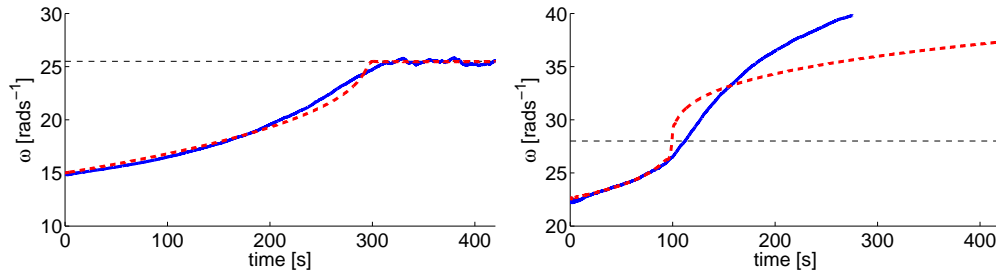


Figure 6.28: Comparison of data from the real robot with the linear model. Top: sensor (acceleration) that leads to convergence. Bottom: Sensor (knee angle) that does not lead to convergence. While the basic properties of the real world data are reproduced by the LTI model there is some differences between the real data and the prediction of the LTI model. The dashed line indicates the estimated resonant frequency. See text for further discussion.

divergent behavior can be observed by using the knee angle sensor instead. For the stable behavior (Fig. 6.28a) the data is $k = 25.5^2$, $C = [0.45, 0]$ and for the unstable behavior $k = 28^2$, $C = [0, 0.12]$ (Fig. 6.28b), all the other parameters are as above. As can be seen in the figures the linear systems reproduce qualitatively the data from the real robot. We are thus confident, that the linear treatment we presented conveys well the basic convergence properties of AFOs in feedback loops.

As we can see for the divergent case the match seems less good, however, already in the converging case we see the fact that the linear model predicts a higher convergence rate for regions close to the target frequency. This same effect leads to the mismatch between the linear model and reality in both cases only in the divergent case the effects become much more visible, since there is no fixed point behavior to which both solutions converge.

It is natural that the model can not fully predict the behavior close to the target frequency, since it was based on results which investigate the convergence behavior only for frequencies which are further away.

From theory to design

The developed theoretical insight can be used in the design of the robot or an experiment. If we understand the phase shift of the different sensory channels (either based on a model or on data) we can chose the sensor which will work best. Furthermore, if no sensor has the appropriate phase shift, then we can use filters to induce additional phase shifts and thus make convergence possible nevertheless.

6.3.6 Conclusions & Discussion

We have shown, that controllers based on adaptive frequency oscillator are able to track the resonant frequency of the robot. Different parameters can influence the frequency, such as mechanical parameters (weight, lengths, spring stiffness etc), but also geometrical “gait” parameters such as the angles of the legs.

In Experiment 4 we have shown that in a compliant robot, such as the presented one, chosen gait pattern is *NOT* necessarily the same as the CPG pattern. This is a fact which is often overseen in the discussion of CPGs applied to robots (and animals). This is in contrast to design methodologies which are aimed at high-gain fully actuated non-compliant robots, where its made sure the commanded trajectories are accurately followed and a influence from the body dynamics is not desired. In the case of a underactuated compliant robot as presented here, the physics of the body has to be taken into account, i.e. the dynamics of the body, the fact that we have distinct flight and stance phases in which the underactuated system reacts differently etc. We can exploit this organizational capability of the robot for certain situations, i.e. to achieve efficient self-organized locomotion with a minimum of control effort. Consequently, in Experiment 5 we show that controllers built with well suited dynamical system which are adaptive and not over-specified can adapt to the bodie’s “preferred” locomotion modes. With this experiment we also showed, that the inter-controller communication is not always mandatory, which could be interesting in the framework of modular or ad-hoc robots.

In a second part of the article we have laid out the theoretical treatment of AFOs in feedback loops and have compared the results of a simple linear model with data from the real robot. This comparison shows that even the simplest spring mass model can account quite well for the convergence effects that are observed. The theoretical treatment of AFO in feedback loops together with a more complete model of the robot (i.e. where the posture angles show up as parameters) will allow to understand most of the effects seen in the experiment in a straight forward manner.

Discussion We can conclude from such experiments that compliant robots offer opportunities and challenges for control. There are two main areas where we lack support for usable, agile robotic legged locomotion. First in the area of activators, and second in the control methodology. Such a robot as presented here definitely lacks certain controllability which severely restricts its practical use. It is a fundamental theoretical fact, that elastic modes decrease the controllability of the plant. In other words, as an example, we can not achieve exact foot placement with this robot. There would be a way around this problem, and again we see it implemented in animals, that allow to use the advantages of both, high accurate control and compliant mechanics. For this we need activators of which we can control the stiffness. In the beginning it would already be interesting just to experiment with activators which can switch from passive to active mode. Stiffness

control would allow precise control for some tasks while allowing self-organized movements for other tasks. Such activators are not a *nice-to-have* feature but an absolute *must* do we ever want to achieve the flexibility and agility with our robot as observed in their natural counterparts. The theoretical aspects of stiffness control, or more general impedance control is already being investigated for robotic tasks which involve contact with the environment [97, 225] and recently also for legged robots with elastic actuators [168]. It will be interesting to bring together those results with adaptive controllers as presented here.

Then, as for the methodology to develop such adaptive controller and the applied concepts, it sums up to the challenges for controller design for self-organizing systems, i.e. controller which can make use of the self-organizing capabilities of the system to be controlled [33]. Ideally we would like to have a system which is able to learn about the system to be controlled. About the intrinsic modes, i.e. we need a controller which feels the intrinsic patterns formed by the underlying system, can modulate, enforce, stabilize or destabilize those modes depending on specified goals. In the here presented system, one of this modes is for example the coordination between front and hind legs, i.e. the phase relationship, another one the resonant frequency.

In [33] it has been proposed to give the systems freedom to self-organize on certain variables of the system (i.e. the phase in our case), i.e. pull out control (in the appropriate way). Here we do exactly that: normally the oscillators are coupled, we removed this coupling and show that the system nevertheless finds good locomotion, in this sense the presented system is an application example of the proposed concepts.

While there are many reports, that biological motor systems are self-organizing [91, 120, 121, 195, 196] we have not methodology at hand for synthesizing such a system or its controller. Ideally we would like the system to be able to recognize, learn and adapt to different possibly co-existing modes. For this traditional control theory is not of big help as it deals mostly with linear (or linearized) systems, in which no self-organization can take place. To develop such adaptive controller which can find and switch between modes, the normal control engineering approach does not work because it usually involves a linearizing step after modeling, by this step we remove all the other attractors in the system, thus a controller which is developed grounded on this model can evidently not exploit different modes.

Arriving with such controllers would mean we could build systems which are less frustrated (i.e. where the activation works in step with the body dynamics instead of forcing “artificial” patterns on the body). Non-frustrated systems mean also less energy consumption, higher efficiency less mechanical stress, wear and tear etc. In Experiment 3 (Fig 6.21) and Experiment 4 (Fig. 6.22) we note that if the system is specified against its “natural”/intrinsic modes, the gaits are less regular which points to the fact that the movement is less robust, this points out that it is important that the controller work with the body.

Summarizing to achieve agile legged robotic locomotion we need

- An appropriate body: self-stabilizing, compliant, with stiffness controlled actuators.
- An appropriate controller which can coordinate with the body and other controllers. The controller needs to be able to adapt to body and environment.
- Appropriate sensors. In order that the controller can get information about the body and its state the robot has to be equipped with appropriate sensors. Interestingly, it turns out that many sensor convey information about the intrinsic modes. It will however, be interesting in what extend redundant sensory information can be exploited to extract more meaningful information.

We showed one building block for such controllers with interesting results and a way how to approach the problem but a lot of work needs to be done before we reach our goal.

Future work Thus in future, the presented research needs to be put forward on the identified two main axes, mechanics and control.

(1) Mechanics – Develop and test systems where we can switch from one control mode to the other, i.e. from high gain to compliant.

(2) Theory of control – We have laid out the theoretical fundament for the understanding of adaptive frequency oscillators in feedback loops. The next large step for the theoretical treatment is a generalization of the understanding to MIMO systems. Furthermore, to advance the theoretical understanding in a next step a comprehensive model of the robot should be developed and the theory applied to this models. More generally we have to put forward a theory of control for self-organizing systems as discussed above.

As a more concrete example, on a robot, it will be interesting to investigate how such controllers can be combined with the control of speed and direction, and how to resolve possibly conflicting goals within the controller architecture.

In addition to the presented ones we have observed many more interesting phenomena, such as higher periods in gaits and bistability amongst other dynamic effects, which will be the focus of future experiments. However, the description of phenomena will take more data gathering, amongst others with a motion tracking system.

Acknowledgments This work is funded by a Young Professorship Award to Auke Ijspeert from the Swiss National Science Foundation.

We would like to thank Fumiya Iida to make PUPPY II accessible for our research.

Additional results We have attempted to replicate the optimality result of the simulation study presented in Section 6.1. However, so far the results do not match completely the simulation results. While the energy consumption, qualitatively scales in the same way (cf. Fig. 6.29a) the velocity results are different (Fig. 6.29b). The reason for that is that even if the activity of the robot has its peak at the resonant frequency, this activity does not necessarily get ideally transformed into forward locomotion at the resonant frequency. If we look at the acceleration sensor data, we see a clear effect of the resonance. However, this activity does not get translated into forward velocity as properly as in the simulation study (with its much simplified mechanics, contact and friction models). In Fig. 6.29b we show the variance of the acceleration on the three axes, normalized on the sum of the variances. While this is not exactly accurate it tells us where the energy goes, i.e. in up-down movements (z-axis), forward-backwards (x-axis) or lateral rocking (y-axis). We see that at the resonant frequency the z-axis sees an increase, i.e. the robot is mostly hopping vertically instead of moving forward. Furthermore, we see that a lot of the energy gets transformed into lateral rocking, this is something which might be improved in future robots and experiments. Another practical problem is that the friction of the feet. The feet tend to slip at higher frequencies, or if the friction of the feet and the ground is higher (e.g. by using a rubber mat on the ground) they tend to generate friction during parts of the swing phase. Furthermore, with the geometry of the robot as it is now, with only one knee joint the posture can not always be chosen optimally as it would lead to problem with the friction of the feet. We can get past some of those problems, by increasing the amplitudes, but this is very demanding for the motors and the mechanics of the robot. So there is a practical upper limit to increasing the amplitude. We can possibly correct such shortcomings in a future robot.

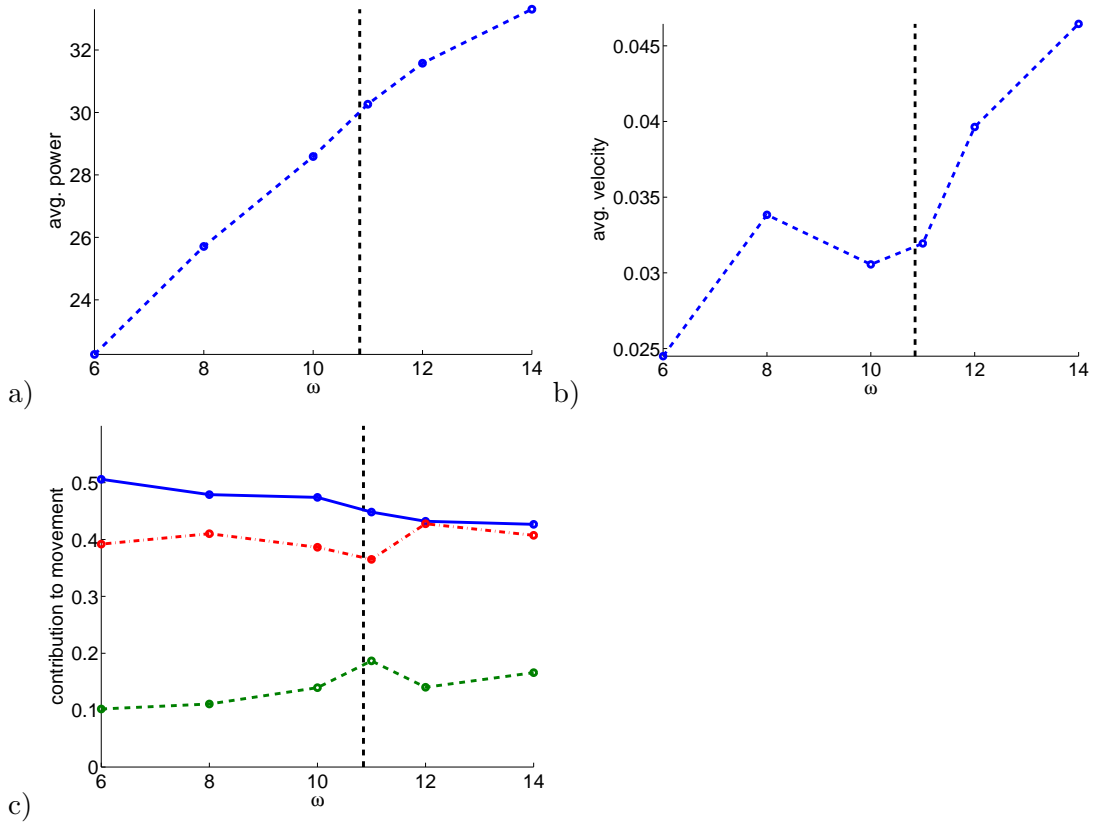


Figure 6.29: Additional results on PUPPY II. a) The average power vs. frequency. Compared to Fig. 6.8 the scaling is qualitatively similar as in the simulation. The vertical line indicates the line found by the adaptive frequency oscillator. b) The average velocity. c) Partition of the movement of the robot vs. the frequency (bold) x-axis (dashed) y-axis (dash-dot) z-axis. Refer to the text for an explanation of the data.

Epilogue

WHILE we have drawn conclusions for each of the presented studies in the respective articles, I would like to conclude the thesis by restating the achieved contributions and drawing a few general conclusions, before finally make a few remarks about future directions of the research that was presented.

7.1 Original contributions

Adaptive frequency oscillators (Chapter 5) – A very general rule for extending oscillators with the capabilities to adapt to the frequencies of external signals has been proposed. The rule has first been proposed on intuitive grounds, then it has been proven¹ for the adaptive frequency Hopf oscillator and its general applicability has been shown by numerical integration. To the best of my knowledge this is the first system which can adapt to frequencies of arbitrary signals in a fully dynamic way and is so general that it can be applied to almost any type of oscillator. Existing adaptive frequency oscillators (e.g. [137,160]) are limited to special types of oscillators or require special input signals (e.g. pulses).

Analysis of AFOs in feedback loops (Chapter 6) – The convergence behavior of AFOs in feedback loop with LTI system has been studied and it has been shown that (1) LTI systems are sufficient to explain the basic convergence behavior of real systems and (2) the phase shift of the system is the determinant for convergence.

Frequency Analysis with AFOs (Chapter 5) – A system has been presented which allows one to find the frequency spectrum of an incoming signal. The system has been analyzed on a macroscopic level by help of the Fokker-Planck formalism. The system performs in that sense a dynamic Fourier

¹ Together with L. Righetti

Transform and is the first of its kind which does frequency analysis by means of dynamical systems only.

The simplest adaptive locomotion toy-system (Chapter 4) – One of the simplest systems to study adaptive locomotion has been proposed. The body contains a very clear body property in form of resonant frequencies. The simple adaptive controller is able to find this property and constantly track it. The system is formulated in the language of dynamical systems. It is arguably one of the simplest adaptive locomotion system which can be formulated, but still proved to be relevant for the development of the controller concept for real robots.

Proof of concept in simulations and real robots (Chapter 6) – The proposed controller concepts have been implemented and proven to work in physics based simulations and real compliant and under-actuated robot.

Engineering view on oscillators (Chapter 3) – An engineering view on oscillators has been given. For this discussion the new concept of radius isochrones has been proposed.

Results on oscillator based control of compliant robots (Chapter 6) – New results on the use of oscillator based controllers for compliant robots have been presented. It has been shown, that the organizational capabilities of the body lead to unexpected results (gait pattern) and can be exploited for simpler control. Furthermore, we have shown how the resonant frequencies depends on gaits and posture and the implications for the control of such robots.

7.2 Discussion & Conclusions

We first discussed a few basic considerations when biologically inspired models and dynamical systems should be used for engineering purposes and showed how adhering to the derived principles leads to more efficient, better performing and simpler solutions.

Based on a set of desired properties which an adaptive locomotion system should possess, we then proposed a simple adaptive system which is able to adapt to the key properties of a compliant robot, namely the resonant frequency. The adaptive locomotion controllers work without fundamental modification for the application to systems that range from toy-system to real under-actuated compliant robots. The controllers are formulated as dynamical systems which brings certain advantages namely 1) fully dynamic description, 2) no separation of learning algorithm and learning substrate, 3) no separation of learning trials or time windows, 4) mathematically rigorous, 5) low dimensional systems. A further advantage is that once we have formulated the system in this way, it is amenable for many of the tools from dynamical systems theory. Such systems do not have an

explicit cost function, which can be problematic for certain applications, e.g. to move as fast as possible. The equivalent of a cost function, i.e. the specification of what the system ultimately achieves is done implicitly via the design of the slow feedback loop.

The key component for these controllers, the adaptive frequency oscillators have been investigated analytically and by numerical simulation and shown to be a versatile and interesting building block. It can be used wherever there is interest in resonant frequencies in a system, to tune to them or avoid them. It delivers information about the frequency component in a signal, this information is directly accessible without further processing by reading out the state variable ω . The adaptive frequency oscillators have only a small number of state variables (3 for a single AFO), yet they possess a large range of capabilities. Those capabilities allow them to be used for tasks which normally need to be accomplished by complicated and resource demanding signal processing algorithms.

7.3 Outlook

This thesis shows one example of the dynamical systems approach to adaptive systems. But a lot of work remains to be done in this subject.

On first sight legged adaptive locomotion might look like a trivial task, but on close look it is far from simple. As a matter of fact, we will not arrive at the goal of having agile robotic locomotion very soon because many key components are missing on different levels, ranging from supporting technology up to theoretical insight. Consequently there are several strands on which the presented work can be extended.

(1) Theory of multi-scale systems and adaptive dynamical systems –

Here fundamental properties of such systems need to be studied. Furthermore, are there general rules for adaptive systems and can we develop general purpose methods to devise the adaptation rule for a given set of specifications? We need to get an “engineering” grip on this question in order to make use of adaptive system in a systematic way in engineering. In our case, the difficulty in proposing a useful multi-scale dynamical system lies in finding an appropriate feedback structure (cf. Chapter 2). We only have proposed an example. It will thus be a great challenge to find general methods for such feedback loops. The old paradox between pre-specification and adaptive capabilities comes up, we discussed this challenge elsewhere in more depth [33].

More concretely for the AFOs, we think it should be feasible to make a more general proof of the convergence of the adaptive frequency oscillator than the one presented in [178]. This would involve expressing the oscillator and the incoming (periodic) signal by (general) Fourier series and working out the perturbation approach on the general series. This rather tedious work remains to be done yet.

As for the AFOs, they promise to be interesting for signal processing applications. However, quite some research has to be done to assess their properties when harnessed for such applications and a careful comparison to other techniques remains to be done. It seems straight forward to implement an AFO in analog electronics and in parallel computing. Such an implementation might be interesting in hindsight to applications (especially in signal processing), and could give such a system an advantage over others.

- (2) AFOs and higher dimensional systems** – What has been presented in the course of this thesis is the application of the controllers to systems with rather low number of degrees of freedom. Yet, interesting systems in robotics – which usually lead to problems for other methods – are higher dimensional (i.e. typically in the range of 10 to 30 DOF, e.g. for quadruped and humanoid robots). So, an evident question to be asked is how would controllers such as we presented behave on such systems and how would one go about the analysis of those systems.

As we have seen in the experiments in Chapter 6, there is an interaction between the “local” controllers (consisting of one AFO each) over the mechanical system. In our experiments we try to exploit this interaction to get coordination. But we could as well imagine situations where the interaction leads to unwanted effects of one DOF to another one, and possibly conflicting adaptation, e.g. different frequencies for different DOF. The possibility of such unwanted interaction of course increases with the numbers of DOF and AFOs in the setup. It will thus certainly be very interesting to try out such AFO based controllers (and other similar ones) on systems with many more DOF. Yet, it is important to note that in quite some applications, e.g. locomotion, it might be sufficient to have only one “central” AFO and force to frequencies of the other oscillators to be the same as the AFO.

As for the analysis, from the systems theoretic view point the means by which the interaction is established (i.e. physical vs. direct “mathematical” coupling) is not of importance. Once the model is there, the analysis proceeds in the same way.

This means, even if so far we have only analyzed what looks like a rather simple case (i.e. LTI SISO systems), this is the first and fundamental step towards the analysis of such more complicated cases. Further analysis means generalizing parts of the system or loosening some of the assumptions made in the analysis, i.e. MIMO (multiple input, multiple output) systems instead of SISO, including time-delays, time varying parameters, non-linearities, etc.

In other words, to understand such situation theoretically the mechanical systems have to be modeled and treated at least as LTI MIMO system. A particular challenge will be to capture the mechanical systems into suitable models. As we have seen the geometry, posture and even the gaits have an influence, i.e. in general we will encounter problems of nonlinear mechan-

ics, modeling of impact forces and other problems of advanced mechanical analysis such as nonholonomic and underactuated systems.

Once the models are established an analysis should be in principle straight forward, yet not necessary simple from the purely technical point of view.

Furthermore, the knowledge gained from the feedback analysis, i.e. the importance of phase shift will help us to correct or to account for possible unwanted effects. Finally, the adaptive system as its formulated in the AFO is surely open for enhancement and adaptation to special needs (e.g. modulation of the adaptation rate, modification of the adaptation rule) the system as we presented merely constitutes the simplest scheme which works for frequency adaptation. It could even be the case that the adaptation scheme should sometimes be turned off, e.g. in non-steady-state situation, such as uneven ground. For sure, in such situations the time scale over which the adaptation works could become much more critical.

The discussion about more sophisticated mechanical systems and models also leads us to a small note about the influence of the morphology on the outcome of the adaptation, and the correspondence of resonant frequency with proper forward locomotion. In the simulation experiments the resonant frequency that the AFOs find clearly corresponds to a nice forward locomotion. In the real robot things become a bit more complex. In some experiments the robot indeed locomotes forward very nicely while in other's the posture is not ideal for forward locomotion. This has per se nothing to do with the adaptation process but is more a problem of the "morphology" of the robot which is different than the simulation models and too limited to replicate exactly the results from the simulation. In future this could be accounted for by building robot with more suited morphologies for these experiments.

On a more general note, suitable models of sufficiently generic mechanical systems are the key to understand what morphologies can offer to adaptive controllers. Based on such models then hopefully methods can be worked out which are general enough to help in the engineering of adaptive agile autonomous robots.

- (3) **Adaptive control of self-organizing systems** – We have shown that it is possible to formulate systems which adapt to the patterns which are formed in a self-organized system. However, in order to fully exploit the framework, important questions have to be solved. Most importantly, methodologies for designing the feedback loops have to be found and important theoretical questions about stability and convergence properties of the devised systems have to be answered. This means we have to investigate the use of the in (1) discussed, to be developed, theory with hindsight on controllability.
- (4) **Robotics** – We are only in the beginning of exploiting compliance for robotic

applications. More sophisticated actuators and mechanics are needed which are robust and simple to use. Furthermore, we need to put forward new experimental systems to test out control approaches and build proof of principle applications.

While the basic results from the simulation could be reproduced on PUPPY II, not all experiments could be reproduced on the real robot. This has to do with differences in the mechanical setup, particularities in modeling friction and contacts in the simulation etc. Yet, I am convinced that the chosen way is an interesting one and should be pursued.

There are several other key parameters for locomotion controller such as offset and amplitudes, but also more “global” parameters, such as gait patterns, which should be investigated as a object of an adaptive system. While the basic ideas of an adaptive dynamical system should be the same, other adaption laws than the adaptive frequency rule have to be found in order to propose such systems. In the end, tuning of the frequency is only a small part of a truly adaptive locomotion controller.

When thinking about the applications of some of the robotic technology which is presented here it is interesting that there is a successful toy robot which exploits the ideas of acting in resonance (the Robo-sapien). It is true that looking at PUPPY is very compelling, it behaves more “life-like”, it always behaves interestingly. I do expect that more such robots will show up on the toy market in near future. But this will only be the beginning, adaptive systems in connection with compliant robots offer so many advantages that in the long run there will be many systems for a large range of applications. There are other domains in robotics such as humanoid robotics and ad-hoc modular self-reconfigurable robots, which could profit of the presented research. Ad-hoc modular robots pose a particular challenge to control engineering since traditional model based approaches as well as off-line optimization strategies are not feasible. Our approach might offer an interesting approach for controllers which are model-free (i.e. without explicit model) and on-line adaptive.

List of Figures

- 3.1 **a)** Limit cycle of the amplitude controlled phase oscillator for $r_0 = 1, g = 10, \omega = 2\pi[\text{rads}^{-1}]$. The arrows show the flow $\dot{\mathbf{q}}$ defined by the F_{ACPO} (3.13). **b)** This figure shows the phase difference established for the following values of $\omega_d = -0.0042, \lambda = 2$ and $g = 1000$. With help of (3.23) predicted value is $\theta_d = 0.2493$ (dashed line). The value from numerical integration is shown with the solid line (mean over $t = [10, 20]$ is $\theta_d = 0.2554$). **c)** The structure of the ACPO-CPG. Note that the connections illustrated by arrows involve rotation matrices (compare to text). 20
- 3.2 $\theta_{R,1,2,3}$ as a function of the chosen gait parameter. $P_{\text{gait}} = 0$ corresponds to the walk pattern, $P_{\text{gait}} = 1$ to trot, and $P_{\text{gait}} = 2$ to the bound. Solid line: $\theta_{R,1}$, dashed line: $\theta_{R,2}$, dash-dotted line: $\theta_{R,3}$. The dots correspond to values that correspond exactly to the values for the different gait patterns. However, also for settings quite far from these points the gait patterns are stable. 24
- 3.3 Results of the numerical integration of the ACPO CPG. **a)** Trajectories of the ACPO-CPG when switching from walk to trot to bound and the corresponding phase difference plots ($\theta_{d,ij}$). Dashed line: $\theta_{d,12}$, solid line: $\theta_{d,13}$, dash-dotted line: $\theta_{d,14}$. The upper figure presents the oscillatory activity (x_i), while the lower figure shows the corresponding phase difference evolution. **b)** phase difference plots for walk to trot (upper figure) and trot to walk (lower figure). The dashed vertical line indicates the time at which P_{gait} is changed. **c)** walk to bound and bound to walk **d)** trot to bound and bound to trot. 26

- 3.4 **a)** Further experiments on the influence of perturbations on the transition speed. Representatively the bound to walk transitions is chosen which is the slowest. Noise is added during the integration procedure (see text). As can be observed the transition is initiated about 1 s earlier then in the case without noise. **b), c)** To illustrate the robustness against perturbation that is inherently built in the structurally stable dynamical system model of the CPG we present the case when the state variable for the left hind leg gets fixed for 0.2s and then released again during walk. The two vertical lines show the time when the legs is fixed and released again. As can be observed, the leg increases in speed in order to catch up with the other legs to fulfill the requirements of the gait pattern. Within less than 0.5 s, the normal gait is re-established. 27
- 3.5 **a)** The schematic illustration of a limit cycle. It is a closed curve in phase space. The stability directions $\mathbf{e}_\phi, \mathbf{e}_r$ are illustrated as well as the projections \mathbf{p}_r and \mathbf{p}_ϕ of a perturbation \mathbf{p} , which has a direction in the phase space, onto those stability directions. **b)** The time series of an hypothetical oscillator. There is a characteristic period T after which the activity of the oscillator and with this the time series repeat. **c)** The limit cycle is a 1-dimensional manifold embedded in a D -dimensional space ($D \geq 2$), we can transform the system into a coordinate system in which the manifold shows particularly simple form and of which the stability directions constitute the base vectors. 37

- 3.6 Illustrating the transformation \mathbb{T} , by help of the isochrones and the radius-isochrones. For each oscillator 16 equally spaced isochrones are used and a varying number of radius-isochrones with a given Δt are plotted in the phase portrait (upper panels) and below the time series are shown. The fine vertical lines indicate the isochrones (only indicating the temporal position on the time series.) We see while they are always equally-spaced in the time series plot, in the phase plot this is not necessarily the case. a) The phase plot of the canonical oscillator in the phase-radius coordinate system PRCS (Eqs. 3.39–3.40). The isochrones form straight and equidistant vertical lines. The radius-isochrones ($\Delta t = [5, 6, 7]s$) form exponentially spaced straight horizontal lines. b) The Hopf oscillator (Eqs.3.66–3.67). The isochrones form straight rays at equal angles, which reflects the polar interpretation of ϕ in the transformation. The radius-isochrones ($\Delta t = [0.7, 1.4, 2.1]s$ outside of the LC and $\Delta t = [0.7, 1.4, 2.1, 3.5]s$ inside) reflect the 3th order convergence behavior of the radius. In the time-series we see the harmonic nature of the limit cycle reflected. c) The Energy oscillator (Eqs. 3.58–3.59). Due to the appearance of the nonlinear energy term only in the first ODE the system loses its circular symmetry. The isochrones and the radius-isochrones ($\Delta t = [2, 2.4, 2.8, 3.2]s$ outside of the LC and $\Delta t = [2, 2.4, \dots, 5.2]s$ inside) get a characteristic deformation. d) van der Pol Oscillator (Eqs.3.78–3.79). This is a strongly nonlinear oscillator. This fact is reflected in the strong deformation of the isochrones. The strong deformation of the radius-isochrones $\Delta t = [0.3, 0.6, 0.9]s$ away from the limit cycle in the upper left and lower right corner of the figure indicates the rapid convergence of the system in that region. It is immediately visible that the transformation from this QCS to the PRCS is a very complicated one. 42

- 3.7 Effect of a small pulse like perturbation on the limit cycle. The perturbation $\mathbf{p}(\mathbf{t})$ arrives when the phase point is at the position marked by a green dot. The phase point is then pushed back to the limit cycle by the stability properties of the system, i.e. it approaches asymptotically the limit cycle. It however retains a phase difference ($\Delta\phi$) in comparison with the unperturbed reference system. The phase difference can be of different amplitude and sign depending on the direction of the perturbation *and* the state the system currently is in when the perturbation arrives. Understanding this fact is key to understanding synchronization phenomena. 45

- 4.1 a) The mechanical sub-system of the adaptive locomotion toy system. It consist of two identical masses connected by a spring. From the mechanics of the system the forces acting on the body can be determined: F_s is the force that the springs exert on the blocks. It is of the same amplitude and opposite sign for the two masses. $F_{r,i}$ are the friction forces acting on the masses. With the help of this forces and Newton's law we are able to derive the system of differential equations that govern the mechanical system (Eq. 4.1).
 b) Schematic of the adaptive locomotion toy-system with its two main parts: The Hopf Oscillator (HO) and the spring mass system (MS). The Hopf Oscillator influences the mechanical system via the spring constant $k_a(z)$. The mechanical in turn disturbs the Hopf oscillator by coupling in the velocity difference d_v as an additive disturbance to the Hopf Oscillator equations. 70
- 4.2 Illustration of the basic mode of locomotion. See text for description. 75
- 4.3 Top panel: Mean energy ($E_p + E_k$) content of the mechanical system for different $\omega_0 = [0, 60]$ at steady state. Bottom panel: Mean velocity. As clearly can be seen we have a broad peak around the resonant frequency of the mechanical system $\omega_m = 14.8324$ 76
- 4.4 (a) This representative plot shows how the adaptation of ω_h increases the velocity of the locomotion system. ω_h starts at 12. The top panel shows the development of ω_h , the second panel shows the position x_1 of M_1 . There is some activity in the system from the beginning, however the excitations gets much stronger the closer ω_h comes to to the resonant frequency of the mechanical system ω_m (vertical line). The steady state for ω_h is around 14.4, which is lower then the calculated resonant frequency of the passive mechanical system: $\omega_m = 14.8324$.
 (b) To illustrate the robustness that is built into the locomotion system by its frequency adaptation we show a representative experiment in which the mass of the bodies is 1kg to 1.5kg at $t=100s$ (vertical line). Immediately, the frequency of the oscillator ω_h starts to adapt to the new resonant frequency of the mechanical system (dash-dotted horizontal line). 77
- 4.5 Adaptation of ω_h with viscous friction scheme. Different initial values for $\omega_h(0) = 0, 1, \dots, 32$ have been chosen. Clearly, the further away the longer ω_h takes to reach its stable steady state. The horizontal lines depict $0.5\omega_m$ and $2\omega_m$, where from the energy diagram (Fig. 4.3) resonant effects have to be expected and their influence on ω_h clearly can be observed here. Refer to text for further description. 78

- 4.6 Comparison of the development of ω_h for viscous and Coulomb friction scheme. The Horizontal line indicates the resonant frequency of the passive mechanical system. (A) Viscous friction. (B) Coulomb friction. See text for further discussion. 79
- 4.7 In order to quantify the steady state behavior of ω_h the mean m_{ω_h} and variance σ_{ω_h} have been measured after the system reached steady state (horizontal lines). Therefore, m_{ω_h} is a measure for (M) and σ_{ω_h} correlates with the distance (U)-(L). Note this figure is illustrative only – the actual values can change. 80
- 4.8 (a) Upper panel: the mean value attained for ω_h dependent on c (note the log scale). Lower panel: Variance for ω_h (note log-log scale). Note that for $c > C_c$ the variance drops to 0, therefore it is not drawn on the log scale. The vertical dotted line indicates the default setting of $c = 0.1$ and the dashed lines indicates the approximate value of C_c . The variance can be fitted with a power law $\sigma^2 \sim \tau^\alpha$. The exponent of the fit is $\alpha = 2.6959$. This behavior is typical for phase transitions.
 (b) Dependence of mean and variance of ω_h on τ_h for steady state behavior. Again, the dotted line indicates the default setting of $\tau = 0.1$ and the dashed lines indicates the approximate value of $\tau_{h,c}$. The variance can be fitted with a power law $\sigma^2 \sim \tau^\alpha$. The exponent of the fit is $\alpha = 1.9903$. (c) The attained mean values m_{v_1} of v_1 after the system reached steady state depending on coupling parameter a . There is a very clear linear relationship $m_{v_1} = qa$. The fit is for $q = 1.5451$ 81
- 4.9 Influence of the friction asymmetry in viscous mode. The z axis is the position of m_1 after 200s for a given setting of ρ_- and ρ_+ . White regions correspond therefore to fast forward locomotion, black to fast backward locomotion. 83
- 4.10 a) At $t = 400$ the feedback from the mechanical system to the Hopf Oscillator is cut by setting $c = 0$. This as well inhibits the frequency adaptation. b) At $t=400$ only the frequency adaptation is cut by setting $\tau = 0$. This means there is still feedback from the mechanical system to the Hopf oscillator. Therefore, the system keeps moving with the same speed. However, it can not react to changing mechanical properties anymore (not shown). 84
- 4.11 M_1 blocked at $t = 100$ (dashed vertical line) and released at $t = 200$ (dash dotted vertical line). 85

- 5.1 We illustrate the coordinate system in which synchronization is most naturally discussed. The figure shows an arbitrary limit cycle. The system is strongly damped in direction perpendicular to the limit cycle \vec{e}_r and marginally stable in direction tangential to the limit cycle \vec{e}_ϕ . This is the reason for the structurally stable limit cycle in the first place and allows for a resetting of the phase on the other hand. Note that the 2-dimensional representation is always valid for discussing a limit cycle since there exists always a 2 dimensional manifold which contains the limit cycle. Refer to text for a discussion of the perturbation \vec{P} 95
- 5.2 Plot of the evolution of ω for four different values of ϵ . Here we set $\mu = 1$, $x(0) = 1$ and $y(0) = 0$, the perturbing force is $F = \cos(30t)$. For every value of ϵ , we see that ω converges to 30, which is the frequency of the input signal. Therefore, the system is able to learn the frequency of the input signal. We also notice that ϵ controls the convergence rate, the higher it is, the faster the system learns. . . 100
- 5.3 Results of the simulation of the first and second order approximations. For a simple input, here $F = \sin(40t)$, $\epsilon = 0.9$, initial conditions are $t_0 = 0$, $w_0 = 30$. The upper figure shows the evolution of the ω variable for the initial dynamical system (Eq. (5.38)), the first order approximation $\omega_\epsilon(t)$ and the 2nd order approximation $\omega_{\epsilon^2}(t)$. The lower figure shows quadratic errors between the initial system and the 2 approximations, for the evolution of ω 102
- 5.4 In this figure, we plotted $\omega(t)$ for several initial conditions, ω_0 . The periodic input is Equation (5.43), $\epsilon = 0.9$. The dotted lines indicates the boundary between the different basins of attraction, corresponding to the different frequency components of the input, that were predicted analytically. 104
- 5.5 The left plot of this figure represents the evolution of $\omega(t)$ when the adaptive Hopf oscillator is coupled to the z variable of the Lorenz attractor. The right plot represents the z variable of the Lorenz attractor. We clearly see that the adaptive Hopf oscillators can correctly learn the pseudo-frequency of the Lorenz attractor. See the text for more details. 105
- 5.6 Frequency spectrum of the Van der Pol oscillator, both plot with $\omega = 10$. The left figure is an oscillator with $\alpha = 10$ and on the right the nonlinearity is higher $\alpha = 50$. On the y-axis we plotted the square root of the power intensity, in order to be able to see smaller frequency components. 107

- 5.7 Plot of the frequency of the oscillations of the Van der Pol oscillator according to ω . Here $\alpha = 50$. There are 2 plots, in dotted line the oscillator is not coupled and in plain line the oscillator is coupled to $F = \sin 30t$. The strength of coupling is $\epsilon = 2$. We clearly see basins of phase-locking, the main one for frequency of oscillations 30. The other major basins appears each $\frac{30}{n}$ (dotted horizontal lines). We also notice small entrainment basins for some frequencies of the form $\frac{30p}{q}$. For a more detailed discussion of these results refer to the text. 108
- 5.8 This figure shows the convergence of ω for several initial frequencies. The Van der Pol oscillator is perturbed by $F = \sin(30t)$, with coupling $\epsilon = 0.7$, $\alpha = 50$. We clearly see that the convergence directly depends on the initial conditions and as expected the different kinds of convergence correspond to the several entrainment basins of Figure 5.7. 109
- 5.9 We show the adaptation of the Van der Pol oscillator to the frequency of various input signals: (a) a simple sinusoidal input ($F = \sin(40t)$), (b) a sinusoidal input with uniformly distributed noise ($F = \sin(40t) + \text{uniform noise in } [-0.5, 0.5]$), (c) a square input ($F = \text{square}(40t)$) and (d) a sawtooth input ($F = \text{sawtooth}(40t)$). For each experiment, we set $\epsilon = 0.7$ and $\alpha = 100$ and we show three plots. The right one shows the evolution of $\omega(t)$. The upper left graph is a plot of the oscillations, x , of the system, at the beginning of the learning. The lower graph shows the oscillations at the end of learning. In both graphs, we also plotted the input signal (dashed). In each experiment, ω converges to $\omega \simeq 49.4$, which corresponds to oscillations with a frequency of $40 \text{ rad} \cdot \text{s}^{-1}$ like the input and thus the oscillator correctly adapts its frequency to the frequency of the input. 111
- 5.10 We show results for several adaptive oscillators. For each oscillator, we give its equation in the right column, ω corresponding to the adaptive parameter. We also specify the values of the different parameters used in the experiments. In the left column we plotted results of the experiment. Each figure is composed of 3 plots. The right one is a plot of the evolution of ω . The left ones are plots of the oscillations (the x variable) and of the input signal F (dashed line), before (upper figure) and after (lower figure) adaptation. . . 113

- 5.11 (a) Typical convergence of an adaptive frequency oscillator (Eqs 5.56–5.58) driven by a harmonic signal ($I(t) = \sin(2\pi t)$). The frequency converges in an oscillatory fashion towards the frequency of the input (indicated by the dashed line). After convergence it oscillates with a small amplitude around the frequency of the input. The coupling constant determines the convergence speed and the amplitude of oscillations around the frequency of the driving signal in steady state. In all figures, the top right panel shows the driving signals (note the different scales). (b–f) Non-harmonic driving signals. We depict representative results on the evolution of $\frac{\omega - \omega_F}{\omega_F}$ vs. time. The dashed line indicates the zero error between the intrinsic frequency ω and the base frequency ω_F of the driving signals. (b) Square pulse $I(t) = \text{rect}(\omega_F t)$, (c) Sawtooth $I(t) = st(\omega_F t)$ (d) Chirp $I(t) = \cos(\omega_c t)$ $\omega_c = \omega_F(1 + \frac{1}{2}(\frac{t}{1000})^2)$ (Note that the graph of the input signal is illustrative only since the change in frequency takes much longer than illustrated.) (e) Signal with two non-commensurate frequencies $I(t) = \frac{1}{2} \left[\cos(\omega_F t) + \cos(\frac{\sqrt{2}}{2}\omega_F t) \right]$, i.e. a representative example how the system can evolve to different frequency components of the driving signal depending of the initial condition $\omega_d(0)$. (f) $I(t)$ is the non-periodic output of the Rössler system. The Rössler signal has a $1/f$ broad band spectrum, yet it has a clear maximum in the frequency spectrum. In order to assess the convergence we use $\omega_F = 2\pi f_{max}$, where f_{max} is found numerically by FFT. The oscillator converges to this frequency. 120
- 5.12 Typical convergence of an adaptive frequency oscillator (Eqs 5.56–5.58) driven by a harmonic signal ($I(t) = \sin(2\pi t)$) and different coupling constants K . The coupling constant determines the convergence speed and the amplitude of oscillations around the frequency of the driving signal in steady state – the higher K the faster the convergence and the larger the oscillations. 121
- 5.13 The structure of the dynamical system that is capable to reproduce a given teaching signal $T(t)$. The system is made up of a pool of adaptive frequency oscillators. The mean-field produced by the oscillators is fed back negatively on the oscillators. Due to the feedback structure and the adaptive frequency property of the oscillators it reconstructs the frequency spectrum of $T(t)$ by the distribution of the intrinsic frequencies. 121

- 5.14 ($N = 1000$, $K = 200$) – a) The teaching signal $T(t)$ (dashed) vs. the output signal $O(t)$ (bold) in the beginning ($t = [0, 1.5]$ s) The output almost immediately tracks the teaching signal since we have a very strong coupling constant. b) $T(t)$ vs $O(t)$ after 1000 s, now the output signal is basically identical to the teaching signal. c) The square root error $e(t) = \sqrt{(O(t) - T(t))^2}$ d) Evolution of the distribution of ω . The traces of the evolution of the ω_i are shown. Thus, we can clearly see the development of the distribution of the intrinsic frequencies from the initial uniform distribution to the distribution which corresponds to the Fourier spectrum of the signal. e) The average Manhattan distance between the distribution of the frequencies of oscillators and the Fourier spectrum (cf. text). f) The fraction of oscillators which have converged. It can be seen that there is fast convergence of the oscillators in the first few seconds. The measure stabilizes at around 0.96. g) The distribution of the intrinsic frequencies ω distribution after $t=1000$ s (bars) the crosses indicate the theoretical value of the Fourier spectrum of the signal. 123
- 5.15 ($N = 1000$, $K = 200$) – Simulation with an initial condition which is further off the end target spectrum. As can be seen due to the negative feedback the oscillators cross over the frequencies which are already covered. This means they take longer to converge but the final distribution is very close to the case presented in Fig. 5.14. c) The count of converged oscillators (bold line) in comparison with the example from before (dashed). 124
- 5.16 ($N = 100$) – a) Convergence over time for different values of K ($T(t) = \sin(10t)$ $\omega(0) \sim U(2, 18)$) as measured by the average Manhattan distance (note the logarithmic scale for the time). We can see that in general larger K mean faster convergence. b) Distance after 1s, 100s 300s, and 5000s for different values of K 125
- 5.17 ($N = 6$, $K = 200$) – The same input signal as in Figs. 5.14 and 5.15. This time we use the minimal number of oscillators ($N = 6$) needed for perfect convergence to the given input signal. It can be seen that in this example the convergence works perfectly. b) shows the histogram after 100 s - see text for further discussion. 126
- 5.18 ($N = 1000$, $K = 200$) – $T(t)$ is a non-stationary input signal (cf. text), in contrast to Figs 5.14 and 5.15 the histogram of the distribution of the frequency ω_i is shown for every 50s, the grey level corresponds to the number of oscillators in the bins (note the logarithmic scale). The thin white line indicates the theoretical instantaneous frequency. Thus, it can be seen that the distribution tracks very well the non-stationary spectrum, however about 4% of the oscillators diverge after the cross-over of the frequencies. 126

- 5.19 ($N = 10000$, $K = 0.1$) – a) The FFT (black line) of the Rössler signal (for $t = [99800, 100000]$) in comparison with the distribution of the frequencies of the oscillators (grey bars, normalized to the number of oscillators) at time 10^5 s. The spectrum of the FFT has been discretized into the same bins as the statistics of the oscillators in order to allow for a good comparison with the results from the full scale simulation. b) Time-series of the output signal $O(t)$ (bold line) vs the teaching signal $T(t)$ (dashed line). 128
- 5.20 $T(t)$ is a harmonic signal a) $c_1(t)$ for Fokker-Planck (dashed) and full-scale simulation ($N = 1000$, $K = 1$) in the noise-less limit ($B(\omega) = 0$) b) The difference between $c_1(t)$ for Fokker-Planck and full-scale simulation. 130
- 5.21 Results from integration of Fokker-Planck and full-scale simulation ($N = 1000$, $K = 1$) for different levels of noise: $\sigma^2 = [10^{-6}, 10^{-2}]$ a)–f) Comparison between the distribution of the large scale simulation (bars) and the Fokker-Planck integration (line), note the logarithmic scale. The continuous distribution $P(\omega, t)$ has been discretized in order to allow for a good comparison with the results from the full scale simulation g) Measures of the convergence in steady state. (Triangles) Fokker-Planck c_1 , (Circles) Full-scale simulation c_1 , (Crosses) Variance of c_1 in the full scale simulation. Clearly visible is that the full-scale simulation and the Fokker-Planck equation show the same qualitative behavior under different levels of noise. Interestingly there is a peak of variance for a level of noise between $\sigma^2 = 10^{-3}$ and 10^{-2} in the full-scale simulation (discussion see text). 132
- 5.22 Comparison between the results of the Fokker-Planck integration and the full scale simulation ($N = 1000$, $K = 1$) for a more complicated signal, namely the signal used in Fig. 5.14. The grey histogram shows the statistics of the full scale simulation and the black line shows the prediction of the Fokker-Planck integration. Note that the statistics of the oscillator does not show more detail since the single oscillator is the lower limit for resolution (zero line in the plot), this resolution could arbitrarily be pushed up by choosing more oscillators. We see that especially in the beginning the match is very good. For longer evolution the Fokker-Planck equation predicts a slightly better convergence than seen in the full scale simulation (cf. text). 133
- 6.1 (a) Integration of the System Eqs. 6.1-6.3 (b) corresponding phase plot, in which the frequency adaptation and the phase locking can be seen. 144

- 6.2 On the top left panel the nonharmonic driving signals are presented. (a) Square pulse (b) Sawtooth (c) Chirp (Note that this is illustrative only since the change in frequency takes much longer as illustrated.) (d) Signal with two non-commensurate frequencies (e) Output of the Rössler system. – We depict representative results on the evolution of $\frac{\omega_d}{\omega_F}$ vs. time. The dashed line indicates the base frequency ω_F of the driving signals. In (d) we show in a representative example how the system can evolve to different frequency components of the driving signal depending on the initial condition $\omega_d(0)$ 144
- 6.3 (a) The mechanical structure of the spring-mass hopper. The trunk is made up of a rigid body M_b on which two legs are attached by rotational joints. The lower part of the leg is attached by a spring-mass system SD . The lower part consist of a small rigid body. The length of the body is 0.5m (b) The coupling structure of the controller and the mechanical system used for the spring-mass hopper. The upper Hopf oscillator is used for the activation of the fore leg and the lower feedback loop for the hind leg. (c) This table presents the parameters that have been used for the simulations, unless otherwise noted. Note that this parameters can be chosen from a wide range and the results do (qualitatively) to a large extent not depend on the exact values of the parameters. Bottom row: Snapshots of the movement sequence of the spring-mass hopper when the frequency is adapted, i.e. steady state behavior (cf also movie [1]). 145
- 6.4 Simulation results of the spring-mass hopper when the rotational joints are not activated. a) Evolution of the intrinsic frequencies of the Hopf oscillators ω_h . Note that the frequencies of both oscillators nearly coincide and therefore only one seems visible. b) Fore limb foot elevation. c) Hind limb foot elevation. The adaptation of the frequency is clearly visible and as can be seen in the feet elevation measurements the activity of the system is increased as hopping starts at around 20 s (arrow). The dashed line depicts the theoretical resonant frequency of the spring-mass system when it would not leave the ground. Due to the lift-off of the feet the real resonant frequency is smaller than the calculated value. 147
- 6.5 Simulation results of the spring-mass hopper when the rotational joints are activated a) The frequencies of the Hopf oscillators ω_h b,c) Foot elevation $y_{f,h}$ d) Displacement of the center of mass of the body x_b . The adaptation of the frequency is clearly visible. As can be seen in the feet elevation measurements and the displacement of the body this adaptation enhances the activity of the leg and initiates a displacement of the body. Interestingly there is a burst of activation (arrow) which increases the adaptation speed before the system settles to steady state behavior. . . 147

- 6.6 Test of the adaptation capability of the controller when the mass is changed. At $t = 40$ s (dashed line) the mass of the body M_b is changed from $m_b = 0.2$ kg to 0.4 kg. See text for discussion. 147
- 6.7 Efficiency ρ vs ω_h . See text for the definition of ρ , details of measurement and experimental protocol. The dashed line indicates the frequency to which the oscillators adapt. It is clearly visible that this corresponds to the maximum of the efficiency. 147
- 6.8 Further results from the simulation study a) total energy consumed by the robot over the simulation run b) The mean velocity achieved by the robot. It can be seen that the neither the energy nor the velocity show an extremum at the resonant frequency. c) Gait pattern (phase difference), depending on the detuning of the controller different gait patterns emerge. d) Energy distribution over the different actuators of the robot. After adaptation, the hind legs contribute more to the locomotion. Hip joints more than the springs: Mean energy A) hind hip joint B) fore hip joint C) hind spring D) fore spring. 150
- 6.9 a) PUPPY II, a robot “dog” with passive dynamics (cf. springs in the knee joints) and several sensor modalities b) Mechanical structure of PUPPY II and sensor placement: 1,3: FSR (Force Sensitive Resistors) 2,4: Potentiometers of the passive joints 5: 3-axis acceleration sensors 6: PSD (Position Sensitive Detector). Circles with a cross denote actuated joints, blank circles denote passive joints. c) Control structure used in the experiments: One of the sensor channels is used to perturb an adaptive frequency Hopf oscillator, the output of the oscillator (a state variable) is used to send motor commands (position control). Thus, this system constitutes a nonlinear feedback loop. 155
- 6.10 Results of adaptation experiments with the real-world robot a) The frequency ω of the oscillator is shown as it changes over time (bold line) adaptation using the z-axis of the inertia sensor: convergence of the frequency adaptation; (dashed line) adaptation using the knee sensor: divergence of the frequency adaptation with increased rate around the resonant frequency b) An experiment showing the advantage of using online adaptive controllers. The body weight is changed from $w_1 = 0.905$ kg to $w_2 = 0.695$ kg. The controller immediately adapts to the changed body property. . . . 157
- 6.11 These snapshots show the hopping movement of the robot after the frequency adaptation has converged. There are moments when the robot has all four legs lifted. 158

- 6.12 In this figure we compare the results of the integration of the full system (Eqs.6.7–6.11) with the results of the approximation (Eq. 6.16): (blue) ω from the integration of the full system, (red dashed) ω predicted by the approximation. The dashed horizontal line marks the resonant frequency of the linear system. 160
- 6.13 A linear system for which the convergence is stable at resonance. a,b) Bode plot for $H(s)$, the dashed line indicates the resonant frequency. Note that the phase has a negative 0 crossing at the resonant frequency, this means the adaptation process has a attractor at the resonant frequency. c) The function $\Delta\omega = \sin(H(s))$. Strictly speaking we need to look at this function to determine stability. d) Time series of the integration of the full system showing the adaptation of the oscillator frequency ω . It is clearly visible how the oscillator frequency adapts to the resonant frequency of the linear system (dashed line), what corresponds to the prediction from the Bode plot and $\Delta\omega$ 163
- 6.14 A linear system for which there is no convergence at resonance. a,b) Bode plot for $H(s)$, note that the phase has no negative 0 crossing at the resonant frequency, this means the adaptation process has no attractor at the resonant frequency, and especially $\Delta\omega$ (c), is always positive with a distinct peak at the resonant frequency. This means divergence of the oscillator frequency ω with an increased rate to be expected around the resonant frequency. d) Time series of ω . The prediction is confirmed by the data obtained by the integration of the full system. 163
- 6.15 a) PUPPY II, a robot “dog” with passive dynamics (cf. springs in the knee joints) and several sensor modalities b) Mechanical structure of PUPPY II and sensor placement: 1,3: FSR (Force Sensitive Resistors) 2,4: Potentiometers of the passive joints 5: 3-axis acceleration sensors 6: PSD (Position Sensitive Detector). Circles with a cross denote actuated joints, blank circles denote passive joints. c) Control structure used in the experiments: One of the sensor channels is used to perturb a controller consisting of one or several adaptive frequency Hopf oscillators, the output of the oscillator (a state variable) is used to send motor commands (position control). Thus, this system constitutes a nonlinear feedback loop. 170

- 6.16 Parameters describing the posture of the robot: center angle, i.e. angle for zero signal $x(t) = 0$, angle corresponding to a signal of amplitude $x(t) = 1$. α_t is the actual position of the leg, α_0 is the offset (compared to a vertical position) of the center position of the leg. Note that the vertical position denotes $\alpha_0 = 0$, legs titled backwards from this position have negative angles, and vice versa. This means the larger this angle, to more tilted forward is the leg. α_1 is the amplitude of the leg for a signal of amplitude 1 (measured against α_0). 172
- 6.17 Experiment 1 to show the online adaptation of the controller. On the left an illustration of the sensor-controller structure. The z-value of the acceleration sensor (A) is used as an input to the oscillator. The signal of the oscillator is used to set the motor position according to Eq. 6.21. On the right the intrinsic frequency ω of the oscillator is shown as it evolves during the experiment. The body weight is changed from $m_1 = 0.905$ kg to $m_2 = 0.695$ kg. The controller immediately starts to adapt to the changed body property. 173
- 6.18 a) The range of posture angles used in the experiment illustrated on the robot. b) The average frequency (squares) found by the adaptive frequency oscillator vs posture, i.e. the angle of the leg. The bars show the standard deviation. 174
- 6.19 Illustration of the effect of the posture angle α_0 on the load distribution on the spring and motor respectively. Of the force acting on the leg (blue), only the part of the force active perpendicular to the foot loads the spring (red), the force acting parallel to the foot will act on the motor (green). Note that this is illustrative only for the principles at work, and that the real case is more complicated (e.g. amongst other things the force vector on the foot is not necessarily vertical). 175
- 6.20 Controller setup with two oscillators. a) Setup with $\theta_d = 0$, i.e. the two oscillator will synchronize in phase, this can also be interpreted as excitatory coupling as denoted by the arrow. b) Setup with $\theta_d = \pi$, i.e. the two oscillator will synchronize in anti-phase. This can also be interpreted as inhibitory coupling as denoted by the circle. 176
- 6.21 Experiment to investigate the influence of the gait pattern on the resonant frequency. a) gait pattern, stance/swing phases, black is stance phase and white is swing phase, H depicts the hind legs and F depicts to fore legs, for simplicity only one leg per pair is shown, the data in each pair looks very similar. Top row for $\theta_d = 0$, it is well visible that the front and hind limbs are active at the same time, while for $\theta_d = \pi$, we clearly see a alternating gait. b) resulting frequency of the adaptation process, the mean is at $\omega = 24.89$ for $\theta_d = \pi$ (alternating gait) and at $\omega_d = 20.02$ 177

6.22	Gait pattern estimated by the knee angle data, black is stance and white is swing phase. a) Coupling $\theta_d = 0$, the first panel shows the gait pattern estimated by the knee angle data, the second panel shows the phase differences estimated by difference of the phase of the Hilbert transform of the knee angle data (in red the average difference). b) The information but this time the angle of the CPG is specified as $\theta_d = \pi$	178
6.23	Controller schema for Experiment 5. No connection between the oscillators for the hind and front leg.	180
6.24	Data from the adaptation experiment with local controllers (Ex. 5). a) Adaptation of the frequencies, at around 400s the frequencies are reset to 6 rads^{-1} . It is clearly visible that there exists an attractor for the convergence process are around 11 rads^{-1} b) The difference between the frequencies for the front and hind leg. It is clearly visible how closely together the two frequencies evolve. c) The phase difference of the two oscillators, as can be seen they phase lock at a value slightly higher than 0.5. And the phase locking is never lost during the whole experiments, i.e. the legs are always well coordinated.	180
6.25	Illustration of the feedback loop of the adaptive frequency oscillator with the linear system and the conventions used. The adaptive frequency oscillator (AFO) is connected to the plant, which is modeled as a linear system $H(s)$ through u (the motor commands) and the sensory feedback from the robot to the AFO is modeled by y	182
6.26	A linear system for which the convergence is stable at resonance. a,b) Bode plot for $H(s)$, the dashed line indicates the resonant frequency. Note that the phase has a negative 0 crossing at the resonant frequency, this means the adaptation process has a attractor at the resonant frequency. c) The function $\Delta\omega = \sin(H(s))$. Strictly speaking we need to look at this function to determine stability. d) Time series of the integration of the full system showing the adaptation of the oscillator frequency ω . It is clearly visible how the oscillator frequency adapts to the resonant frequency of the linear system (dashed line), what corresponds to the prediction from the Bode plot and $\Delta\omega$	185
6.27	A linear system for which there is no convergence at resonance. a,b) Bode plot for $H(s)$, note that the phase has no negative 0 crossing at the resonant frequency, this means the adaptation process has no attractor at the resonant frequency, and especially $\Delta\omega$ (c), is always positive with a distinct peak at the resonant frequency. This means divergence of the oscillator frequency ω with an increased rate to be expected around the resonant frequency. d) Time series of ω . The prediction is confirmed by the data obtained by the integration of the full system.	185

- 6.28 Comparison of data from the real robot with the linear model. Top: sensor (acceleration) that leads to convergence. Bottom: Sensor (knee angle) that does not lead to convergence. While the basic properties of the real world data are reproduced by the LTI model there is some differences between the real data and the prediction of the LTI model. The dashed line indicates the estimated resonant frequency. See text for further discussion. 186
- 6.29 Additional results on PUPPY II. a) The average power vs. frequency. Compared to Fig. 6.8 the scaling is qualitatively similar as in the simulation. The vertical line indicates the line found by the adaptive frequency oscillator. b) The average velocity. c) Partition of the movement of the robot vs. the frequency (bold) x-axis (dashed) y-axis (dash-dot) z-axis. Refer to the text for an explanation of the data. 191

List of Tables

3.1	(a) The table shows the phase differences corresponding to the three most common gaits observed in quadrupeds. (b) The table shows the 3 different rotation angles that are needed in the construction of the ACPO-CPG. (c) Connection scheme used for the ACPO-CPG.	24
3.2	Nomenclature, conventions and common abvrevations used to discuss oscillators in this article.	35
3.3	Common design goals and the required properties of the oscillator.	48
3.4	Table classifying some of the contribution of the field oscillators applied to robotics and related modeling. The contributions are classified according the the design method as discussed in Section 3.2.4. The labels in each case correspond the design goals identified in Section 3.2.3: (1) Timing: Design that influence the phase of the oscillator: (a) influence on (relative) phase, (b) instantaneous frequency, and (c) average frequency. (2) Design that influences the geometry of the oscillator: (a) influences on r , (b) the design of T^{-1} / output filter. The column “R/A” indicates whether the resulting system is reactive or adaptive. This table has sparsely populated columns which point to open research question.	63
5.1	This table summarizes the maximum errors of the simulation for the first and second order approximations discussed from Figure 5.3	102

Bibliography

- [1] Movies of the spring-mass hopper are available at <http://birg2.epfl.ch/movies/full/hopper-exp1.mpg>
<http://birg2.epfl.ch/movies/full/hopper-exp2.mpg>
<http://birg2.epfl.ch/movies/full/hopper-exp3.mpg>.
- [2] A movie of the robot experiment is available at <http://birg.epfl.ch>.
- [3] *Open Dynamics Engine Documentation*. Available online at <http://ode.org>.
- [4] J.A. Acebron and R. Spigler. Adaptive frequency model for phase-frequency synchronization in large populations of globally coupled nonlinear oscillators. *Physical Review Letters*, 81:2229–2232, 1998.
- [5] J.A. Acebron and R. Spigler. Uncertainty in phase-frequency synchronization of large populations of globally coupled nonlinear oscillators. *Physica D: Nonlinear Phenomena*, 141(1–4):65–79, 2000.
- [6] R.M. Alexander. Elastic energy stores in running vertebrates. *Am. Zool.*, 24:85–94, 1984.
- [7] R.M. Alexander. *Elastic Mechanisms in Animal Movement*. Cambridge University Press, Cambridge, 1988.
- [8] V.I. Arnol'd. Remarks on the perturbation theory for problems of mathieu type. *Russ Math Surv*, 38(4):215–233, 1983.
- [9] Y.I. Arshavsky, T.G. Deliagina, and G.N. Orlovsky. Pattern generation. *Current Opinion in Neurobiology*, 7(6):781–789, 1997.
- [10] J.E.A. Bertram. Constrained optimization in human walking: const minimization and gait plasticity. *J Exp Biol*, pages 979–991, 2005.
- [11] J.E.A. Bertram and A. Ruina. Multiple walking speed-frequency relations are predicted by constrained optimization. *J Exp Biol*, 209:445–453, 2001.

- [12] E. Bicho, P. Mallet, and G. Schöner. Target representation on an autonomous vehicle with low-level sensors. *Int J Robotics Research*, 19(5):424–447, 2000.
- [13] R. Blickhan. The spring-mass model for running and hopping. *J. Biomechanics*, 22(11–12):1217–1227, 1989.
- [14] R. Blickhan and R.J. Full. Similarity in multilegged locomotion: bouncing like a monopode. *Journal of Comparative Physiology*, 173:509–517, 1993.
- [15] Roman Borisyuk, Mike Denham, Frank Hoppensteadt, Yakov Kazanovich, and Olga Vinogradova. Oscillatory model of novelty detection. *Computation in neural systems*, 2001.
- [16] G. Brambilla, J. Buchli, and A.J. Ijspeert. Adaptive four legged locomotion control based on nonlinear dynamical systems. In *From Animals to Animats 9. Proceedings of the Ninth International Conference on the Simulation of Adaptive Behavior (SAB'06)*, volume 4095 of *Lecture Notes in Computer Science*, pages 138–149. Springer Verlag, 2006.
- [17] T.G. Brown. The intrinsic factors in the act of progression in the mammal. *Proceedings of the Royal Society of London. Series B*, 84(572):308–319, 1911.
- [18] T.G. Brown. The factors in rhythmic activity of the nervous system. *Proceedings of the Royal Society of London. Series B*, 85(579):278–289, 1912.
- [19] J. Buchli. Locking behavior in extended nerve cell models, 2003. MSc Thesis – Institute of Neuroinformatics, ETH / UNI Zürich.
- [20] J. Buchli. *Foreword – Mobile Robots, moving intelligence*. Advanced Robotics Systems International and pro literatur Verlag, Mammendorf, 2007.
- [21] J. Buchli, editor. *Mobile Robots, moving intelligence*. Advanced Robotics Systems International and pro literatur Verlag, Mammendorf, 2007.
- [22] J. Buchli, F. Iida, and A.J. Ijspeert. Finding resonance: Adaptive frequency oscillators for dynamic legged locomotion. In *Proceedings of the IEEE/RSJ International Conference on Intelligent Robots and Systems (IROS)*, pages 3903–3909. IEEE, 2006.
- [23] J. Buchli and A.J. Ijspeert. Distributed central pattern generator model for robotics application based on phase sensitivity analysis. In A.J. Ijspeert, M. Murata, and N. Wakamiya, editors, *Biologically Inspired Approaches to Advanced Information Technology: First International Workshop, BioADIT 2004*, volume 3141 of *Lecture Notes in Computer Science*, pages 333–349. Springer Verlag Berlin Heidelberg, 2004.

- [24] J. Buchli and A.J. Ijspeert. A simple, adaptive locomotion toy-system. In S. Schaal, A.J. Ijspeert, A. Billard, S. Vijayakumar, J. Hallam, and J.A. Meyer, editors, *From Animals to Animats 8. Proceedings of the Eighth International Conference on the Simulation of Adaptive Behavior (SAB'04)*, pages 153–162. MIT Press, 2004.
- [25] J. Buchli and A.J. Ijspeert. Self-organized adaptive legged locomotion in a compliant robot. 2007. Unsubmitted manuscript.
- [26] J. Buchli, A.J. Ijspeert, M. Rabinovich, and A. Selverston. Dynamical principles in neuronal systems and robotics – guest editorial. *Biological Cybernetics*, 96(6):517–518, 2006.
- [27] J. Buchli, L. Righetti, and A.J. Ijspeert. Adaptive dynamical systems for movement control. In *Proceedings of 3rd International Symposium on Adaptive Motion in Animals and Machines – AMAM 2005*, page 7. Verlag ISLE, Ilmenau, 2005. Abstract.
- [28] J. Buchli, L. Righetti, and A.J. Ijspeert. A dynamical systems approach to learning: a frequency-adaptive hopper robot. In *Proceedings of the VI-IIth European Conference on Artificial Life ECAL 2005*, Lecture Notes in Artificial Intelligence, pages 210–220. Springer Verlag, 2005.
- [29] J. Buchli, L. Righetti, and A.J. Ijspeert. Adaptive dynamical systems: A promising tool for embodied artificial intelligence. In *Proceedings of 50th anniversary summit of artificial intelligence*, July 2006. Abstract.
- [30] J. Buchli, L. Righetti, and A.J. Ijspeert. Adaptive frequency oscillators applied to dynamic walking II. Adapting to resonant body dynamics. In *Proceedings of Dynamic Walking*, 2006. Abstract.
- [31] J. Buchli, L. Righetti, and A.J. Ijspeert. Engineering entrainment and adaptation in limit cycle systems – from biological inspiration to applications in robotics. *Biological Cybernetics*, 95(6):645–664, 2006.
- [32] J. Buchli, L. Righetti, and A.J. Ijspeert. Frequency analysis with coupled nonlinear oscillators. *SIAM Journal on Applied Dynamical Systems*, 2007. Submitted.
- [33] J. Buchli and C.C. Santini. Complexity engineering: Harnessing emergent phenomena as opportunities for engineering. In *Reports of the Santa Fe Institute's Complex Systems Summer School 2005*. Santa Fe Institute, 2005.
- [34] M. Buehler, R. Battaglia, R. Cocosco, G. Hawker, J. Sarkis, and K. Yamazaki. SCOUT: a simple quadruped that walks, climbs, and runs. In *Proceedings ICRA*, volume 2, pages 1707–1712, 1998.

- [35] P.L. Buono. Models of central pattern generators for quadruped locomotion. ii. secondary gaits. *Journal of Mathematical Biology*, 42(4):327–346, 2001.
- [36] P.L. Buono and M. Golubitsky. Models of central pattern generators for quadruped locomotion. i. primary gaits. *Journal of Mathematical Biology*, 42(4):291–326, 2001.
- [37] C.C. Canavier, R.J. Butera, R.O. Dror, Baxter D.A., J.W. Clark, and J.H. Byrne. Phase response characteristics of model neurons determine which patterns are expressed in a ring circuit model of gait generation. *Biological Cybernetics*, 77:367–380, 1997.
- [38] J.G. Cham, S.A. Bailer, J.E. Clark, R.J. Full, and M.R. Cutkosky. Fast and robust: hexapedal robots via shape deposition manufacturing. *The International Journal of Robotics Research*, 21(10):869–882, 2002.
- [39] J.G. Cham, J.K. Karpick, and M.R. Cutkosky. Stride period adaptation of a biomimetic running hexapod. *Int. Journal of Robotics Research*, 23(2):141–153, 2004.
- [40] S. Chevallier, A.J. Ijspeert, D. Ryczko, F. Nagy, and J.M. Cabelguen. Organisation of the spinal central pattern generators for locomotion in the salamander: biology and modelling. *Brain Research Reviews*, 2006. Submitted.
- [41] A.H. Cohen. Effects of oscillator frequency on phase-locking in the lamprey central pattern generator. *Journal of Neuroscience Methods*, 21(2–4):113–125, 1987.
- [42] A.H. Cohen. Control principles for locomotion - looking toward biology. In *AMAM 2003*, 2003.
- [43] A.H. Cohen, G.B. Ermentrout, T. Kiemel, N. Kopell, K.A. Sigvardt, and T.L. Williams. Modelling of intersegmental coordination in the lamprey central pattern generator for locomotion. *Trends in Neurosciences*, 15(11):434–438, 1992.
- [44] A.H. Cohen, L. Guan, J. Harris, R. Jung, and T. Kiemel. Interaction between the caudal brainstem and the lamprey central pattern generator for locomotion. *Neuroscience*, 74(4):1161–1173, 1996.
- [45] A.H. Cohen, P.J. Holmes, and R. Rand. The nature of coupling between segmented oscillations and the lamprey spinal generator for locomotion: a mathematical model. *J. Math. Biol.*, 13:345–369, 1982.
- [46] A.H. Cohen and P. Wallen. The neural correlate of locomotion in fish. "fictive swimming" induced in a in vitro preparation of the lamprey spinal cord. *Exp. Brain Res.*, 41:11–18, 1980.

- [47] J.J. Collins and S.A. Richmond. Hard-wired central pattern generators for quadrupedal locomotion. *Biological Cybernetics*, 71(5):375–385, 1994.
- [48] J.J. Collins and I.N. Stewart. Coupled nonlinear oscillators and the symmetries of animal gaits. *Journal of Nonlinear Science*, 3:349–392, 1993.
- [49] Steve Collins, Andy Ruina, Russ Tedrake, and Martijn Wisse. Efficient Bipedal Robots Based on Passive-Dynamic Walkers. *Science*, 307(5712):1082–1085, 2005.
- [50] J.D. Crawford. Introduction to bifurcation theory. *Rev Mod Phys*, 63(4):991–1037, 1991.
- [51] A. Crespi, A. Badertscher, A. Guignard, and Ijspeert. A.J. Swimming and crawling with an amphibious snake robot. In *Proceedings of the 2005 IEEE International Conference on Robotics and Automation (ICRA 2005)*, pages 3035–3039, 2005.
- [52] A. Crespi and A.J. Ijspeert. AmphiBot II: An amphibious snake robot that crawls and swims using a central pattern generator. In *Proceedings of the 9th International Conference on Climbing and Walking Robots (CLAWAR 2006)*, pages 19–27, 2006.
- [53] M. de Lasa and M. Buehler. Dynamic compliant quadruped walking. In *ICRA 2001*, volume 3, pages 3153–3158, 2001.
- [54] F. Delcomyn. Neural basis for rhythmic behaviour in animals. *Science*, 210:492–498, 1980.
- [55] J.M. Dixon, J.A. Tuszyński, and D. Sept. Orthogonal trajectories and analytical solutions of the Van der Pol equation without forcing. *Physics Letters A*, 239:65–71, February 1998.
- [56] J. Duysens and H.W.A.A. van de Cromment. Neural control of locomotion; part 1: The central pattern generator from cats to humans. *Gait & Posture*, 7(2):131–141, 1998.
- [57] D. Eck. Finding downbeats with a relaxation oscillator. *Psychological Research*, 66:18–25, 2002.
- [58] V.M. Eguíluz, M. Ospeck, Y. Choe, A.J. Hudspeth, and M.O. Magnasco. Essential nonlinearities in hearing. *Phys Rev Lett*, 84(22):5232–5235, 2000.
- [59] G. Endo, J. Nakanishi, J. Morimoto, and G. Cheng. Experimental studies of a neural oscillator for biped locomotion with q rio. In *Proceedings of the 2005 IEEE International Conference on Robotics and Automation*, pages 598–604, Barcelona, Spain, 2005.

- [60] C. Engels and G. Schöner. Dynamic fields endow behavior-based robots with representations. *Robotics and Autonomous Systems*, 14(1):55–77, 1995.
- [61] B. Ermentrout. An adaptive model for synchrony in the firefly *pteroptyx malaccae*. *J. Math. Biol.*, 29:571–585, 1991.
- [62] G.B. Ermentrout and D. Kleinfeld. Traveling electrical waves in cortex: Insights from phase dynamics and speculation on a computational role. *Neuron*, 29:33–44, 2001.
- [63] G.B. Ermentrout and N. Kopell. Multiple pulse interactions and averaging in systems of coupled neural oscillators. *Journal of Mathematical Biology*, 29:195–217, 1991.
- [64] G.B. Ermentrout and N. Kopell. Inhibition-produced patterning in chains of coupled nonlinear oscillators. *SIAM J. Appl. Math.*, 54(2):478–507, 1994.
- [65] M.J. Feigenbaum. Universal behavior in nonlinear systems. *Los Alamos Science*, 1(1):4–27, 1980.
- [66] M.S. Fischer and R. Blickhan. The tri-segmented limbs of therian mammals: kinematics, dynamics, and self-stabilization - a review. *J Exp Zool*, 305A(11):935–952, 2006.
- [67] R. FitzHugh. Impulses and physiological states in theoretical models of nerve membrane. *Biophysical J.*, pages 445–466, 1961.
- [68] G. Franklin, J.D. Powell, and A. Emami-Naeini, editors. *Feedback Control of Dynamic Systems*. Addison-Wesley Longman Publishing, Boston, 3rd edition, 1993.
- [69] Y. Fukuoka, H. Kimura, and A.H. Cohen. Adaptive dynamic walking of a quadruped robot on irregular terrain based on biological concepts. *The International Journal of Robotics Research*, 3–4:187–202, 2003.
- [70] R.J. Full and D.E. Koditschek. Templates and anchors: neuromechanical hypotheses of legged locomotion on land. *Journal of Experimental Biology*, 202:3325–3332, 1999.
- [71] M. Galicki, L. Leistriz, and H. Witte. Learning continuous trajectories in recurrent neural networks with time-dependent weights. *IEEE Transactions on Neural Networks*, 10(4), 1999.
- [72] L. Gammaitoni, P. Hänggi, P. Jung, and F. Marchesoni. Stochastic resonance. *Reviews of Modern Physics*, 70(1):223–287, 1998.
- [73] H. Geyer, A. Seyfarth, and R. Blickhan. Spring-mass running: simple approximate solution and application to gait stability. *J. Theor. Biol.*, 232(3):315–328, 2004.

- [74] H. Geyer, A. Seyfarth, and R. Blickhan. Compliant leg behaviour explains basic dynamics of walking and running. *Proc. Roy. Soc. Lond. B*, 273(1603):2861–2867, 2006.
- [75] L. Glass and M.C. Mackey. *From Clocks to Chaos, The rhythms of life*. Princeton University Press, 1988.
- [76] M. Golubitsky and I. Stewart. Nonlinear dynamics of networks: the groupoid formalism. *Bull. Amer. Math. Soc.*, 2006.
- [77] M. Golubitsky, I. Stewart, P-L. Buono, and J.J. Collins. Symmetry in locomotor central pattern generators and animal gaits. *Nature*, 401:693–695, Oct 1999.
- [78] M. Golubitsky, I. Stewart, P.L. Buono, and J.J. Collins. A modular network for legged locomotion. *Physica D*, 115(1–2):56–72, 1998.
- [79] I. Grabec and W. Sachse. *Synergetics of Measurement, Prediction and Control*. Springer Series in Synergetics. Springer Verlag Berlin Heidelberg, 1997.
- [80] T. M. Griffin, R. KRam, S.J. Wickler, and D.F. Hoyt. Biomechanical and energetic determinants of the walk-trot transition in horses. *J. Exp. Biol.*, 207:4215–4223, 2004.
- [81] S. Grillner. Control of locomotion in bipeds, tetrapods and fish. In V.B. Brooks, editor, *Handbook of Physiology, The Nervous System, 2, Motor Control*, pages 1179–1236. American Physiology Society, Bethesda, 1981.
- [82] S. Grillner. Neurobiological bases of rhythmic motor acts in vertebrates. *Science*, 228(4696):143–149, 1985.
- [83] S. Grillner, T. Degliana, Ö. Ekeberg, A. El Marina, A. Lansner, G.N. Orlovsky, and P. Wallén. Neural networks that co-ordinate locomotion and body orientation in lamprey. *Trends in Neuroscience*, 18(6):270–279, 1995.
- [84] S. Grillner, Ö. Ekeberg, A. El Manira, A. Lansner, D. Parker, J. Tegner, and P. Wallen. Intrinsic function of a neuronal network – a vertebrate central pattern generator. *Brain Research Reviews*, 1998.
- [85] S. Grossberg, C. Pribe, and Cohen M.A. Neural control of interlimb oscillations i. human bimanual coordination. *Journal of Mathematical Biology*, 77(2):131–140, 1997.
- [86] A.K. Gutmann, B. Jacobi, M.T. Butcher, and J.E.A. Bertram. Constrained optimization in human running. *J Exp Biol*, 209:622–632, 2006.
- [87] H. Haken. *Synergetics. An introduction*. Springer Verlag Berlin Heidelberg, 3rd edition, 1983.

- [88] H. Haken. Synergetics—an interdisciplinary approach to phenomena of self-organization. *Geoforum*, 16(2):205–211, 1985.
- [89] H. Haken. *Advanced Synergetics. Instability Hierarchies of Self-Organization Systems and Devices.*, volume 20 of *Springer Series in Synergetics*. Springer Verlag Berlin Heidelberg, 2nd edition, 1987.
- [90] H. Haken and M. Haken-Krell. *Entstehung von biologischer Information und Ordnung*, volume 3 of *Dimensionen der modernen Biologie*. Wissenschaftliche Buchgesellschaft, Darmstadt, 1989.
- [91] H. Haken, J.A.S. Kelso, and H. Bunz. A theoretical model of phase transitions in human hand movements. *Biological Cybernetics*, 51:347–356, 1985.
- [92] B. Hasslacher and M.W. Tilden. The biology and technology of intelligent autonomous agents. *Robotics and Autonomous Systems*, 15(1–2):143–169, 1995.
- [93] Brosl Hasslacher and Mark W. Tilden. Theoretical foundations for nervous networks. volume 411, pages 179–186. AIP, 1997.
- [94] S. Haykin. *Neural Networks: A Comprehensive Foundation*. Prentice Hall; ISBN: 0132733501, 2nd edition, July 1998.
- [95] N.C. Heglund and C.R. Taylor. Speed, stride frequency and energy cost per stride: how do they change with body size and gait? *J Exp Biol*, 138(1):301–318, 1988.
- [96] A.L. Hodgkin and A.F. Huxley. Propagation of electrical signals along giant nerve fibres. *Proceedings of the Royal Society of London. Series B, Biological Sciences*, 140(899):177–183, October 1952.
- [97] N. Hogan. Impedance control - an approach to manipulation. i - theory. ii - implementation. iii - applications. *ASME, Transactions, Journal of Dynamic Systems, Measurement, and Control*, 107:1–24, 1985.
- [98] E. Hopf. Abzweigung einer periodischen Lösung von einer stationären Lösung eines Differentialsystems. *Ber. Math.-Phys., Sächs. Akad. d. Wissenschaften, Leipzig*, pages 1–22, 1942.
- [99] D.F. Hoyt and R. Taylor. Gait and the energetics of locomotion in horses. *Nature*, 292:239–240, 1981.
- [100] F. Iida. Cheap design approach to adaptive behavior: Walking and sensing through body dynamics. In *International Symposium on Adaptive Motion of Animals and Machines*, 2005.

- [101] F. Iida, G.J. Gomez, and R. Pfeifer. Exploiting body dynamics for controlling a running quadruped robot. In *Proceedings of the 12th Int. Conf. on Advanced Robotics (ICAR05)*, pages 229–235, 2005.
- [102] F. Iida, Y. Minekawa, J. Rummel, and A. Seyfarth. *Intelligent Autonomous Systems 9*, chapter Toward a human-like biped robot with compliant legs, pages 820–827. IOS Press, 2006.
- [103] F. Iida and R. Pfeifer. "Cheap" rapid locomotion of a quadruped robot: Self-stabilization of bounding gait. In F. Groen et al., editor, *Intelligent Autonomous Systems 8*, pages 642–649. IOS Press, 2004.
- [104] A.J. Ijspeert. A connectionist central pattern generator for the aquatic and terrestrial gaits of a simulated salamander. *Biological Cybernetics*, 84(5):331–348, 2001.
- [105] A.J. Ijspeert. Vertebrate locomotion. In M.A. Arbib, editor, *The handbook of brain theory and neural networks*, pages 649–654. MIT Press, 2003.
- [106] A.J. Ijspeert, A. Crespi, and J.M. Cabelguen. Simulation and robotics studies of salamander locomotion. Applying neurobiological principles to the control of locomotion in robots. *Neuroinformatics*, 3(3):171–196, 2005.
- [107] A.J. Ijspeert, A. Crespi, D. Ryczko, and J.M. Cabelguen. From swimming to walking with a salamander robot driven by a spinal cord model. *Science*, 2007. In print.
- [108] A.J. Ijspeert, J. Hallam, and D. Willshaw. Evolving swimming controllers for a simulated lamprey with inspiration from neurobiology. *Adaptive Behavior*, 7(2):151–172, 1999.
- [109] A.J. Ijspeert and J. Kodjabachian. Evolution and development of a central pattern generator for the swimming of a lamprey. *Artificial Life*, 5(3):247–269, 1999.
- [110] A.J. Ijspeert, J. Nakanishi, and S. Schaal. Learning attractor landscapes for learning motor primitives. In *Advances in Neural Information Processing Systems 15 (NIPS2002)*, 2002.
- [111] Auke Jan Ijspeert, Jonas Buchli, Allen Selverston, Mikhail Rabinovich, Martin Hasler, Wulfram Gerstner, Aude Billard, Henry Markram, and Dario Floreano (Editors). *Dynamical principles for neuroscience and intelligent biomimetic devices*. EPFL, 2006. ISBN 978-2-8399-0134-5.
- [112] E.M. Izhikevich. Resonate-and-fire neurons. *Neural Networks*, 14:883–894, 2001.

- [113] S. Jezernik, G. Colombo, M. Morari, and V. Dietz. Relearning gait in spinal cord injured and stroke persons using robotic technology. In *Proceedings of the Workshop on European Scientific and Industrial Collaboration (WESIC 2001)*, pages 425–431, 2001.
- [114] V.K. Jirsa and J.A.S. Kelso, editors. *Coordination Dynamics: Issues and Trends*. Springer, 2004.
- [115] E. R. Kandel, J. H. Schwartz, and T. M. Jessell, editors. *Principles of Neural Science*. McGraw-Hill Professional Publishing; ISBN: 0830577016, 4th edition, January 2000.
- [116] B.A. Kay, J.A.S. Kelso, E.L. Saltzman, and Schöner G. Space-time behavior of single and bimanual rhythmical movements: Data and limit cycle model. *Journal of Experimental Psychology: Human Perception & Performance*, 13(2):178–192, 1987. a lot of dots missing, see also kay87html.pdf.
- [117] J. A. S. Kelso, J. P. Scholz, and G. Schöner. Nonequilibrium phase transitions in coordinated biological motion: critical fluctuations. *Physics Letters A*, 118(6):279–284, 1986.
- [118] J. A. S. Kelso, J. P. Scholz, and G. Schöner. Dynamics governs switching among patterns of coordination in biological movement. *Physics Letters A*, 134(1):8–12, 1988.
- [119] J.A.S. Kelso. *Dynamic patterns : the self-organization of brain and behavior*. MIT Press, 1995.
- [120] J.A.S. Kelso and J.J. Jeka. Symmetry breaking dynamics of human multilimb coordination. *Journal of Experimental Psychology*, 18(3):645–668, 1992.
- [121] J.A.S. Kelso, D.L. Southard, and D. Goodman. On the nature of human interlimb coordination. *Science*, 203(4384):1029–1031, 1979.
- [122] R. Kempter, W. Gerstner, and J.L. van Hemmen. Hebbian learning and spiking neurons. *Phys Rev E*, 59:4498–4514, 1999.
- [123] A. Kern and R. Stoop. Essential role of couplings between hearing nonlinearities. *Physical Review Letters*, 91, 2003.
- [124] H.K. Khalil. *Nonlinear Systems*. Prentice Hall, New Jersey, 2002.
- [125] H. Kimura, S. Akiyama, and K. Sakurama. Realization of dynamic walking and running of the quadruped using neural oscillator. *Auton. Robot.*, 7:247–258, 1999.
- [126] H. Kimura and Y. Fukuoka. Biologically inspired adaptive dynamic walking in outdoor environment using a self-contained quadruped robot: Tekken2. In *Proceedings IROS 2004*, 2004.

- [127] H. Kimura, Y. Fukuoka, and A.V. Cohen. Biologically inspired adaptive dynamic walking of a quadruped robot. In S. Schaal, A.J. Ijspeert, A. Billard, S. Vijayakumar, J. Hallam, and J.A. Meyer, editors, *From Animals to Animats 8. Proceedings of the Eighth International Conference on the Simulation of Adaptive Behavior (SAB'04)*, pages 201–210. MIT Press, 2004.
- [128] S. Kirkpatrick, C.D. Gelatt, and M.P. Vecchi. Optimization by simulated annealing. *Science*, 220(4598):671–680, 1983. <http://dx.doi.org/10.1126/science.220.4598.671>.
- [129] N. Kopell. *Neural control of rhythmic movements in vertebrates.*, chapter Toward a Theory of Modelling Central Pattern Generators. John Wiley and Sons, New York, 1988.
- [130] N. Kopell and G.B. Ermentrout. Symmetry and phaselocking in chains of weakly coupled oscillators. *Communications on Pure and Applied Mathematics*, 39:623–660, 1986.
- [131] N. Kopell and G.B. Ermentrout. Coupled oscillators and the design of central pattern generators. *Mathematical Biosciences*, 90(1–2):87–109, 1988.
- [132] N. Kopell and G.B. Ermentrout. Phase transitions and other phenomena in chains of coupled oscillators. *SIAM J. Appl. Math.*, 50(4):1014–1052, 1990.
- [133] M.A. Kramer, R. Herschel, and J.M. Calo. Sensitivity analysis of oscillatory systems. *Applied Mathematical Modelling*, 8(5):328–340, 1984.
- [134] Y. Kuramoto. *Chemical oscillations, Waves, and Turbulence*. Springer Verlag Berlin Heidelberg, 1984.
- [135] Y. Kuramoto. Collective synchronization of pulse-coupled oscillators and excitable units. *Physica D: Nonlinear Phenomena*, 50(1):15–30, 1991.
- [136] L.D. Landau and E.M. Lifshitz. *Statistical Physics*, volume 5 of *Course of theoretical physics*. Pergamon Press London Paris, 1959.
- [137] E.W. Large. Resonance and the perception of musical meter. *Connection Science*, 6(2–3):177–208, 1994.
- [138] E.W. Large. Modeling beat perception with a nonlinear oscillator. In *Proceedings of the Eighteenth Annual Conference of the Cognitive Science Society*, 1996.
- [139] L. Leistriz, M. Galicki, H. Witte, and E. Kochs. Training trajectories by continuous recurrent multilayer networks. *IEEE Transactions on Neural Networks*, 13(2):283–291, March 2002.
- [140] F.L. Lewis. *Applied Optimal Control and Estimation*, chapter Introduction to Modern Control Theory. Prentice-Hall, 1992.

- [141] M.A. Lewis, R. Etienne-Cummings, M. Hartmann, Z.R. Xu, and A.H. Cohen. An in silico central pattern generator: silicon oscillator, coupling entrainment, and physical computation. *Biological Cybernetics*, 88:137–151, 2003.
- [142] D. Liechti and J. Buchli. Biology-based neural network control of the robotic orthosis lokomat, 2002. Technical Report – Automatic Control Laboratory, ETH Zürich.
- [143] S. Mallat, editor. *A wavelet tour of signal processing*. Academic Press, 2nd edition, 1999.
- [144] D. Marbach and A.J. Ijspeert. Online optimization of modular robot locomotion. In *Proceedings of the IEEE Int. Conference on Mechatronics and Automation (ICMA 2005)*, pages 248–253, 2005.
- [145] J. Marx. How cells step out. *Science*, 302(5643):214–216, 2003. Science News Focus. Cell Biology.
- [146] The MathWorks Inc. Matlab web site. <http://www.mathworks.com>.
- [147] K. Matsuoka. Sustained oscillations generated by mutually inhibiting neurons with adaptation. *Biol. Cybern.*, 52:367–376, 1985.
- [148] K. Matsuoka. Mechanisms of frequency and pattern control in the neural rhythm generators. *Biol. Cybern.*, 56:345–353, 1987.
- [149] T. McGeer. Passive dynamic walking. *International Journal of Robotics Research*, 9:62–82, 1990.
- [150] T.A. McMahon. The role of compliance in mammalian running gaits. *J. Exp. Biol.*, 115(1):263–282, 1985.
- [151] F. Menzer, J. Buchli, D.M. Howard, and A.J. Ijspeert. Nonlinear modelling of double and triple period pitch breaks in vocal fold vibration. In *Proceedings of the 6th Pan European Voice Conference, PEVOC 6*, 2005.
- [152] F. Menzer, J. Buchli, D.M. Howard, and A.J. Ijspeert. Nonlinear modelling of double and triple period pitch breaks in vocal fold vibration. *Logopedics Phoniatics Vocology*, 31:36–42, 2006.
- [153] O. Michel. Webots: Professional mobile robot simulation. *International Journal of Advanced Robotic Systems*, 1(1):39–42, 2004.
- [154] R.E. Mirollo and S.H. Strogatz. Synchronization of pulse-coupled biological oscillators. *SIAM Journal on Applied Mathematics*, 50(6):1645–1662, 1990.

- [155] J. Morimoto, G. Endo, J. Nakanishi, S. Hyon, G. Cheng, D. Bentevegna, and C.G. Atkeson. Modulation of simple sinusoidal patterns by a coupled oscillator model for biped walking. In *Proceedings of the 2006 IEEE International Conference on Robotics and Automation*, pages 1579–1584, May 2006.
- [156] J. Nakanishi, J. Morimoto, G. Endo, G. Cheng, S. Schaal, and M. Kawato. Learning from demonstration and adaptation of locomotion with dynamical movement primitives. *Special issue of Robotics and Autonomous Systems*, 2003. To appear.
- [157] V.I. Nekorkin and M.G. Velarde, editors. *Synergetic Phenomena in Active Lattices*, volume 79 of *Springer Series in Synergetics*. Springer Verlag Heidelberg, 2002.
- [158] J. Nishii. A learning model for oscillatory networks. *Neural Networks*, 11(2):249–257, 1998.
- [159] J. Nishii. Learning model for coupled neural oscillators. *10*, 10:213–226, 1999.
- [160] J. Nishii, Y. Uno, and R. Suzuki. Mathematical models for the swimming pattern of a lamprey, i. analysis of collective oscillators with time-delayed interaction and multiple coupling. *Biological Cybernetics*, 72:1–9, 1994.
- [161] T. Nishikawa, F.C. Hoppensteadt, and Y.C. Lai. Oscillatory associative memory network with perfect retrieval. *Physica D*, 197:134–148, 2004.
- [162] D. Noble. Modeling the heart - from genes to cells to the whole organ. *Science*, 295:1678–1682, 2002.
- [163] M. Okada, D. Nakamura, and Y. Nakamura. Hierarchical design of dynamics based information processing system for humanoid motion generation. In *Proceedings AMAM 2003*, 2003.
- [164] M. Okada, K. Tatani, and Y. Nakamura. Polynomial design of the nonlinear dynamics for the brain-like information processing of whole body motion. In *Proceedings of ICRA 2002*, volume 2, pages 1410–1415. IEEE, 2002.
- [165] J. Peinke, J. Parisi, O.E. Rössler, and R. Stoop. *Encounter with Chaos. Self-Organized Hierarchical Complexity in Semiconductor Experiments*. Springer Verlag Berlin Heidelberg, 1992.
- [166] A. Pikovsky, M. Rosenblum, and J. Kurths. *Synchronization, A universal concept in nonlinear sciences*, volume 12 of *Cambridge Nonlinear Science Series*. Cambridge University Press, Cambridge, UK, 2001.
- [167] R. Playter, M. Buehler, and Raibert M. Bigdog. *Proceedings of SPIE*, 6320, 2006.

- [168] G.A. Pratt, P. Willisson, C. Bolton, and A. Hofman. Late motor processing in low-impedance robots: Impedance control of series elastic actuators. In *Proceedings of the 2004 American Control Conference*, pages 3245–3251, 2004.
- [169] J. Pratt. *Exploiting Inherent Robustness and Natural Dynamics in the Control of Bipedal Walking Robots*. PhD thesis, Massachusetts Institute of Technology, Cambridge, Massachusetts, 2000.
- [170] J. Pratt and Pratt G. Exploiting natural dynamics in the control of a planar bipedal walking robot. In *Proceedings of the Thirty-Sixth Annual Allerton Conference on Communication, Control, and Computing*, 1998.
- [171] C. Pribe, S. Grossberg, and Cohen M.A. Neural control of interlimb oscillations ii. biped and quadruped gaits and bifurcations. *Journal of Mathematical Biology*, 77(2):141–152, 1997.
- [172] M. Raibert and J.K. Hodgins. *Biological Neural Networks in Invertebrate Neuroethology and Robotics*, chapter Legged Robots, pages 319–354. Academic Press, 1993.
- [173] M.H. Raibert. Trotting, pacing and bounding by a quadruped robot. *Journal of Biomechanics*, 23:79–98, 1990.
- [174] E.A. Rietman, M.W. Tilden, and M. Askenazi. Analog computation with rings of quasiperiodic oscillators: the microdynamics of cognition in living machines. *Robotics and Autonomous Systems*, 45(3):249–263, 2003.
- [175] L. Righetti, J. Buchli, and A.J. Ijspeert. From dynamic hebbian learning for oscillators to adaptive central pattern generators. In *Proceedings of 3rd International Symposium on Adaptive Motion in Animals and Machines – AMAM 2005*. Verlag ISLE, Ilmenau, 2005. Full paper on CD.
- [176] L. Righetti, J. Buchli, and A.J. Ijspeert. From dynamic hebbian learning for oscillators to adaptive central pattern generators. In *Proceedings of 3rd International Symposium on Adaptive Motion in Animals and Machines – AMAM 2005*, page 45. Verlag ISLE, Ilmenau, 2005. Abstract.
- [177] L. Righetti, J. Buchli, and A.J. Ijspeert. Adaptive frequency oscillators applied to dynamic walking I. Programmable pattern generators. In *Proceedings of Dynamic Walking*, 2006. Abstract.
- [178] L. Righetti, J. Buchli, and A.J. Ijspeert. Dynamic hebbian learning in adaptive frequency oscillators. *Physica D*, 216(2):269–281, 2006.
- [179] L. Righetti, J. Buchli, and A.J. Ijspeert. Programmable central pattern generators. In Auke Jan Ijspeert, Jonas Buchli, Allen Silverston, Mikhail Rabinovich, Martin Hasler, Wulfram Gerstner, Aude Billard, Henry Markram,

- and Dario Floreano (Editors), editors, *Dynamical principles for neuroscience and intelligent biomimetic devices*, pages 129–130. EPFL, 2006. ISBN 978-2-8399-0134-5.
- [180] L. Righetti and A.J. Ijspeert. Design methodologies for central pattern generators: application to crawling humanoids. In *Proceedings RSS 06*, 2006.
- [181] L. Righetti and A.J. Ijspeert. Programmable central pattern generators: an application to biped locomotion control. In *Proceedings of the 2006 IEEE International Conference on Robotics and Automation*, 2006.
- [182] H. Risken. *The Fokker-Planck Equation*, volume 18 of *Springer Series in Synergetics*. Springer, 1984.
- [183] F. Rosenblatt. The perceptron: a probabilistic model for information storage and organization in the brain. *Psychol Rev*, 65(6):386–408, 1958.
- [184] O.E. Rössler. An equation for continuous chaos. *Phys Lett A*, 57(5):397–398, 1976.
- [185] A. Ruiz, D.H. Owens, and S. Townley. Existence, learning, and replication of periodic motions in recurrent neural networks. *IEEE Transactions on Neural Networks*, 9(4):651–661, July 1998.
- [186] D. Rumelhart, D. Hinton, and G. Williams. *Parallel Distributed Processing*, chapter Learning internal representations by error propagation. MIT Press, Cambridge, 1986.
- [187] J. Rummel, F. Iida, and A. Seyfarth. *Intelligent Autonomous Systems 9*, chapter One-legged locomotion with a compliant passive joint, pages 566–573. IOS Press, 2006.
- [188] C.M.P. Santos. *Attractor Dynamics Based Generation of Timed Robotic Trajectories*. PhD thesis, Universidade do Minho Escola de Engenharia, Dept. de Electronica Industrial, Guimaraes, Portugal, September 2003.
- [189] C.M.P. Santos. Generating timed trajectories for an autonomous vehicle: A non-linear dynamical systems approach. In *2004 IEEE International Conference on Robotics and Automation*. IEEE, IEEE, 2004.
- [190] J. P. Scholz, J. A. S. Kelso, and G. Schöner. Nonequilibrium phase transitions in coordinated biological motion: Critical slowing down and switching time. *Physics Letters A*, 123(8):390–394, 1987.
- [191] G. Schöner. Learning and recall in a dynamic theory of coordination patterns. *Biol. Cybern.*, 62:39–54, 1989.

- [192] G. Schöner. Recent developments and problems in human movement science and their coceptual implications. *Ecological Psychology*, 7(4):291–314, 1995.
- [193] G. Schöner and M. Dose. A dynamical systems approach to task-level system integration used to plan and control autonomous vehicle motion. *Robotics and Autonomous Systems*, 10(4):253–267, 1992.
- [194] G. Schöner, M. Dose, and C. Engels. Dynamics of behavior: Theory and applications for autonomous robot architectures. *Robotics and Autonomous Systems*, 16(2–4):213–245, 1995.
- [195] G. Schöner, W.Y. Jiang, and J.A.S. Kelso. A synergetic theory of quadrupedal gaits and gait transitions. *Journal of theoretical Biology*, 142:359–391, 1990.
- [196] G. Schöner and J.A.S. Kelso. Dynamic pattern generation in behavioral and neural systems. *Science*, 239(4847):1513–1520, 1988.
- [197] G. Schöner and J.A.S. Kelso. A dynamic pattern theory of behavioral change. *J. Theor. Biol.*, 135:501–524, 1988.
- [198] G. Schöner and J.A.S. Kelso. Dynamic patterns of biological coordination: Theoretical strategy and new results. In J.A.S. Kelso, A.J. Mandell, and M.F. Shlesinger, editors, *Dynamic Patterns in complex systems*, pages 77–102, 1988.
- [199] G. Schöner and J.A.S. Kelso. A synergeric theory of environmentally-specified and learned patterns of movement coordination. I Relative phase dynamics. *Biological Cybernetics*, 58:71–80, 1988.
- [200] G. Schöner and J.A.S. Kelso. A synergetic theory of environmentally-specified and learned patterns of movement coordination. II Component oscillator dynamics. *Biological Cybernetics*, 58:81–89, 1988.
- [201] G. Schöner and C.M.P. Santos. Control of movement time and sequential action through attractor dynamics: A simulation study demonstrating object interception and coordination. In *SIRS 2001*, 2001.
- [202] I. Schreiber and M. Marek. *Modeling the Dynamics of Biological Systems*, volume 65 of *Springer Series in Synergetics*, chapter Dynamics of Oscillatory Chemical Systems. Springer Verlag Berlin Heidelberg, 1995.
- [203] A.I. Selverston and J. Ayers. Oscillations and oscillatory behavior in small neural circuits. *Biological Cybernetics*, 95(6):537–554, 2006.
- [204] A. and Seyfarth. Swing-leg retraction: a simple control model for stable running. *The Journal of Experimental Biology*, 206:2547–2555, 2003.

- [205] M.L. Shik, F.V. Severin, and G.N. Orlovsky. Control of walking by means of electrical stimulation of the mid-brain. *Biophysics*, 11:756–765, 1966.
- [206] S. Skogestad and I. Postlethwaite. *Multivariable Feedback Control*. John Wiley & Sons, Chichester, 1996.
- [207] J.J.E. Slotine and W. Li. *Applied Nonlinear Control*. Prentice Hall, New Jersey, 1991.
- [208] D. Somers and N. Kopell. Rapid synchronization through fast threshold modulation. *Biological Cybernetics*, 68:393–407, 1993.
- [209] J.C. Spall. An overview of the simultaneous perturbation method for efficient optimization. *Johns Hopkins Apl Technical Digest*, 19(4):482–492, 1998.
- [210] S. Still and M.W. Tilden. Coupled oscillators and walking control: a hardware implementation of a distributed motor system. In N. Elsner and R. Wehner, editors, *Proceedings of the 26th Goettingen Neurobiology Conference*, volume 2, page 262, 1998.
- [211] R. Stoop, J. Buchli, and M. Christen. Phase and frequency locking in detailed neuron models. In *2004 Int. Symposium on Nonlinear Theory and its Applications (NOLTA 2004)*, pages 43–46, 2004.
- [212] R. Stoop, J. Buchli, G. Keller, and W.H. Steeb. Stochastic resonance in pattern recognition by a holographic neuron model. *Physical Review E*, 67, 2003.
- [213] S. Strogatz. *Nonlinear Dynamics and Chaos. With applications to Physics, Biology, Chemistry, and Engineering*. Addison Wesley Publishing Company, 1994.
- [214] S.H. Strogatz. The mathematical structure of the human sleep-wake cycle. *Lecture Notes in Biomathematics*, 69, 1986.
- [215] S.H. Strogatz. From kuramoto to crawford: exploring the onset of synchronization in populations of coupled oscillators. *Physica D: Nonlinear Phenomena*, 143(1–4):1–20, 2000.
- [216] S.H. Strogatz and I. Stewart. Coupled oscillators and biological synchronization. *Scientific american*, 269(6):68–74, 1993.
- [217] G. Taga. Emergence of bipedal locomotion through entrainment among the neuro-musculo-skeletal system and the environment. *Physica D: Nonlinear Phenomena*, 75(1–3):190–208, 1994.
- [218] G. Taga. A model of the neuro-musculo-skeletal system for human locomotion. I. Emergence of basic gait. *Biological Cybernetics*, 73(2):97–111, 1995.

- [219] G. Taga. A model of the neuro-musculo-skeletal system for human locomotion. II. real-time adaptability under various constraints. *Biological Cybernetics*, 73(2):113–121, 1995.
- [220] G. Taga. A model of the neuro-musculo-skeletal system for anticipatory adjustment of human locomotion during obstacle avoidance. *Biological Cybernetics*, 78(1):9–17, 1998.
- [221] G. Taga, Y. Yamagushi, and H. Shimizu. Self-organized control of bipedal locomotion by neural oscillators in unpredictable environment. *Biological cybernetics*, 65:147–159, 1991.
- [222] M.W. Tilden. Adaptive robotic nervous systems and control circuits therefor. US Patent No. 5325031, 1994.
- [223] K. Tsuchiya, S. Aoi, and K. Tsujita. Locomotion control of a multi-legged locomotion robot using oscillators. In *2002 IEEE Intl. Conf. SMC*, volume 4, 2002.
- [224] K. Tsujita, K. Tsuchiya, and A. Onat. Adaptive gait pattern control of a quadruped locomotion robot. In *IROS 2001*, 2001.
- [225] T. Valency and M. Zacksenhouse. Accuracy/robustness dilemma in impedance control. *Journal of Dynamic Systems, Measurement, and Control*, 125:310–319, 2003.
- [226] V. Vapnik. *Statistical Learning Theory*. Wiley, New York, 1998.
- [227] B.W. Verdaasdonk, H.F.J.M. Koopman, and F.C.T. van der Helm. Resonance tuning in a neuro-musculo-skeletal model of the forearm. *Biological Cybernetics*, 96(2):165–180, 2007.
- [228] W. Wang and J.J.E. Slotine. On partial contraction analysis for coupled nonlinear oscillators. *Biological Cybernetics*, 92(1):38–53, 2005.
- [229] B. Webb, J. Wessnitzer, S. Busch, J. Schul, J. Buchli, and A. Ijspeert. Resonant neurons and bushcricket behaviour. *Journal of Comparative Physiology A*, 193(2):285–288, 2007.
- [230] P. Werbos. *Beyond regression: New tools for prediction and analysis in the behavioral sciences*. PhD thesis, Harvard Univ., Cambridge MA, 1974.
- [231] K. Wiesenfeld. New results on frequency-locking dynamics of disordered josephson arrays. *Physica B*, 222(4):315–319, 1996.
- [232] C. Wilbur, W. Vorus, Y. Cao, and S.N. Currie. *Neurotechnology for biomimetic robots*, chapter A Lamprey-Based Undulatory Vehicle. Bradford/MIT Press, Cambridge London, 2002.

-
- [233] M.W. Williamson. Exploiting natural dynamics in robot control. In *Proceedings Fourth European Meeting on Cybernetics and Systems Research (EM-CSR '98)*, 1998.
 - [234] A.T. Winfree. *The Geometry of biological time*. Springer Verlag, 2nd edition, 2001.
 - [235] H. Yuasa and M. Ito. Coordination of many oscillators and generation of locomotory patterns. *Biological Cybernetics*, 63:177–184, 1990.
 - [236] P. Zegers and M.K. Sundareshan. Trajectory generation and modulation using dynamic neural networks. *IEEE Transactions on Neural Networks*, 14(3):520–533, 2003.

Jonas Buchli

Curriculum Vitae

born July 1, 1977 in Solothurn Switzerland
Citizen of Safien GR, Switzerland

Education

2003–2007	PhD candidate at the Biologically Inspired Robotics Group, EPFL
2003	Graduation: dipl. El.Ing. ETHZ (equivalent to MSc EE)
1997–2003	Studies in Electrical Engineering ETH Zürich
1997	Matur Typ C (mathematisch naturwissenschaftliche Matur) (general qualification for university entrance, mathematical/natural science type) Kantonsschule Solothurn

Research interests

Application of Complex Systems knowledge in Engineering
Self-Organization and Emergent Phenomena in Complex Systems
Nonlinear Dynamical Systems
Robotics
Information Concepts
Theory of Computation
Computational Neurosciences & Theoretical Biology

Academic experience

Supervision of nine student projects (master and semester projects)
Co-organization of two international conferences
Reviewer for international conferences and journals
Main guest-editor of a special issue on “Dynamical principles in neuronal systems and robotics”
Teaching in Nonlinear Dynamical Systems

Industrial experience

Experience in SW/HW development
Independent engineering and consulting for the paragliding industry

Publications

Journal publications

- [1] J. Buchli and A.J. Ijspeert. Self-organized adaptive legged locomotion in a compliant robot. 2007. Unsubmitted manuscript
- [2] J. Buchli, L. Righetti, and A.J. Ijspeert. Frequency analysis with coupled nonlinear oscillators. *SIAM Journal on Applied Dynamical Systems*, 2007. Submitted
- [3] B. Webb, J. Wessnitzer, S. Busch, J. Schul, J. Buchli, and A. Ijspeert. Resonant neurons and bushcricket behaviour. *Journal of Comparative Physiology A*, 193(2):285–288, 2007
- [4] J. Buchli, L. Righetti, and A.J. Ijspeert. Engineering entrainment and adaptation in limit cycle systems – from biological inspiration to applications in robotics. *Biological Cybernetics*, 95(6):645–664, 2006
- [5] L. Righetti, J. Buchli, and A.J. Ijspeert. Dynamic hebbian learning in adaptive frequency oscillators. *Physica D*, 216(2):269–281, 2006
- [6] F. Menzer, J. Buchli, D.M Howard, and A.J. Ijspeert. Nonlinear modelling of double and triple period pitch breaks in vocal fold vibration. *Logopedics Phoniatrics Vocology*, 31:36–42, 2006
- [7] R. Stoop, J. Buchli, G. Keller, and W.H. Steeb. Stochastic resonance in pattern recognition by a holographic neuron model. *Physical Review E*, 67, 2003

Conference publications

- [1] J. Buchli, F. Iida, and A.J. Ijspeert. Finding resonance: Adaptive frequency oscillators for dynamic legged locomotion. In *Proceedings of the IEEE/RSJ International Conference on Intelligent Robots and Systems (IROS)*, pages 3903–3909. IEEE, 2006
- [2] G. Brambilla, J. Buchli, and A.J. Ijspeert. Adaptive four legged locomotion control based on nonlinear dynamical systems. In *From Animals to Animats 9. Proceedings of the Ninth International Conference on the Simulation of Adaptive Behavior (SAB'06)*, volume 4095 of *Lecture Notes in Computer Science*, pages 138–149. Springer Verlag, 2006
- [3] L. Righetti, J. Buchli, and A.J. Ijspeert. From dynamic hebbian learning for oscillators to adaptive central pattern generators. In *Proceedings of 3rd International Symposium on Adaptive Motion in Animals and Machines – AMAM 2005*. Verlag ISLE, Ilmenau, 2005. Full paper on CD

- [4] F. Menzer, J. Buchli, D.M. Howard, and A.J. Ijspeert. Nonlinear modelling of double and triple period pitch breaks in vocal fold vibration. In *Proceedings of the 6th Pan European Voice Conference, PEVOC 6*, 2005
- [5] J. Buchli, L. Righetti, and A.J. Ijspeert. A dynamical systems approach to learning: a frequency-adaptive hopper robot. In *Proceedings of the VI-IIth European Conference on Artificial Life ECAL 2005*, Lecture Notes in Artificial Intelligence, pages 210–220. Springer Verlag, 2005
- [6] R. Stoop, J. Buchli, and M. Christen. Phase and frequency locking in detailed neuron models. In *2004 Int. Symposium on Nonlinear Theory and its Applications (NOLTA 2004)*, pages 43–46, 2004
- [7] J. Buchli and A.J. Ijspeert. A simple, adaptive locomotion toy-system. In S. Schaal, A.J. Ijspeert, A. Billard, S. Vijayakumar, J. Hallam, and J.A. Meyer, editors, *From Animals to Animats 8. Proceedings of the Eighth International Conference on the Simulation of Adaptive Behavior (SAB'04)*, pages 153–162. MIT Press, 2004
- [8] J. Buchli and A.J. Ijspeert. Distributed central pattern generator model for robotics application based on phase sensitivity analysis. In A.J. Ijspeert, M. Murata, and N. Wakamiya, editors, *Biologically Inspired Approaches to Advanced Information Technology: First International Workshop, BioADIT 2004*, volume 3141 of *Lecture Notes in Computer Science*, pages 333–349. Springer Verlag Berlin Heidelberg, 2004

Abstracts

- [1] J. Buchli, L. Righetti, and A.J. Ijspeert. Adaptive dynamical systems: A promising tool for embodied artificial intelligence. In *Proceedings of 50th anniversary summit of artificial intelligence*, July 2006. Abstract
- [2] L. Righetti, J. Buchli, and A.J. Ijspeert. Programmable central pattern generators. In Auke Jan Ijspeert, Jonas Buchli, Allen Selverston, Mikhail Rabinovich, Martin Hasler, Wulfram Gerstner, Aude Billard, Henry Markram, and Dario Floreano (Editors), editors, *Dynamical principles for neuroscience and intelligent biomimetic devices*, pages 129–130. EPFL, 2006. ISBN 978-2-8399-0134-5
- [3] L. Righetti, J. Buchli, and A.J. Ijspeert. Adaptive frequency oscillators applied to dynamic walking I. Programmable pattern generators. In *Proceedings of Dynamic Walking*, 2006. Abstract
- [4] J. Buchli, L. Righetti, and A.J. Ijspeert. Adaptive frequency oscillators applied to dynamic walking II. Adapting to resonant body dynamics. In *Proceedings of Dynamic Walking*, 2006. Abstract

- [5] J. Buchli, L. Righetti, and A.J. Ijspeert. Adaptive dynamical systems for movement control. In *Proceedings of 3rd International Symposium on Adaptive Motion in Animals and Machines – AMAM 2005*, page 7. Verlag ISLE, Ilmenau, 2005. Abstract

Technical Reports & Misc

- [1] J. Buchli, A.J. Ijspeert, M. Rabinovich, and A. Selverston. Dynamical principles in neuronal systems and robotics – guest editorial. *Biological Cybernetics*, 96(6):517–518, 2006
- [2] J. Buchli. *Foreword – Mobile Robots, moving intelligence*. Advanced Robotics Systems International and pro literatur Verlag, Mammendorf, 2007
- [3] J. Buchli and C.C. Santini. Complexity engineering: Harnessing emergent phenomena as opportunities for engineering. In *Reports of the Santa Fe Institute’s Complex Systems Summer School 2005*. Santa Fe Institute, 2005
- [4] J. Buchli. Locking behavior in extended nerve cell models, 2003. MSc Thesis – Institute of Neuroinformatics, ETH / UNI Zürich
- [5] D. Liechti and J. Buchli. Biology-based neural network control of the robotic orthosis lokomat, 2002. Technical Report – Automatic Control Laboratory, ETH Zürich

Books

- [1] Auke Jan Ijspeert, Jonas Buchli, Allen Selverston, Mikhail Rabinovich, Martin Hasler, Wulfram Gerstner, Aude Billard, Henry Markram, and Dario Floreano (Editors). *Dynamical principles for neuroscience and intelligent biomimetic devices*. EPFL, 2006. ISBN 978-2-8399-0134-5
- [2] J. Buchli, editor. *Mobile Robots, moving intelligence*. Advanced Robotics Systems International and pro literatur Verlag, Mammendorf, 2007